CARDIFF UNIVERSITY

SCHOOL OF ENGINEERING

Thesis Titled:

COMBUSTION DYNAMICS IN A LEAN PREMIXED COMBUSTOR WITH SWIRL FORCING AND FUEL CONDITIONS

By

OKON ANIEKAN A.

Thesis submitted in fulfilment of the requirements for the degree of Doctor of Philosophy

December, 2017

Acknowledgment

To the Almighty God, the King of kings and Lord of lords, I give Him all the Glory.

My heartfelt gratitude goes to my supervisors: Dr Agustin Valera-Medina, Dr Yiqin Xue and Dr Richard Mash for their support and guidance. Their invaluable discussions, comments, revisions, advice and encouragement contributed immensely to the overall success of this study.

I would also like to thank Dr Roger Grosvenor and Dr Andrew Crayford for their assistance. I sincerely appreciate the help of the technical team of the Mechanical Engineering workshop especially Mr Malcom Seaborne, Mr Andrew Rankmore, Mr Paul Malpas and Mr Stephen Mead.

My sincere thanks go to my sponsors, Niger Delta Development Commission (NDDC), Nigeria and University of Uyo, Nigeria, for all their financial support and encouragement.

I am so grateful to my family for their patience, encouragement and support throughout the entire period of the programme.

To my friends and colleagues: Hayder Kurji, Fares Hatem, Mohammed Alfahaam, Ali Alsaegh, Abbas Alfarji, Ali Alzugaibi, Oula Fatla, Fatima Shkal, Julian, Hua, Den and many others, I say many thanks for your assistance and goodwill.

This work is dedicated to my little daughter Sophia, my wife Emem and my mother Hannah

Summary

Fossil fuels still account for a large percentage of global energy demand according to available statistics. Natural gas is increasingly gaining the share of these fuels due to the retired coal and nuclear plants. The more stringent emission standards have also put natural gas ahead of other fuels as a result of its efficiency, cost, environmental attributes as well as the operational efficiency of the gas turbine, an engine that uses this fuel. A standard low emission combustion technique in gas turbines is the dry low NOx combustion, with lean fuel and fuel-air premixed upstream of the flame holder. However, this condition is highly susceptible to combustion instabilities characterised by large amplitude oscillations of the combustor's acoustic modes excited by unsteady combustion processes. These pressure oscillations are detrimental both to the efficiency of performance as well as the hardware of the system.

Although the processes and mechanisms that result in instabilities are well known, however, the current challenges facing gas turbine operators are the precise understanding of the operational conditions that cause combustion instabilities, accurate prediction of the instability modes and the control of the disturbances.

In a bid to expand this knowledge frontier, this study uses a 100kW swirl premixed combustor to examine the evolution of the flow structures, its influence on the flame dynamics, in terms of heat release fluctuation and the overall effects on the pressure field, under different, swirl, fuel and external excitation conditions. The aim is to determine the operational conditions whose pressure oscillation is reduced to the barest minimum to keep the system in an excellent running condition. The results of this study are expected to contribute towards the design of a new control system to damp instabilities in gas turbines.

Publications

1. Aniekan Okon*[1] Agustin Valera-Medina[1], Yiqin Xue[1], Ali Al-Zughaibi[1] "Flow dynamics perturbations of a forced swirl premixed combustor for efficient and low emissions combustion". Journal Paper- Flow, Turbulence and Combustion, Springer, (under review).

2. Aniekan Okon*[1] Agustin Valera-Medina[1], Yiqin Xue[1], Ali Al-Zughaibi[1] "Acoustic Mode suppression of an enhanced Lean Premixed Combustor with Methane- CO2 Fuel Blends". Journal Paper- Fuel, Elsevier,(under review).

3. Okon Aniekan*,Valera-Medina Agustin, Kurji Hayder, Xue Yiqin, "Acoustic dynamics of a swirl premixed combustor with different operating conditions" 9th International Conference on Applied Energy, ICAE 2017, 21-24 August 2017, Cardiff, UK.

4. Hayder Kurji, Agustin Valera-Medina, Aniekan Okon, Cheng Tung Chong "Combustion and emission performance of CO2/CH4/biodiesel and CO2/CH4/diesel blends in a swirl burner generator" - 9th International Conference on Applied Energy, ICAE2017, 21-24 August 2017, Cardiff, UK.

5. Hayder Kurji, Agustin Valera-Medina, Aniekan Okon, Cheng Tung Chong "Carbon dioxide blends to reduce emissions under premixed combustion" 13th International Conference on Energy for a Clean Environment. Sao Miguel, Azores, Portugal, 2 - 6 July, 2017.

6. A. Okon*, A. Valera, H. Kurji, Y. Xue, R. Mash, "Effects of flame temperature on combustion instabilities of a premixed burner" 8th European Combustion Meeting, 18-21 April 2017, Dubrovnik, Croatia.

7. H. Kurji; Aniekan Okon; A. Valera-Medina; C. Cheng-Tung "Reduction of emissions by using various syngases with different injection strategies under premixed combustion mode" 2016 International Conference for Students on Applied Engineering (ICSAE), Newcastle University. Year:2016 Pages: 407 - 412, DOI: 10.11-09/IC-SAE- 2016.7810226IEEE Conference Publications

8. Aniekan Okon; Hayder Kurji; Agustin Medina; Yiqin Xue "Heat release rate and pressure fluctuation of lean premixed flame at different forcing levels", 2016 International Conference for Students on Applied Engineering (ICSAE), Newcastle University. Year: 2016, Pages: 232 236, DOI: 10.1109/ICSAE.-2016.-78-10194IEEE Conference Publications.

Table of Contents

Contents

List of Figures

List of Tables

List of Abbreviations

ACD	Autocorrelation decay
AMV	Axial Mean Velocity
CAM	Combustor Acoustic Mode
CCS	Carbon Capture and Storage
CFD	Computational Fluids Dynamics
CH_4	Methane
CIVBCO	Combustion Induced Vortex Breakdown
CO	Carbon Monoxide
CO_2	Carbon Dioxide
COP	Conference of Parties
CRZ	Central Recirculation Zone
CTA	Constant temperature anemometer
DLE	Dry Low Emission
DLR	Diameter to Length Ratio
DNS	Direct Numerical Simulation
DOQ	Data acquisition
ERZ	External Recirculation Zone
EU	European Union
FDF	Flame describing function
FDIDF	Flame double input describing function
FFT	Fast Fourier Transform
FTF	Flame Transfer Function
HMFR	High momentum flow region
HSP	High speed Photography
HWA	Hot Wire anemometry
IEPE	Integrated electronic piezoelectric
LDA	Laser Doppler Anemometry
LES	Large Eddy Simulation
LPM	Lean premixed
NO	Nitrous oxide
NOx	Nitrous oxides
OECD	Organization for Economic Cooperation for Development
OSCILOS	Open source combustion instability low order simulator
PACT	Pilot scale advanced capture technology
PDF	Probability Density Function
PDF	Probability density function
PVC	Pressing Vortex Core
RANS	Reynolds -Averaged Navier-Stokes
Re	Reynolds Number
UHC	Unburned Hydrocarbons
UN	United Nation
URANS	Unsteady Reynolds-Averaged Navier-Stokes

ABSTRACT

Natural gas is increasingly gaining the share of fossil fuels due to the retired coal and nuclear plants. The more stringent emission standards, efficiency and cost, have also put natural gas ahead of other fuels such as coal and oil. A standard low emission combustion technique in gas turbines is the dry low NOx combustion. However, its running conditions are highly susceptible to combustion instabilities, characterised by large amplitude oscillations of the combustor's acoustic modes excited by unsteady combustion processes. These pressure oscillations are detrimental both to the efficiency and hardware of the system.

Although the processes and mechanisms that cause these instabilities are well known, however, the current challenges facing gas turbine operators are the precise understanding of the operational conditions that cause combustion instabilities, accurate prediction of the instability modes and the control of the disturbances. In a bid to expand this knowledge frontier, this study uses a 100kW swirl premixed combustor to examine the evolution of the flow structures, its influence on the flame dynamics and the overall effects on the pressure field, under different, swirl, fuel and external excitation conditions.

The results of this study revealed that at both flow and flame fields, the increased swirl strength with a corresponding increase in the size of the CRZ and high turbulence all enhanced mixing and flame anchorage, however, the high turbulence resulted in increased heat release fluctuations. An increased forcing moved the high turbulence velocity regimes down to the dump plane and split them into smaller scales especially within the shear layers with extreme forcing conditions. Thus the heat release oscillation peaked at a higher swirl strength and a low forcing frequency but decreased with increased forcing. The heat release oscillation also reduced significantly with the blend of methane with CO_2 due to the interplay of the thermodynamic properties.

These dynamics in the flow and flame fields were observed to have corresponding effects on the acoustic field. The increased swirl strength, increased the acoustic instabilities, with further increase with low forcing frequencies. The blend of methane with CO_2 suppressed the acoustic instability modes to the barest minimum especially at a low percentage of CO_2. In most cases, the reduced instabilities became more efficient at the leaner mixture. Thus the control of the flow and flame fields via the variation of the geometry of the swirl nozzle and fuel mix kept the

combustor in a stable running condition with promising potentials for an active control design for the system.

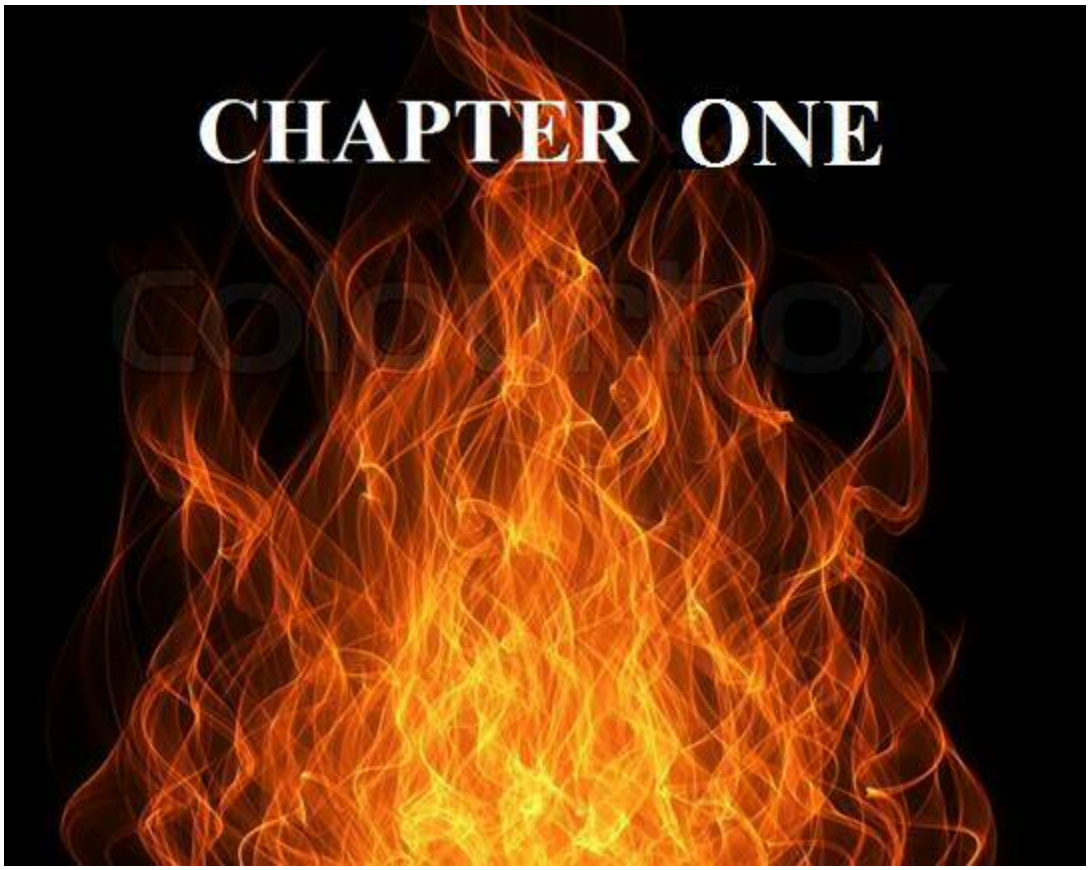
CHAPTER ONE

CHAPTER ONE:

INTRODUCTION

"We can create a more sustainable, cleaner and safer world by making wiser energy choices."
-- Robert Alan Silverstein

This chapter looks at the global energy demand, sources and its supply, with attention on natural gas as one of the purest forms of fossil fuel. The operation of gas turbines as the conventional combustion engines that use natural gas are reviewed. Pollutant emissions from combustion engines and its policy framework are also examined. The pollutant formation, (with emphasis on oxides of nitrogen), control and the operability challenges in gas turbines are also reviewed. Section 1.1 looks at the global energy demand; section 1.2 considers the global energy consumption by sector; section 1.3 describes the energy sources and supply. Section 1.4 discusses natural gas as the purest form of fossil fuels with expected higher demand in the future; section 1.5 looks at gas turbines as the combustion engines that burn natural gas. Section 1.6 considers combustion emissions, its formation, and the policy framework by institutions, section 1.7 considers the various techniques for the control of the pollutants while section 1.8 considers the impacts of these control methods on the operability of the system. The summary of the chapter, objectives of the study and the thesis structure are outlined in sections 1.9, 1.9.1 and 1.9.2 respectively.

1.1 Global Energy Demand

Energy plays a significant role in human life and its development. It drives industrial machines, powers homes, propels aircraft, automobiles, marine engines, etc. The global demand for energy has continued to increase since the advent of civilization. The growth became rapid in the last few decades due to increasing human population, modernization, and urbanization. It is projected that the increase in global energy demand would rise sharply in the near future. According to the Energy Information

Administration (EIA) [1], the world energy demand will rise by 56 percent between 2010 and 2040, Figure1.1. According to the projection, energy demand will increase from 524 quadrillions Btu in 2010 to 630 quadrillions Btu in 2020 and 820 quadrillions Btu in 2040. The forecast also indicates that a substantial percentage of this increase will come from the developing countries outside the Organization for Economic Cooperation for Development (Non-OECD) countries due to the expected growth in economic activities and expansion in population. The 2012 World Energy Outlook [2], also projected a 60% increase in the Non-OECD countries energy demand from 2010 to 2035, Figure1.2.

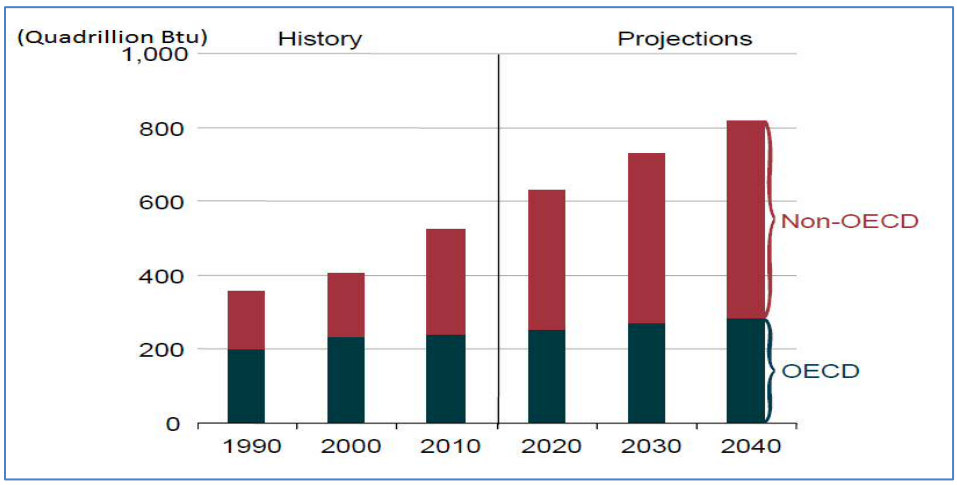

Figure 1. 1 Global Energy Demand Projection [3].

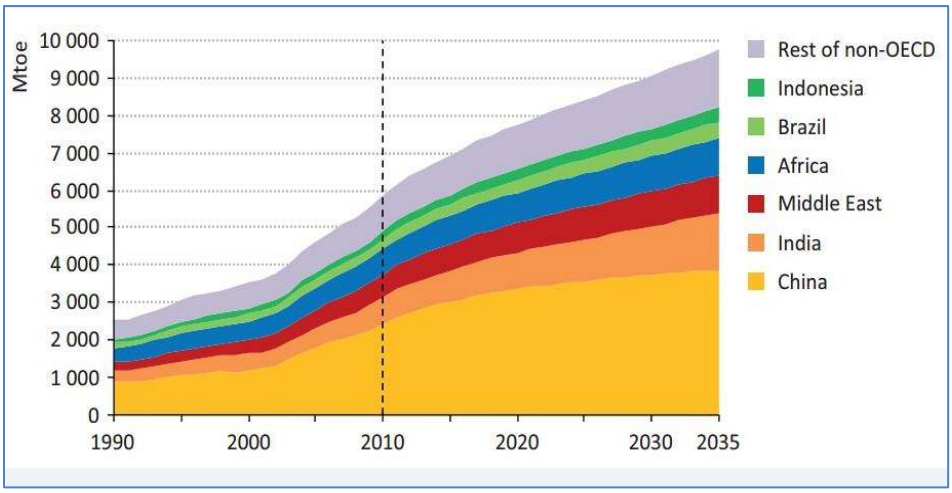

Figure 1. 2 Non- OECD Energy Demand by Regions [2].

The above projections indicate that the global energy demand will continue to rise in the future and therefore requires a concerted effort to secure energy to meet the future demand.

1.2 Energy Consumption by Sectors

Energy consumption could be classified into four broad categories, these are:

- Commercial: This is mainly electricity consumed in commercial buildings such as mercantile, health care, warehouse, services, education, offices, etc. The consumptions include cooking, office equipment, water heating, local heating, ventilation, cooling, lighting, etc.
- Industrial: These are energy consumption industries which include textile mills, wood product, printing, chemical, petroleum, coal product, metals, non-metallic mineral products, machinery, etc.
- Transportation: Energy consumption in transportation comes from light and heavy duty vehicles, rail, aviation and marine vehicles. Examples are trucks, salon cars, trains, aircraft, rocket, ship, and submarines.
- Residential: Energy consumed in residential houses is mainly for space heating, air conditioning, water heating, appliances, electronics, etc.

Changes in economic activities alter the energy demand in these sectors with a corresponding impact on the overall global energy demand.

1.3 Energy Sources and Supply

The world energy sources are classified into renewable and non-renewable energy, Figure1.3. Non-renewable energy includes; fossil fuels (oil, natural gas, coal) and nuclear power, while renewable energy is made up of solar, hydro, wind, geothermal, biomass and tidal energy. The choice of these energy sources is influenced by many factors including environmental, economic, technical, safety, etc. A greater percentage of global energy supply comes from non-renewable energy sources. The Renewable Energy Policy Network [4], estimated the renewable energy share of the global energy consumption in 2013 to be 19%, while 78% came from fossil fuels and 3% from nuclear energy, Figure 1.4.

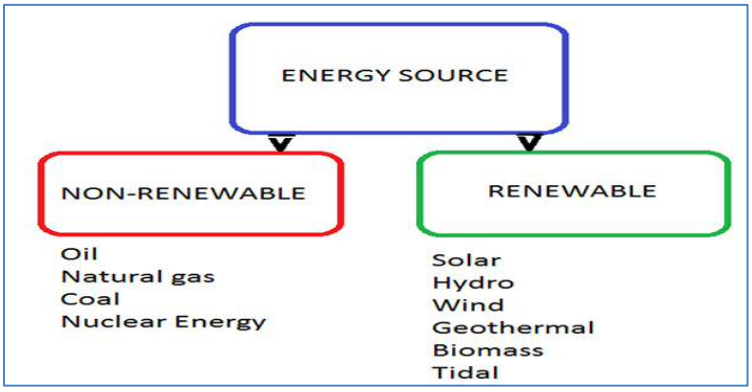

Figure 1. 3 Global Energy Sources

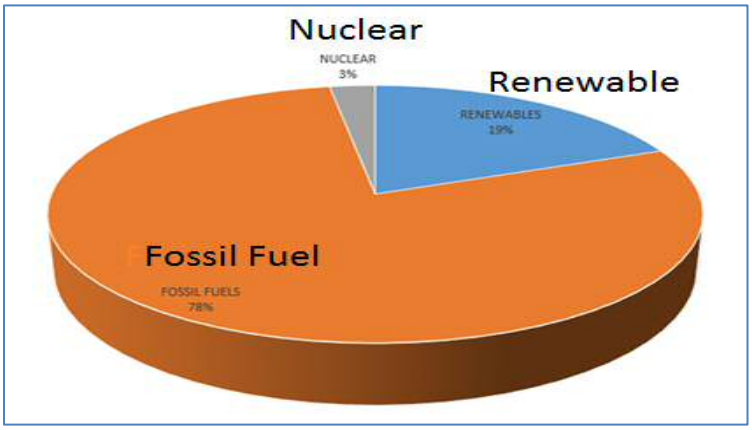

Figure 1. 4 Share of global energy supply in 2013, [4].

These statistics indicate the dominance of the non-renewable energy in the global energy landscape. Although there has been a tremendous growth in the renewable energy, the sector is still faced with the challenges of intermittency and unreliability. Thus, the future of global energy will continue to depend heavily on non-renewable energy sources. Statistics also show that the power sector to electricity generation recorded about 38% of the global primary energy in 2012 [2]. Accordingly, EIA [5] forecast that this share of the power sector to electricity generation will rise to 42% in 2035 due to population and economic growth. Fossil fuels will account for about 63% of the total inputs to power generation in 2035, according to the report. This would be due to the low carbon technologies becoming more prominent, that the percentages of oil and coal will be reduced in the share of fossil fuel to power generation whereas the share of natural gas would rise substantially due to its availability, lower prices, ease

of operation and environmental concern. The projections, therefore, point to the fact that natural gas will play a dominant role in the global energy security in the future.

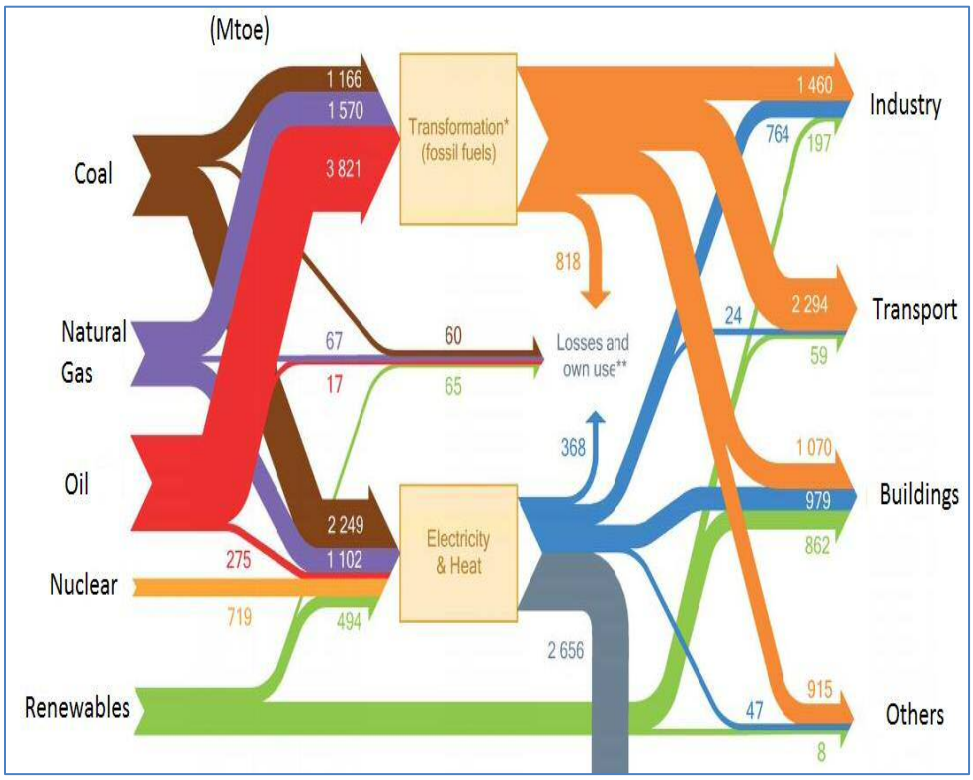

Figure 1. 5 Global Energy System [5].

1.3.1 Gas Turbine Combustor

The combustor has a combustion chamber with fuel injectors which inject a steady stream of fuel and air into the chamber. The fuel mixes with the air and burns to produce high temperature, high-pressure gas streams which expand in the turbine to generate power. Modern gas turbine combustors are designed to meet the current requirements such as combustion efficiency, emissions, alternative or flexible fuels, size, and operability. Based on its configuration, combustors are classified as:

- Can: Can combustors comprise of multiple burners evenly spaced around the turbine (Figure 1.12a).
- Annular: Annular combustors have a single continuous chamber that encircles the turbine (Figure 1.12b).

- ❖ Can-annular: A Can-annular combustor is a compromise between annular and can combustors. A group of can burners is arranged inside a single annular casing (Figure 1.12c).

The design of these combustors is quite critical in the overall performance of the system.

1.4 Natural Gas and the future of global energy

Natural gas is increasingly gaining the share of non-renewable energy mix due to the retired coal and nuclear plants. The more stringent emission standards have also put natural gas ahead of other non-renewable fuels. Figure 1.5 and 1.6, show the contributions of natural gas to the global sectoral energy consumption. The issue of efficiency, cost, and environmental attributes all make natural gas one of the most preferred among the non-renewable energy sources.

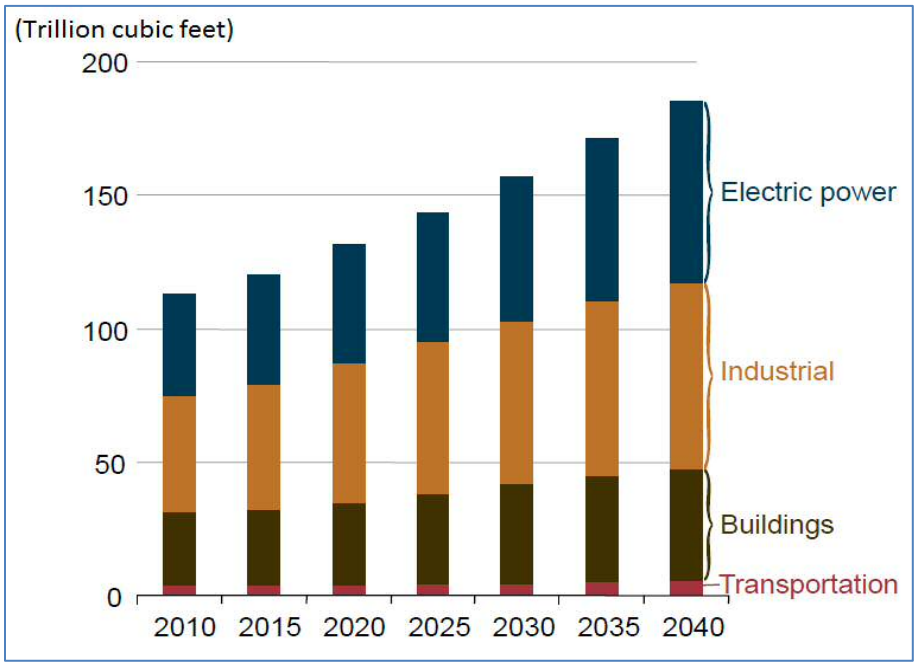

Figure 1. 6 World natural gas consumption by sector [3].

Figure 1.6 shows a massive increase in natural gas demand by industrial and electricity generating sectors in 2040. Also, Figure 1.7 shows the projection of the fuel consumption in the U.S. from 1990 to 2040. It points out that while petroleum reduced from 40% of the total fuel consumption in 1990 to 36% in 2013 and down to 33% in 2040, coal remained at 18% between 2013 and 2040. But natural gas increased from

23% in 1990 to 27% in 2013 and up to 29% in 2040, still agree with the fact that natural gas will dominate other fuels for industrial power and electricity generation.

1.4.1 The North American Natural Gas

The US recent energy development has culminated in a far reaching impact on the global energy landscape. The surge in the US tight and shale gas production as a result of new technologies to unlock the gases at low output prices has lowered the demand for oil. North American shale and tight gas have continued to increase the US domestic gas production due to the discovered new sources. According to forecast [5], the shale gas production in the US will increase from 24 trillion cubic feet in 2015 to about 33 trillion cubic feet in 2040, Figure 1.8. This increase will change the energy economy as more will be invested in the natural gas sector. Apart from industrial power and electricity generation, natural gas will play an influential role in providing the power for the transportation industry in the near future.

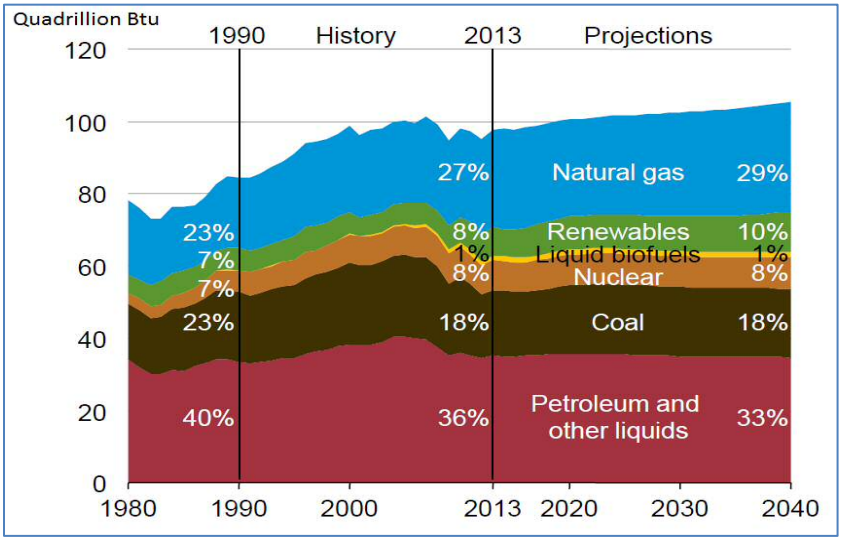

Figure 1. 7 US Energy Consumption and projection from 1980 – 2040 [1].

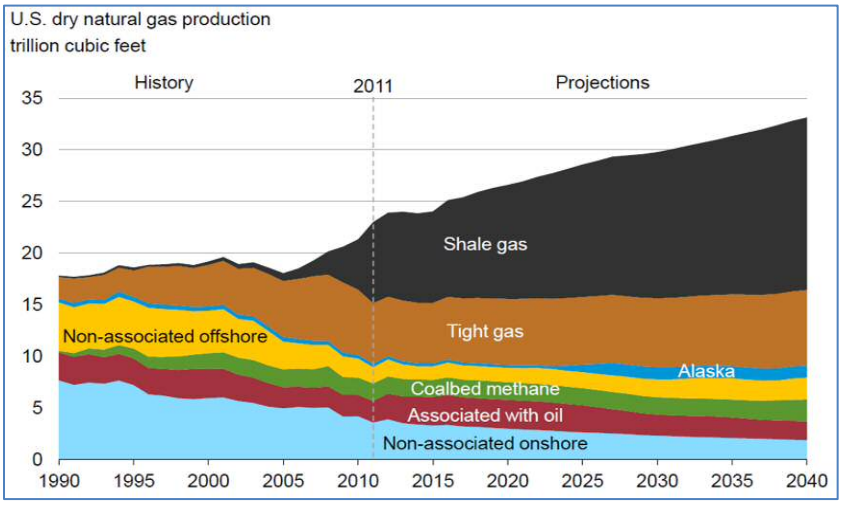

Figure 1. 8 U.S. Natural Gas Projections [5]

Another projection [6] sees an increment in the US electricity generation from natural gas from 25% in 2011 to 30% in 2040, Figure 1.9. This increase will be due to the reduction in the amount of electricity generated from coal as a result of the environmental concern and the availability of natural gas.

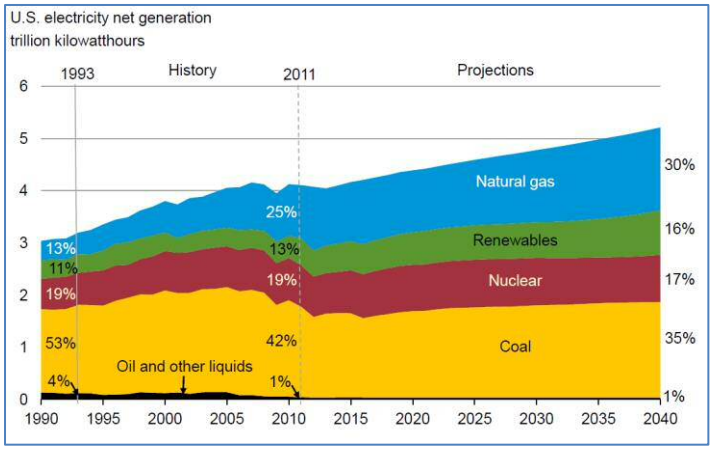

Figure 1. 9 U.S. Electricity-mix Projections [6].

These projections all conclude that natural gas will dominate the non-renewable energy sector in the future due to its availability, the ease of usage, and environmental concern, and therefore requires a more effective and efficient approach of converting it to power during combustion. The above scenarios all point to the fact that natural gas would be needed in large quantities to drive engines and supply the much-needed energy to the world, now and in the future. The efficiency in converting this fuel to

power becomes of utmost importance to reduce cost and protect the environment, thus the most preferred engine for this purpose is gas turbine.

1.5 The Gas Turbine Engines

Gas turbines are used for power generation. They work as an internal combustion (IC) engine. As the name implies, air- fuel mixture is burnt to produce hot gases which spin a turbine to generate power. It burns continuously and utilizes fuels like natural gas, synthetic fuels, fuel oil, etc. The fuel provides the input heat that burns to generate heat energy which may be used directly for industrial purposes or made to power cooled fans to produce thrust for electricity generation, aero, and marine propulsion. A gas turbine is made up of different sections as shown in Figures 1.10 and 1.11.

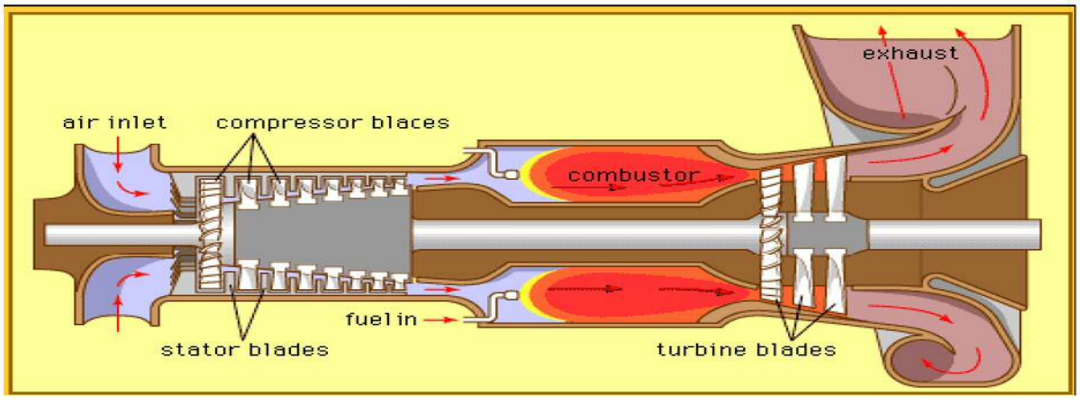

Figure 1. 10 A schematic view of a cut section of a gas turbine [7]

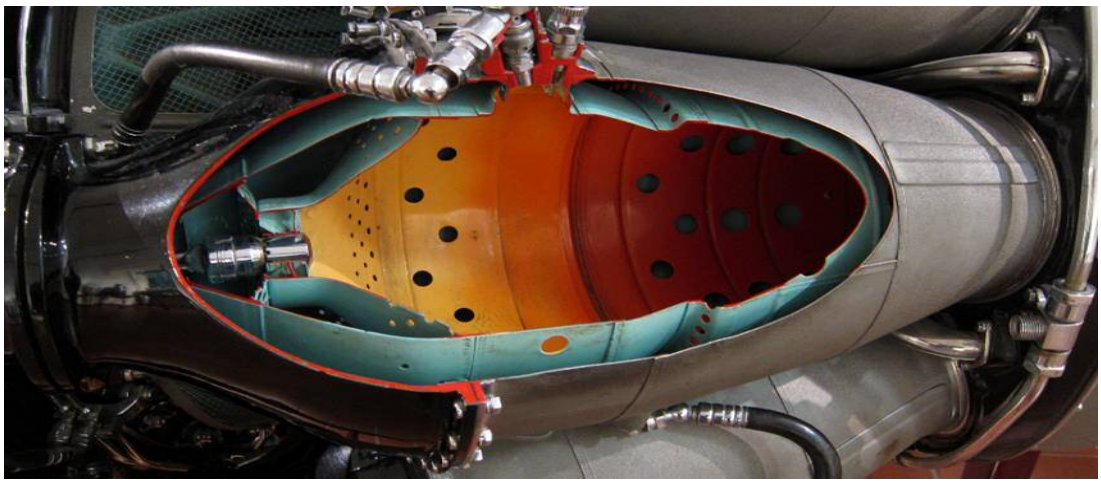

Figure 1. 11 A cut section of the combustion chamber of a gas turbine [8]

The compressor raises the air pressure from the inlet passage with the atmospheric condition to a high pressure, and it flows to the combustor, Figure 1.11, for

combustion. As a result, the temperature, velocity and the volume of gas flow are increased and then directed to spin the turbine blades to generate the thrust. The compactness, smooth running and the relative simplicity of the gas turbine design make it more preferable to other engines. With the expected dominance of natural gas in the global fuel mix, gas turbine will contribute tremendously to power generation in the coming future.

1.5.1 The Turbine

The turbine is made up of an array of stationary and rotating aerofoil-section blades. The hot combustible gases expand through the turbine and rotate the blades which are attached to a common shaft to turn both the compressor and the power generator.

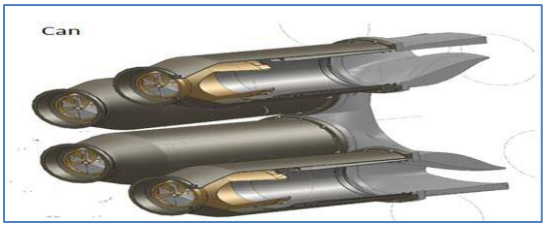

(a)

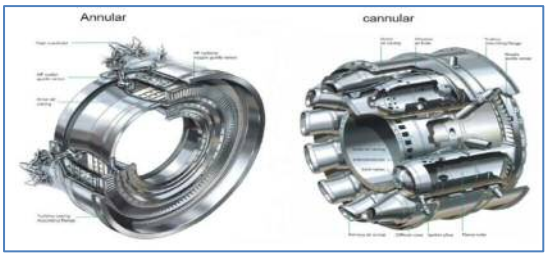

(b) (C)

Figure 1. 12 Gas turbine combustors classified by configurations [9]

1.6 Emissions Concerns

Pollutant emissions from combustion processes are of immense concern to humans given their impact on health and environment. The primary pollutants emitted by gas turbines which use natural gas are oxides of nitrogen, unburned hydrocarbons (UHC) and carbon monoxide CO. The oxides of nitrogen are nitric oxides NO and nitrogen dioxide NO2. A large quantity of NO is produced and later oxidized to NO2 in the

atmosphere. Thus these oxides of nitrogen are referred to as NOx. The nature of pollutant formation is such that the concentration of CO and UHC are highest at low-power condition and diminish with increase in power. In contrast, NOx is relatively insignificant at low power setting and attains maximum values at the highest power condition where the turbine is required to operate. Therefore emphasis is laid on NOx emissions in gas turbine combustion using natural gas.

1.6.1 Harmful Impacts of NOx Emissions

The following are the major adverse effects of NOx combustion emissions on health and environment.

Global Warming: One of the gases from the exhaust stream of a gas turbine is nitric oxide NO, a greenhouse gas. With other gases, they accumulate in the atmosphere causing a gradual rise in the earth's temperature which is a leading cause of climate change and global warming.

Acid Rain: NOx reacts with other gases in the atmosphere to form acids. This acid reaches the earth surface through rain, snow, fog, etc. The acid rain makes streams and lakes acidic thereby rendering them unsuitable for aquatic habitation.

Ground Level Ozone: NOx reacts with volatile organic compounds in the presence of heat and sunlight forming ground level ozone. This mixture presents serious health issues such as damage to lungs tissues. Ozone also damages vegetation as well as the reduction in crop yield.

Water Quality Deterioration: NOx loading in water bodies such as coastal estuaries distorts the chemical balance of nutrients of aquatic life.

NOx combustion emissions are therefore very destructive to human existence, and it becomes imperative to adopt technologies capable of reducing these emissions to its minimum in gas turbine combustion.

1.6.2 NOx Formation in Gas Turbine

Thermal NOx is formed by the reaction of atmospheric nitrogen. Its formation is influenced by three main factors. First, it is mostly attributed to the high flame temperature of combustion. A greater amount of NOx is formed at a temperature above

1900k and increases with increase in temperature [10]. Also, the formation of NOx increases with increase in the combustion residence time. The fuel-air mixture also influences its formation. Rich mixtures with high adiabatic temperature form more pollutants while lean fuel mixtures reduce pollutant formation to the barest minimum. The formation of NOx reaches its peak at the equivalence ratio of 1 (stoichiometric mixture) and decreases with fuel leanness. The inhomogeneity of the reactant mixture also results in equivalence ratio fluctuations. Thus areas of inadequate mixing may have a rich mix and become prone to pollutant formation. Therefore, to operate the gas turbine in a low pollutant regime, as required by emissions regulations, these factors need to be considered.

1.6.3 Government Policy Framework on Emissions

The world is earnestly looking forward to a low emissions future as the risk becomes more severe with an increase in global temperature, resulting in flooding, food and water shortages, coastal erosion, desertification, etc. It, therefore, requires urgent actions if a severe global catastrophe is to be avoided. The governments of the world had agreed to limit global warming to a maximum of 2C above the pre-industrial level to avoid the worst impact of climate change, in the December 2015 - 21st Conference of the Parties (COP) to the UN Framework convention on climate change in Paris. Pledges were made by many countries of the world on their intentions to reduce their emission levels. In their separate submissions, European Union targeted the reduction by 40% of the 1990 levels by 2030. The US pledged a reduced emission by 26 to 28% in 2025 against the 2005 baseline, and the Russian Federation promised a 25 to 20% reduction of the 1990 level while China pledged to cut about 60 to 65% of the 2005 levels by 2030. It is therefore certain that a large percentage of these emissions reduction will come from fossil fuel combustion. It, therefore, becomes imperative to adopt combustion technologies capable of reducing combustion emissions to its lowest.

1.7 NOx Emissions Control

Nitrogen oxides emission control is done in two ways: first by modifying the combustion processes to prevent its formation and the second by treating the product gases to remove or destroy the oxides. The inertness, insolubility of NO and running

cost remain a major challenge to the second method. The combustion process modification is therefore preferred. The following are the techniques used for reducing NOx emissions in gas turbines, using combustion processes.

1.7.1 Selective Catalytic Reduction

This method converts NOx in the gas turbine exhaust stream into molecular nitrogen and water. This is achieved by injecting ammonia into the stream together with a catalyst. Ammonia mixes with the engine exhaust stream and flows through the catalyst (usually vanadium pentoxide), and NOx is then reduced to N_2 and H_2O. A major challenge of this method is the inappropriate control system to feed the required amount of ammonia and the need for a continuous monitoring system that can give feedback to the ammonia supply mechanism under different load conditions [10]. Also, the large volume and weight of the ammonia supply device become another drawback.

1.7.2 Exhaust Gas Recirculation

In this method, the flame temperature is reduced by recirculating cooled combustion products back into the combustion zone. Wilkes and Gerhold [11] recorded about 50% reduction of emissions with a recirculation rate of 20% at base load condition. The technique can be easily applied to standard production combustors but needs an intercooler between the exhaust and the inlet, thus making it suitable for only large combined cycle plants.

1.7.3 Water Injection

Adding water or steam into the combustion zone of gas turbine serves as a heat sink to lower the combustion temperature. Although this technique is not suitable for aero engines, it is appropriate for large stationary engines due to the availability of water. The water or steam is injected into the flame either through the nozzles upstream of the combustor, fuel or into the air stream [12]. Although this technique is very effective in reducing NOx emission, it is however faced with many drawbacks. Apart from the high running cost, it increases fuel consumption by about 2 to 3% [13], as extra fuel is used to heat the water to the combustion temperature. Also, pure water is required for the process to prevent deposit and corrosion of the hot sections

downstream of the combustor. Water treatment is therefore needed, and this also adds extra running cost to the system.

1.7.4 Dry Low NOx Combustion

The disadvantages of water and steam injection led to the development of the dry low-NOx combustors. As the name implies, dry low NOx combustion stems from the fact that low pollutant emissions mainly NOx is achieved without injecting water or steam into the combustion zone. One way of achieving this is to thoroughly premix fuel and air upstream of the combustion zone to supply the zone with an entirely homogeneous mixture of fuel and air. Also, the combustion zone runs with lean fuel, which means that extra air is added to the combustion zone. This excess air reduces the flame temperature with a corresponding reduction in NOx emissions [10]. However running a combustor in this condition subjects the system to many operability challenges.

1.8 System Operability Challenges

A dry low NOx combustor operating in a lean premixed condition is highly susceptible to combustion instabilities [14]. Combustion instabilities can lead to a flashback where the flame front propagates from its anchorage within the combustion chamber upstream of the fuel/air mixing section [15] [16]. This is destructive since it introduces high amplitude waves into the premixing chamber. Combustion instability can also come as blow-off, where the flame disappears from its anchorage and moves downstream of the combustion chamber [17] [18] usually to the turbine sections. This is a serious challenge as this affects the performance of the turbine unit due to temperature variations. The most challenging of all is the thermo-acoustic instabilities where the acoustic modes of the combustor are excited by the unsteady heat release forming high-pressure waves in the combustor [19][20]. Thermo-acoustic instability is detrimental to both the performance as well as the structural makeup of the system, due to the advanced heat transfer, thermal stress on the walls of the combustor and mechanical load oscillation. These result in high cost of system downtime, inspection, and maintenance. In extreme cases the entire system is shattered, Figure 1.13.

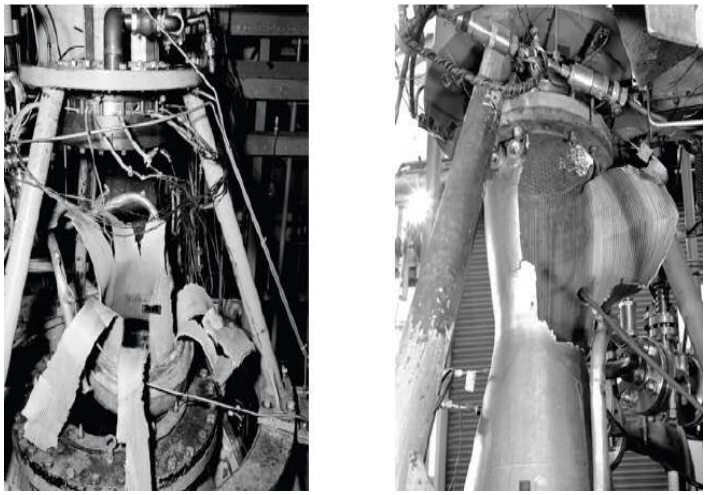

Figure 1. 13 Destructive effects of thermoacoustic instability [14].

1.9 Summary

This chapter concludes that energy is quite essential in the human development and its demand will continue to increase in the future. Statistics show that fossil fuel sources still provide about 78 percent of global energy consumption while renewable provides the rest with its attendant intermittency and unreliability. The gas turbine converts one of the purest forms of fossil fuel (natural gas) to power via combustion. With pollutant emissions concern, new techniques have been developed to reduce emissions in gas turbines to the barest minimum. One of these techniques is dry low NOx combustion where the combustion zone runs with lean fuel, which means that extra air is added to the combustion zone to reduce the flame temperature and thus the reduction in NOx emissions. However, this technique subjects the system to severe operability challenges, as the system is highly susceptible to combustion instabilities. This is detrimental to both the efficiency and the hardware of the system. The major challenges currently facing combustion experts are adequate knowledge of the operating conditions that cause combustion instability, accurate prediction and control of the instability modes.

1.9.1 Objectives

This research has the following primary objectives:

- Design, manufacture, and characterization of the operability limits of a new burner.
- Evaluation of the combined effect of swirl and forcing on the flow field.
- Evaluation of the of the flame response to swirl, fuel and forcing conditions.
- Evaluation of the acoustic dynamics and mode stability of the combustor in response to different swirl, fuel and forcing conditions.

1.9.2 Thesis Structure

Chapter 1: An introduction that assesses the global energy demand and supply as well as the future energy scenarios. It also focuses on combustion efficiency, emissions, policy framework, and techniques.

Chapter 2: A review of the knowledge frontiers on the essential areas such as fundamental processes and mechanisms of flow, flame and acoustic field dynamics, fuel blend and basic acoustic control techniques in combustors.

Chapter 3: This chapter reviews the techniques, instrumentation and experimental procedures of the study.

Chapter 4: The flow field velocity and coherent structures evolution for different swirl flows, and forcing levels are investigated.

Chapter 5: The flame dynamics and heat release fluctuations for various swirl, forced and fuel conditions are studied.

Chapter 6: The dynamic pressure and the acoustic modes of the combustion chamber are investigated for various flow, flame and forcing conditions.

Chapter 7: A Low Order Combustion Instability network model is simulated using experimental data to predict the eigen values of the combustion chamber during combustion, to serve as the basis for comparison with the experimental values. Statistical validation of the acoustic mode dynamics are also performed.

Chapter 8: This chapter discusses the results of this study. It relates the contributions of the inlet flow field characteristics and the flame dynamics on the dynamic pressure of the combustor and how the operating conditions have influenced the overall acoustic intensity of the system.

Chapter 9: Conclusion and future work - This chapter provides a summary of the key findings obtained in this study. It also suggests further work which could be carried out to expand this knowledge frontier.

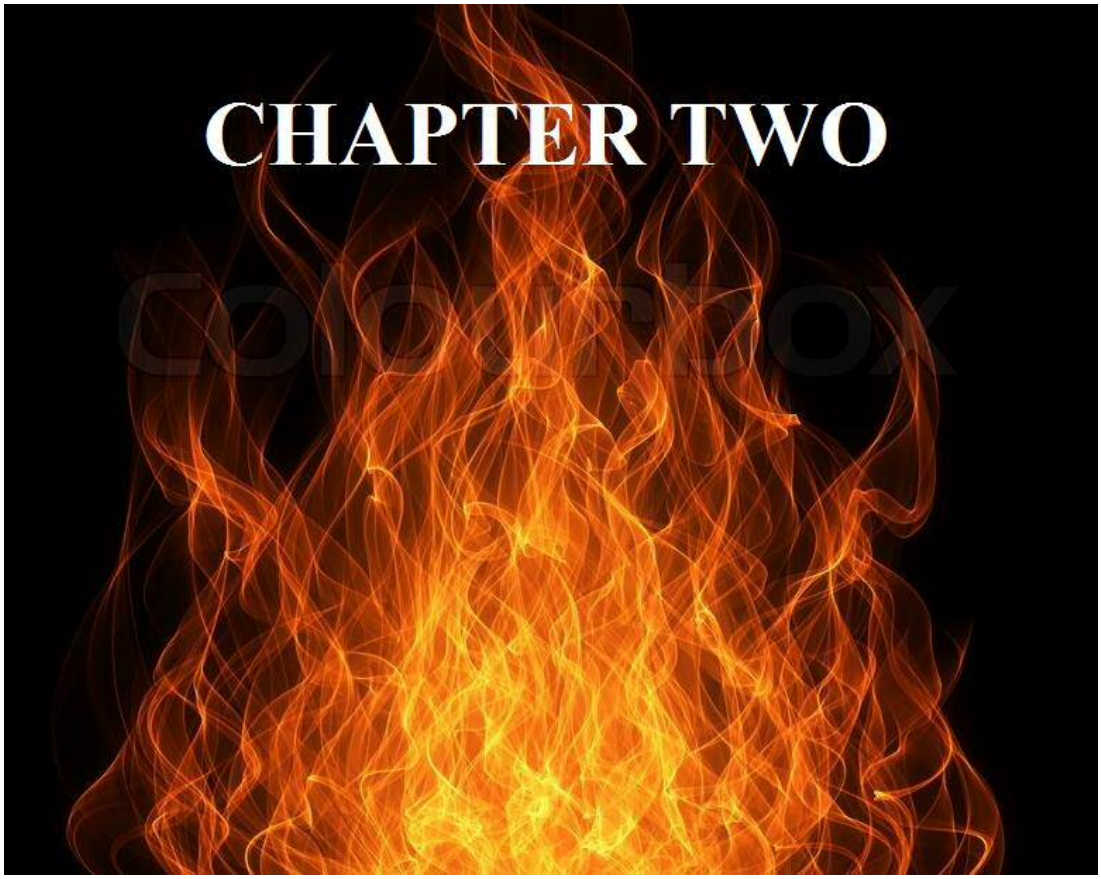
CHAPTER TWO

CHAPTER TWO:

LITERATURE REVIEW

It can scarcely be denied that the fundamental phenomena which first led mankind into chemical inquiries are those of combustion.

-- William Crookes

This chapter begins with the review of the fundamentals of gaseous fuels combustion in a confined volume (combustor), with emphasis on lean premixed swirl flames. The fuel-air flow structures and injection into the flame zone, which are crucial to the flame anchorage are also reviewed. The flame response to inlet flow fluctuation regarding flame model and the impact of fuel blends on the model is also examined. Finally, combustion instabilities induced by the coupling of the flow, flame and pressure fields are critically examined. The conditions that lead to the formation, growth and saturation, as well as the control of combustion instabilities, are also reviewed.

2.1 Fundamentals of Combustion

Practical combustion systems like gas turbines have flame stabilized at a fixed point while combustion mixture is continuously supplied. It is essential therefore that fuel and air mix properly in the flame zone and with the hot combustibles, for an enhanced thermal performance. Combustion processes are influenced by many factors such as fuel-air mixture and injection, fuel-air composition, transport phenomenon, flame dynamics, etc. A full understanding of these factors is quite necessary for combustion engineers.

2.1.1 Mixture and Injection

Fuel-air mixing and injection play a crucial part in combustion processes. Based on these factors, flames are classified as:

Diffusion flame: In a diffusion flame, fuels and the oxidizer (air) enter separately into the combustion chamber where they mix and burn with a continuous mutual diffusion [21][22]. The reactions occur in the combustion zone with the reactants being converted to combustion products downstream of the chamber. These products are then diluted by secondary air to reduce the temperature at the exit of the combustor to a level suitable for the turbine blades.

Premixed flame: As the name implies, premixed flames have fuel and oxidizer mixed at the molecular level in a separate chamber upstream of the flame. Premixed flames propagate in a mixture of fuel and air due to heat conducted from the burned hot products to fresh cold reactants. Premixed flames occur as a thin, propagating flame that is stretched and distorted by turbulence [23]. Flames are also classified as homogeneous if there is a complete vaporization of the mixture before entering the flame zone, often obtained in gaseous fuels. Heterogeneous flames result when the fuel is not completely vaporized before entering the flame zone, this is common to liquid fuels.

2.1.2 Fuel- Air Ratio

The fuel-air ratio has significant effects on the combustion physics. It is the ratio of air to fuel in the fuel-air mixture at a given time. The unit of measurement may be in mass, volume or mole. The fuel-air ratio in mass flow rate is usually used. The Stoichiometric fuel-air ratio gives a precise quantity of air for the complete combustion of a given fuel. The addition of more air makes the combustion fuel-lean, and the addition of less air makes the combustion fuel-rich. However, it is more convenient to measure how much the combustion is less or much of air from its stoichiometric ratio. This is called equivalence ratio. Combustion is described as lean if the equivalence ratio is less than 1 and rich if the equivalence ratio is greater than 1. Thus, a lean combustion of 0.8 has a 20% excess air. Lean- premixed (LPM) flames, therefore share the characteristics of both lean and premixed flames. LPM flame characteristics are more susceptible to combustion challenges.

2.1.3 Speed of Flame Propagation

A flame is known to be a chemical change which occurs within a thin fluid layer with steep temperature gradient and luminescence as a result. The flame zone is therefore an interface between the burned gases and unburned mixture, where the former propagates into the latter, [10]. Depending on the speed of propagation within the burned and unburned gases interface, combustion is classified as *deflagration*, occurring below 1m/s and *detonation* which is a shock wave propagating at a supersonic velocity. In gas turbine combustion, the flame falls within deflagration. The flame is also described as being *laminar* or *turbulent* depending on the nature of fluid flow.

2.1.3.1 Laminar Flames

A fundamental property of combustible mixture is the flame burning velocity. It is defined as the velocity with which a plane flame front moves in a direction normal to its surface through the adjacent unburned gas. The rate of propagation is determined partly by the rate of chemical reaction in the thin flame zone and by heat and mass transfer from the flame to the unburned gas [24]. The following parameters determine the flame-burning velocity; flame radiation, temperature, and local gas properties such as viscosity, diffusion coefficient, pressure and equivalence ratio. Experimental results [25][26], have shown that the burning velocity of hydrocarbon fuels is approximately 0.43m/s at atmospheric temperature and pressure.

2.1.3.2 Turbulent Flames

In gas turbines, the interaction between the flame and unburned gases is usually turbulent. This causes the flow to exhibit irregular behaviour both in space and time because of fluctuations in all variables which behave rather randomly. Eddies are the major causes of fluctuations in turbulent flames. They stir the flow and increase the mean transport of flow quantities. A fundamental turbulent theory says that eddies are of a continuous range of large to small sizes in turbulent flow [27] and that the largest eddies are determined by the geometry of the flow configuration. Turbulence is usually described by Fourier's transformation of the turbulent quantity from space/ time domain to frequency domain. Turbulence could be simulated numerically via direct numerical simulation DNS, Large Eddy Simulation, (LES) or Reynolds averaged Navier-Stokes (RANS), [28].

2.1.4 Flame Stabilization in the Flame Zone

In continuous combustion systems like gas turbines, fuel–air streams (in the case of premixed flames), move at speed higher than the standard burning velocity. The combustion process is thus achieved by stabilizing the flame with continuous ignition at a particular point in the flow, where the combustion flame front propagates into the high-speed stream at a fixed flame speed. Flames, in this case, are classified based on the type of mechanism used to "hold" or stabilize the flame. Swirl - stabilized flames have axial or radial swirl positioned upstream of the exit nozzle to provide swirling flames for efficient fluid mixing and flame stabilization [29 - 31]. Swirl stabilized flames are common in gas turbine combustion. The use of bluff - stabilized flames has been reported by many researchers [32] [33]. A bluff body is placed in the high-speed gas stream as a mechanism to stabilize the flame. Bluff flames are found to be very useful in ramjet combustors and turbo-jet afterburners. In tangential stabilized flames, one or two tangential inlet(s) introduce(s) the fuel-air mixture which rotates and exits the nozzle to the flame zone. The flow rate is varied in the inlet ducts using inlet inserts [34]. In the three mechanisms, the common features are the fluid mixing and flame stabilization. This study uses a swirl-stabilized flame.

2.1.5 Combustion Operability Challenges

Combustion processes come with different operability difficulties such as blow-off, flashback, auto-ignition, combustion instability etc. These challenges are briefly discussed:

2.1.5.1 Blowoff

Blowoff is the physical disappearance or extinction of the flame from its anchorage. It could be very disastrous especially when the flame fails to reignite at high pressure and low temperature [23]. Low NOx combustors usually operate in the lean region thereby "pushing" the combustion process to the blowoff limit. In gas turbines, this phenomenon could be very problematic as the flame gets to the turbine section of the system and results in excessive temperature variation of the turbine blades, a problem which reduces its performance. Many studies have analysed the occurrence of blowoff in combustors [35] [36]. The causes of blowoff have been attributed to equivalence ratio variation with the inlet flow velocity [37], increased flame velocity [38], Damkohler number variation [39] etc.

2.1.5.2 Flashback

The opposite problem of *blowoff* is *flashback*; here the flame physically propagates upstream of the flame anchorage into the premixing passage of the system which was not designed for high temperature. Flashback is a fundamental feature of all premixed combustors. It occurs when the inlet mixture flow velocity is smaller than the flame speed [24]. Flashback destroys the hardware of the system, a typical example is shown in Figure 2.1, [40].

Figure 2. 1 Destruction of burner assembly by acoustic dynamics: Left – damaged, Right – new [40].

Even though lean combustion reduces flame speed, but engine cycle factors such as high pressure, temperature, turbulence, pre-ignition reactions of the gas mixture as a result of the increased resident time could raise the flame speed [41], thereby making the system susceptible to flashback. It is also reported [42] [43] that the swirl strength could cause the flow to move into the swirling compartment, where the attached flame to the centre body propagates upstream and flashes – back. Flashback is also linked to fuel blends especially that of hydrogen with increased flame speed.

2.1.5.3 Auto-Ignition

It refers to the fuel mixture pre-ignition before entering the combustion chamber [44] The chemical time scales are controlled by the fundamental ignition time based on premixed gases at control pressure and temperature, [45]. This occurrence is enhanced

by the addition of higher order of hydrocarbon of methane-based fuel blends, especially at higher temperatures (T 1300K), [46]. This added hydrocarbon reduces the ignition delay of the fuel blends, [44]. There has been a growing concern of this combustion challenge [47], as it could seriously destroy the sub-components of the premixed and injection sections of the combustor and exerts extreme back pressure on the compressor blades which can affect its performance.

2.1.5.4 Combustion Instability

It refers to the damaging pressure oscillations associated with the combustion heat release rate. Combustion instabilities are caused by a coupling between the unsteady heat release and the inherent acoustic waves within the combustor. The fluctuations in the velocity-thermodynamic state variables induce another fluctuation in the heat release rate which equally excites acoustic oscillations and the acoustic oscillations, in turn, generate the velocity and thermodynamic state variable fluctuations thereby completing the instabilities loop, [48]. More details of this phenomenon are given in the later part of this chapter. In this study, the focus is on combustion instability of lean premixed swirl- stabilized turbulent flames. The interactions between the chemical reaction, fluid dynamics and heat and mass transfer that cause this destructive phenomenon are critically examined.

2.2 Flow Dynamic and Mechanisms

Fuel-air mixing and injection into the combustion chamber play a vital role in achieving an efficient and clean combustion in gas turbines. For gaseous fuels, the fuel and air, as well as the combustibles in the flame zone, mix optimally. The use of liquid fuels requires further atomisation into droplets before being fed into the air stream entering the combustion zone. In premixed combustion, swirl injectors provide mechanisms which generate swirling flows characterized by high shear stress and turbulence with various flow structures needed to stabilize the flame. Recent advances in this area have been reported [49] [43]. These flow mechanisms interact with the chamber acoustics to generate combustion instabilities as examined in this section.

2.2.1 Swirl Configuration

Swirling flow geometries are classified into axial and radial swirls. The axial swirls have vanes with flat or twisted blades while radial swirls have blades or tangential

injection inlets [50] [51], Figure 2.2. A single or multiple swirl assembly could be used to obtain the desired swirling conditions.

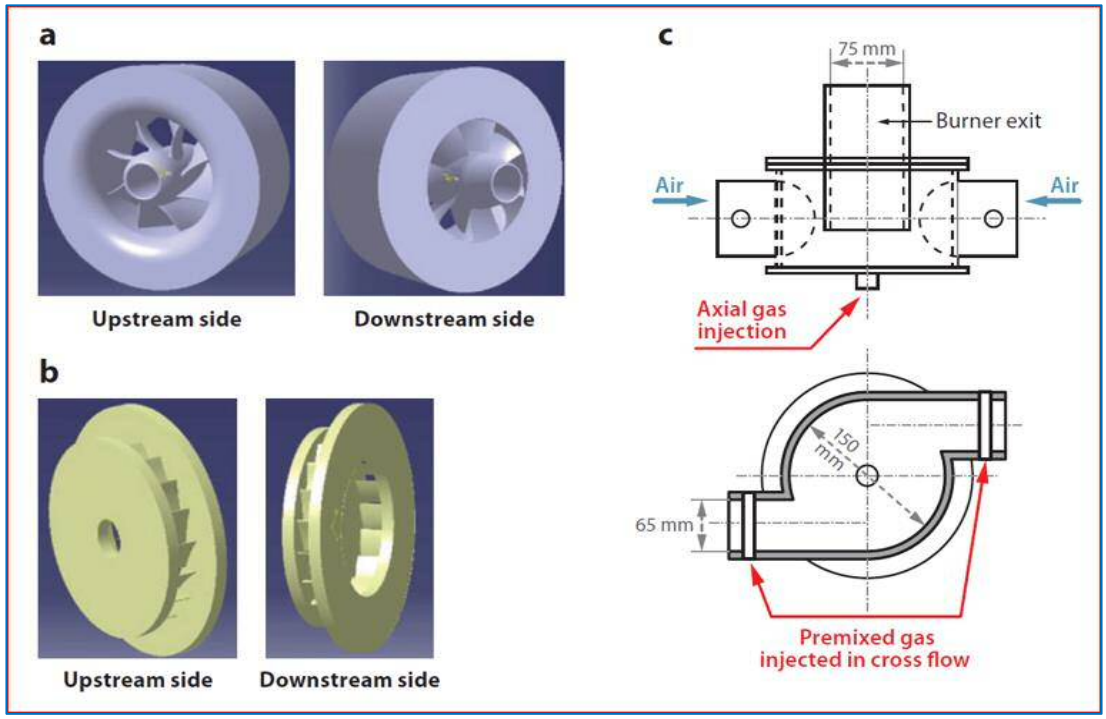

Figure 2. 2 Swirl Configurations

[(a) Axial swirler, (b) Radial Swirler [52], (c) Tangential inlet Swirler [53] [54].

An important parameter of the swirling flow is the swirl number S, which is defined as the ratio of the axial flux of the tangential momentum to the product of the axial momentum flux and a characteristic radius [55] [56] given as

$$S = \frac{\quad}{\quad} \tag{2.1}$$

where Rn and Rh denote the radii of the centre body and the inlet duct respectively. In radial swirl flow, the geometric swirl number is given as

$$S_g = \frac{\quad}{\quad} \tag{2.3}$$

where r_{eff} is the effective radius at the centre of the inlet pipe, re, the exit radius and A_t, the total area of the tangential inlet,[57] [58]. This swirl number uses inlet conditions while ignoring the pressure variation effects across the flow.

2.2.2 Flow Characteristics of Swirl Injectors

The swirl generates different flow structures in the flow field. The three primary structures are the vortex breakdown-induced Central recirculation zone (CRZ), processing vortex core (PVC) and the Shear layers (SL).

2.2.2.1 Vortex Breakdown- Induced CRZ

Vortex breakdown is a major flow structure of the swirling flows in gas turbine swirl flow combustion. It occurs as an abrupt change in the core of a slender vortex which usually develops downstream into a recirculation bubble or a spiral pattern [59]. This region is characterized by the occurrence of the internal stagnation points and reversed flows which provide the dominant flame stabilization mechanism. The importance of this flow structure to the combustion system has been reported by many studies, [60] [61- 63]. Many theories have been proposed as the basis for the formation and evolution of vortex breakdown. Squire [64], and Benjamin [65] wave theories attribute the vortex breakdown to the existence of the critical state which separates a supercritical from a subcritical flow state. While disturbances propagate downstream in the supercritical flow, standing waves exist with disturbances propagating both downstream and upstream in the subcritical flows. Leibovich and Stewnrtson [66], Jones [67] and Ludwieg [68] are of the view that vortex breakdown is as a result of hydrodynamic instability which results from the response of the flow to spiral disturbances. Vortex breakdown is also attributed to flow stagnation being analogous to boundary layer separation or flow stagnation processes.

Sarpkaya [69] and Sarpkaya [70] experimentally observed three kinds of vortex breakdown namely: (i) axisymmetric, which usually occurs at high swirl numbers, (ii) spiral which occurs at low swirl numbers and (iii) the double helix which prevails when the vortex core expands and swirls. Lu et al. [71] conducted a large eddy simulation (LES) analysis to investigate the formation of vortex breakdown in a coaxial swirl injector. A Reynolds number of 1.25×10^5 and two swirl numbers were used, Figure 2.3.

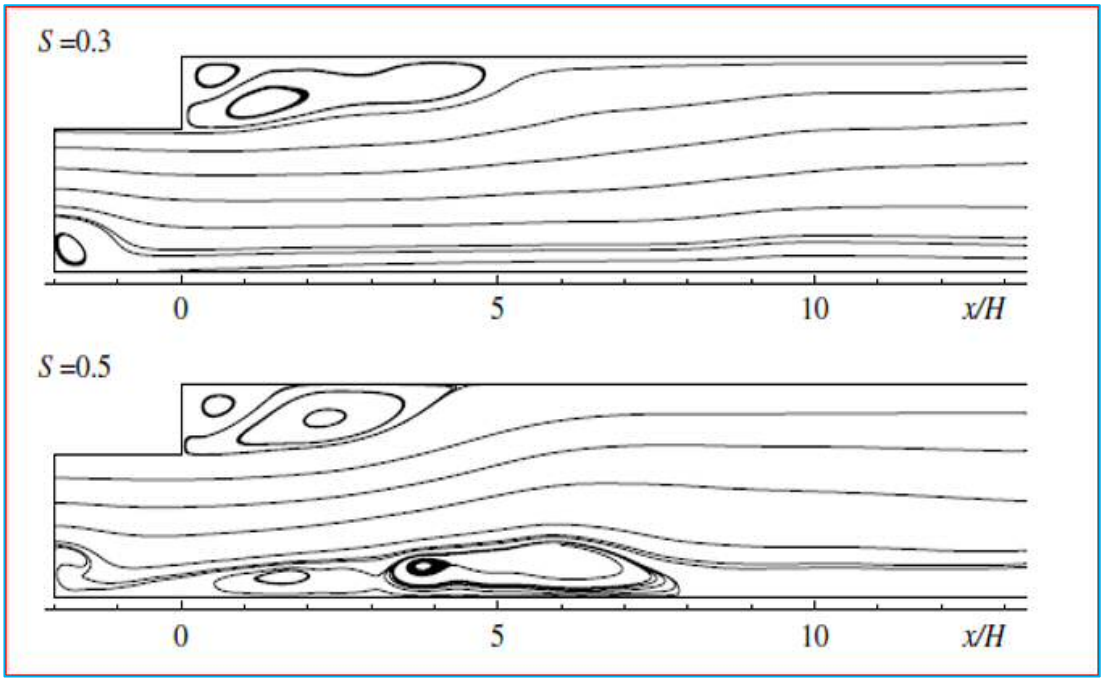

Figure 2. 3 Streamlines based on mean axial and radial velocity components [S= 0.3 and 0.5], [71].

For a low swirl number of S= 0.3, Figure 2.3, no vortex breakdown was observed, but a vortex breakdown induced recirculation was observed with a high swirl number of S= 0.5, which was attributed to the differences in the radial and axial pressure gradient. Wang-et al. [72], also performed an LES analysis of the flow structure evolution using a radial entry swirl injector. Two swirl numbers S= 0.35 and 0.49 and a Reynolds Number of 2x 10^5 were used. For the low-swirl number, Figure 2.4 (a), S= 0.35, a stable bubble vortex breakdown was observed downstream of the centre body while a complex structure was observed at the higher swirl number, Figure 2.4 (b), S= 0.49.

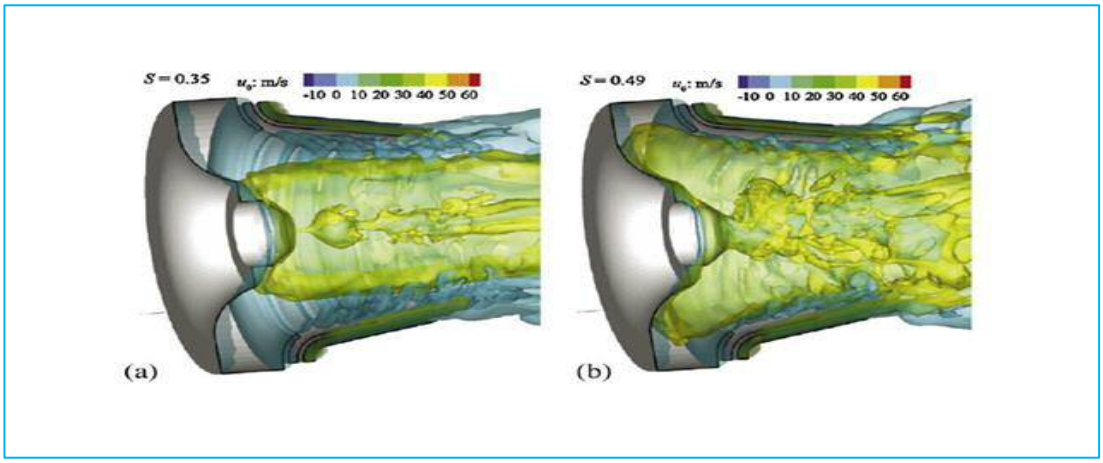

Figure 2. 4 An iso-surface of azimuthal velocities [(a) low swirl number (b) high swirl number], [72].

2.2.2.2 Precessing Vortex Core

Processing Vortex Core (PVC) is another important swirling flow structure. It plays a central role in stabilizing the flame in the combustion chamber [73] [74]. PVC is a three-dimensional asymmetric flow structure which is formed when the central vortex core starts precessing around the axis of symmetry at a well-defined frequency [53] [75]. PVC is highly influenced by the vortex breakdown and its recirculation zones, usually with a high Reynolds Number flow. According to Syred & Beer [76], the PVC is usually located on the boundary of the reverse flow zone. The precession frequency depends largely on the linear flow rate, swirl number and chamber configuration [59]. According to Syred [77], the frequency of PVC in the isothermal condition is characterized by Strouhal and swirl Number. PVC is also affected by the confinement ratio Do/De, swirl number and equivalence ratio. Wang and Hsiao [78], performed an LES simulation of a CFM56 gas turbine swirl injectors. It was observed that the low-pressure core was initially found to align with the axial axis downstream of the fuel nozzle and thereafter departs from the centerline at the stagnation point of the flow reversal while being extended downstream spirally in the opposite direction to the main flow rotation.

The visualization of PVC under combustion condition has been performed in many studies [77], [79- 81]. They all proved that PVC is helical in shape and wraps itself around the reversed flow boundary, Figure 2.5.

Figure 2. 5 PVC visualization of swirling flames, [79] [77].

It is worthy to note that although PVC improves combustion efficiency by enhanced turbulent intensity and mixing, it could also be a potential source of combustion instability if its resonance couples with the low-frequency acoustic oscillation in the combustion chamber.

2.2.2.3 Shear Layers

As the flow exits the injector, the velocity differential between the jet and ambient flow develops a strong shear layer. Large-scale coherent structures are generated in this region which moves downstream due to the Kelvin-Helmholtz (K-H) instabilities [59]. These structures have great impact on the combustion process as they modulate the mixing of the fuel with the oxidant and the hot combustibles. The coherent structure is enhanced by the presence of the swirl where an azimuthal shear layer and centrifugal instability is produced when the circulation decreases in the outward direction. In cases where the azimuthal velocity is comparable to the axial velocity as in high swirl number flows, vortex breakdown could take place. Many studies on shear layers and its structures have been conducted experimentally [82] [83], theoretically [84] [85] and numerically [86] [87].

In their experimental studies, Liang and Maxworthy [88] examined the vortical flow structures and their dynamic evolution. It was observed that for non-swirling and weakly swirling jets, the Kelvin –Helmholtz (K-H) instabilities in the axial shear layer formed vortex rings, but with the introduction of swirling motion, the axial and azimuthal shear layers became unstable and changed to a modified form of the K-H instability. Wang and Hsieh [72] numerically studied the prevalence of large-scale structures in swirl injectors using a radial –entry swirl injector. The results (Figure 2.6), show the snapshot of two cross sections at different swirl numbers of the vorticity magnitude fields. Two counter-rotating flows with varying velocities merged at the trailing edges of the guide vanes due to the opposition of the swirl vane angles. The shear layer instability together with the helical and centrifugal instabilities generated large asymmetric structures on the flow. At a high swirl number, the centre recirculation flow was observed to intersect with the outer shear layer resulting in a complex flow field near the injector exit.

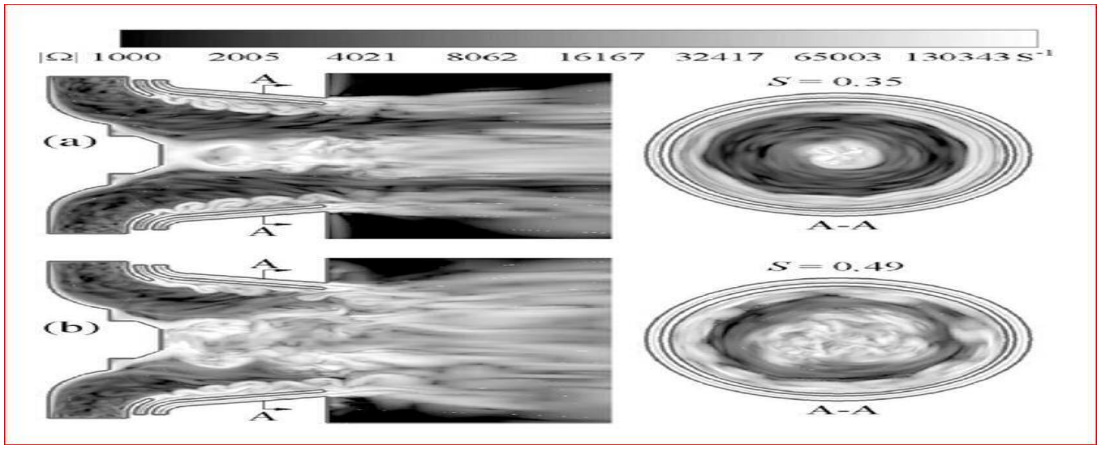

Figure 2. 6 Snapshots of vorticity magnitude contours [(a) low swirl number and (b) high swirl number], [72].

These show the existence of shear layers and its complex coherent structures in swirling flows and its capability to induce combustion instabilities. All these, point to the fact that combustion systems largely depend on the flow stream to the flame zone. The inherent structures of the flow are affected by the swirl configuration, swirl - number, and nozzle parameters. Therefore swirling flows remain an important aspect of the study of combustion instability in gas turbines.

2.2.2.4 Velocity Profiles in Swirl Flows

The velocity profile of swirling flows changes with variation in the blade angle or swirl number. When a certain threshold value of the swirl number is exceeded, a CRZ is developed with a backflow on the axis of the injector. According to Candel and Durox [75], Durox [89], this occurs when the blade angle shifts from = 38 degrees to = 42 degrees with a substantial change in the flow structure. The axial velocity reaches its minimum being relatively flat for blade angle below 38 degrees, Figure 2.7.

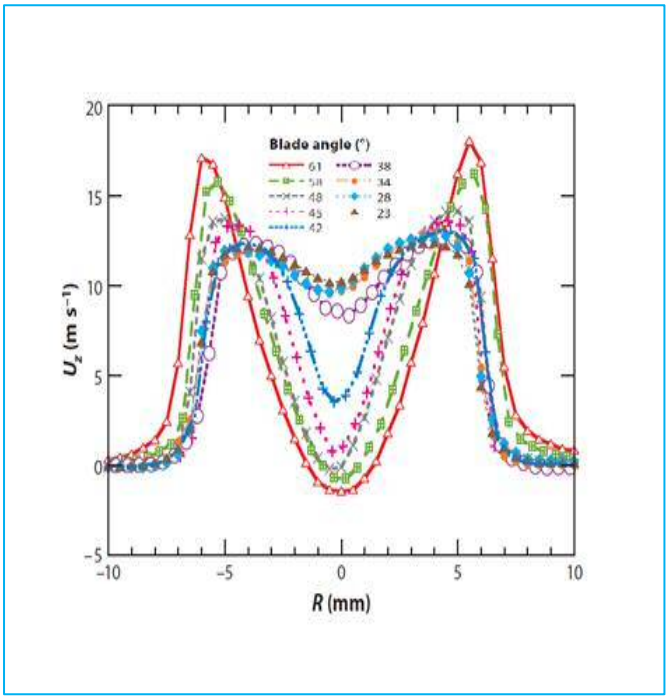

Figure 2. 7 Velocity profiles of swirl injector at different blade angle [89].

Above this value, the axial velocity decreases and takes negative values on the centerline at the blade angle above 48 degrees. The above scenarios prove that coherent structures of the flow field are highly influenced by the swirl strength and could be used as the basis to control the flow – flame interactions which impact greatly on the acoustic modes of the combustors.

2.3 Combustion Instability and Mechanisms

Combustion instabilities are destructive both to the hardware and system performance, especially when the oscillation is near to the structural resonant frequency of the system. Some of its consequences are thermal stress on combustor walls, enhanced heat transfer, severe vibrations, oscillatory mechanical loads, blowoff, flash back, etc. Combustion instabilities stem from the coupling between the unsteady combustion process and the inherent acoustic modes within the combustor, [90 - 92] as depicted in Figure 2.8.

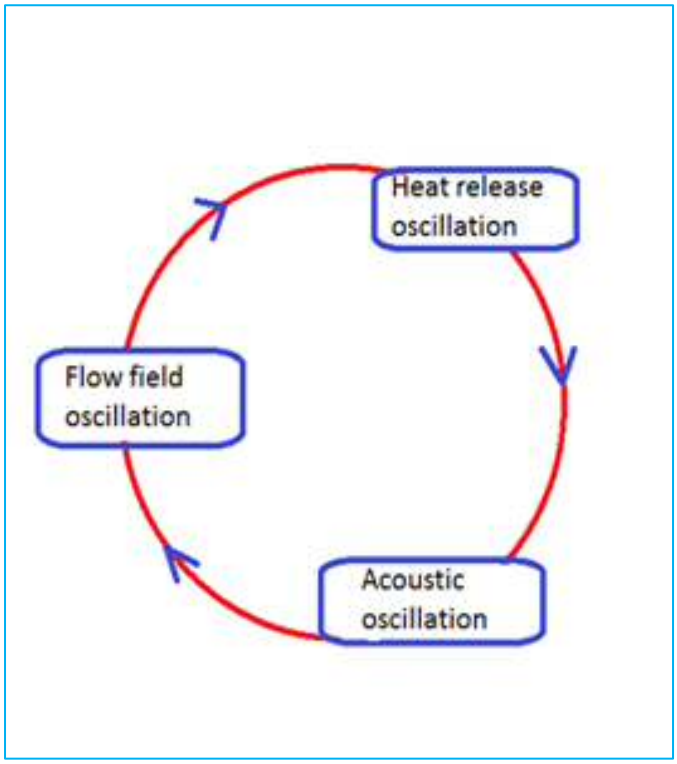

Figure 2. 8 Feedback loop of combustion instability

The waves propagate within the combustion chamber, interact with the boundaries of the combustion zone with a time delay which depends on the size, geometry of the combustion chamber, speed of sound and the impedance at the boundary of the combustion chamber, [93] [50] [94] [95]. In the flow field, flow or mixture perturbation could be caused by any of the following processes:

- Fluctuation in the air supplied to the combustor
- Variations in fuel supply to the nozzles
- Aerodynamic disturbances of the fluid in the combustor
- Mal-distribution of fuel in the combustion zone

When any of these happens, it gives rise to a cycle of extinction and re-ignition in the localized regions of the flame resulting in a periodic heat release, which produces acoustic waves with a broad frequency bandwidth [19]. The waves propagate within the combustion chamber and reflect to the combustion zone, [24]. The dynamic pressure, in turn, fluctuates the flow field, altering the velocity profiles and reactant composition (equivalence ratio), thereby producing periodic heat release,[48] [96]. Thus these processes synchronize to form a feedback loop generating oscillations with

an amplitude which grows, dampen or remains same at each cycle of the loop depending on the relative energy balance.

2.3.1 Rayleigh Criterion

Rayleigh criterion gives the conditions under which a periodic heat addition initiates and sustains acoustic oscillation resulting in combustion instabilities. Rayleigh [97] states that an acoustic field gains energy when the average time product of the heat addition and pressure perturbation is greater than zero. This condition occurs when the heat is added in phase with pressure, i.e. when the magnitude of the phase between the pressure (and heat-release (oscillations is less than 90 degrees (0 | |). Also, the acoustic field loses energy when heat is added out of phase with pressure, where the magnitude of the phase between the pressure and heat-release oscillations is greater than 90 degrees but less than 180, (90 | |). It, therefore implies that the unsteady heat release performs work on the gas when the expansion occurs in phase with the pressure [98]. This theory is expressed thus:

(2.14)

Where , , V, T, and Li represent the combustor pressure fluctuation, heat release oscillation, combustor volume, period of oscillation and the i-th acoustic energy loss respectively. The left hand-side of the expression, therefore, represents the acoustic driving term, where energy is added to the system and the right-hand side represents the damping term, where the acoustic energy is dissipated out of the system. The expression also shows that having and in phase is not sufficient for instability to occur until the energy of the acoustic driving term is greater than that of the damping term, [19] [99]. Instability growth and damping are therefore a balance between these two terms. In combustion instability control as would be seen later, while the active control approach focuses on the left-hand side of the expression to keep the pressure and heat release fluctuation out of phase, the passive control method seeks to increase the energy loss term of the right-hand side of the expression.

2.3.2 Acoustic Driving Processes

Heat release fluctuation is the dominant acoustic driver when properly coupled with the combustor's dynamic pressure as stated by Lord Rayleigh, [97]. This heat release

fluctuation is caused by many processes such as vortex structure – flame shape interaction [100] [101], acoustic velocity interaction with flame [102], acoustic coupling with fuel feedline [103] [104], mixing induced equivalence ratio perturbations [105], reactant products atomization and vaporization oscillations [103] etc. These heat release oscillations add energy to the acoustic field if the magnitude of the characteristic timescale of the heat-addition process is of the order of some integer multiple of the acoustic period [98]. These processes depend on the combustor design, operating condition, process characteristics etc. Assuming that the aforementioned heat release–fluctuation processes are represented by processes 1 to 5 respectively and the dynamic pressure in Figure 2.9. With the period of 0.004s of the dynamic pressure of the combustor, the five processes cause heat release fluctuations at different time delays. The figure shows that the characteristic time of process 5 is of the order of the period of the pressure wave of 0.004s. This satisfies the Rayleigh's criterion, thereby adding energy to the acoustic field. But the time scales of other processes differ. However, due to multiple acoustic modes of the combustor, process 2 could also add energy to the acoustic field since its characteristic time is a multiple (0.008) of the pressure wave.

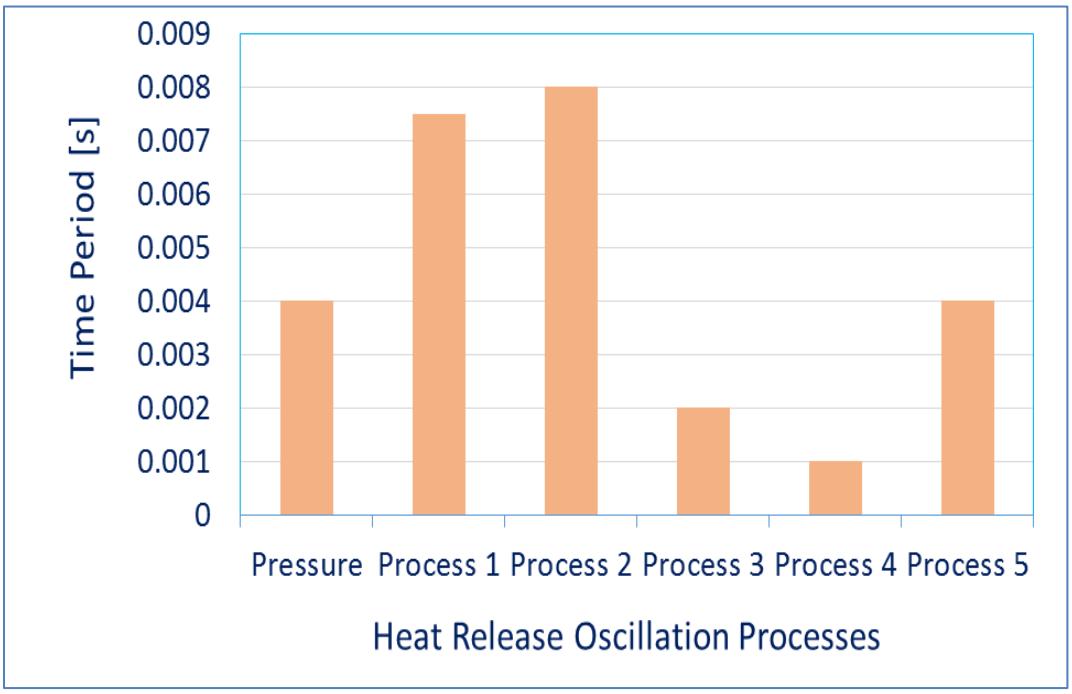

Figure 2. 9 Heat release oscillation response to periodic pressure

In combustion instability control therefore, these time scales of these processes are altered in such a way that they are not of the same order or multiple of the pressure wave time scale.

2.3.3 Acoustic Damping Processes

Acoustic driving and damping processes are two major determinants of thermo-acoustic instabilities within the combustion chamber as illustrated by Rayleigh criterion. Acoustic energy within the combustor is dissipated by the following three processes:

- **Viscous and Heat Transfer:** Acoustic energy is transferred to vertical velocity fluctuation as it comes in contact with the rigid wall due to the no-slip condition of the boundary. Thus the energy of the reflecting sound wave is smaller than the incident wave. The magnitude of the energy loss is given thus:

  (2.15)

  Where is the viscous or thermal transport time scale, and f, the frequency of propagation. At sharp edges, flow separation also converts acoustic energy to vorticity.

- **Convection and Radiation:** Within the duct, the acoustic energy is dissipated by convection due to the movement of the mean fluid out of the system. This damping mechanism is given mathematically:

  (2.16)

  Where f, and represent the frequency, duct diameter and the speed of sound respectively. The magnitude of the fluid motion is sensitive to the mean flow Mach number, thus low velocity mean flow has a significant effect on the system damping.

- **Transfer of Energy between Acoustic Modes:** Acoustic oscillations within the combustor are made of tones with different frequencies. Thus acoustic energy is transferred between the excited and unexcited modes. In nonlinear combustors, acoustic energy is transferred from a certain frequency f_0 to higher harmonics ($2f_0$, $3f_0$) or sub-harmonics ($f_0/2$, $f_0/3$) [98]. The energy is

transferred from the narrow band, coherent oscillations to spectrally distributed, incoherent oscillations by random modulation processes.

2.3.4 Growth and Saturation of Combustion Instabilities

Instabilities within the combustor, initiate and grow exponentially until saturation sets in depending on the balance between the driving and damping processes. The sequence is summarized as follows:

- The oscillation amplitude increases (depending on the energy addition and dissipation balance).
- With this increase, the energy addition and dissipation processes then become dependent on the oscillation amplitude.
- The oscillation amplitude reaches its peak when the time average of addition and removal becomes equal to each other.
- This maximum oscillation amplitude is called limit cycle amplitude

This instability is viewed in linear and nonlinear states. The system becomes linearly unstable as a result of small disturbances while nonlinear states result from large disturbances. Linear unstable states are not usually observed in real life until they evolve to nonlinear states. The transition of these states is illustrated by the famous hypothetical amplitude – dependent driving H (A) and damping, D (A) process, Figure 2.10.

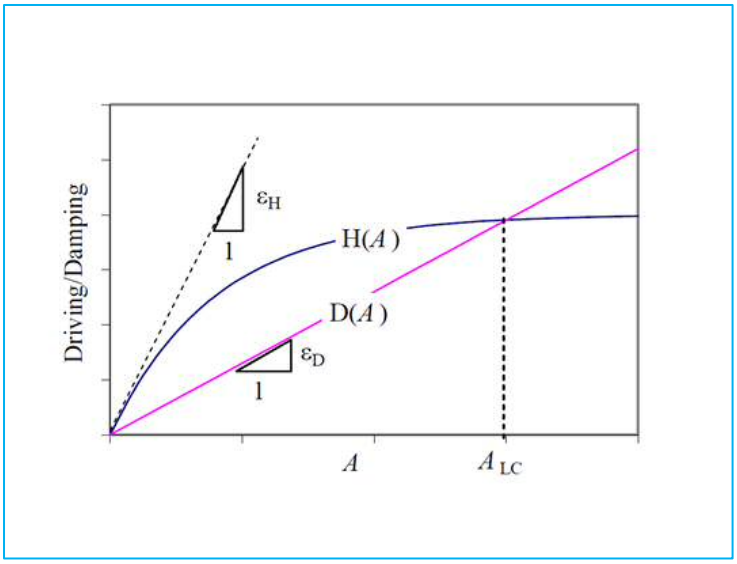

Figure 2. 10 Dependence of acoustic driving and damping processes on instability amplitude [98]

The intersection of the two curves at the origin gives a zero amplitude – equilibrium point. Away from this point, H(A) becomes larger than D(A) with further growth of the instability. The difference between these curves increases with oscillation amplitude signifying the increase in the amplitude of growth rate with oscillation amplitude. The driving and damping processes are represented by a linearized expression when the amplitude of oscillation is small which shows that combustor's linear processes control the balance between the driving and damping processes when the oscillation amplitude is small and could determine the frequency and growth rate of the combustor's inherent oscillation [98]. Nonlinear processes control features such as limit cycle, mode switching of the oscillation as the driving and damping processes remain instability- amplitude dependent. The nonlinearity is observed as the acoustic driving process H(A) saturates and intersects with the damping process D(A) at the limit cycle amplitude of the instability. At the limit cycle, the time average driving mode equals the damping mode and no net energy are supplied to the oscillations, [106][107].

2.4 Flame Dynamics

Apart from flow structures, combustion processes remain very critical in combustion instabilities of burners. Combustion processes are quantified in terms of a flame model which describes the flame behaviour with respect to fluctuations in input parameters such as the velocity of the flow field. Flame model in this study relates the heat release response to inlet velocity fluctuation. A flame transfer function (FTF) is measured as the ratio of heat release rate fluctuation to inlet axial velocity perturbation. This technique has been used in many studies [108] [109] [96], and could be obtained analytically [110] [111], numerically [112 - 114] and experimentally [115 - 118]. In most cases, experimental determination of FTF is preferred because of the high fidelity of the experimental approach in capturing the highly complex interaction between the flow and flame fields.

2.4.1 Linear Flame Transfer Function

A linear flame transfer function relates the heat release rate to small inlet velocity fluctuations [119 - 123], expressed as:

— — (2.3)

where is the heat release fluctuation, velocity fluctuation, and are their mean values respectively. An excited linear flame transfer function is given by:

Function = ——— (2.4)

which relates the heat release rate fluctuations to the relative velocity fluctuations for a given harmonic modulation frequency [108]. By Fourier's transformation, equation (2.4) becomes

—— = FTF ( ) —— (2.5)

where Q ( ) and U ( ) represent the complex perturbations and FTF ( ) defines the flame transfer function. According to Ewald, [120], assuming sinusoidal waveforms, the perturbations can be conveniently expressed by a pointer rotating in the complex plane with a real amplitude denoted by a hat ^ and a phase angle

= (2.6)

= (2.7)

Thus the transfer function finally becomes

FTF ( ) = —— – (2.8)

Many studies [124 - 129], have used this framework in flame characterization. However, this model lacks the capability to predict the nonlinear features of the flame dynamics such as mode switching, instability triggering, hysteresis, limit cycle etc. To characterize these features, the flame model must be able to capture the nonlinear regime of the flame where these dynamical features manifest.

2.4.2 Nonlinear Flame Transfer Function

The linear flame transfer function is extended to a nonlinear regime [130 -133] [112], known as the Flame Describing Function (FDF) given as:

$$F = \frac{}{} G \tag{2.9}$$

where denotes the normalised heat release fluctuation rate and the normalised inlet velocity oscillation impinging on the flame. This extended model is expressed in the frequency domain as gain G and phase which are functions of the forcing frequency ( ) and amplitude . In this case, it is assumed that the flame responds to the harmonic forcing with similar frequency but with a gain and phase shift which depend on the forcing amplitude and frequency.

2.4.3 Flame Describing Function

Flame describing function framework has been utilized in many studies to quantify the flame nonlinear response to flow oscillations. Dowling [133] developed a nonlinear oscillation theory of the flame heat release rate. The theory assumes that the main nonlinearity in the combustion zone is the flame heat release rate, which essentially saturates with forcing conditions. The amplitudes of fluctuations were found to be sufficiently small that the acoustic wave remains linear. However, the time evolution of the oscillations was determined by the numeric integration and inclusion of nonlinear effects which led to limit cycle of finite amplitude. The predicted results were compatible with the experimental and linear theory. It was concluded that flame describing function has the capability to estimate the limit cycle amplitude of the system. This theory was later experimented by Balachandran [131], with a lean partially premixed combustor. The amplitude dependence of the flame response to inlet velocity fluctuations and local heat release rate were examined. The heat release response became nonlinear at certain inlet velocity amplitudes which depended on the forcing frequencies, amplitudes and equivalence ratios. It was observed that the rolled up of the flame shear layers into vortices was the major cause of the nonlinearity.

The flame nonlinearity was also investigated experimentally by Bellows [134]. The measurement of the amplitude dependence of the flame response was taken at several points corresponding to various flow velocity amplitudes and forcing frequencies. It

was observed that the flame exhibited varieties of behaviour at the nonlinear regime. The phase difference between the flow oscillation and the heat release also showed a significant dependence on amplitude. Vortex roll-up and unsteady flame lift were also identified to be an important mechanism responsible for the saturation of the flame with large velocity fluctuations. These two mechanisms responsible for the heat release nonlinear response to imposed acoustic oscillations were further studied experimentally by Bellows [135], to reveal how these mechanisms lead to the flame nonlinear response. It was found that the vortex roll-up keeps the flame area destruction rate of the propagating flame at the same pace with the disturbance amplitude. Thus the flame surface area does not grow proportionally with the disturbance amplitude. The unsteady flame lift-off causes the flame attachment point to move off the centre body to a downstream location for part of the cycle, where the flame surface area decreases due to the merging of flame branches. These two mechanisms are attributed to the flame area reduction by the flame propagation normal to itself.

Noiray et al. [132] conducted an experimental study to quantify the flame describing function of an unconfined laminar burner by associating the nonlinear flame behaviours to the frequency domain analysis of the burner acoustics. With the coupling of the flame model with an acoustic model, the limit cycle was predicted, which was in good agreement with experimental results. The flame linear-nonlinearity transition was found to depend entirely on the amplitude level of the perturbations impinging on the flame. This experimental study was verified analytically by Heckl [136]. The nonlinear flame heat release rate was computed using a generalized n- model with amplitude dependence coefficients and multiple time-lag. The FDF was then measured using experimental coefficients. The results showed a good agreement with the experimental study.

Durox, [108] experimentally measured the FDF of four different flame geometries namely: single conical flame, V-flame, M-flame and a collection of small conical flames stabilized on a perforated plate. The results showed the evolution of the gain and phase shift with the level of oscillation modulation and the steady-state of the configuration, thus revealing the strong influence of the imposed oscillation and the injection geometries on the nonlinearity of the flame. Palies et al. [122], demonstrated

the FDF framework with a geometric burner configuration: a confined swirling flame comprising an upstream manifold and downstream injection unit. The nonlinear flame dynamics was evaluated as a function of the frequency and amplitude of perturbations impinging on the combustion region. An experimental study was also conducted by Kim and Hochgreb [137] to analyse the forced response of swirling lean premixed flames to high amplitude acoustic forcing using a double-swirled, double-channel annular laboratory- scale stratified burner. Various flame shapes like an M-shaped flame, dihedral V-flame and a toroidal detached flame were used for the study. It was found that the modification of the stabilization mechanism has a substantial impact on the nonlinear response of the flames with high amplitude acoustic forcing.

The experimental study of Balachandran [131], was recently tested numerically by Han and Morgans [138]. A large Eddy Simulation (LES) with an Open Source computational fluid dynamics code was used to characterize the nonlinear response of a turbulent premixed flame to acoustic velocity oscillation. Harmonically varying velocity fluctuations were achieved by imposed forcing frequencies and normalized forcing amplitudes. The numerically obtained FDF showed a good agreement with experimental results, thus confirming the capability of LES to quantify FDF. Orchini and Juniper [139] recently suggested the extension of the FDF framework to Flame Double Input Describing Function (FDIDF) by forcing the flow field with multiple amplitudes and frequencies. The calculation of a non-static flame FDIDF was presented using a G- equation- based laminar conical flame.

The above studies confirm the potential of the flame FDF framework to measure a reliable flame model required to predict combustion instabilities. These studies, reveal that the gain of the flame describing function decreases as the fluctuation frequency increases and that, for a given frequency, it becomes constant up to a certain level of perturbation and starts to decrease as the perturbation level increases further. The former and the latter are usually referred to as linear and nonlinear flame response respectively. This flame behaviour plays an important role in combustion instability of the system [133] [140].

2.4.4 Effects of Fuel Blends on flame dynamics

Fuel composition is very crucial in combustion processes, both in terms of thermal efficiency and pollutant emissions. This section assesses the scenarios of fuel blends and its effects on combustion systems.

2.4.4.1 Fuel Flexibility Scenarios

The blend of natural gas with unconventional gases such as carbon dioxide and hydrogen has become popular nowadays in gas turbine combustion for emission reduction and a boost in gas supply. These blends of fuel change the chemical kinetics of the base fuel (natural gas), thus making it more prone to combustion instabilities. An effective means of mitigating CO_2 emission is by Carbon Capture and Sequestration (Storage) (CCS). A large percentage of CO_2 emission comes from power plant such as gas turbine, thus providing a veritable opportunity for CCS to be applied in large scale systems. The process of CO_2 capture requires the separation of CO_2 from the exhaust gas before being captured. Exhaust gas recirculation (EGR) is, therefore, an effective technique to increase the concentration of CO_2 in the exhaust. CO_2 is selected from a portion of the exhaust gas and recycled back into the air inlet section, thus replacing nitrogen in the air and creating a CO_2 rich combustion and subsequently higher CO_2 concentration in the flue gas. The UK Carbon Capture and Storage Research Centre [141] is currently embarking on a Pilot Scale Advanced Capture Technology (PACT), with the main focus on Exhaust Gas Recycle (EGR) in gas turbines. Raising the concentration of CO_2 in the exhaust makes the operation both economically and technically viable for effective and efficient carbon capture from the gas turbine exhaust gases. Several recent studies investigating EGR in gas turbines have been published, [142 -146] , and the general conclusion is that EGR is a realistic method for improving the performance of power generation systems integrated with chemical absorption CO_2 capture technology.

2.4.4.2 Methane Blends

Methane (CH4) has almost similar properties with natural gas. Although natural gas has about 97% of methane, the remaining 3% of the composition is inert gas which does not take part in the combustion process. The energy release and dilatant range depend on its geographical location, with variation in prices. Pure methane has a calorific value of about 55MJ/KG which is suitable for gas turbine combustion. At the

laboratory scale, pure methane is usually used to represent natural gas which gives consistent combustion characteristics. The air to fuel ratio of 17.16 by mass is the equivalence ratio of methane obtained from the basic combustion equation:

$$CH_4 + 2(O_2 + 3.76N_2) = CO_2 + 2(H_2O) + 2(3.76N_2) \quad (2.10)$$

$$AFR_{stoich} = \text{——————} = \text{———} \quad (2.11)$$

The equivalence ratio then gives the ratio of stoichiometric air-fuel to the actual air-fuel mass flow rate:

$$= \text{————} \quad (2.12)$$

For equivalence ratio greater than 1, the mixture is rich, less than 1, the mixture is lean and, an ideal stoichiometric state. Addition of CO_2 to methane-air combustion presents a lot of physical, chemical and thermodynamic changes to the combustion system. The combustion equation is given as

$$CH_4 + aCO_2 + 2(O_2 + 3.76N2) = (a+1)\ CO_2 + 2(H_2O) + 2(3.76N_2) \quad (2.13)$$

where the molar fraction of carbon dioxide to methane is denoted by a. CO_2 addition to pure methane reduces the calorific value of the mixture [23], the turbulent flame speed and flame temperature as well as the NOx formation, [147 - 151]. The general view is that CH4/air- CO_2 flame has a reduced flame temperature compared to the CH4/air flame with corresponding strain rate especially when radiant effects are considered.

Park et al. [152] observed that the addition of CO_2 to methane-air mixture has a diluent effect due to the relative reduction in the concentration of the reactive species and direct chemical effects as a result of the breakdown of CO_2 through the reaction of third-body collision and thermal dissociation. It was also the view of Park et al. that the heat capacity of CO_2 is much higher than air and its absorption coefficient is quite high, that the addition of CO_2 to the fuel mixture is expected to change the flame axial velocity gradient (strain rate). Rokke [146] experimentally investigated the effect of methane blend with N_2, CO_2 and O_2 in a combustion system. The results showed that

the addition of CO_2 and N_2 decreased the NOx formation while the combustion stability limit depended largely on the mass-based additive to fuel ratio. Lewis et al. [153], experimentally demonstrated the effect of methane blend with CO_2 in a proprietary power derivative gas turbine. It was shown that the presence of CO_2 drastically decreased the high momentum flow velocity while increasing the central recirculation zone velocity, since the CO_2's high specific heat increases the pressure differential which drives the recirculation. Therefore the blend of methane with gases like CO_2 and Hydrogen alters the composition of the mixture with corresponding changes in the flame describing function of the system. It, therefore, calls for a thorough examination of the effects of fuel blend on flame describing function and the corresponding effects on acoustic modes of the system, in view of the promising diverse range of fuel supply in the future.

2.5 Combustion Instability Diagnostics

Acoustic dynamics of a combustor is modeled based on the fundamental equations of mass, momentum and energy conservation. Here two cases are considered; the conservation of mass, momentum and energy leading to Navier-Stokes equations [154] and a reactive flow balance equation [122].

2.5.1 Conservation of Mass, Momentum and Energy

The conservation of mass, momentum and energy leads to Navier-Stokes equations:

$$\frac{\partial}{\partial} + \rho \ . U = 0 \tag{2.17}$$

$$\rho\frac{\partial}{\partial} = - \ p + \frac{\partial}{\partial} \tag{2.18}$$

where p is the pressure, ρ the density, u velocity and $\sigma_{i,j}$ the viscous stress tensor. The remainder of this analysis follows from Dowling and Stow [154]. Incorporating the basic thermodynamic properties, the conservation equations from equation (2.17) and (2.18) give the energy equation:

$$\rho\frac{\partial}{\partial} - = - \ . (pu) + q + \ . (K \ T) + \frac{\partial}{\partial}(\sigma_{i,j}u_i) \tag{2.19}$$

where k is the conductivity and q is the rate of heat added to the fluid per unit volume. Thus equation (2.18) becomes

— = — + q + .(k) + — (2.20)

Entropy S is defined by the thermodynamic relation Dh = TDS + (1/) Dp, thus equation (2.20) becomes:

— = q + .(k) + — (2.21)

This shows that heat release, heat transfer and viscous effects result in increased entropy for a material particle. By taking the curl of equation (2.18) and using equation (2.17) form the equation for the vorticity, = x u:

— – = – u + — x + – x –—— (2.22)

The first term of the right-hand side of equation (2.22) denotes the intensification of local vorticity by the stretched vortex lines. The second term implies that vorticity could be created when the pressure and density gradient are not aligned, the last term shows the generation of vorticity by viscous effects. With the assumption of inviscid flow, ideal gas and constant specific heats, the flow is assumed to have a steady uniform mean flow and a small perturbation of equation (2.17):

P(x, t) = + (x, t) (2.23)

where the over bar represents the uniform mean flow and the prime represents small perturbations. And the linearized equations for the perturbation, (2.21) and (2.22) are given as:

— + . = 0 (2.24)

— + – = 0 (2.25)

— = (2.26)

— = 0 (2.27)

where = + and = 0. Combining equation (2.24) and (2.26) and using = / - / = 0 give the inhomogeneous wave equation:

— — - = — — (2.28)

Where c is the speed of sound.

It must be noted that equation (2.27) is not coupled to either the pressure or the entropy. For no unsteady heat release, the pressure in equation (2.28) and entropy in equation (2.26) are not also coupled. Therefore any perturbation is thought of as the summation of these three disturbances, (a) vorticity disturbances, (b) entropy disturbances and (c) acoustic (pressure) disturbances. However, these disturbances are independent and could be treated separately. In the case of acoustic (pressure) disturbance = 0, =0 hence = . Since = 0, equation (2.28) becomes the wave equation with convection for as

— — = 0 (2.29)

and the corresponding given in equation (2.25). In this case, entropic disturbances and vortical disturbances, are convected out of the system with the flow, leaving only the acoustic perturbation to propagate with the speed of sound.

2.5.2 Conditions across Flame Zone and Associated Boundary Conditions

Considering a thin flame zone in a plane x=0 and given that the heat release per unit area is Q_A. A discontinuity occurs in the flow parameter across the flame. If conditions $x=0_-$ and $x=0_+$ are denoted by 1 and 2 respectively. From equation 2.17, 2.18 and 2.20, it is clear that

= (2.30)

= (2.31)

= (2.32a)

where H= h +1/2 gives the stagnation enthalpy. The mean flow is evaluated, since Q_A is known from the fuel composition and its equivalence ratio. A flame model then

describes the response of to the flow perturbation. The combustion system has both inlet and outlet boundary conditions which influence the system.

In most test rigs, the outlet discharges into the atmosphere or an open space, in which the condition is modeled as an open end, where (r, , t) = 0. The inlet is also modeled as open end where (r, , t) = 0, if it is supplied via a plenum chamber. Choked inlet and outlet to the combustion system are modeled for compressor exit and turbine inlet respectively. The conditions for a compact choked outlet and a compact choked inlet boundary conditions are given in equations 2.32b and 2.32c respectively, [155 -157].

2— + — - — = 0 (2.32b)

2— + — = — - — + (– 1) — = = 0 (2.32c)

An acoustic source could also be driven across the chamber and the acoustic impedance of the inlet and outlet are measured experimentally using appropriate sensors.

2.5.3 Acoustic Mode Prediction

Three methods are considered, these are plane wave solution, reactive flow balance and dynamic pressure signal techniques.

2.5.3.1 Plane Wave Solution

Considering a duct with a uniform cross-sectional area, for a mean temperature and a no mean flow density, the unsteady flow parameters are only functions of the axial space coordinate x and time t. Then the general solution of the wave equation (2.29) is given as

$$(x, t) = f(t - x/\ ) + g(t + x/\ ) \quad (2.33)$$

where the functions g(t) and f (t) are arbitraries. The linearized momentum equation (2.25) then becomes

— = –— = —— - —— (2.34)

which is

= — - — (2.35)

Given a frequency of , f(t) is then written as Re where the circumflex indicates the complex amplitude. From this notation equations 2.33 and 2.35 become

(x) = + (2.36)

(X) = —(-) (2.37a)

The resonant frequency is obtained from the application of the boundary condition at the end of the duct. For instance with a large plenum connected to the duct end at x=0 and a constriction at x=l, the boundary conditions are given as

(0) = (l) = 0 (2.37b)

Then equation 2.36 implies = which follows from equation 2.37a that

cos — = 0 (2.37c)

The solution then becomes

= = - — (2.38)

This gives the resonant frequency of a duct describing the oscillation of pressure without decay, with corresponding mode shapes:

= Sin ——— (2.39)

= —Cos ——— (2.40)

Where is an arbitrary

When heat is added at a rate q(x, t) per unit volume, the pressure oscillations satisfy the one-dimensional wave equation of equation (2.28) with = 0 as

— — - — = — — (2.41a)

where the right-hand side gives the level of impact that the addition of heat has on the pressure disturbance. If heat release oscillation rate is dependent on the local pressure with a time delay of , then

(x, t) = —— (x, t –) (2.41b)

The pressure oscillation is obtained by substituting for in equation 2.41a and seeking a separable solution, = Re ( ). By applying suitable boundary conditions to (x) of the form in equations 2.39 and 2.40, the equation for the resonant frequency is thus given as:

(2.42)

When = 0, the roots of equation (2.42) are the undamped resonant organ-pipe frequency . When 0, = 0, the quadratic equation of equation (2.42) for is solved:

(2.43)

Thus making complex. Since the time dependence is , -In (becomes the growth rate of the disturbance. Therefore = exp [ ], indicating that the oscillation grows exponentially if is positive and damps if is negative. These agree with the Rayleigh Criterion of phase and antiphase of heat-pressure coupling.

2.5.3.2 Reactive Flow Balance Method

In this approach, a reactive flow balance equation is coupled to the flame model, and jump conditions at the specific point are analysed. The remainder of this subsection follows from the work of Palies [122].

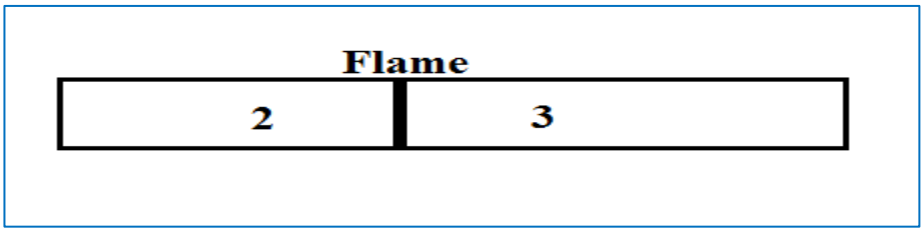

Figure 2. 11 A compact flame in a cylindrical duct

For a flame established in a cylindrical duct Figure 2.11, the flow area changes across the flame. If S_2 denotes the upstream area of 2 and S_3 denotes the downstream area of 3, a jump condition relating the perturbed variables of S_2 and S_3 could be derived. Here the flame is regarded as compact with regards to the wavelength. The balance equation is integrated over the flame volume, and the Green's theorem is applied. An integrated volumetric flux of the heat release perturbation in the control volume is obtained.

—— (2.44)

The three sections of the experimental combustor: plenum, injection and the flame tube are designated by the length l_1, l_2 and l_3 respectively. Their corresponding areas are S_1, S_2 and S_3. The flame is assumed to be compact with respect to the wavelength, and it is stabilised where the flow area changes abruptly between section l_2 and l_3. Thus this theoretical approach uses this geometry to drive a jump condition that relates the upstream and downstream variables to predict the resonant frequency and other thermos-acoustic characteristics of the system.

2.5.3.3 Real-time Measurement of Dynamic Pressure Signal

A practical way of investigating combustion instabilities in a combustor is by the analysis of the pressure signals and the visualisation of the flame structure. The pressure signals recorded by pressure transducers located at different ports within the combustion chamber are analysed to determine the scale invariance combustion acoustics of the system using visibility algorithms. Lieuwen [158] characterised a combustor's transition across stability boundaries by correlating the pressure signals to the operating parameters such as the cycles of oscillation, mean inlet velocity, frequency mode etc. Fourier's transformation of the combustor's dynamic pressure gives well-defined frequencies of the combustor oscillation [159]. The magnitudes of these frequencies give an idea of the stability state of the combustor. Cross correlation measures the similarity of two signals with respect to their relative lag to each other. At maximum cross-correlation magnitude, two signals have maximum overlap as a function of the time lag, [160]. The time lag at the maximum overlap of two pressure signals serves as the time delay of the oscillating acoustic signal.

2.6 Combustion Instability Control

To take full advantage of the efficient and low emissions continuous combustors, operating in a lean premixed combustion condition, the instabilities within the system need to be accurately predicted and incorporated into the system design phase to suppress the destructive phenomenon. As combustion instability stems from the coupling between the inherent acoustics and the unsteady heat release rate, controlling it, therefore, requires the interruption of the coupling between the acoustic waves and the unsteady heat release or an outright damping of the oscillation. There are two major approaches to controlling combustion instabilities; these are *passive* and *active* control techniques. Acoustic dampers are commonly used in rocket engines and afterburners, but less emphasis is placed on land based gas turbines. The disparity stems from the fact that whereas high frequencies in the range of kHz are encountered in rocket engines and afterburners, low frequencies in the range of hundreds of Hz are found in land-base gas turbines which require physical larger dampers. Thus the large size of the damper alters the engine packaging. The following subsections give detailed discussion of these techniques.

2.6.1 Passive Control

Controlling combustion instability passively involves reducing the susceptibility of the combustion processes to acoustic oscillation through design modifications [161] [162] or by removing energy from the sound waves [163]. A hole in the wall of the combustor could release acoustic energy from the chamber which could return to the feedback loop, thereby serving as a potential source of acoustic damping. This view was noted by Putnam, [164] thus: "To solve an oscillatory combustion problem, drill a hole, if that doesn't work, drill two holes''. This statement demonstrates the efficacy of holes in the burner liner to reduce combustion oscillation. By reducing the acoustic energy, the stability of the oscillating system is enhanced. However, in modern premixed gas turbines, dilution holes are completely avoided within the burner liner since the flow is being controlled to meet some performance index. An effective acoustic damping technique in modern combustors is the use of acoustic resonators [162]. These dampers enhance acoustic dissipation within the combustor thereby increasing the damping term in the Rayleigh criterion leading to the reduction in the acoustic energy within the system.

2.6.2 Active Control

In active control of combustion instability, the incipient instability is detected and suppressed. Early studies in the 1950s rocket motor instability had suggested the active control method of introducing perturbations into the combustion chamber via an actuator to decouple the heat-release- acoustic pressure loop to keep the system in a stable running condition. A huge success has been achieved by many organisations with the used of active control to suppress thermos-acoustic instability in gas turbines. The United Technologies Research Centre [165] is reported to have suppressed up to about 16-dB of combustion instabilities in a full-scale single combustor and attenuation of about 6.5-dB in a different combustor. Also, ABB Alstom investigators [166], have also reported a successful instability control. Delaat [167] used an open-loop fuel modulation testing and closed-loop instability control testing with a high – frequency fuel modulation valve. Accordingly, the valve has an inherent control system with a mean flow loop that keeps the mean fuel flow constant while perturbing the fuel flow at about 1000Hz. Active control is sub-divided into Open-Loop and Closed- Loop control system.

2.6.2.1 Open – Loop Control System

Open-loop control action does not depend on the combustion chamber response to control input. Instead, a fixed stimulus is provided to alter the instability coupling and suppress it, [10]. This is to provide oscillation in the physical variable of the flow and heat release which has a substantial influence on the control system. Some of the actuators commonly used are flow valves with periodic flow mechanisms, acoustic drivers etc. The efficacy of these actuators for the control system has been discussed by McManus and Pointsot [168]. According to them, this method is advantageous because control system instability remains a common feature in closed-loop active control. However, accurate calibration of the actuator remains a major task of this control technique.

2.6.2.2 Closed-Loop Control System

Feedback control is a key feature of a closed-loop control system. Both the input and the output of the continuous combustion system is monitored. Where instability is noticed, the input is appropriately adjusted to suppress the instability as measured by

the output sensor. The following are the basic requirements of an active control system in gas turbine control:

- The key variables such as heat release, pressure, and flow velocity are measured using sensors in most cases.
- The heat release and dynamic acoustics are modeled.
- The actuation capability is provided
- The control algorithms are provided to produce optimised actuation signal [169].

The output sensor usually a pressure transducer measures a time-varying parameter of the combustion chamber such as the dynamic pressure and passes the information to the controller. The controller processes the data and based on the processed data, applies an appropriate signal through an actuator to suppress the acoustic perturbation. Many studies [170 - 172] have reported the successful attenuation of combustion instabilities of both rocket engines and land-based gas turbines.

2.6.3 Actuation System for Active Control

Actuation technology plays a crucial role in the product development of active instability control systems in gas turbines. Flow modulating devices are usually used to actively control combustion instability. Two common devices for this purpose are fuel injectors and loudspeakers. While the former adds or reduces the mass flow (which alters the heat release), the latter adds additional velocity which affects the heat release and acoustics [173]. Many studies on the use of these actuation systems in instability closed-loop control have been reported [174 - 176].

2.6.3.1 Fuel Injectors

The fuel injection system is made up of the fluidic and electromechanical parts. The electromechanical part produces an electromechanical field which pushes a spring–loaded poppet. The movement of the poppet controls the aperture of the injector which modulates the flow rate [177] [178]. In this case, the transfer function between the voltage to the poppet position and the mass flow rate from the injector is derived from the Bernoulli, Continuity and Kirchhoff voltage laws [179].

2.6.3.2 Loud Speakers

The actuation system of a loud speaker converts electrical energy into acoustic energy. Thus the actuator dynamics is prescribed by a transfer function between the voltage into the speaker and the acceleration of the loud speaker diaphragm, which is given as

=———————— (2.45)

where represent the friction, stiffness, calibrating gain and the mass property respectively. The effect of this actuation on the combustion system is thus modeled [180]. Table 2.1 gives some published work on the used of fuel and loudspeaker as actuators [181-185] [175][176] [33]. The main challenge now is to accurately capture the interacting mechanism of the flow, flame and the wave fields using a simple and effective actuating technique.

Table 2.1: Fuel and loudspeaker actuators in combustion instability active control.

S/N	Reference	Actuator	Sensor	Experiment/I	Controller Type
1	Dines(1983)	Loudspeaker	CH*	E	Phase - Shift
2	Heckl (1988)	Loudspeaker	P'	E	Phase - Shift
3	Lang et al. (1987)	Loudspeaker	P'	E/M	Phase - Shift
4	Poinsot et al. (1979)	Loudspeaker	P'	E	Phase - Shift
5	Blonbou et al. (2000)	Loudspeaker	P' , OH	E	Neural Network
6	Murugappan et al. (2003)	Loudspeaker	P'	E	LQG-LTR
7	Hathou et al. (1998)	Loudspeaker	P'	M	LQR
8	Gulati & Mani (1992)	Loudspeaker	P'	E	Compensator/Phase- Shift

2.7 Summary

Combustion processes of practical systems such as gas turbines play crucial roles in the enhancement of thermal performance, reduced emissions and better operability. Factors such as fuel-air mixture and injection, fuel-air composition, flow structures, flame dynamics etc. are used to classify flames. One of these classifications is lean premixed flame with high thermal performance and low emission, but with a high susceptibility to combustion disturbances such as blowoff, flashback, autoignition and combustion instabilities. In swirling flows, the coherent flow structures produce flow rotation with inherent flow pressure gradient which causes flow reversal resulting in vortex-induced CRZ. This region of high flame stretch enhances the recirculation of hot gases with cold flow, reduced NOx formation, anchors and stabilizes the flame. A very important parameter of this flow structure is the swirl number (S) which relates

the axial flux of tangential momentum to the axial momentum flux. A change in this number alters the flow structure with huge impact on the flame and pressure fields. The flame also responds to oscillations in the chamber. The flame behaviour is quantified in terms of flame model which relates the heat release response to inlet velocity fluctuations. In the linear regime, the flame model holds for small oscillation amplitudes but lacks the capability to capture some dynamical features such as limit cycle, mode shape, mode switching, hysterias etc. In order to evaluate these dynamical features, the flame model is extended to the nonlinear regime called the Flame Describing Function (FDF) expressed in terms of Gain and Phase of the heat release fluctuation for different modulating frequencies and oscillation amplitudes. Combustion instabilities caused by a coupling between the unsteady heat release and the dynamic pressure is also influenced by fuel blends, due to changes in the heat release rate. The major challenges currently facing combustion experts are adequate knowledge of the precise operating conditions that cause combustion instabilities, accurate prediction and control of the instability modes. At the moment, there is a limited knowledge of the contributions of each of these factors as well as their combined effect on combustion instabilities. There is a curiosity that the combined effects of these factors could be a potential tool for the control of the destructive oscillation. This study, therefore, focuses on the characterization of the effect of each of these factors on the flow - flame field and their combined effects on the acoustic field.

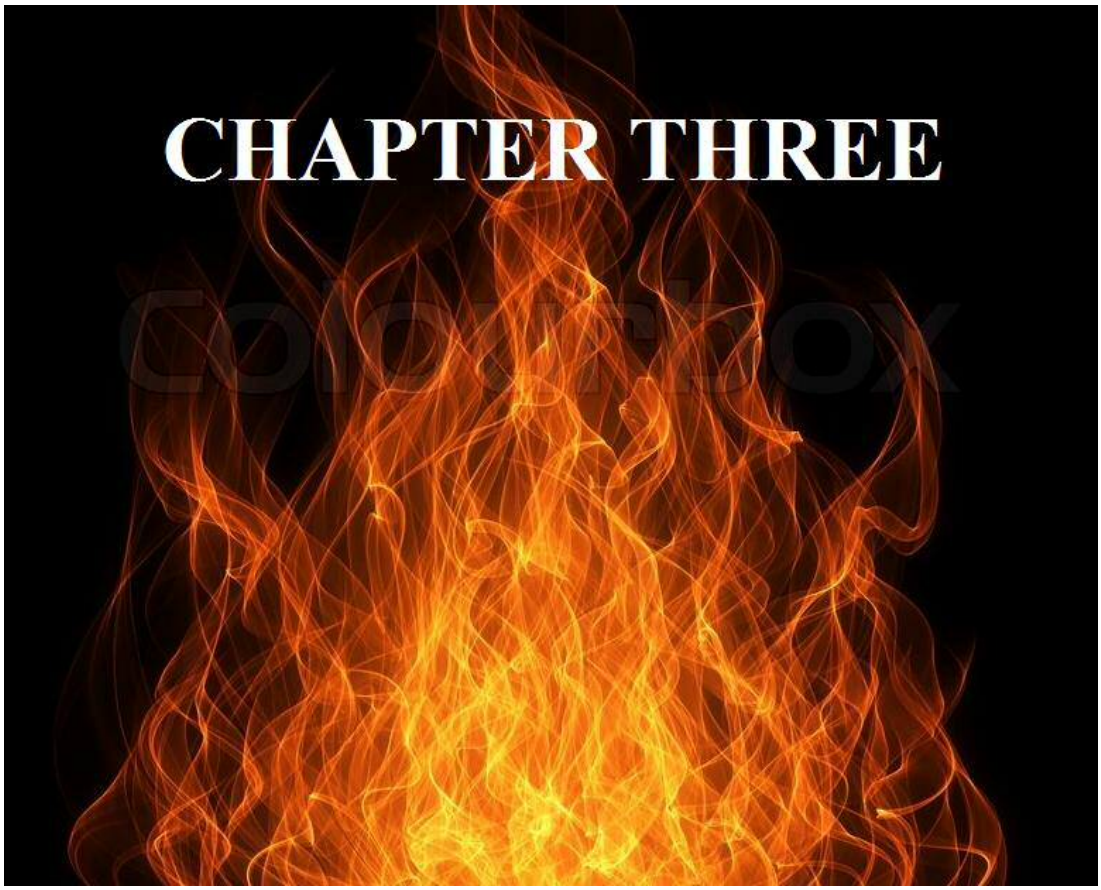
CHAPTER THREE

CHAPTER THREE:

EXPERIMENTAL DESIGN, SETUP AND MEASUREMENT TECHNIQUES

"All life is an experiment. The more experiments you make the better"

--Ralph Emerson

This chapter presents the experimental procedures and measurement techniques of the parameters under investigation, as well as a Low Order combustion simulation used in validating the experimental results. Section 3.1 describes the design, manufacture and setup of the combustor, section 3.2 focuses on the measurement techniques and the instrumentation used for the experimental study, section 3.3 briefly describes a Low Order combustion software (OSCILOS) utilised in this study, and finally, section 3.4 summarises the chapter.

3.1 System Design and Manufacture

This study commenced with the design and manufacture of a 100kW combustor to boost combustion studies in the research group. A 3D model of the combustion system was designed using a CAD software (Solid Works). Figures 3.1 show the design of some of the parts of the burner. Figures 3.1 (a-d) show the 2-D design and their corresponding 3-D versions of some of the parts while (e) and (f) show the assembly of the entire system with a snapped picture of the whole combustor in Figure 3.2, while a detailed setup of the rig is given in Appendix A1 and A2. It is made up of the plenum for fuel-air premixing, injection section and an external flame confinement. A loudspeaker placed at the bottom of the plenum provides an excitation of the flow mixture. The production of the rig was done in the Cardiff School of Engineering Workshop. The system uses gaseous fuel only and could be used for various fundamental studies in efficient and clean combustion.

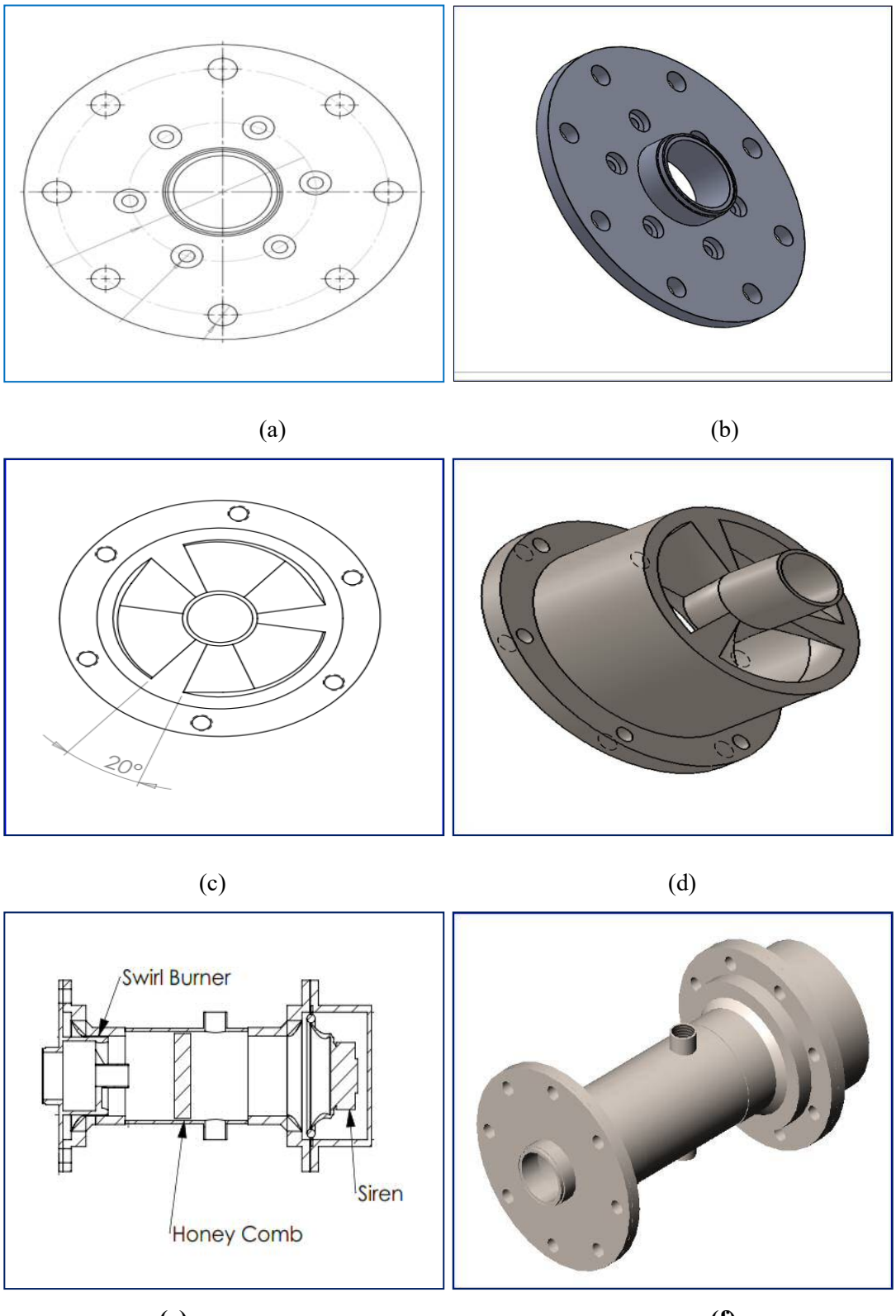

Figure 3. 1 Burner Design

[a, b-Swirl Plate; c, d- Pre-swirl vane; e, f–burner assembly]

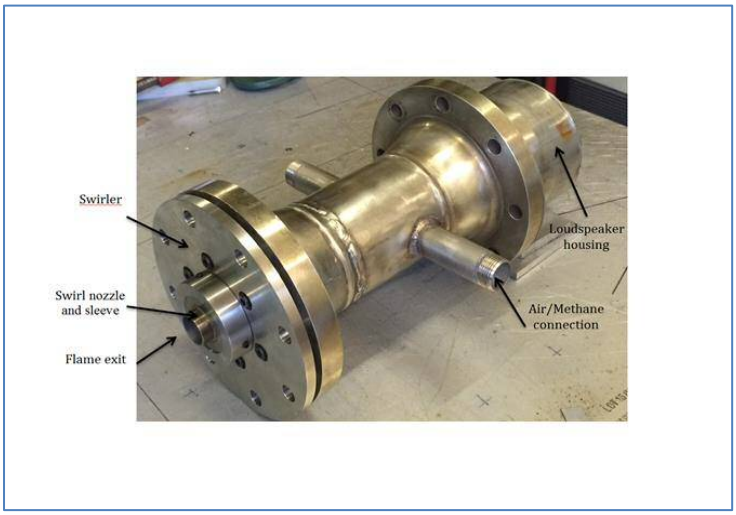

Figure 3. 2 A picture of a newly manufactured swirl premixed burner

3.1.1 The Swirl Configurations

As was discussed in the previous chapter, the geometrical configuration of the swirl nozzle plays a crucial part in modifying the flow and flame fields of the burner. Swirling flows in a premixed combustor is characterized by its swirl number (S), which is defined as the ratio of the axial flux of the tangential momentum to the product of the axial flux of axial momentum and a characteristic radius [75]. In this study, two swirl numbers were used, Figure 3.3. The first swirl with a swirl number of 1.05 is made up of four tangential inlets while the second swirl with a higher swirl number of 1.50 has nine tangential inlets both symmetrically distributed.

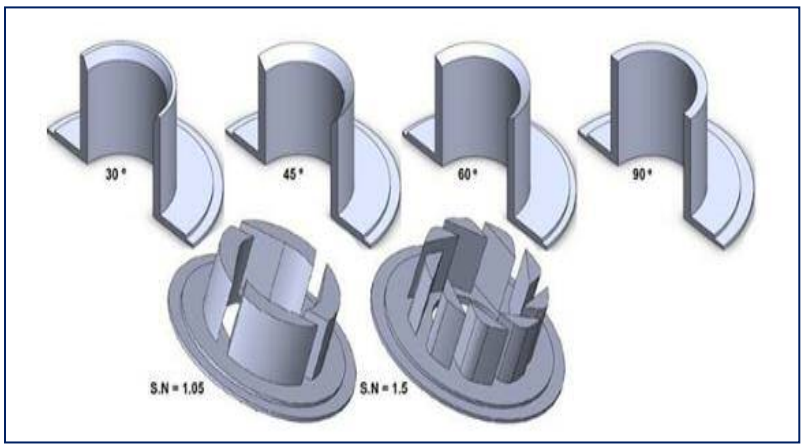

Figure 3. 3 Geometric swirl configurations with divergent nozzle angles

The premixed fuel – air mixture exits into the flame zone via the nozzle. Thus the geometry of the nozzle is equally important in combustion processes. The length and

divergent angle of the nozzle also play a crucial role in flame stabilization. In this study, the internal diameter of the nozzle was kept constant at 28mm, to maintain the same swirl number while the divergent angle and the length of the nozzle were varied, Figure 3.3. The nozzle length is 15 and 30mm for the two swirl numbers.

3.1.2 Rig Set-up and Installation

Figure 3.4, shows the set-up of the experimental rig. At the bottom of the 102mm, internal diameter plenum is a WS13E – 8 Ohm Visaton loud speaker which receives signals of known parameters from a signal generation system. At 110mm above the loudspeaker's diaphragm are two inlet tubes of 40mm internal diameter each, set opposite to each other to supply fuel/air mixture to the plenum, the positioning of the two tubes enhances the fluid mixing process. The air and fuel are fed to the inlet tube at 175mm and 125mm respectively from the plenum. A honeycomb is placed in the plenum chamber 66mm from the fuel/air supply to straighten the flow and to remove large scale perturbation of the flow stream. The injection unit has an 80mm internal diameter section with three pre-swirl vanes attached to a centre shaft which runs through the swirl nozzle. The vanes provide the initial swirling flow which acts as the holder for the swirl nozzle. The swirl nozzle provides an exit for the reactant mixture to the flame zone. The flame is confined with an 80-mm internal diameter and 400mm long quartz tube, which opens to the air.

The excitation system consists of a 5MHz TG503 Thandar signal generator connected to a 200MHz, four channel digital storage TDS2024c Tektronix oscilloscope to read the generated signal. The signal strength is increased via an amplifier, and the final output signal is measured with the remaining channels of the oscilloscope. This output signal is fed to a 152mm diameter, 8 ohms loudspeaker. Thus a signal of known amplitude and frequency is used to excite the flow field to alter the flow velocity profile with corresponding effects on the flame field.

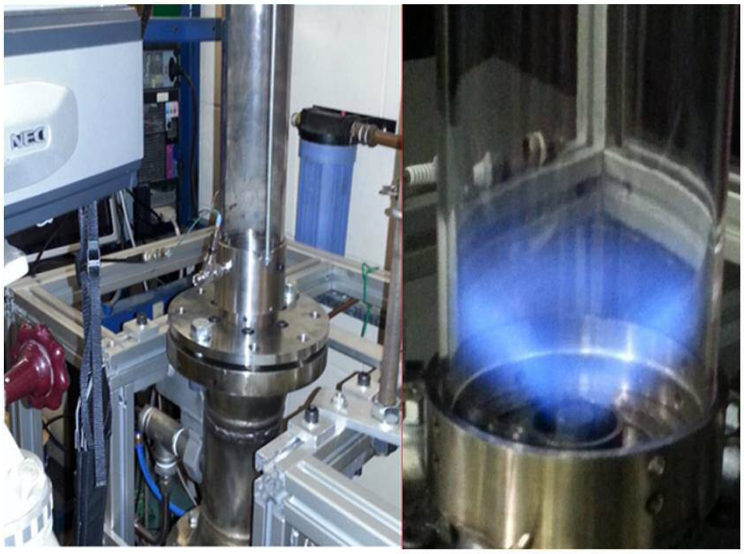

Figure 3. 4 A setup of the swirl premixed burner

3.2 Measurement Techniques and Instrumentation

Highly sensitive instruments were used for the study. Key areas of measurement were the velocity of the flow field, flame heat release rate (chemiluminescence) and the dynamic pressure field. Both intrusive and nonintrusive techniques were deployed for the measurement.

3.2.1 Velocity Profile Measurement

The profiles of the flow field being an important aspect of this study were characterised using a constant temperature anemometer and a Laser Doppler Anemometry LDA. These instruments are briefly described.

3.2.1.1 Constant Temperature Anemometer (CTA)

A Constant Temperature Anemometry system is an intrusive measurement technique which works on the principle of the cooling effects of a sensor placed in a flowing fluid. With its frequency response in the range of kHz, and its sensitivity to low flow velocities, CTA remains an accurate technique for measuring turbulent velocity in swirling flows. The sensor's (hot wire) temperature is kept constant by an electronic circuitry which provides a feedback control loop for the system. The circuitry produces a continuous voltage which varies with the instantaneous velocity of the flow. Thus

the fluctuating voltage becomes a direct measurement of the velocity fluctuation. In this study, a MiniCTA 54T42 hardware with a single channel, Figure 3.5, was used to measure the mean and turbulent levels of the axial velocity of the inlet flow to the combustor.

Figure 3. 5 CTA Hardware for data acquisition [186]

3.2.1.2 The Sensor (Hot Wire)

The sensor is a thin wire suspended by two or more prongs, Figure 3.6. The prongs come with different configurations to measure one, two and three-dimensional flows. The wire is the heating element by current from the electronic circuit via the prongs. The prongs also provide support to the wire.

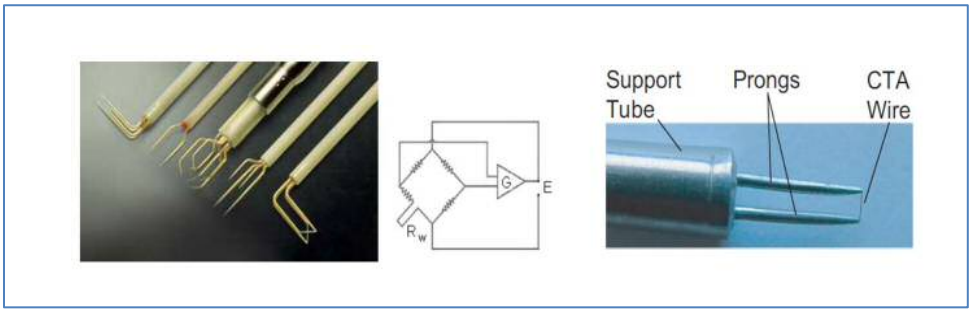

Figure 3. 6 Constant Temperature Anemometer probes

[Centre: Wheatstone bridge, E = bridge voltage, Rw = wire résistance], Source: Dantec Dynamics [187].

For the temperature of the wire to be kept constant, the electronic circuit supplies current to the sensor to keep its resistance constant in spite of the cooling of the wire by the flowing fluid. Thus the circuit voltage E becomes the heat transfer to the

flowing fluid which measures its velocity. The heat transfer from the hot wire to the fluid is given by the equation [188].

$$= K \quad — \quad —— \tag{3.1}$$

Where is the heat flux, K, A, and B, are the probe constants obtained by the calibration of the hot wire, the sensor temperature and the fluid temperature. The heat flux is obtained from the power loss in the wire as voltage E and the wire resistance R_w thus

$$= — \tag{3.2}$$

A curve fit serves as a transfer function between the voltage and the calibration velocity.

3.2.1.3 Laser Doppler Anemometry

In the isothermal and combusting conditions, the velocity fluctuations of the flow field were measured using Laser Doppler Anemometry (LDA). This technique is widely used for fluid flow measurement in gases and liquids. The measurement gives the mean and turbulent velocity profiles of the flow field. It is directional sensitive, nonintrusive in principle and has a high spatial and temporal resolution, thus suitable for measuring reversing, chemically reacting flows even in a high-temperature environment which are not suitable for intrusive sensors. Figures 3.7 show a schematic view of the LDA setup.

LDA is made up of sub-systems namely: a laser with continuous beams, beam transmitting optics, photo detecting optics and processors. The laser produces a continuous beam, and a glass crystal with a vibrating piezo crystal (Bragg) generates acoustical waves which act as an optical grid. The Bragg cell produces two beams of the same intensity but different frequencies which are then focused onto the optical fibres and then brought to a probe. The beams from the fibre intersect in the probe volume which is then focused by a lens.

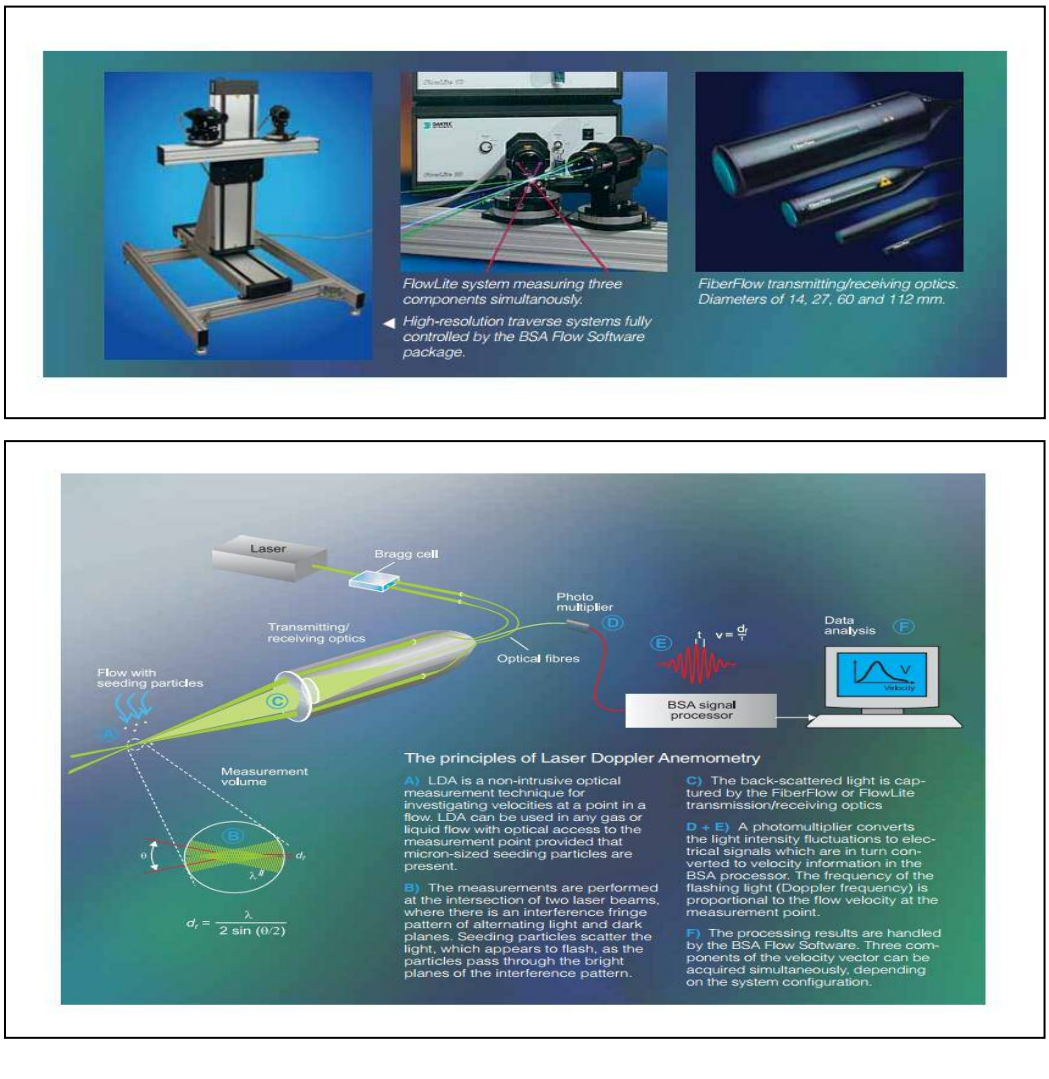

Figure 3. 7 A schematic view of a LDA Setup and operation

Source: Dantec Dynamics, [189].

The light intensity is varied by the interference between the laser beams. The flow field velocity is measured from the light scattered by the seeding particle in the flow through the probe volume. This produces parallel planes of high light intensity called fringes. The fringe distance d_f is given by the wavelength of the laser light and the angle between the beams:

$$= \frac{\quad}{\quad} \tag{3.3}$$

Thus each particle that passes through the probe volume scatters light proportional to the local light intensity. The scattered light contains a Doppler shift, the Doppler frequency f_D, which is proportional to the velocity component perpendicular to the

bisector of the two laser beams, which corresponds to the X-axis of the probe volume,[189]. The scattered rays of light are collected by a receiver lens and focused on a photodetector. An interference filter mounted before the photo detector passes only the required wavelength to the photodetector. The photodetector then converts the fluctuating light intensity to an electrical signal which is filtered and amplified by the signal processor. The fringe spacing d_f gives the information about the distance travelled by the particle. The Doppler frequency f_D provides information about the time ($t = 1/f_D$), thus the fluid velocity v is determined as

$$v = d_f \times f_D \quad 3.4$$

3.2.2 Flame Field Measurement

An accurate measurement of flame dynamics is very crucial in combustion, as this parameter plays a vital role in characterizing and predicting unsteady combustion behaviour such as blow off, flashback, combustion instabilities, combustion noise, pulsed combustion etc. Nonintrusive techniques are usually preferred for this purpose to capture the heat release chemiluminescence in the flame zone, to ensure that the measurement instruments do not interfere with the flow field. The intensity of light emitted by the flame is known to be proportional to the chemical production rate of the molecules [134]. Thus chemiluminescence is related to the chemical rate of reaction. Many studies [190] [191], have used chemiluminescence roughly as a measure of reaction and heat release rate.

The spectral analysis of electromagnetic radiation of energy stored in a body is used as a function of its wavelength, where the distribution is known as the emission spectrum, determined by the electronic system of the reactant composition. Changes in the oscillatory energy of the atoms and the rotational energy of the molecules alter the position of individual bands in the band system and the fine structure of individual bands respectively. The radicals OH*, CH*, C2* and CO2* make up the chemiluminescence spectrum of hydrocarbon flames, emitting light in narrow spectral bands. The wavelength of radiation is the distinctive characteristic of each radical. They have a wavelength of 308nm, 431nm and 513nm for OH*, CH* and C2* respectively while CO2* appears as a continuous radiation spectrum, Figure3.8.

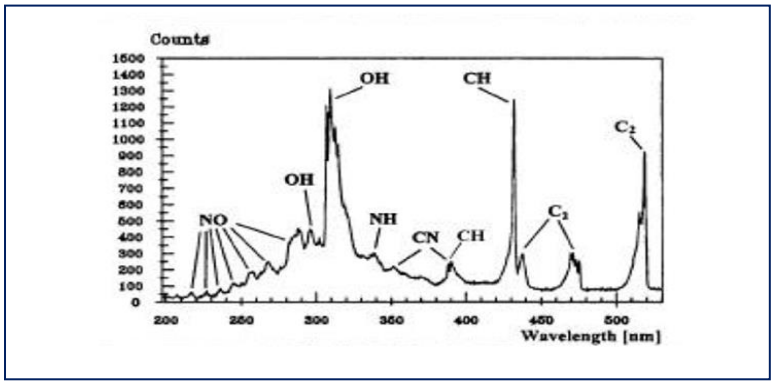

Figure 3. 8 Emission spectrum band of hydrocarbon fuel radicals, [192].

The shape and size of the flame could also be used to characterise the operational boundary in terms of flashback and blowoff limits of the burner.

3.2.2.1 Flame Shape and Radicals Measurement

Two cameras were used for the measurement of the flame dynamics. While the digital camera measured the flame shape kinematics, the high-speed camera measured the heat release fluctuation rate, as described below.

- **Digital Camera**

A high-quality Sony DSCHX400V Digital compact camera was used to capture the flame images and their evolutions with different operating conditions to obtain the operational limits (flashback/blowoff limits) of the burner.

- **High-Speed Camera**

A Photron Fastcam APX-RS high-speed camera operating at 1000 frames/s with a 105 mm, 1:2.8 Nikon lens was used to measure the CH* chemiluminescence of the flame. The repetition rate was fixed at 60 Hz to provide an overview of CH* fluctuation for different cases. The intensity of the weak chemiluminescence from the flame was enhanced by an image intensifier. Here a photocathode converts the weak intensity incident light from the flame to photoelectrons and passes it to the microchannel plate where the electrons are multiplied, and a phosphor screen reconverts the electrons to a light of a high intensity which is then captured by the high-speed camera. The CH* images were captured on PC using a Photron FASTCAM PFV software and thereafter analysed with Matlab – based codes.

3.2.3 Pressure Measurement

The real time dynamic pressure of the combustion chamber was measured using five Kistler Piezo electronic Sensors, given in Table 3.1. Two - 211B6, Figure 3.9 and one - 701A sensors, were mounted 20mm downstream of the flame while one -701A and 601A, Figure 3.10, were positioned 100mm upstream of the swirl. The details of theses sensors are also provided.

Table 3.1: Kistler Pressure Transducers and their Sensitivities, [193][194].

Model	Sensitivity	No. of Sensor
211B6	100Mv/Psi	2
701A	-80PC/bar	2
601A	-16PC/bar	1

The core of the sensors has a synthetic crystal usually a quartz and operates on the principle of piezoelectricity, where the pressure to be measured acts on the sensor's diaphragm and then converted to a proportional force which acts on the crystal. A proportional pressure is produced by the compressed crystal using charges which are picked-up by sensor electrodes and carried to the plug. The charged signal is finally converted to a readable voltage, by a charge amplifier.

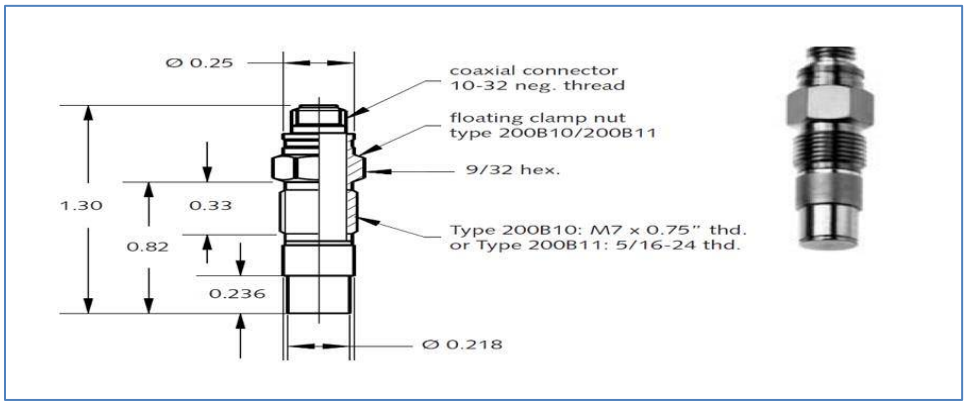

Figure 3. 9 Voltage output Model 211B Pressure Transducer

Source; Kistler Instrument Corp, [193].

These sensors give either charge or voltage output. For the charge output sensors, the sensitivity is given in pico-coulombs per unit of pressure (pC/bar), where the pressure applied to these sensors produces negative charge signals and are then converted to a positive voltage signal via an external amplifier. They require no power since charge

signals are produced when pressure is applied to the piezoelectric material. Voltage output sensors are made up of an integrated electronic circuit which converts a charge into a voltage signal. Since this sensor delivers a voltage signal, its sensitivity is given in millivolt per unit of pressure (mV/psi). The sensors produce direct positive signals. They are powered by an electronic circuit (IEPE- Coupler) which supplies constant current excitation to the sensors. Model 211B6 is a voltage output while Models 701A and 601A are charge output.

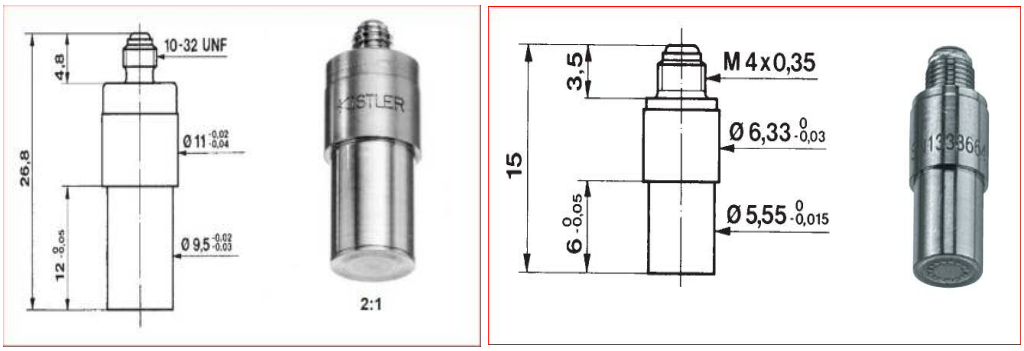

(a) (b)

Figure 3. 10 A charge output Kistler Pressure Transducer

[(a) Model 701A, (b) Model 601A], [193], Source; Kistler Instrument Corp, [194].

The multi-channel amplifier has an integrated digital and analogy output DAQ which is connected to a PC via Ethernet cable for data logging. The sensors were flush mounted on the wall of the combustor within the flame zone. The calibration was done at the factory by determining the sensor output in response to a known input. A calibrated pressure with a dead-weight tester was applied to a standard secondary sensor. The standard sensor was then used to calibrate the test sensors by applying pressure to both sensors simultaneously as stated in the calibration certificate.

3.2.4 Data Acquisition Techniques

The experimental data was accurately acquired and processed to provide accurate information for the study. This subsection describes the data acquisition techniques that were used for all the instrument.

3.2.4.1 Velocity Fluctuation

A dedicated data acquisition for Laser Doppler Anemometry (LDA) measurement is a Windows Software Package- BSA Flow Software, which works together with Dantec Dynamics' LDA processors and optical LDA systems to provide an integrated velocity measurement through its flexible user's interface. The measurement matrix was designed to measure 621 points: 23 points with a 2mm step on the horizontal axis by 27 points with a 2mm step on the vertical plane. In each case, the seeding particle count was kept at 10000, which was far above the minimum accuracy level of 2000 [195]. The user interface of the software shows and records the mean and root mean square velocities of the 621 points. The system parameters and settings are given in Appendix A4.

Stream Ware is also a Windows based software [186], which works with the CTA hardware to measure the velocity profiles. With the synchronisation of a DAQ Assistant (DAQ) from the National Instrument, the complete system is controlled by Stream Ware Basic which performs the following tasks: hardware setup, automatic probe calibration and data acquisition. The acquired data was converted and reduced to give the mean and root mean square velocities of the flow field. It also provides a database for the storage of the acquired data. Full detail is given in Appendix A5.

3.2.4.2 Flame and Heat Release Fluctuation

The CH* images from the high-speed videos were reconstructed to obtain the qualitative views of the chemiluminescence intensity as well as the quantitative values using a standard Matlab - based software, "Imatool" , Appendix B1, and validated with another Matlab - based code details given in Appendix B2.

3.2.4.3 Dynamic Pressure Fluctuation

A practical way of investigating combustion instabilities in a combustor is by analysing the pressure signals of the combustion chamber. The dynamic pressure signals were recorded with the pressure transducers located at different ports within the combustion chamber. They were then analysed to obtain the combustion acoustic modes of the system. With this technique, Lieuwen [158] characterised a combustor's transition across instability boundaries by correlating the pressure signals to the

operating parameters such as the cycles of oscillation, mean inlet velocity, frequency mode, etc. The Fourier transformation of the combustor's dynamic pressure gives well-defined frequencies of combustor oscillation [159]. The power spectrum of these frequencies gives an idea of the stability state of the combustor. Cross correlation measures the similarity of two signals with respect to their relative lag to each other. At maximum cross-correlation magnitude, two signals have maximum overlap as a function of this time lag [160]. The time lag at the maximum overlap of two pressure signals serves as the time delay of the oscillating acoustic signal. The mean velocity fluctuation at the flame holder location could also be obtained with the two microphone technique, where the forcing frequency, dynamic pressure by the two sensors (simultaneously recorded) and their common distance from each other, are all combined in the frequency domain to obtain the mean velocity fluctuations.

A Model 5165A – 4- Channel Kistler Lab. Amplifier was used to convert the signals from the pressure transducers to digital values. The settings of the Amplifier were configured in a standard web-browser with a graphical user interface offering an accurate measurement of the time series of the dynamic pressure of the system. The analogue time series were sampled for all the experimental tests at 6.25 kHz for 2 seconds. Full detail is given in Appendix A6.

3.3 Low Order Combustion Instability Simulator (OSCILOS)

A combustion instability simulator called Open Source Combustion Instability Low-Order Simulator (OSCILOS) [93], was used to predict the Eigen frequencies of the combustor during combustion. The simulated results serve as the basis for comparison with the eigen values obtained from the time signals of the dynamic pressure of the combustor measured with pressure transducers. The flame describing function (FDF) obtained in terms of gain and phase is fed into the thermos-acoustic model to predict the frequency of resonant modes, instability growth rate (positive and negative growth rates), mode structure and the time evolution of disturbances. OSCILOS is an open source code designed to simulate combustion-driven instability written in Matlab / Simulink. This program was developed by a combustion research group at the Department of Mechanical Engineering, Imperial College London, UK. It can

simulate both longitudinal and radial combustor geometries as a network of connected modules, Figure 3.11, where the acoustic waves are modeled as 1-D plane waves.

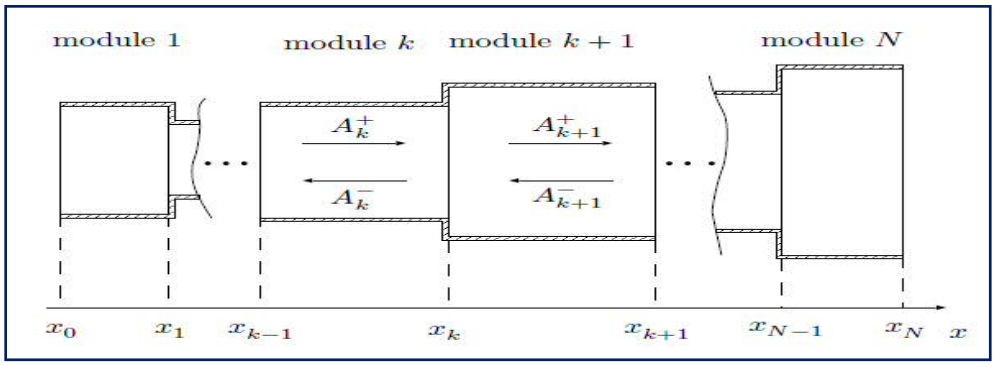

Figure 3. 11 A schematic view of the longitudinal acoustic element [93].

3.3.1 Acoustic Waves Propagation

The combustion chamber consists of several cylindrical tubes with different sectional areas. Representing the distance along the longitudinal axis as x, and the inlet and outlet of section K as $x= x_{k-1}$ and $x= x_k$ respectively, a flame located at $x =x_n$ becomes the heat source. The premixed gases are ignited and turned to burned gases. As a result, a weak disturbance is induced within the combustor with plane acoustic waves which propagate in both directions. The pressure, velocity and density in section k are expressed thus:

(3.5)

—— (3.6)

— — (3.7)

where and represent the amplitude of the downstream and upstream acoustic waves respectively, E_k denotes the amplitude of entropy waves and , , are time delays.

3.3.2 Flame Model

A linear flame transfer function as discussed in chapter two describes the linear response of heat release rate fluctuation to inlet velocity and equivalence ratio fluctuations expressed in the Laplace domain as

— — — (3.8)

where , represent the flame response to velocity oscillations and mixture inhomogeneity .

The normalized heat release rate perturbation could also be expressed as a function of normalised velocity oscillation in the unburned gases as

— — (3.9)

where u represents unburned gases.

The flame model thus describes the response of the normalised heat release fluctuation rate to the normalised velocity fluctuations. OSCILOS has four prescriptions of the flame transfer function; the first three are represented by equations 3.10, 3.11 and 3.12. Equation 3.10 is the Crocco's famous *n-* model, 3.11 is *n-* model filtered by a first order model and 3.12 is *n-* model filtered by a second order model, , [133],[196].

(3.10)

— (3.11)

————— (3.12)

Where and denote the gain and time delay respectively, = 2 f and represent cut –off frequency of the filter and damping coefficient of the second low pass filter respectively.

The fourth model, equation 3.13, is a user- defined model, by supplying the numerator coefficient b and the denominator coefficient a.

(3.13)

The afore-mentioned models are linear in nature, however in practical combustors, flames feature a nonlinear response to flow perturbation [197], [123], [122], [28]. As discussed in chapter two, linear flame models lack the capabilities to predict nonlinear features of combustion instabilities. Also, the framework of flame describing function (FDF) presents the response of heat release rate as linear for small oscillations level and a weakly nonlinear regime for larger disturbance amplitudes. An analytical nonlinear FDF can be prescribed from the option provided in OSCILOS, experimental or CFD data could be loaded and fitted.

3.3.3 Boundary Conditions

The combustor reflection coefficients are prescribed by the inward and outward propagating waves at the end of the combustor. Thus the pressure reflection coefficients at the inlet and outlet are given as R1 and R2 respectively, which are expressed as,[93].

(3.14)

(3.15)

The compressor outlet and turbine inlet in the case of gas turbines are considered as choked inlet and choked outlet respectively. These choked interfaces are regarded as boundaries for the system analysis with the selection of the appropriate values for R1 and R2 for the simulation.

3.3.4 Eigen Frequency Simulation

The thermal properties of the gas mixture which are basically the flow properties and the mean heat are correctly prescribed, the flame models are loaded, and the boundary conditions are specified, the simulation is run in the eigen mode panel. In this study, the simulation results serve as the basis for comparison with the eigen frequencies obtained from the time-series signals of the dynamic pressure of the combustor. A good agreement of the experimental and simulated results would be an indication of the accuracy of the entire study.

3.4 Summary

A new 100kW combustor was designed and manufactured for experimental investigations in lean premixed combustion. In this study, the combustion system was influenced by three main factors: the first was the swirl strength of the flow field where two swirl numbers of 1.05 and 1.50 with four and nine tangential inlets, respectively, were used to vary the flow swirl strength. The second was the external excitation, where a loudspeaker at the bottom of the plenum was used to control the amplitude of the acoustic oscillations. Its variation enables an accurate measurement of the flame to acoustic perturbation. Finally, the fuel was used as an important factor of the flame field dynamics, where methane was used as a baseline fuel for the comparison of the effects of CO_2 blend with methane in the flame and acoustic fields.

The main areas of measurement were the velocity of the flow field, the flame heat release rate (chemiluminescence) and the dynamic pressure field. Both intrusive and nonintrusive techniques were deployed for the measurement. The velocity profile of the flow field was measured with LDA and CTA, and a digital camera was used for the measurement of the flame shape kinematics. A high-speed camera was also used for the measurement of the flame heat release fluctuation, while a real-time dynamic pressure of the combustion chamber was measured using Kistler Piezo-electronic sensors. An open loop forcing of the flow field was carried out, and its effects on the flow, flame and pressure fields were characterized under different swirl and fuel conditions. Combustion instabilities within the combustor were investigated by spectral and statistical analysis of the time-series of the dynamic pressure signals. A combustion instability simulator was also used to predict the eigen frequencies of the combustor during combustion, for comparison with the experimental results.

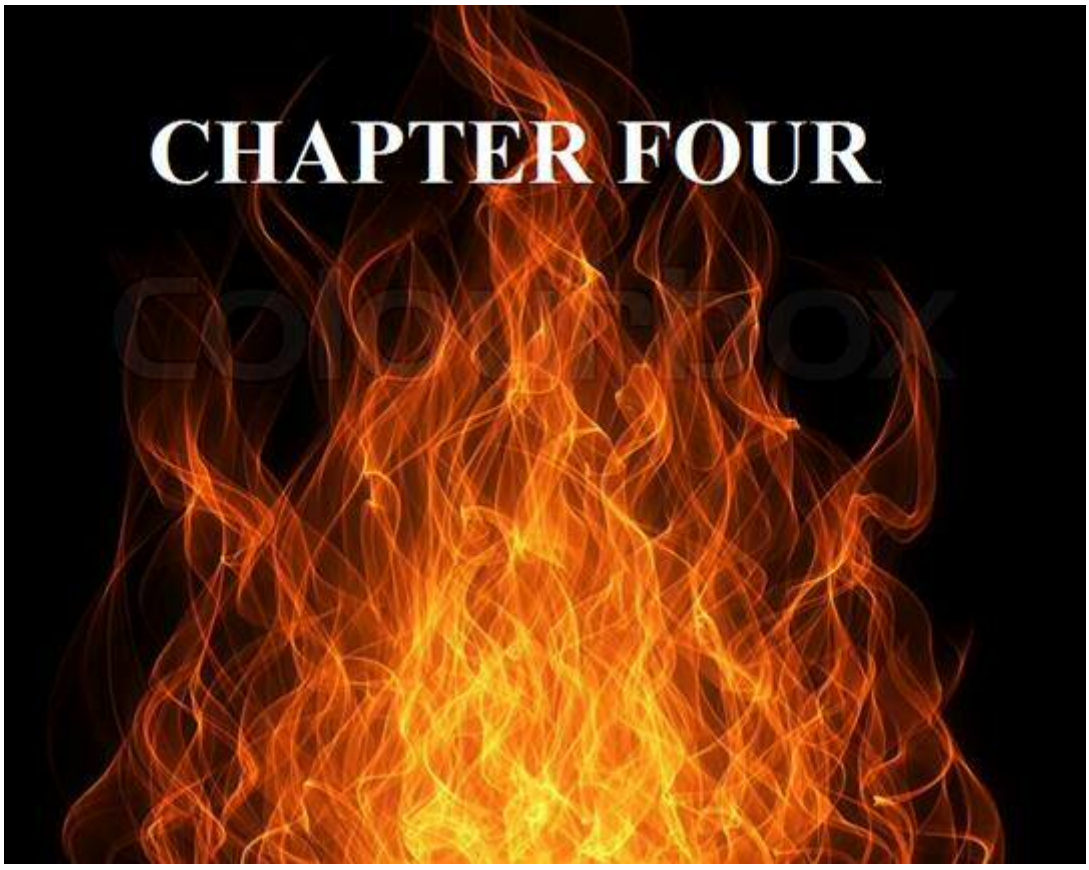
CHAPTER FOUR

CHAPTER FOUR:

FLOW FIELD FLUCTUATIONS WITH SWIRL AND FORCING

An experiment is a question which science poses to nature, and a measurement is the recording of nature's answer" – Max Planck

Swirling flows are common to many lean premixed gas turbines. The flow features serve to stabilize the flame and enhance efficient and clean combustion. Swirling flows affect the flame either by the coupling of large scale unsteady flows with the combustor's wave or by altering the flame structure and combustion intensity, all leading to heat release rate fluctuation which is central to combustion instabilities. This chapter measures the velocity profiles of the flow field at different swirl geometry and forcing conditions under isothermal condition, with a view to assessing the contributions of the swirl intensity and forcing on the fluctuations of the velocity profiles. Section 4.1 defines the domain boundaries of the flow field which lies mainly within the CRZ. All the parameters are measured within this domain. Section 4.2 validates the velocity profiles values by comparing the results obtained from the LDA to those of the Hot Wire Anemometry. Section 4.3 considers the effects of the flow swirl strength on the mean axial velocity and turbulence intensity of the flow field. Section 4.4 and 4.5 repeat the investigation of section 4.3 but with additional influence of external excitation of the flow field and finally, section 4.6 summarises the results obtained.

4.1 Flow Field Matrix

The flow was measured from the centre zero flow axis with a radius (R) of 23mm and a vertical distance of 54 mm with 2mm step, Figure 4.1. To globalise these distances, the vertical axis is normalised as the ratio of the vertical distance (y) to the internal diameter of the nozzle (D), and the horizontal axis as the ratio of the probe distance from the zero axis of the flow (r) to the overall radius of measurement (R).

The diameter of the nozzle is 28mm and the total measurement point within the matrix is 621 (27x23).

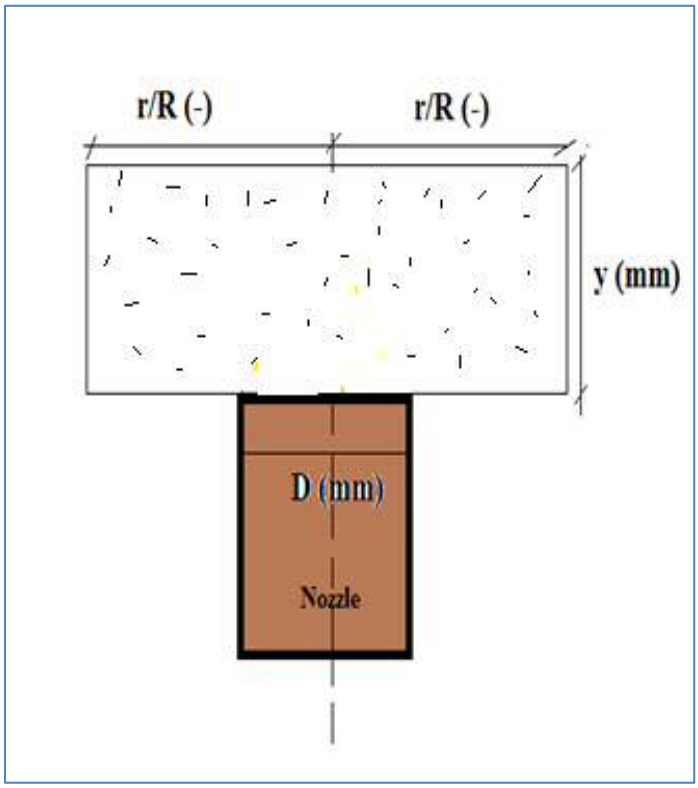

Figure 4. 1 Flow Field Domain Definition

The measurements were taken at isothermal conditions with the flow rate kept constant at 2.44g/s, with two swirl conditions (S=1.05 and 1.50).

4.2 Validation of Velocity Profile Measurement

Laser Doppler Anemometer (LDA) was used mainly for the measurement of the velocity profiles of the flow field, however, an intrusive Constant Temperature Anemometer (CTA) was used to validate the velocity values of the LDA. Figures 4 .2 give the mean velocity profile obtained from LDA and CTA with the same conditions for two vertical distances from the dump plane. These positions are y/D = 0.3571 (y=10mm) and y/D =1.0714 (y = 30mm). For the swirl number of 1.50, the velocity profiles show the existence of a well-known flow structure called the central recirculation zone (CRZ) due to high swirl intensities, where there is a steep pressure

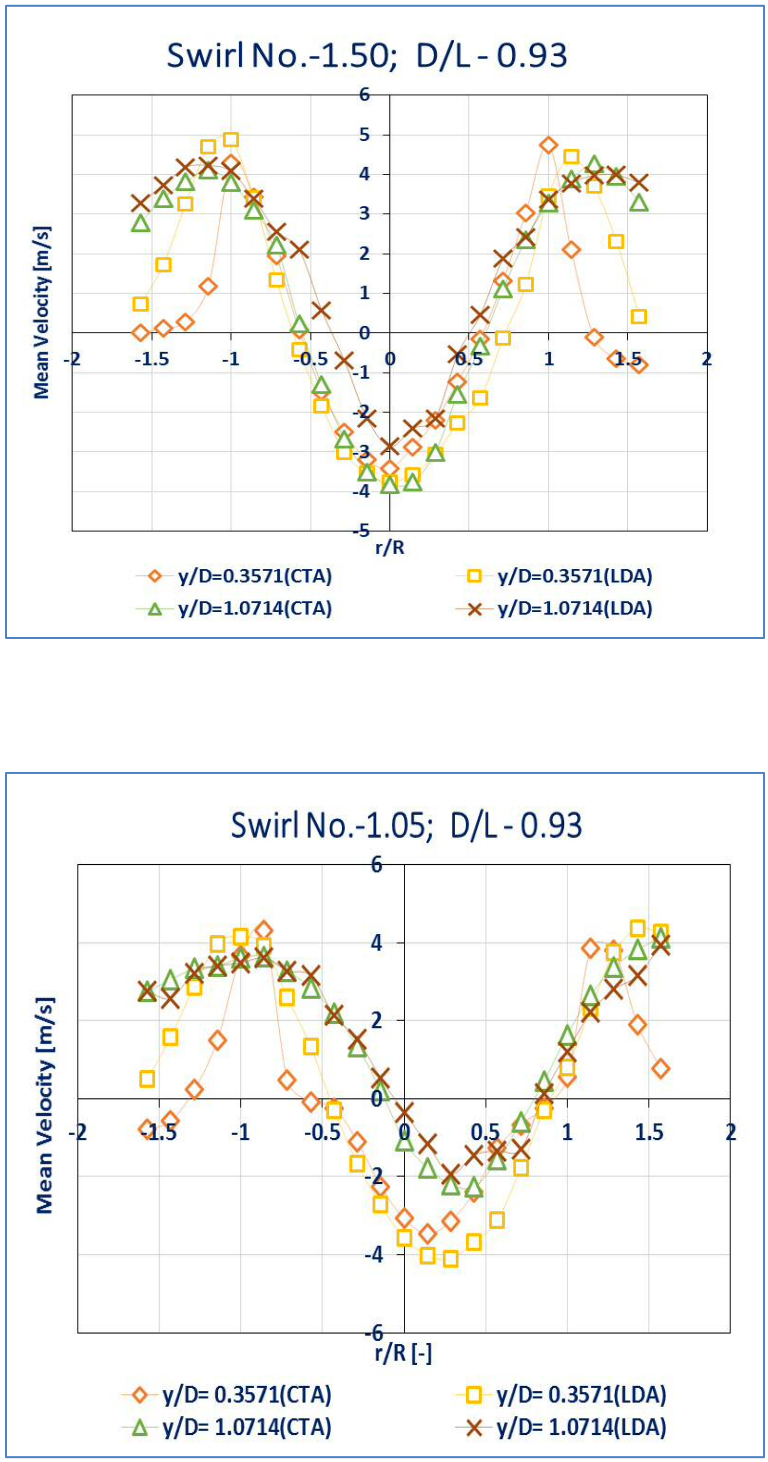

Figure 4. 2 Mean velocity profiles measured with LDA and CTA

gradient in the radial direction to balance the centrifugal forces which lead to a low - pressure core around the centre line. This phenomenon has been reported in many published works [43][77]. This mechanism eventually leads to a positive gradient

generated along the axial axis resulting in a flow reversal, a region with negative velocities. This mechanism is treated extensively in the later part of this section.

The flow reaches a maximum mean velocity of 5m/s at the high momentum flow region and reduces towards the zero axes to a negative velocity of -4m/s at the axis. The results obtained from the two techniques agree at many points in both vertical distances especially in the high momentum flow regions (-1 r/R -0.5 and (0.5 r/R 1), with insignificant differences in the reversed flow regions. The validation was also tested with the decreased swirl number of 1.05 with a reduced swirling strength. The recirculation zone moves towards zero value with increased vertical distance and shifts slightly away from the flow axis. The velocity profiles in both locations of the measurement probe also show good agreement.

The velocity profiles were further validated with the turbulence intensity of the flow field for the two swirl numbers. Figures 4.3 show high turbulence intensities in the shear layers of the flow field which reduces with increase in the vertical distance (y/D), Figure 4.3(a). The high turbulence scale close to the dump plane is attributed to the high velocity of fresh inlet gases which flow in opposite direction with the recirculated flow. The inlet velocity weakens downstream of the flow resulting in weak shear layers with low turbulence scales. For the first probe distance of y/D = 0.3571, a high turbulence intensity of 42% for LDA and 45% for CTA was observed at a horizontal position of r/R = -0.6 and turbulence values of 25% for LDA and 24% for CTA at a distance of r/R = 0.6, which are within the shear layers of the flow field. At a higher position of y/D = 1.0714, minor variations were observed in the measurement of the two techniques around the shear layers.

In the lower swirl number of 1.05, Figure 4.3 (b), the measurements in the two vertical probe positions also became very close both in the shear layers and other regions of the flow field, thus proving the accuracy of the LDA measurement. The LDA was then used in the remaining flow measurement of the study due to the fragility of the CTA.

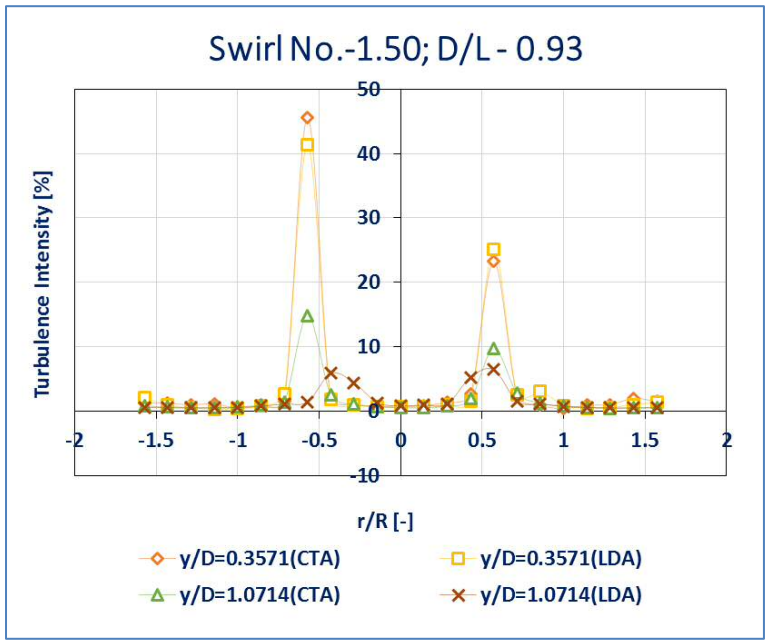

(a)

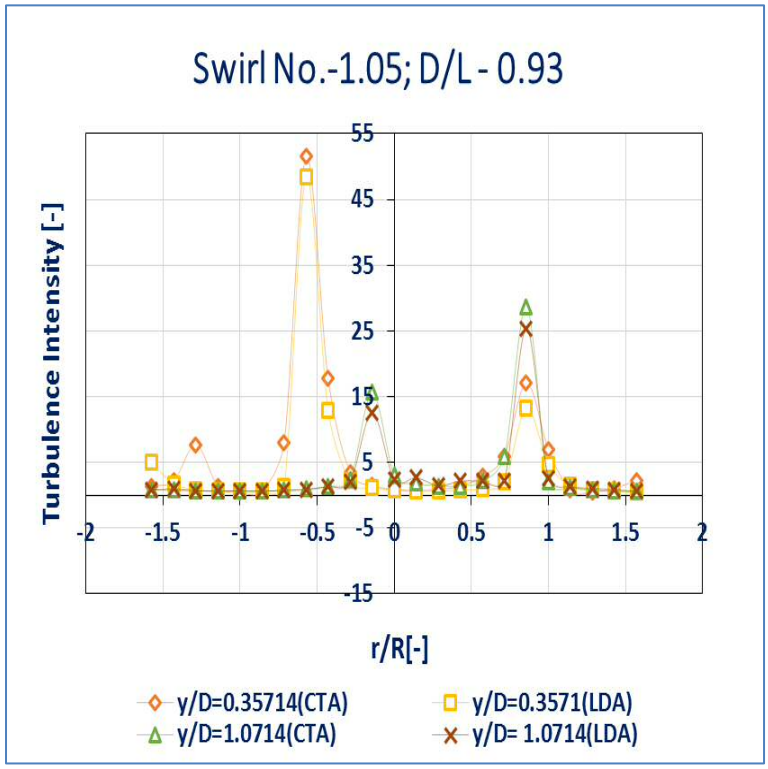

(b)

Figure 4. 3 Turbulence velocity profiles measured with LDA and CTA

4.3 Velocity Profile Variations: Swirl Number Dependence

Swirl number has a profound effect on the velocity of the flow field with a corresponding impact on the flame heat release when the flow perturbations are convected to the flame zone. This section assesses the mean and turbulence velocity variations as a function of the swirl strength.

4.3.1 Mean Axial Velocity Fluctuations: Swirl Geometry Dependence

Two swirl geometries of swirl number of 1.50 and 1.05 were used and the nozzle geometries were kept constant. Figures 4.4 give the mean velocity profiles of the swirling flows for the swirl number of 1.50 for a nozzle diameter to length ratio (D/L) of 0.89 for three ranges of vertical distances of the flow field, (a) 0 y/D 0.3571, (b) 0.4285 y/D 0.7142, (c) 0.7857 y/D 1.0714, respectively. For the range of 0 y/D 0.357, Figure 4.1 (a), the maximum negative velocity of -3.75m/s was found at the centre of the flow axis which indicates the central recirculation of the flow field which spans -0.5 r/R 0.5 with the nozzle diameter at -1 r/R 1. Away from the reversed flow, the mean velocity increases to a maximum value of 4.87m/s at both sides of the high momentum flow regions and then reduces in value away from these regions due to the influence of the ambient air. Within this range of vertical distance, the mean velocity shows marginal variations with the 2mm vertical distance increment, especially in the reversed flow region, which represents the uniformity of the mean velocity within these regions closer the dump plane.

As the measurement probe moves downstream to a range of 0.4285 y/D 0.7142 Figure 4.4 (b), the intensity of the recirculation increases as the maximum negative velocity reaches -4.2m/s. Here the 2mm increment in the vertical height shows no change in velocity except for y/D = 0.7142 which shows minor variations with the rest of the velocity regimes. Further down the flow, 0.7857 y/D 1.0714, Figure 4.4(c), the highest negative velocity returns to -4m/s with increased velocity variations with the 2mm step probe positions. Along the flow axes, the maximum negative velocities span between -4m/s and about 2.8m/s, a range wider than the previous two flow regions. This implies that in the downstream of the flow field, the mean velocity varies in every 2mm step, with corresponding changes in the chemical time scale in each of

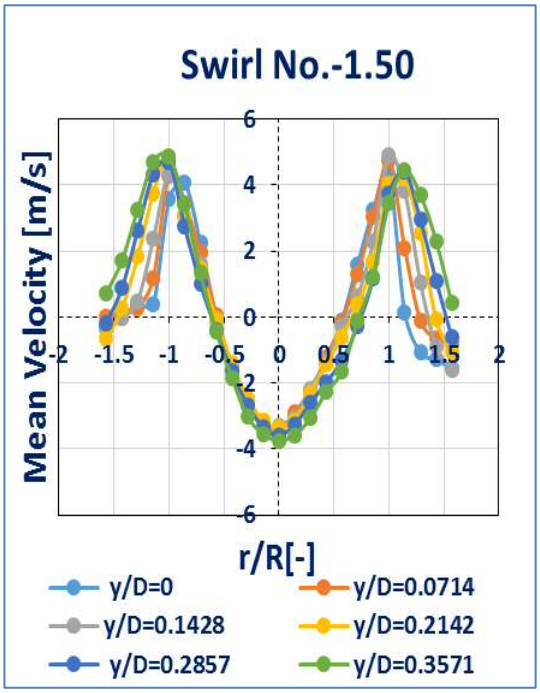

(a)

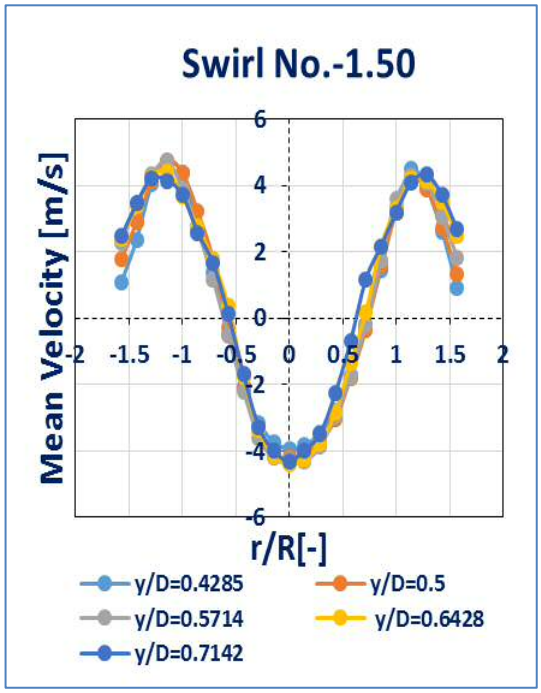

(b)

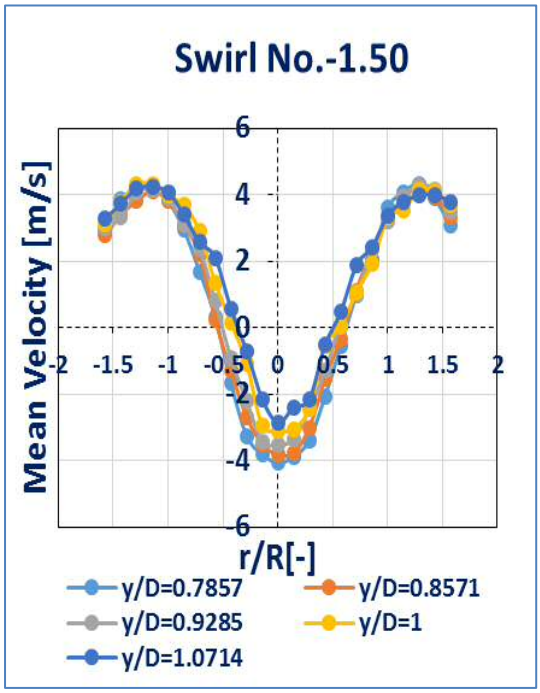

(c)

Figure 4. 4 Mean velocity variations across the vertical axis of the flow field

[(a) 0≤ y/D ≤ 0.3571, (b) 0.4285≤ y/D ≤ 0.7142, (c) 0.7857≤ y/D ≤ 1.0714]

the regions due to changes in the flame speed. Consequently, the heat release rate also fluctuates in these regions. These changes could be attributed to the change in the direction of flow in the HMFR as some gas mixtures enter the reversed flow zone. Thus the presence of localised velocity profiles of the flow with changes in both vertical and horizontal distances are evident.

Figure 4.5 shows the evolution of the mean velocity profiles as the swirl number reduces to 1.05 in three vertical positions of 0 y/D 0.3571, 0.4285 y/D 0.7142 and 0.7857 y/D 1.0714. For the flow field near the dump plane, 0 y/D 0.3571 (a), the mean velocities are seen to be almost similar in both swirl strengths but the CRZ shifts away from the flow axes with the reduced swirl strength. This shift could have a significant impact on the precessing vortex core whose frequency plays a major role in the flame – flow interactions.

Further downstream of the flow, 0.4285 y/D 0.7142 (b), the decreased swirl strength gradually decreases the intensity of the reversed flow in the CRZ as the negative velocity regimes decreases from -4m/s at point 3 (P3) to about -2.3m/s at a higher vertical distance of P4. The CRZ also decreases in size and further shifts away from the flow axes to about r/R = 0.4. At the extreme downstream of the flow field, 0.7857 y/D 1.0714 (c), there is a further reduction in the swirl strength of the lower swirl number. Here at P5 and P6, the negative velocities of the lower swirl strength reduce to a similar value of about -2.12m/s. Also, the negative velocity regime of the higher swirl number at P6 moves farther away from the velocity profiles of P5. In all these it is worthy of note that self-sustaining oscillations impinging on the shear layer are fundamental sources of flow noise and structural loading [198]. The frequency of oscillation is expressed by the Strouhal Number at the shear layer separation as:

St =— (4.1)

where St - Strouhal number, – mean velocity, frequency of oscillation, – initial momentum thickness of the shear layer.

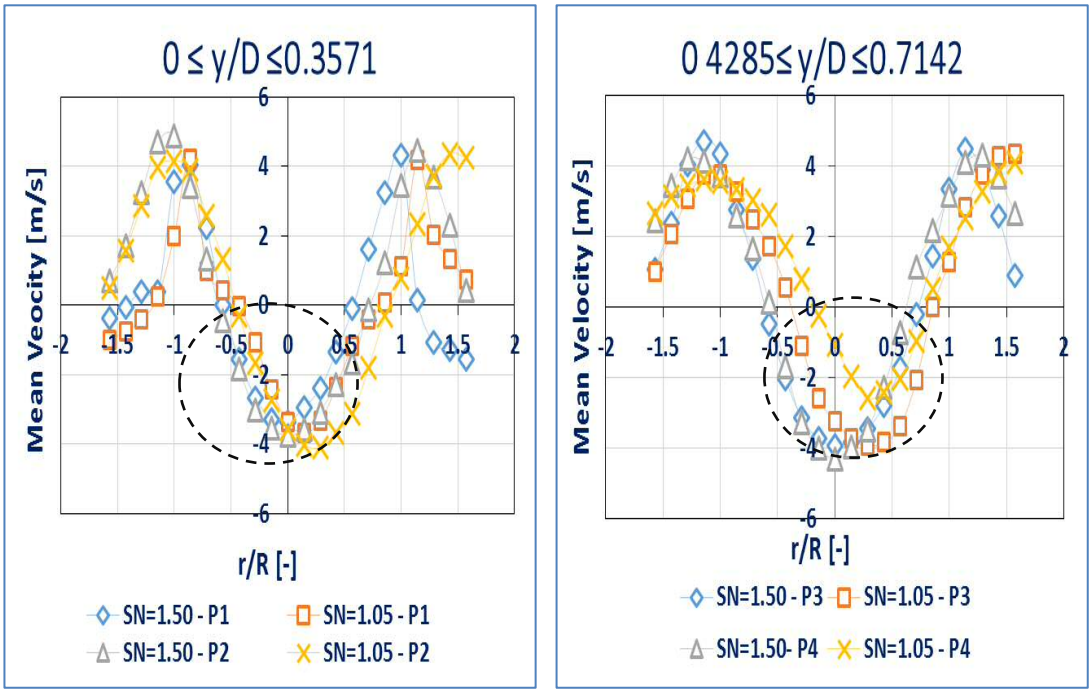

(a) (b)

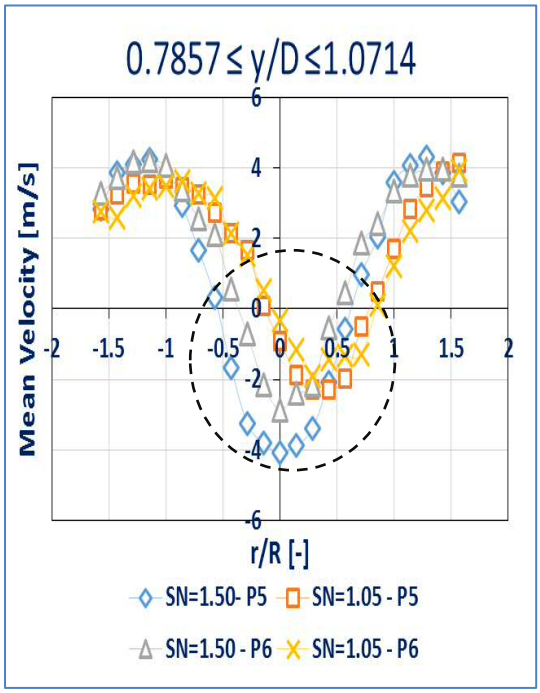

(c)

Figure 4. 5 Mean velocity profiles variations with Swirl Number

Thus the mean velocity substantially affects the oscillation frequency in this case. The evolution of the mean velocity as a result of the variation in the swirl number causes fluctuation in the flow oscillation frequency. If this frequency coincides with other oscillation frequencies like PVC, heat release or dynamic pressure could lead to the amplification of the resultant acoustic mode of the sytem. It is also evident here that the reduction in the swirl strength via the swirl number, reduces the size of the CRZ as well as the flow reversal intensity. The position of the CRZ is also shifted from the axis of the flow with a reduced swirl strength. This is capable of reducing the combustion convective time scales, as the distance between the flow exit from the nozzle and the flame centre of mass is reduced. Time scales of combustion system which are linked to instabilities as expressed:

$$+ \quad = KT \tag{4.2}$$

Where denotes the convective time delay, (the time required for the equivalence ratio perturbation or vortex shedding to convect from its formation point to the centre of mass of the flame) and denotes the chemical time delay, while T and K denote acoustic period and a constant related to the combustor chamber acoustics, respectively [199].

4.3.2 Turbulence Intensity Fluctuations: Swirl Number Dependence

The effect of the swirl strength on the turbulent intensity of the flow field was also assessed. In all the results, a high turbulence intensity was observed in the shear layers of the flow. These layers separarte the CRZ and the HMFR. The turbulence level in other parts of the flow remains less than 1% except at the outer recirculation zone where pockets of turbulence were observed. With a higher swirl numberof 1.50, Figure 4.6, 0 y/D 0.3571 (a), the turbulent intensities at the shear layers rise to about 50% on the left hand side at r/R = -0.6 and about 33% on the right hand side at r/R = 0.65. Away from the HMFR, turbulence intensities of about 20% were observed due to the interaction of the swirl flows with the ambient air.

Downstream of the flow at 0 y/D 0.3571, Figure 4.6 (b), the turbulence level reduces drastically to about 20% on the left hand side but the right hand side remains the same, while the turbulence in the outer recirculation zone disappears. As the swirl number reduces to 1.05 Figure 4.6 (c), the high turbulent intensity of about 50% is only observed at y/D = 0 and y/D = 0.0714 on the left hand side and a turbulence of 45% on the right hand side at y/D = 0. Other regimes in the shear layers remain at about 15% and 10% outside the HMFR. The high turbulence in the shear layers also shifts away from the flow axes. The dynamics of the turbulent intensity is further evident at a higher vertical axis of 0.7857 y/D 1.0714, Figure 4.6 (d), as the turbulence on the left hand side almost appears at the centre of the flow axes with fluctuations in turbulent intensities across the distances. Thus the increased swirl number increases the size of the CRZ, with enhanced mixing and a high turbulence around the shear layers.

The above results have demonstrated the impact of the swirl number on the mean and turbulence velocities of the swirling flows. It changes the intensity of the reverse flow, the size and the shape of the CRZ, with respect to the axis of the flow. This is expected to have strong impact on combustion processes when these variations wrap with with the flame front. Changes in the mean velocity are capable of changing the Strouhal number or the frequency of oscillation impinging on the shear layers, a fundamental contributor to heat release fluctuations.

Most importantly, the results have shown the changes in both the mean and turbulence velocities with as little as 2mm change in the vertical axes of the flow with different swirl conditions which could further complicate the flow and flame fields with corresponding impact on the acoustic fields. With the introduction of variable swirl numbers, the range of turbulence flows could be regulated to give an optimal flow condition that gurantees the stability of the system.

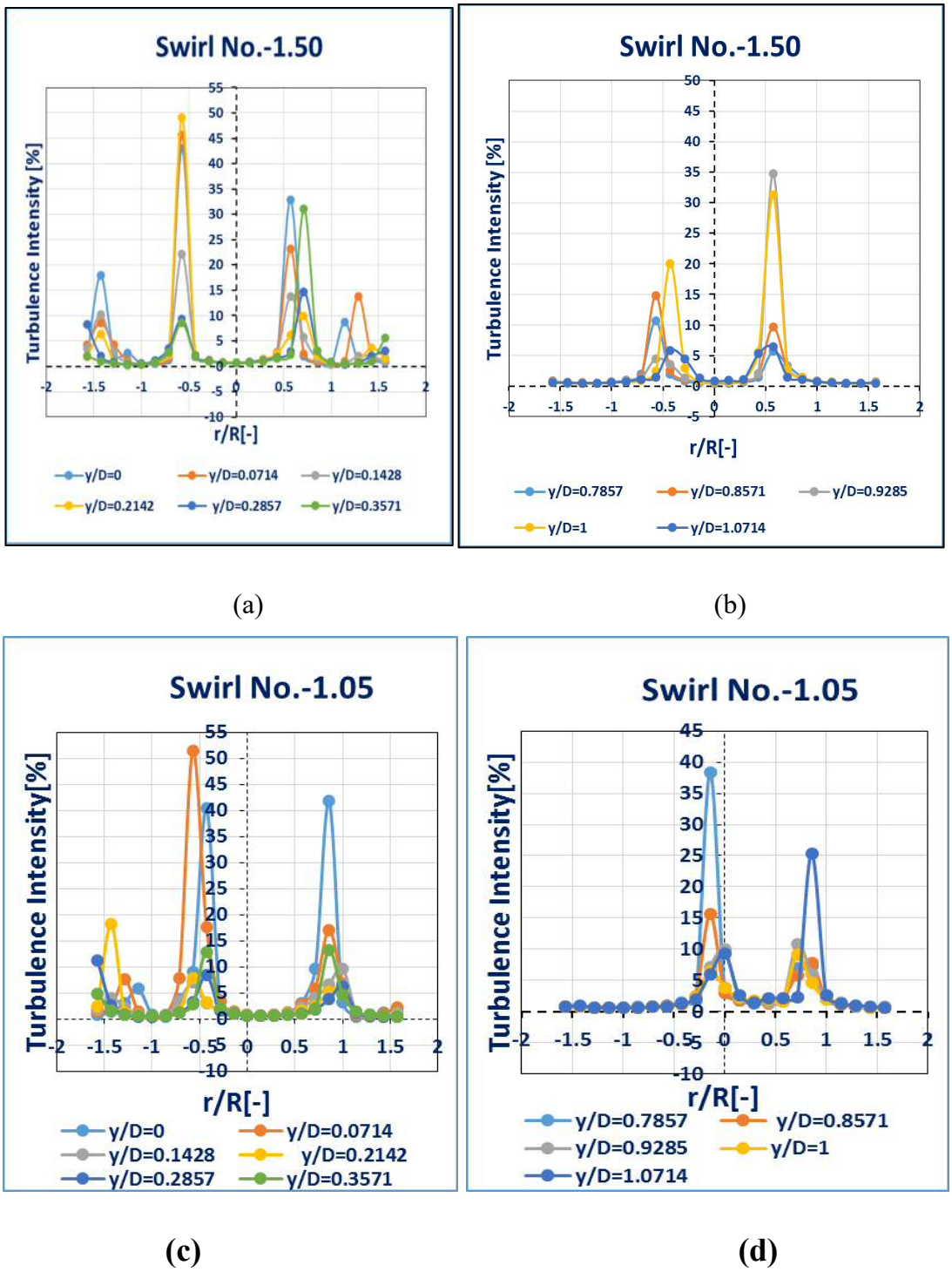

Figure 4. 6 Turbulence Flow Variations with Swirl Number

4.4 External Forcing and Swirl Effects on AMV

The contributions of the external excitation of the flow field, as well as the swirl strength to the variations in axial mean velocity (AMV) in the localised vortical structures, are examined. Figures 4.7 show the variations in the velocity gradient tensor: (a) du/dx and (b) du/dy of the flow field with a swirl number of 1.50 at no excitation condition. These mean velocity variations are convected by the flow to the flame field leading to the distortion of the flame front with a time delay which causes

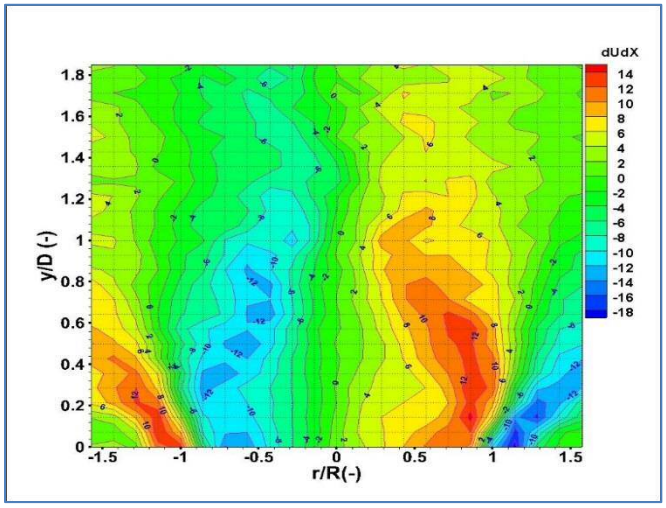

(a)

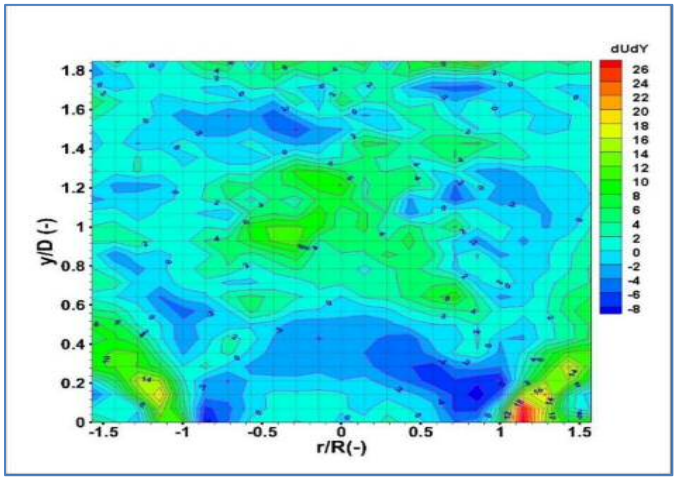

(b)

Figure 4. 7 Velocity gradient tensor: (a) du/dx, (b) du/dy

oscillation in the heat release rate, [43] [117]. When the mass flow is excited with a discrete sinusoidal frequency f_0, the swirl injector responds correspondingly with periodic oscillations of the mass flow rate as reported in the work of Cohem and Hibsman [165] and given by the equation:

$$= \quad [1 + \quad)] \tag{4.3}$$

Where denotes the forcing frequency and , the mean mass flow. By continuity equation, the mass flow fluctuations also oscillate the velocity fields.

$$— + \ . (\tag{4.4}$$

The variations in the swirl intensities also have profound effects on the velocity profiles, thus a good understanding of the combined effects of forcing and swirl strength could be advantageous in modulating the flow oscillation and by extension the heat release oscillation. This section, therefore examines the axial mean velocities within the vortical structures with discrete forcing frequencies using two swirl numbers.

4.4.1 Case I: AMV Variations with Swirl Number of 1.50 and Forcing

Case - I uses a geometrical swirl number of 1.50 with three conditions (unforced and two forced conditions), to examine the axial mean velocities within the vortical structures of the flow field at a constant mass flow rate of 120 l/m. Figure 4.8 shows the vortical structures of the swirling flow without forcing (case 1a). The CRZ here is seen to lie at the horizontal distance of -0.5 r/R 0.5 which is half the radius of the nozzle exit -1 r/R 1, with zero as the centre of the flow axis (r is the radius of the measurement probe from the centre zero and R is the radius of measurement). The negative velocity reversed flow in the CRZ is made up of eight different mean velocity regimes designated by the dotted lines, with different intensities in circumferential modes and different shapes and sizes with respect to the dump plane. These velocity regimes range from -4m/s to -0.5m/s within the CRZ, with the length of the CRZ which lies between 0.8 y/D 1.73 from the dump plane. Because of high swirling strength, it is also observed that some of the velocity regimes in the CRZ have penetrated the inlet annulus which may lead to flashback instability.

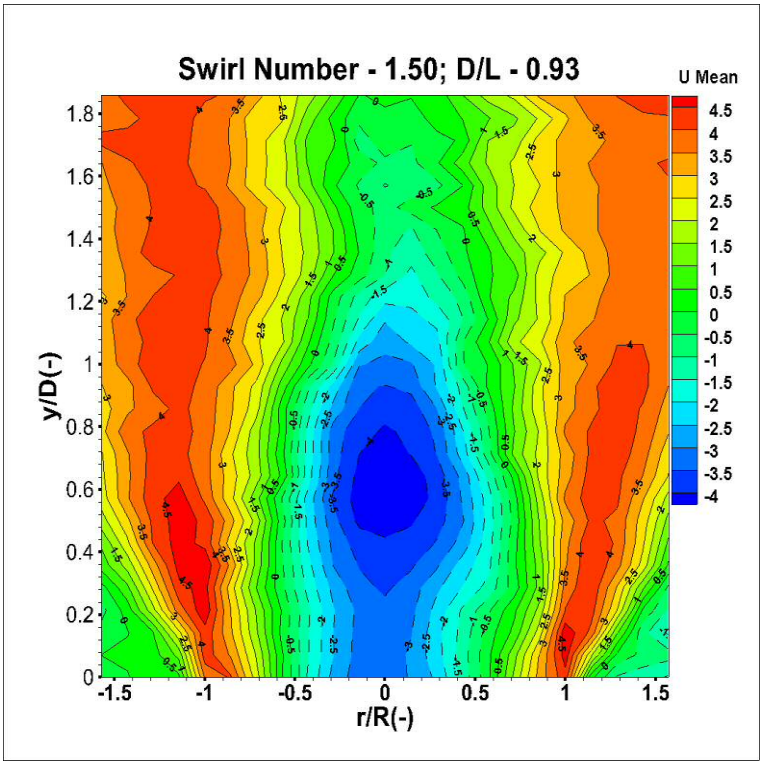

Figure 4. 8 Contour plot of mean axial velocity (Case Ia)

[S – 1.50, Forcing Amplitude 0.2; No Forcing]

The shear layers also show substantial variations from 0.5m/s just after the velocity stagnation layer to 2.5m/s then followed by the high momentum flow region from a velocity of 3.0 m/s to the peak value of 4.5m/s. Any change in the number, incremental values or the size of these velocity profiles produces corresponding effects on other processes both in the flow, flame and acoustic fields. The CRZ length controls the flame length which is a very important component of the convective time scale, a key parameter in combustion instability. The changes in the mean velocity, length and the position of the recirculation zone remain very critical as instabilities is linked to both the length and chemical time scales of the combustion system.

Figures 4.9 present the axial mean velocity profiles for the forcing frequencies of 110Hz (case Ib) and 210Hz Figure 4.10 (case Ic) respectively. The changes in the velocity profiles with reference to the unforced flow are evident. With the forcing frequency of 100Hz, the high mean velocity regime in the reversed flow was reduced from -4.0m/s to 3.5m/s with an increment of 0.5m/s of successive velocity regimes to the highest value of 4m/s in the HMFR.

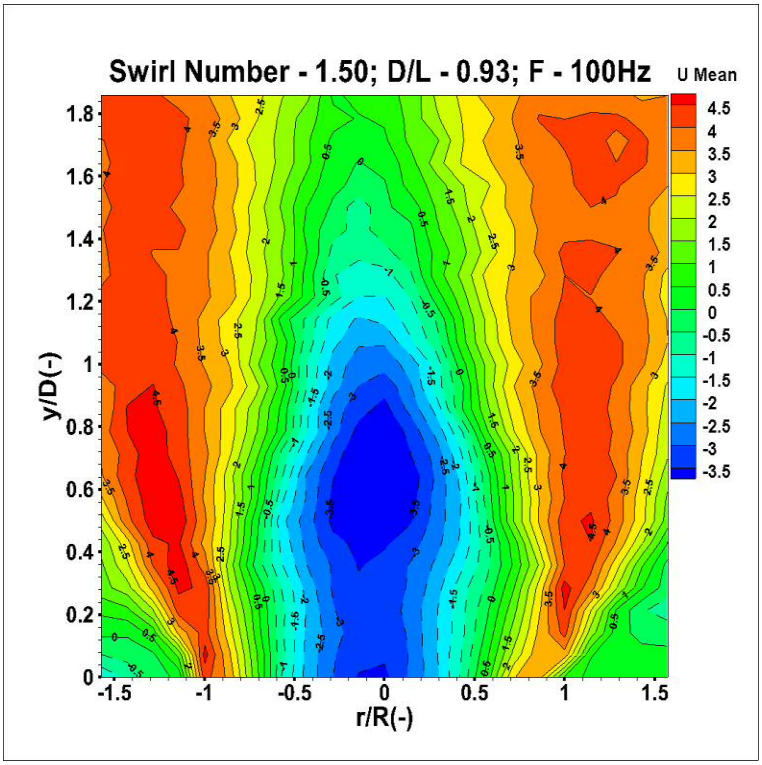

Figure 4. 9 Contour plot of mean axial velocity (Case Ib)

[S – 1.50, Forcing Amplitude 0.2; Forcing – 100Hz]

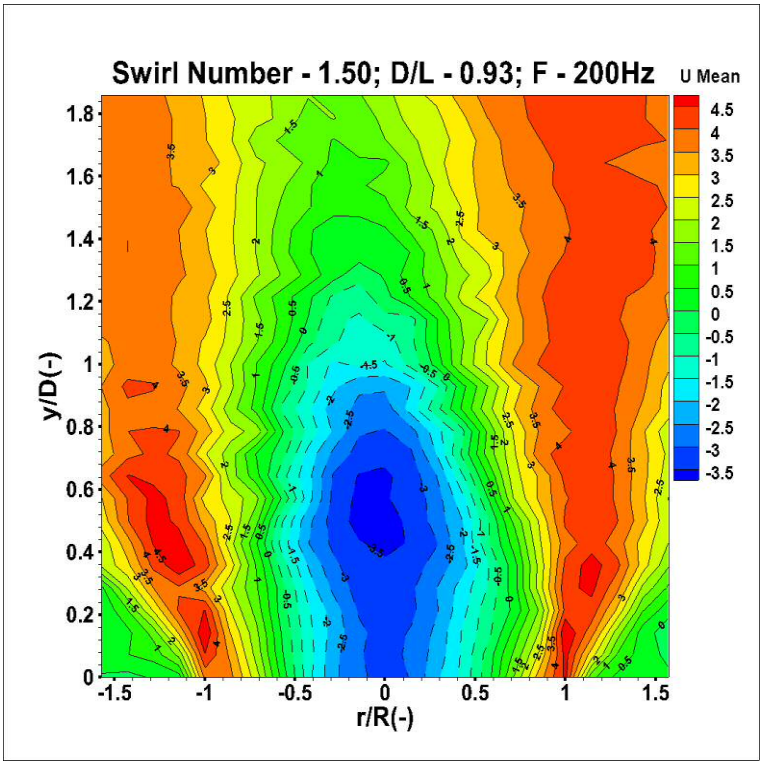

Figure 4. 10 Contour plot of mean axial velocity (Case Ic)

[S – 1.50, Forcing Amplitude 0.2; Forcing – 200Hz]

The number of flow regimes in the CRZ is also reduced from eight in the unforced flow to seven and remains same with increased forcing frequency of 210Hz (Ic). As shown in the figures above, in each forcing condition, changes in the CRZ, shear layers and HMFR were highly significant. Figure 4.11 compares the width and the length of the CRZ as well as its location with respect to the dump plane.

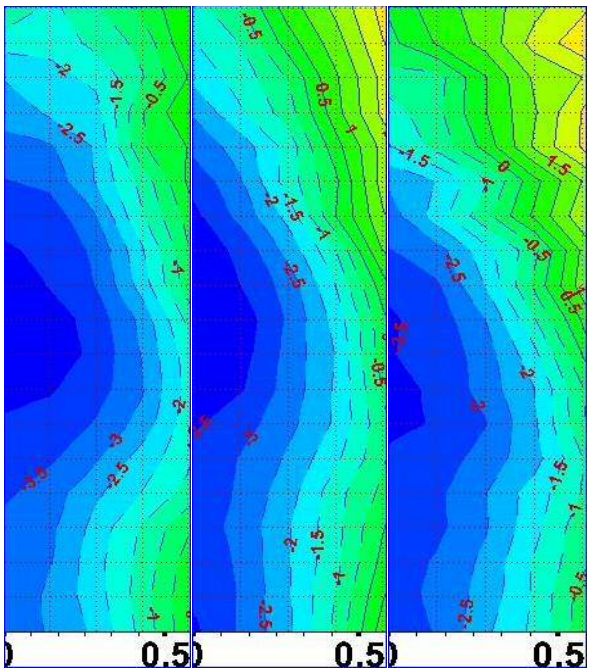

Ia: No forcing Ib: 100Hz Ic: 200Hz

Figure 4. 11 Variations in the width and length of the CRZ with different forcing frequencies: S= 1.50.

The two forcing conditions reduced the number of velocity regimes in the reversed flow region as well as the length of the CRZ downstream of the flow field. It can be seen that increased forcing draws the high recirculation region towards the dump plane, increases the width of the CRZ and lowers the entire recirculation region towards the exit nozzle. With these, the convective time between the gas mixture exit and the complete reaction of the mixture at the flame zone could be significantly varied due to the changes in the length of the CRZ. These show that the size of the CRZ could be further varied at constant swirl strength by different forcing levels. The use of a variable swirl [89], thus provides a wider range of control of the reversed flow intensity, by extension the control of the flame and acoustic dynamics.

The variations in the size and location of the CRZ also have corresponding effects on other vortical structures such as the shear layers. Figure 4.12 compares the variation in the HMFR and shear layers with the three cases.

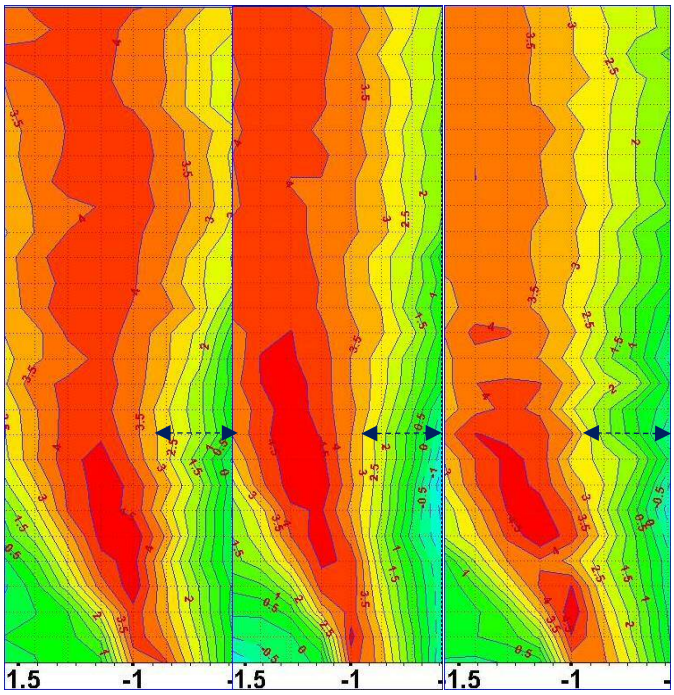

Ia: No forcing Ib: 100Hz Ic: 200Hz

Figure 4. 12 Variations in the width and length of the HMFR with different forcing frequencies: S= 1.50.

With increased forcing, the width of the HMFR is reduced and the entire region is moved away from the CRZ as it draws near the dump plane, thus the width of the shear layers becomes widened as indicated by the black arrows. The high mean velocity regimes in the HMFR are drastically reduced in length and are pushed towards the dump plane. At a higher forcing frequency of 200Hz, the region becomes split into small domains. As would be shown in the next chapter, this widening of the entire flame size increases the total flame surface area, a parameter which controls the global heat release [131] and the fluctuation of these flame structures results in oscillation in the heat release rate.

4.4.2 Case II: AMV Variations with Swirl Number of 1.05 and Forcing

The evolution of the axial mean velocities within the vortical structures of the flow field with variations in the level of forcing was also examined with a reduced swirl strength with a swirl number of 1.05. Figure 4.13 shows the flow structure of the localised mean velocity variations for the above-mentioned swirl condition with no external excitation. The reduction in the swirl number produces many changes both in the CRZ and the HMFR. The number of the velocity regimes in the reversed flow of the unforced condition is reduced to seven, indicated by the dashed lines with a maximum negative velocity of -3.5m/s. The same maximum velocity regime was observed at the tip of the nozzle rotating and penetrating the annulus, with many of these negative velocity regimes penetrating the nozzle. The swirling strength becomes stronger with the appearance of a higher negative velocity regime of -4m/s while the -3.5m/s velocity merges with the one penetrating the nozzle at the forcing frequency of 110Hz, Figure 4.14. The CRZ also elongates and the oval section of the velocity regimes moves slightly further away from the dump plane.

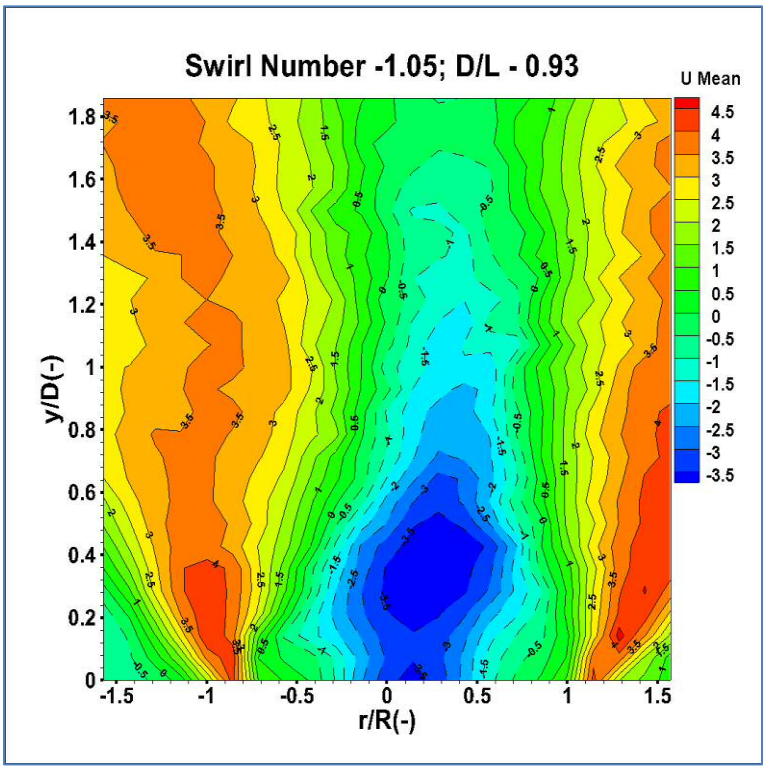

Figure 4. 13 Contour plot of mean axial velocity [S – 1.05, No Forcing] (Case IIa)

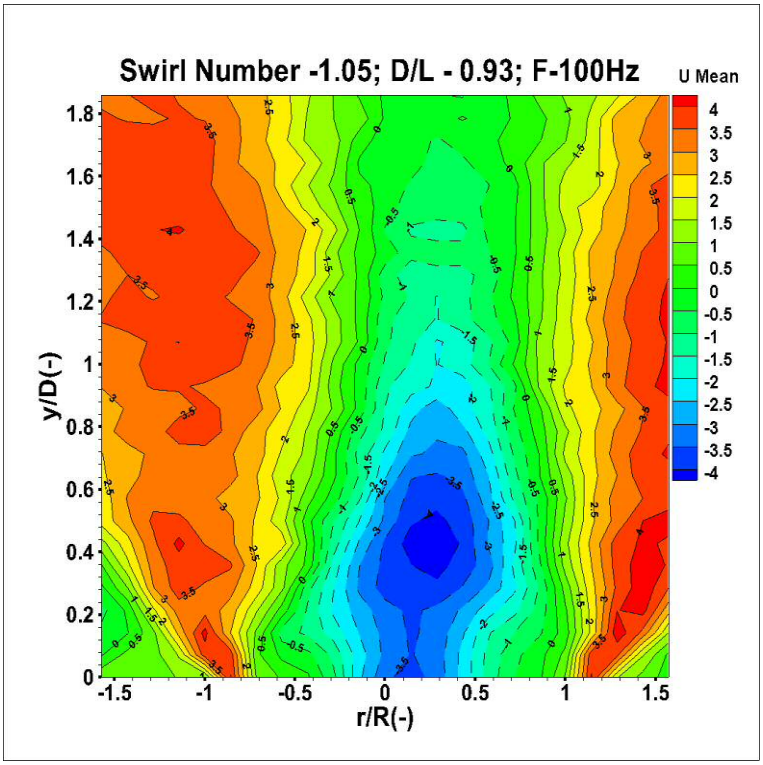

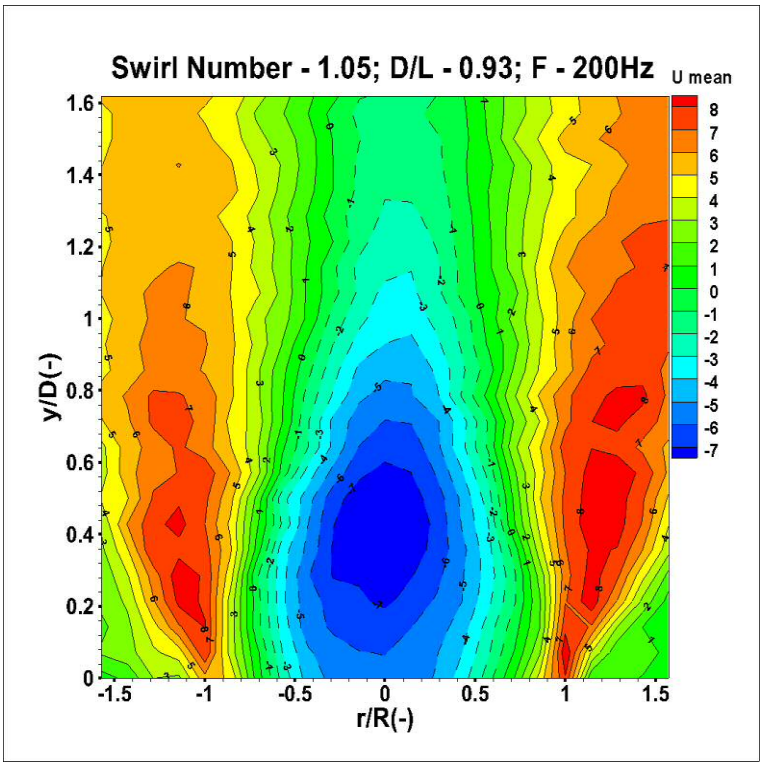

Figure 4. 14 Contour plot of mean axial velocity [Case IIb and IIc]

[S – 1.05, Forcing-100Hz (up) (case IIb) and Forcing – 200Hz (down)(caseIIc)]

Case IIc with a forcing frequency of 200Hz experiences a higher negative mean velocity of -7m/s with enlarged sizes of the velocity regimes. The -6m/s regime circulates close to the dump plane while the –5m/s regime actually penetrates the nozzle annulus. The CRZ increases both in length and in width and draws the high velocity regimes nearer to the dump plane. As was the case in the higher swirl number, this reduced swirl strength also shows the evolution of the position and size of the CRZ with increased excitation. Figure 4.15 compares the sizes and the locations of the CRZs of the three cases. From the figures, it can be seen that the bahaviour of the CRZ of this lower swirl strength at various conditions are similar to those of the higher swirl strength although in this case, with a smaller length of the CRZ. With increased forcing, the regions with higher mean velocities are drawn towards the exit nozzle with enlarge width of the CRZ. Also with increased forcing, the axis of the CRZ which was initially away from the centerline of the nozzle gradually aligns with the flow axes.

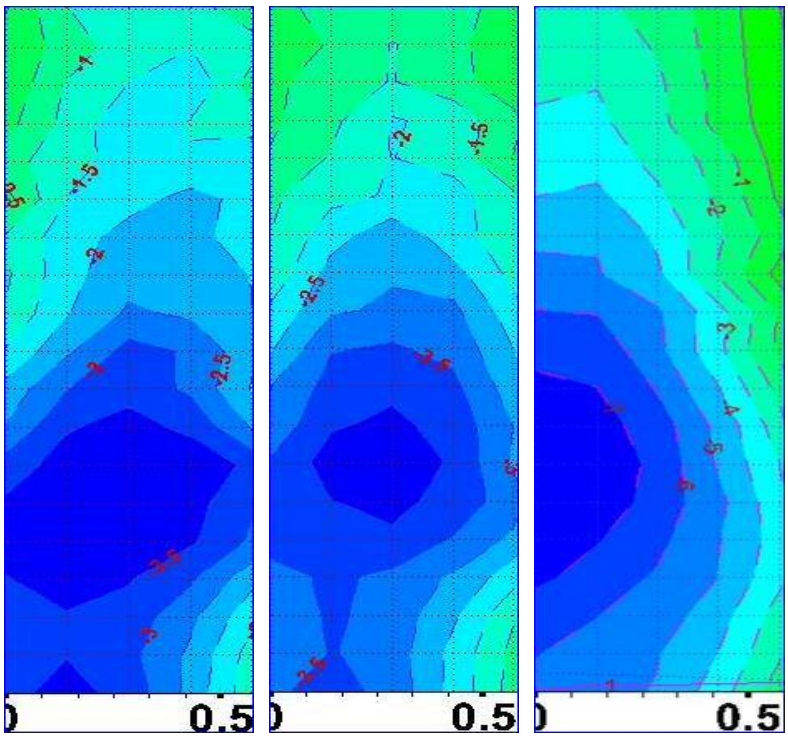

IIa IIb IIc

Figure 4. 15 Variations in the width and length of the CRZ with different forcing frequencies: S= 1.05

[Case IIa: Swirl Number – 1.05, Forcing - 0Hz Case IIb: Swirl Number – 1.05, Forcing - 100Hz Case IIc: Swirl Number – 1.05, Forcing - 200Hz].

4.4.3 Comparison of Swirl Strength and Forcing on Flow Conditions

Figures 4.16 and 4.17 compare the mean velocity profiles of the CRZ and the HMFR respectiely, for the two swirl numbers with the forced conditions. Their differences are summarised thus:

- A higher swirl number of 1.50 possess a higher swirl strength than the 1.05 swirl.
- The increased swirl strength increases the turbulence both in the shear layers and the HMFR.
- In both cases, the 100Hz forcing frequency stretches the length of the CRZ with increase number of velocity regime entering the nozzle annulus.
- In both cases, the higher forcing frequency of 200Hz increases the size of the CRZ and draws the high velocity regimes further upstream of the flow closer to the nozzle dump plane.
- The higher swirl number of 1.50 shows a slimmer width of the HMFR but an expended shear layers and vice versa as a result of increased turbulence.
- In each of the swirl number, the size of the HMFR reduces while the shear layers expands with increased turbulence as the forcing frequency is increased.
- The high velocity regimes in the HMFR becomes split with increased forcing frequency.

These results all agree with many swirl flow studies [43][59] [53] [200].

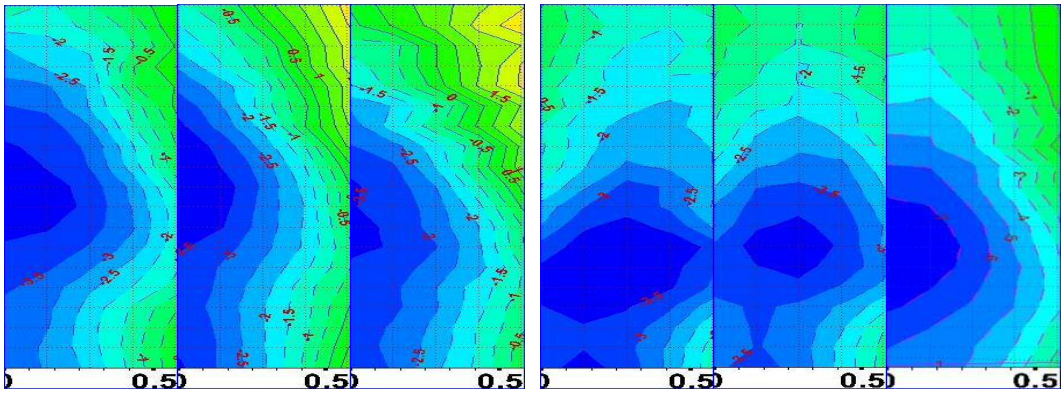

Ia Ib Ic IIa IIb IIc

Figure 4. 16 Mean velocity profile variations in the CRZ with different swirl and flow conditions.

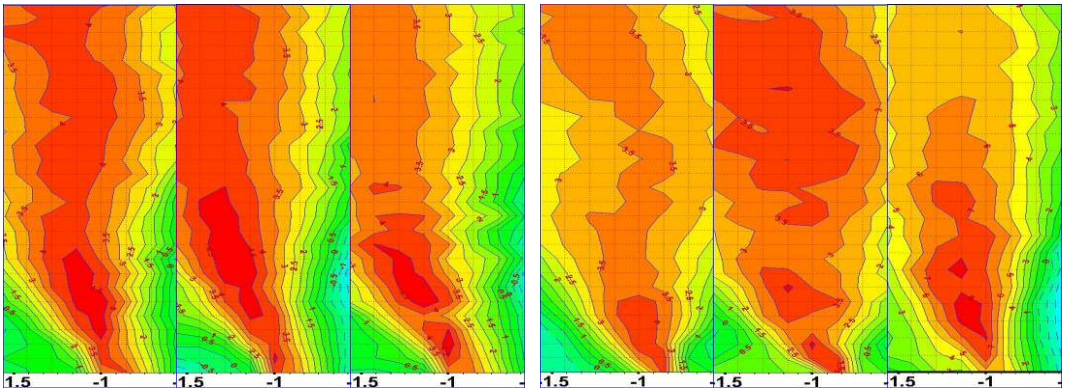

Ia Ib Ic IIa IIb IIc

Figure 4. 17 Mean velocity profile variations in the HMFR with different swirl and flow conditions

Figure 4.18 compares the variation in the height of the mean velocity regimes in the CRZ of the two swirl numbers with the three flow conditions.

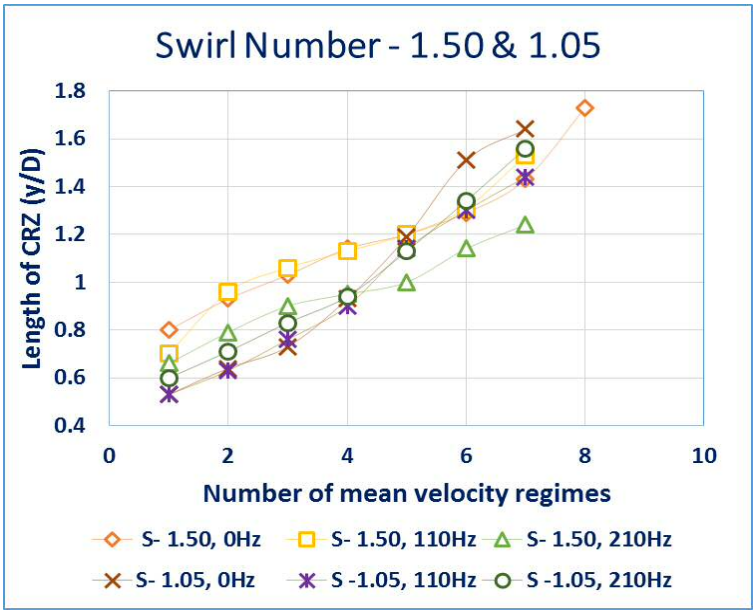

Figure 4. 18 Fluctuation of the length of the negative velocity regimes in the CRZ with different swirl and forced flows

The swirl number of 1.50 has the highest number of negative velocity regimes but reduces when forced with the other two forcing frequencies. The length of various negative velocity regimes in terms of the vertical distance y/D downstream of the flow increases slightly with the 100Hz forcing and reduces significantly with the 200Hz. In the 1.05 swirl number the length of the velocity regimes remains same in the high

velocity region but reduces significantly at lower negative velocity regimes with the two forcing frequencies.

The above discussions all show that the size of the CRZ which represents the intensity of the reversed flow is controlled by the swirl number. The results further reveal that the level of the reversed flow could be further altered by forcing the flow with discrete sinusoidal frequencies. Therefore the use of the swirl number and frequency could provide a wide range of the magnitude of the reversed flow. This range of reversed flow could be advantageous since the size of the CRZ is a key factor of the acoustic period of the combustor.

4.5 External Forcing and Swirl Effects on Flow Turbulence

Changes in the swirl number and forcing have corresponding effects on the turbulence scale of the flow field resulting in flame speed and flame surface area oscillation. They all culminate in flame heat release fluctuations, a dominant factor which influences combustion instability. This section considers the evolution of the turbulence levels in terms of the root mean square velocity within the vortical structures of the flow field, under isothermal conditions. Three cases are considered: The first being the lower swirl number with a nozzle diameter to length ratio of 0.93, the second case uses a higher swirl number with the same diameter to length ratio and finally the last case uses similar higher swirl number with a diameter to length ratio of 1.86.

4.5.1 Case I: Swirl Number of 1.05; Nozzle DLR of 0.93

Case 1 investigates the evolutions of the localised turbulence level with a low swirl number of 1.05 and four forcing conditions. Figure 4.19 presents the turbulence velocity profiles of the unforced flow, Figures 4.20 show the profiles for the 100 and 150 Hz forcing, while Figure 4.21 shows the profiles for 200Hz forcing. In all the profiles the effects of both the swirl strength and forcing are quite significant. With no forcing, the turbulence levels range from 1 to 4m/s with the highest level of 4m/s in the shear layers due to an enlarged width of the CRZ close to the dump plane (y/D 2). These high levels of turbulence cover large circular areas within these regions on the two shear layers. The next successive turbulence region of 3.6m/s becomes elongated and moves downstream of the flow field to y/D = 0.5. There is a reduction in the turbulence scale of the other successive regimes downstream of the flow to a

turbulence of 1.8m/s. The level of turbulence in the CRZ is observed to be lower within the range of 2.6 m/s because of the reduced pressure. Changes in the localised turbulence is evident especially in the shear layers with the forcing. Changes in the turbulence levels were evident with the forcing of the flame with a frequency of 100Hz. There was a reduction in the size of the high turbulence regimes such as 4.0 and 3.8 m/s as they also move closer to the dump plane. The number of turbulence zone was also increased indicated by the more complex "velocity line" especially within the HMFR.

The increased forcing of 150Hz further reduced the sizes of the high turbulence regimes with the splitting of the low turbulence profiles around the CRZ. Other lower turbulence regions became slender in size and elongated downstream of the flow. With further increase in the forcing frequency to 200Hz, the number of turbulence regions was drastically reduced evidently by the fewer regular turbulence domains. However, the turbulence levels within small regions near the dump plane became extremely high to the range of 0.7m/s.

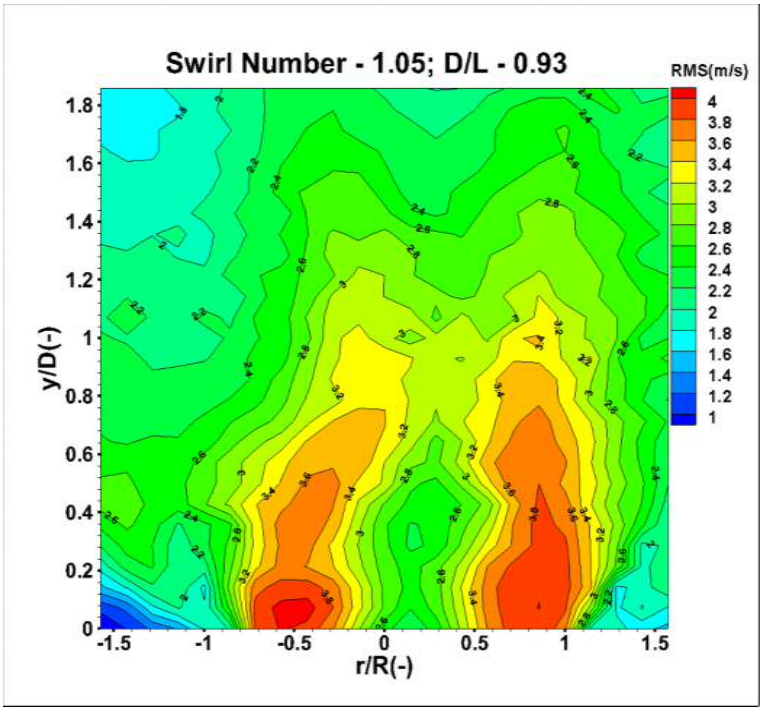

Figure 4. 19 Turbulence velocity profiles [S-1.05; No Forcing]

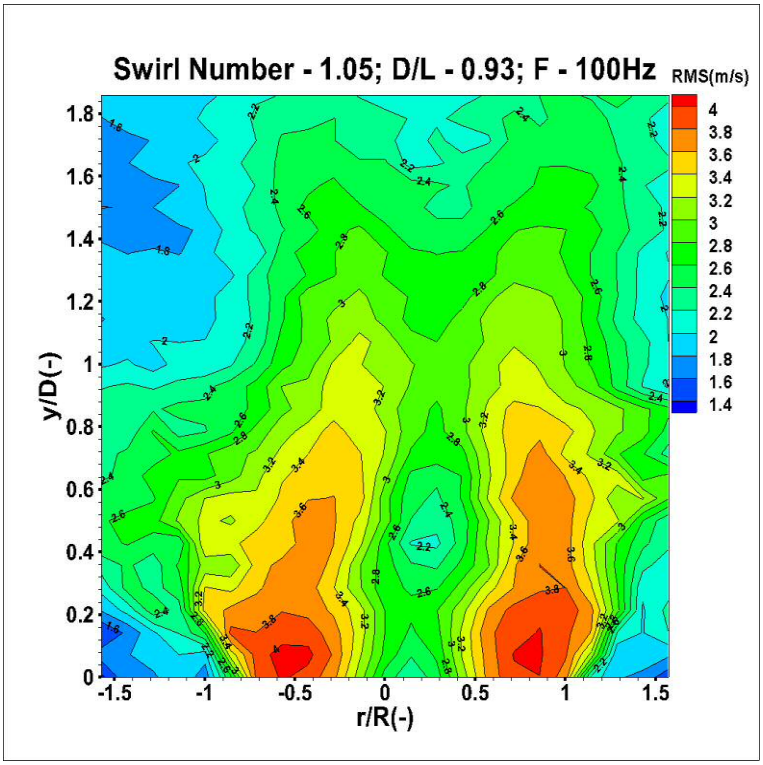

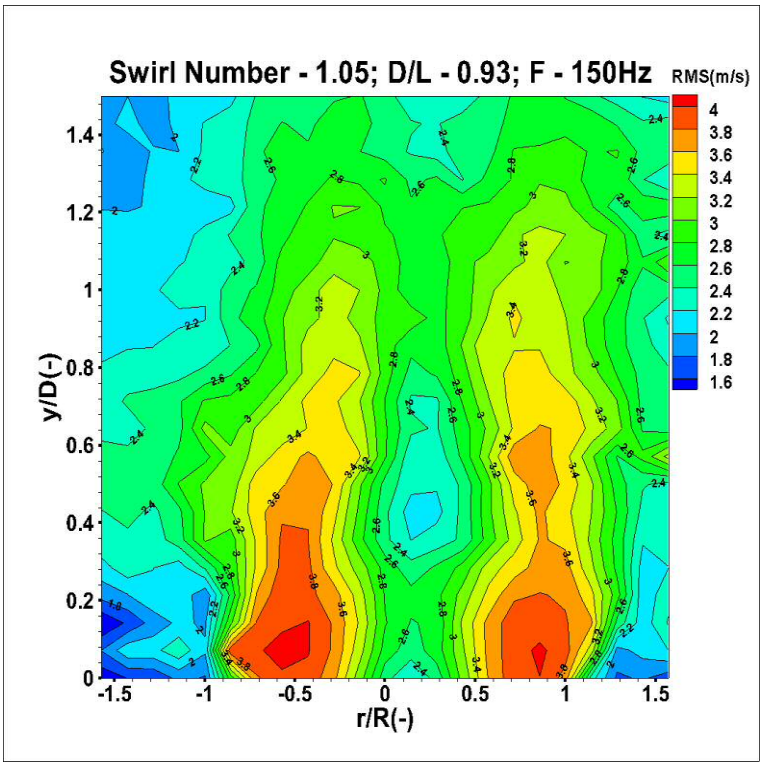

Figure 4. 20 Turbulence velocity profiles [S-1.05; Forcing – 100Hz (up); 150Hz (lower)]

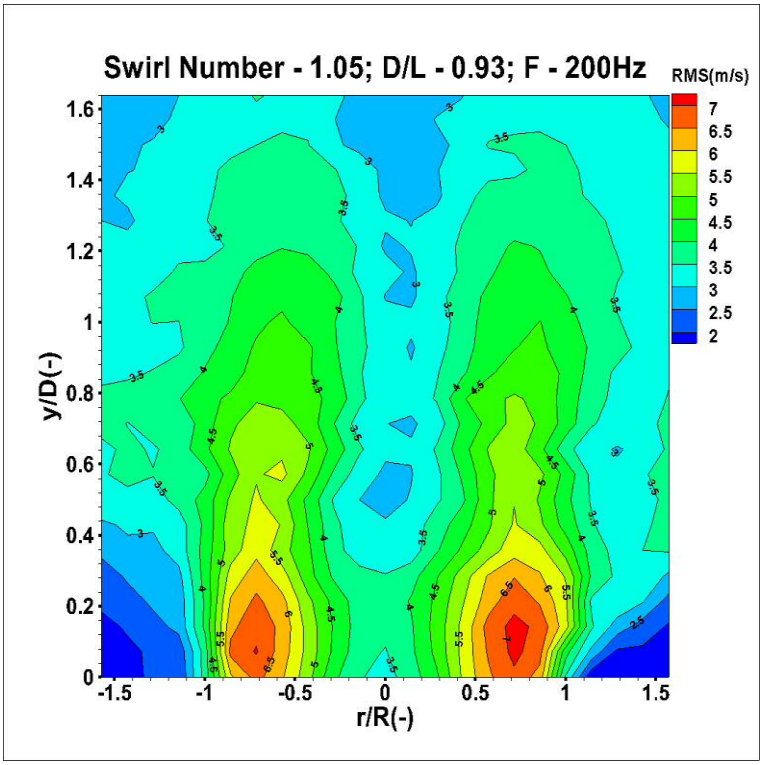

Figure 4. 21 Turbulence velocity profiles [S-1.05; Forcing – 200Hz]

These have clearly shown the combined effects of the swirl and forcing on the turbulence scale of the flow field. With this specific swirl number of 1.05, forcing resulted in the reduction of the sizes of the high turbulence regimes in different domains of the flow field and pushed the regions closer to the dump plane. Also, there was a reduction in the complexities of the turbulence level at higher forcing levels. These variations in turbulence scale across the flow field modulate the flame surface areas and flame speed with corresponding impacts on the convective and chemical time scales respectively. The overall impact on the flame is the fluctuation in the gain and phase of heat release rate.

4.5.2 Case II: Swirl Number of 1.50; Nozzle DLR of 0.93

The turbulence fluctuations in the flow field was also examined with three forcing conditions with an increased swirl strength of S= 1.50. Figure 4.22 presents the plot for case I of the unforced flame with a swirl number of 1.50. The increased swirl strength elongates the high turbulence regions and moves them away from the dump plane on the left hand side of the shear layers. While on the right hand side, the width of the high turbulence region remains almost the same, but is also detached from the dump plane and moves down the flow field. This is because the increased swirl number has increased the size of the CRZ and stretched it down stream of the flow, thus

developing a stretched turbulence level along the shear layers which are due to the interactions between the HMFR and the CRZ. The increased swirl strength also complicates the turbulence scale of the flow field due to the increased flow recirculation which goes in opposite direction with the HMFR region. A reduced turbulence region was also observed at the downstream of the CRZ region which could be attributed to the reduced pressure and the flow reversal.

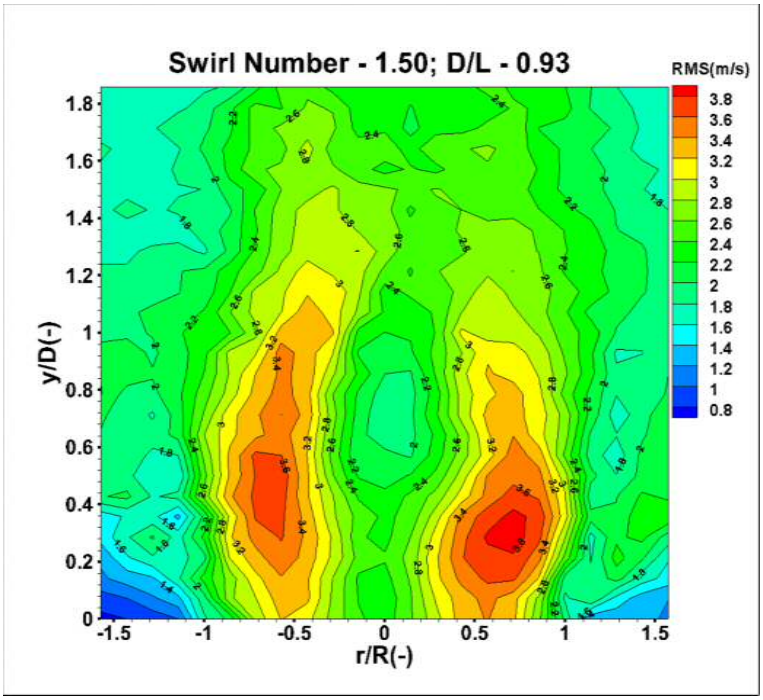

Figure 4. 22 Turbulence Variations in shear layers (S-1.50; D/L-0.93)

In the other two cases, forcing frequencies of 100 and 200Hz were applied to assess the flow field response to the combined effects of the increased swirl and forcing, Figures 4.23. With 100Hz forcing frequency, the high turbulence region of 3.8 m/s disappeared while reducing the sizes of other high turbulence domains as compared to the unforced flow

The high turbulence regions moved further away from the dump plane and the turbulence structures become more regular which indicates the uniformity of the turbulence scale of the flow. With increase forcing of 200Hz, on the left hand side, the 3.6m/s turbulence changes to a rectangular geometry while the 3.4m/s irregular regime was stretched longer towards the opposite shear layer which separates the outer recirculation zone. There was a reduction in the length of the other lower turbulence

regimes as the broader section moves closer to the nozzle. On the right hand side, the high turbulence regions also moved upstream of the flow with regular structures.

These results show that increased swirl strength increases the length of the turbulence region along the shear layers and complicates the turbulence scale of the flow field due to the increased size of the CRZ and swirl intensity respectively. With forcing, the high turbulence regions disappears, the sizes of others are reduced while the entire turbulence structures became more regular.

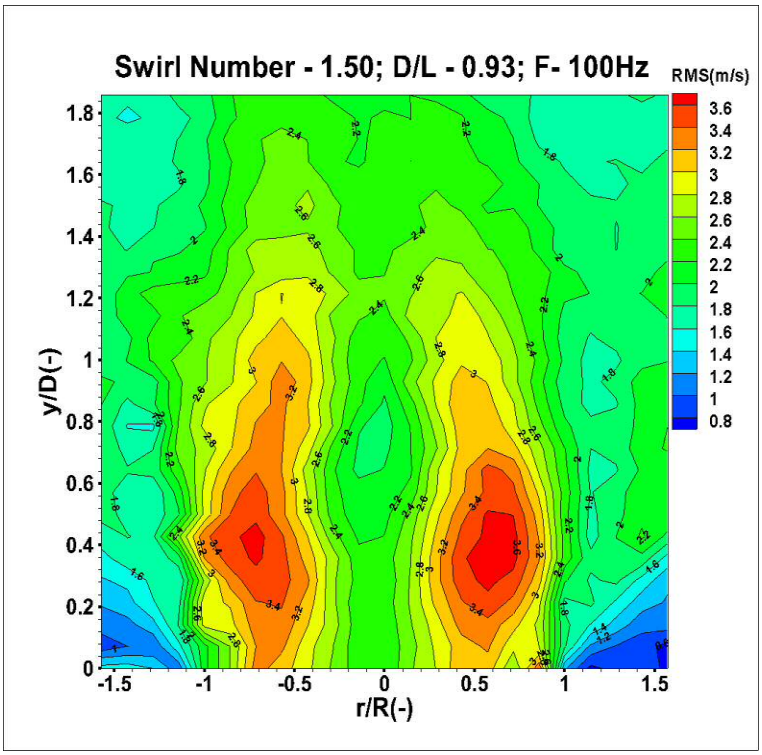

Figure 4-23 (a): Turbulence Variations in shear layers (S-1.50; D/L-0.93; F- 100Hz.

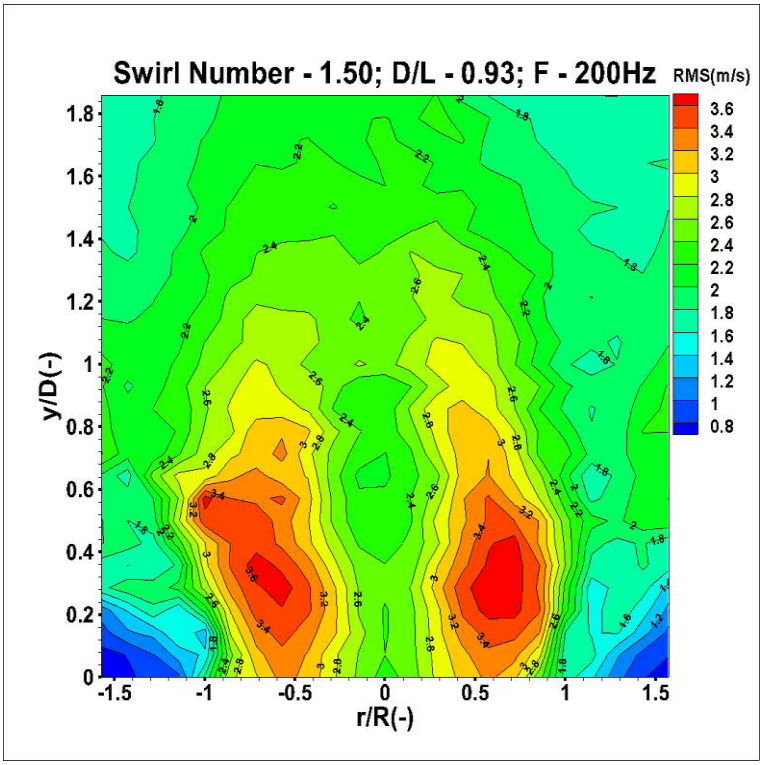

(b)

Figure 4. 23 Turbulence Variations in shear layers (S-1.50; D/L-0.93; F- 200Hz

4.5.3 Case III: Swirl Number of 1.50; Nozzle DLR of 1.86

Case III repeats the same swirl number of 1.50 of case II but with a change in the nozzle diameter to length ratio of 1.86 which means that the nozzle length is reduced by half. The effects of this reduction on the turbulence scale of the flow field were then investigated. Figures 4.24 show the turbulence variations for the 100 and 150Hz forced flames. These flow conditions produced significant changes in the turbulence scales compared to case I and II. In comparing the 100Hz forcing conditions of case II and III, it was observed that the width and length of the turbulence regions around the shear layers became significantly reduced to thin short regions very close to the exit nozzle.

Successive reduced turbulence regimes along the shear layers became very regular with larger domains downstream of the flow with similar turbulence scales. The width of the turbulence regions was further reduced with the increased forcing of 150Hz. The sizes of the high turbulence regimes became very small and were pushed very

close to the dump plane. The region of low turbulence downstream of the flow also increased as indicated by the deep blue colour map. With further increased in forcing level to 200Hz, the turbulence level downstream the flow was further reduced to the range of 1.8 to 1.6 m/s which covered larger regions downstream of the flow. There was also a reduction in the length of the thin turbulence structures around the shear layers, an example being the reduction of the 2.2 m/s turbulence regime from the height of y/D = 1.4 in the 150Hz forced condition to below y/D = 1.2 in the 200Hz forced condition, Figure 4.25.

It is therefore evident that the variation in the length of the nozzle can influence the fluctuations in the turbulence scale of the flow field. In this particular case, the reduction in the nozzle length reduced the length of the flame and a reduced interaction between the air that penetrate the nozzle and the incoming fresh gas mixture. As a result, the turbulence concentrated along the shear layers with more regular structures around the flame zone near to the dump plane. Just as in other previous cases, the forcing also affected the turbulence scale with a reduction in the sizes of the turbulence structure which moved further closer to the nozzle at high forcing levels

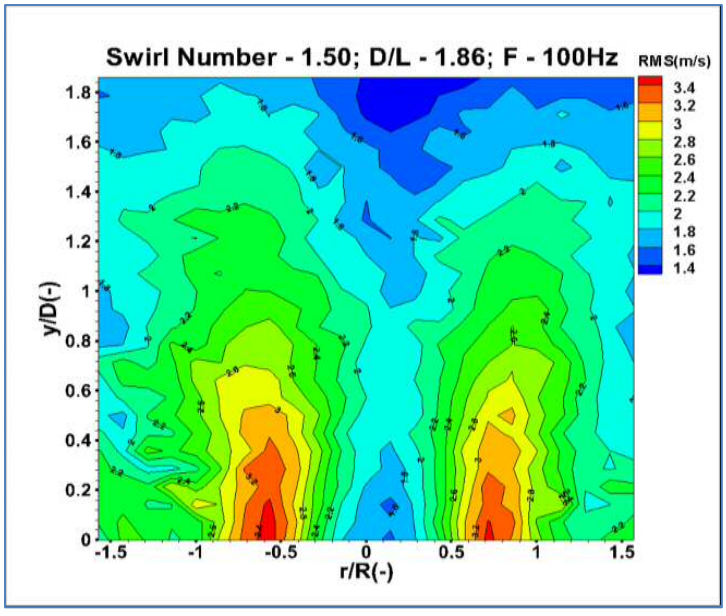

Figure 4-24 (a): Turbulence velocity profiles [S-1.50; D/L -1.86; Forcing – 100Hz

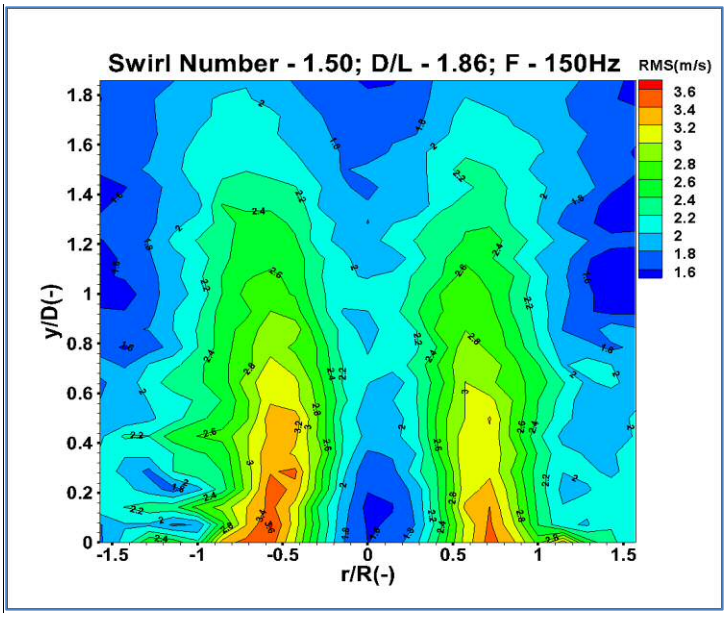

(b)

Figure 4. 24 Turbulence velocity profiles [S-1.50; D/L -1.86; Forcing –150Hz

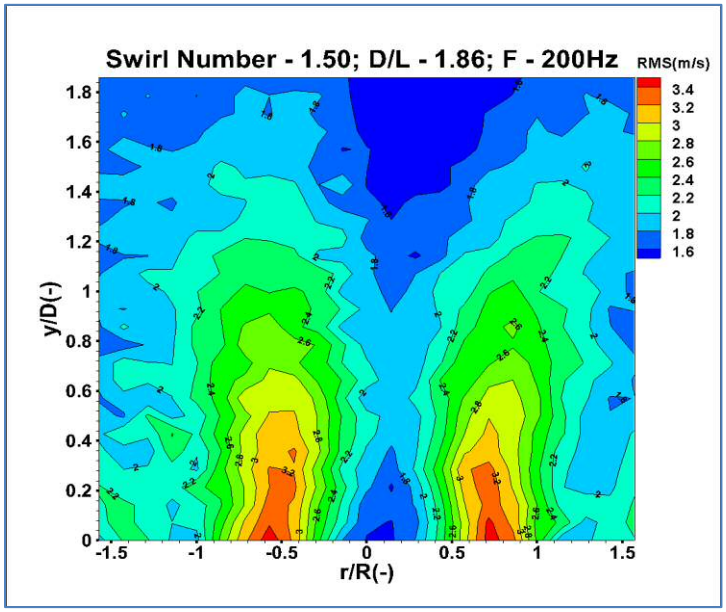

Figure 4. 25 Turbulence Variations in shear layers (S-1.50;D/L-1.86)

4.5.4 Comparison of Turbulence Cases

Figures 4.26 compare the turbulence levels of the three cases. It is clearly shown that turbulence in the flow field is a very important parameter that influences the combustion chemical and convective time scales, depending on the swirl and forced conditions. Increasing the swirl strength elongates the turbulence region down the shear layers. The region could also be pushed towards the dump plane by reducing the nozzle length. Apart from the swirl and nozzle geometries, forcing provides another path to influencing the turbulence scales. With increased forcing, the width and the length of the turbulence zone within the shear layers are reduced, but with high turbulence intensities. From the stand point of combustion instability control, these variations in turbulence with different swirl and forcing conditions could serve as the basis to modulate the chemical and convective time scales of the combustion system and control the heat release rate in such a way that the dynamic pressure and the heat release signals are kept out of phase.

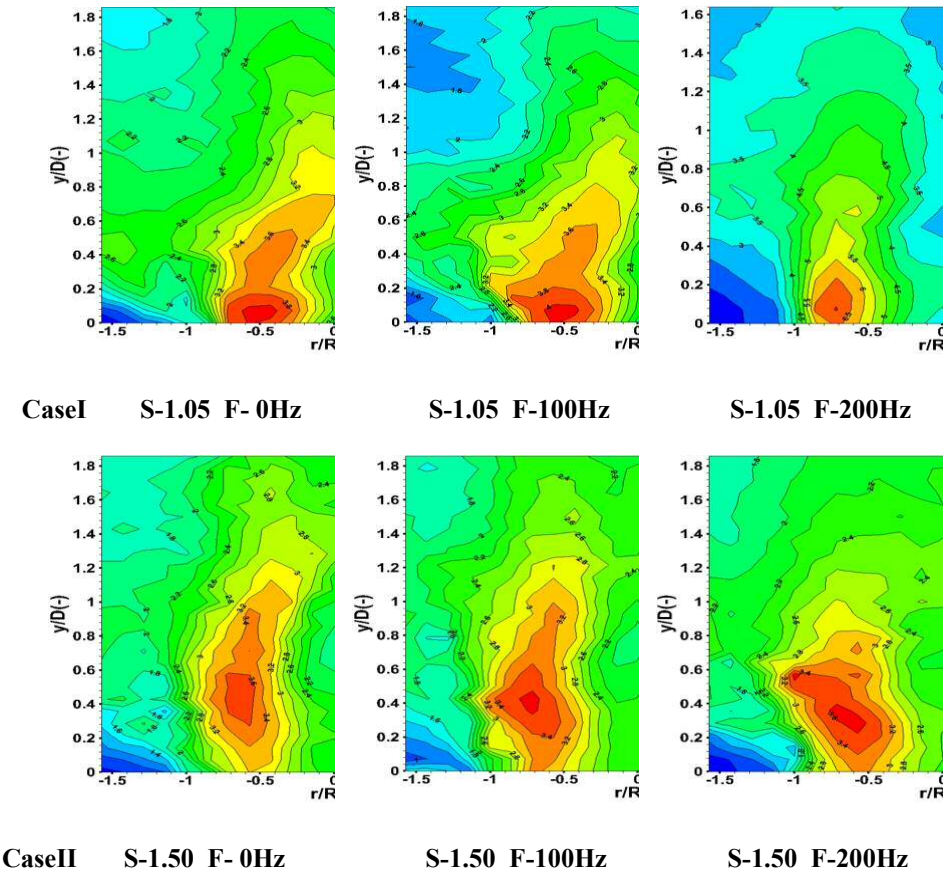

Figure 4-26 (a): Turbulence Variations in the shear layers of the flow field with various swirl and forced conditions.

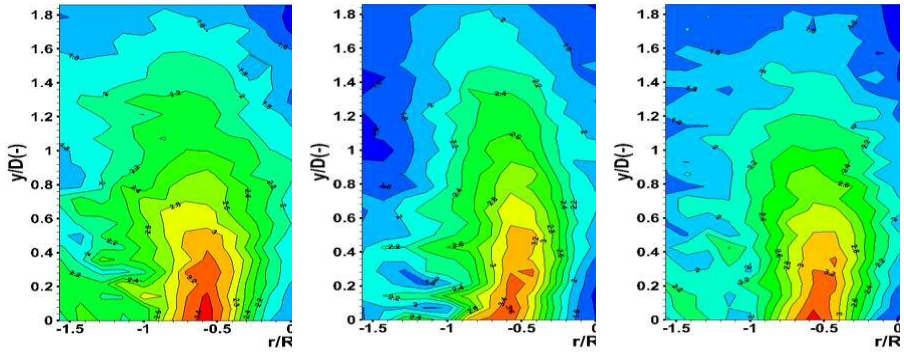

Case III S-1.50 F- 100Hz S-1.50 F-150Hz S-1.50 F-200Hz

(b)

Figure 4. 26 Turbulence Variations in the shear layers of the flow field with various swirl and forced conditions

4.6 Summary

The vortical structures of the flow field change with variations in the swirl and forcing conditions. This evolution is convected to the flame with the resulting contortion and convolution effects which lead to heat release fluctuations. With appropriate conditions of the heat release oscillation with the dynamic pressure of the combustor, the inherent acoustic mode is excited which could grow to destructive amplitudes at limit cycle. This chapter used the mean axial velocities and turbulence intensities of the flow field at various swirl and forcing conditions to examine the evolution of the vortical structures.

The results showed that increased swirl number increased the swirl strength by increasing both the length and width of the CRZ; increased the turbulence scale and aligned the CRZ with the flow axis. In contrast, a reduced swirl number reduced the swirl strength and the turbulence level and pushed it away from the flow axis. The increased swirl strength also reduced the size of the HMFR and expanded the shear layers with increased turbulences in both regimes. It was also observed that the turbulence regions could be pushed towards the dump plane by reducing the length of the nozzle. The flow structures were also influenced by external excitation, as increased forcing increased the width of the CRZ slightly and moved the high-velocity regimes closer to the dump plane. At a higher forcing frequency, the high-velocity regimes in the HMFR became split into smaller domains. Apart from this evolution of

the turbulence region, forcing generally increased the turbulence intensities within the vortical structures.

In general, the velocity profiles of the flow field are altered by the swirl and forcing conditions which are subsequently convected to the flame field with resulting heat release fluctuations. Thus the combustion convective and chemical time scales could be varied by changing the shape, size and location of the vortical structures in the flow field via the swirl and forcing conditions. Therefore, the control of the flow field has a corresponding influence on both the flame and acoustic fields and could serve as a potential approach to active control of the resulting combustion instabilities.

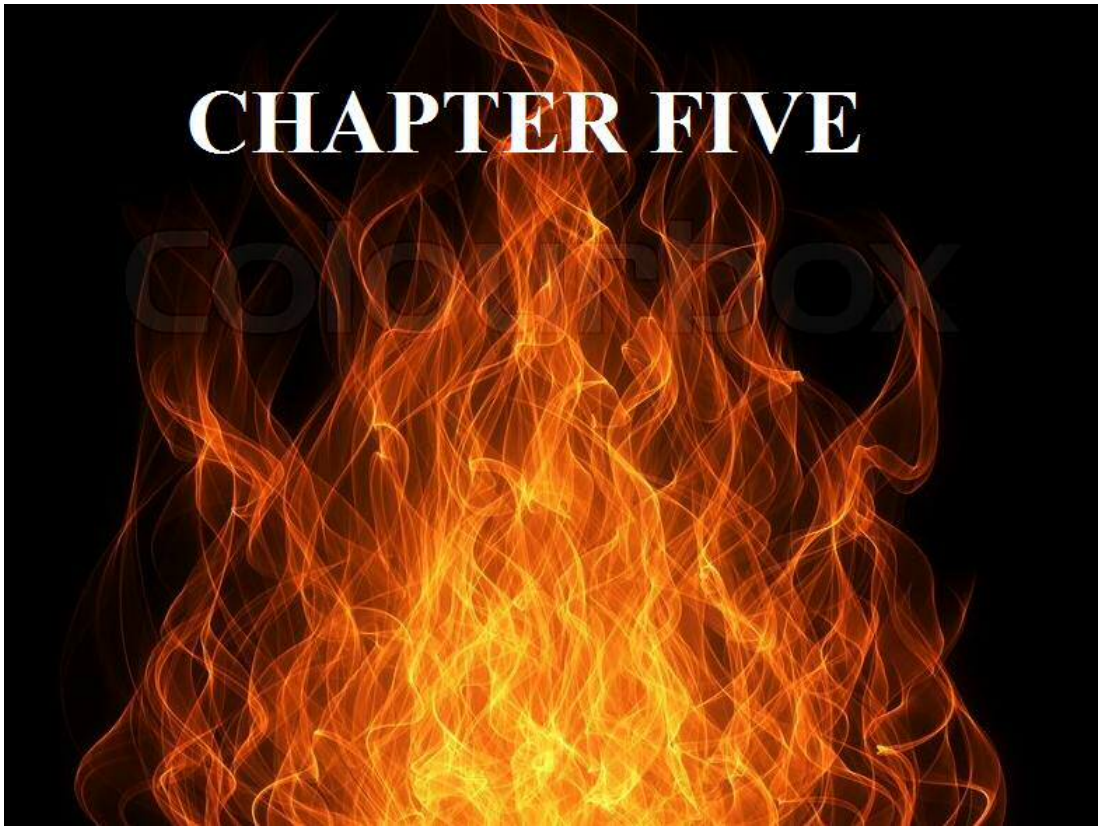
CHAPTER FIVE

CHAPTER FIVE:

FLAME DYNAMICS CHARACTERIZATION

"Talent is a flame. Genius is a fire."

Bern Williams

Confined flames respond significantly to acoustic driving and coupling processes. The driving processes perturb the flow field resulting in mechanisms such as flame rollup, flame surface area oscillation, flame front annihilation etc, all culminating in heat release rate and acoustic oscillations. The coupling processes involve the reaction of the flame to acoustic wave motion in terms of upstream modulation, composition inhomogeneity and strain rate. Thus heat release fluctuation is as a result of many complex acoustic – flow mechanisms. In this chapter, flame stability limits are first characterised, being a newly designed and manufactured burner. Then followed by the investigation of heat release rate response to flow, fuel and forcing conditions. Section 5.1 characterises the flame at different operating conditions including open and confined flames, variations in swirl geometries and fuel blends, etc. Section 5.2 deals with heat release fluctuation induced by the flow structure convection to the flame zone, with emphasis on the perturbations caused by the combustor geometrical variations. Section 5.3 discusses the heat release oscillation as a response to swirl, fuel blends and external excitation, and finally, Section 5.4 concludes the chapter.

5.1 Burner - Flame Characterization

The burner was run under different conditions to assess its flame behaviour and to determine its stability limits. The fuel was methane and air as the oxidant with two swirl geometries: S = 1.05 and S = 1.50. A nozzle diameter of 28mm and length of 30mm with a bluff rod of about the same length at the centre. The fuel and air were kept at ambient temperature and pressure and the system was run with open and confined flame conditions.

5.1.1 Open Flame

The fuel and air flow rates were varied to give different equivalence ratios and flame power. The flashback and blowoff limits were characterised for different flow rates, so as to provide safe operational boundaries for the burner in an open flame condition. Table 5.1 gives the values of the fuel flow rate of 0.116g/s and 0.133g/s with corresponding air flow rates, equivalence ratio and flame power. Figure 5.1 also gives the flame pictures for each fuel – flow mixture of the 0.116g/s fuel combustion captured using a digital camera. The second picture, Figure 5.1 (2) with an air flow rate of 0.116g/s and the equivalence ratio of 9.84 has a yellowish and sooty flame which penetrates the nozzle annulus. This condition serves as the flashback limit for the open flame. It must be noted here that this stable yellow flame at such a high equivalence ratio is attributed to the contribution of the ambient air to the combustion process as the flame would have required more air to get such stable condition if the flame was confined.

The flame gradually becomes more stabilised with a blue flame with yellow bands at the centre, as the air flow rate increases. The CRZ becomes well developed and gradually leaves the annulus and moves downstream of the flame zone. In the seventh picture Figure 5.1(7), with an equivalence ratio of 1.64, the yellow band at the centre of the flame disappears, and the flame becomes completely blue, well-structured and stabilised. The CRZ also attains its maximum width, with strong recirculation mixing of the cold fresh mixture with the hot gases.

Table 5.1(a): Fuel – air composition for open flames [S= 1.50]

S/N	Fuel(l/min)	Fuel (g/s)	Air(l/min)	Air (g/s)	Equ. Ratio	Power (kW)
1	10.5	0.116	0	0	0	5.82
2	10.5	0.116	10	0.204	9.84	5.82
3	10.5	0.1169	20	0.408	4.92	5.82
4	10.5	0.1169	30	0.612	3.28	5.82
5	10.5	0.1169	40	0.816	2.46	5.82
6	10.5	0.1169	50	1.02	1.96	5.82
7	10.5	0.1169	60	1.224	1.64	5.82
8	10.5	0.1169	70	1.429	1.4	5.82
9	10.5	0.1169	80	1.633	1.23	5.82
10	10.5	0.1169	90	1.837	1.09	5.82
11	10.5	0.1169	100	2.041	0.98	5.82
12	10.5	0.1169	110	2.245	0.89	5.82

Table 5.1 (b): Fuel – air composition for open flames[S= 1.05]

S/N	Fuel(l/min)	Fuel (g/s)	Air(l/min)	Air (g/s)	Equ. Ratio	Power (kW)
13	12	0.133	0	0	0	6.66
14	12	0.133	20	0.408	5.62	6.66
15	12	0.133	30	0.612	3.75	6.66
16	12	0.133	40	0.816	2.81	6.66
17	12	0.133	50	1.02	2.25	6.66
18	12	0.133	60	1.224	1.87	6.66
19	12	0.133	70	1.429	1.6	6.66
20	12	0.133	80	1.633	1.4	6.66
21	12	0.133	90	1.837	1.25	6.66
22	12	0.133	100	2.041	1.12	6.66
23	12	0.133	110	2.245	1.02	6.66
24	12	0.133	120	2.449	0.93	6.66

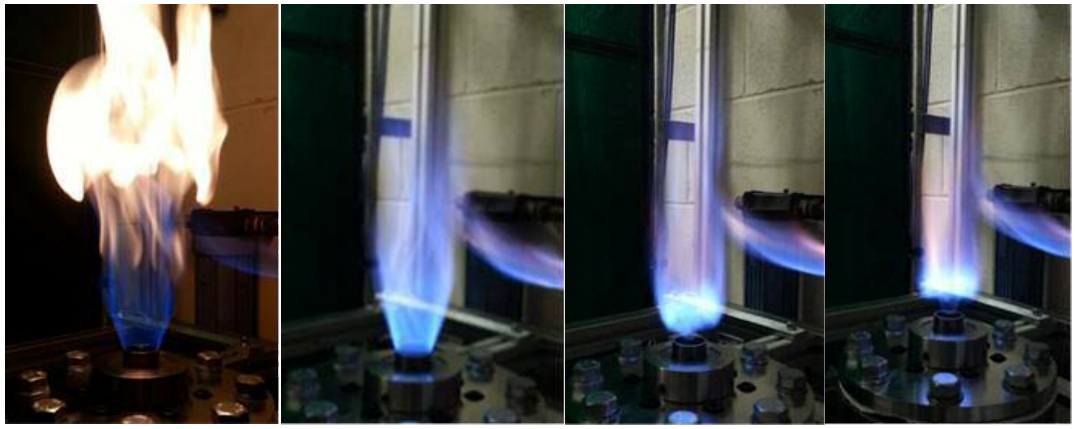

(1) (2) (3) (4)

(5) (6) (7) (8)

(9) (10) (11) (12)

Figure 5. 1 Open flames at various equivalence ratios for a fuel mass flow rate of 0.116g/s

[The numbering follows the serial number (1-12) of Table 5 -1]

Away from this fuel-air mixture, the flame size starts to elongate and gradually becomes thin and unstable with gradual oscillations as the flame becomes leaner until the blowoff limit was finally reached at an air flow rate of 2.245g/s , Figure 5.1(12). At this point, the very thin and oscillating blue flame was completely detached from the anchorage beyond which the flame was extinct. Table 5.1b, serial number 13 to 24, give the fuel-air composition for an increased fuel flow rate of 0.133g/s at 6.66kW. A similar trend in flame evolution was also observed but with increased flame size and turbulence. The flashback was moved to 0.408g/s while the blowoff was increased to 2.449g/s of air flow rate. In all practical combustion systems, the flames are confined. Thus the behaviour of an open flame can only be used to project or estimate the behaviour of a confined flame with suitable geometries.

5.1.2 Confined Flame

The flame was confined with a cylindrical quartz tube of 400mm long and 84mm internal diameter. This confinement shields the flame from the ambient air. The temperature and pressure were kept at atmospheric condition. The fuel and air flow rates were also varied to give stable combustion regimes. Table 5.2 gives the fuel-air mixture for the combustion, where the fuel was kept constant at 0.116g/s, and 0.133g/s while the air was varied in each case to give different equivalence ratio and flame power. Figure 5.2 shows the flame pictures of the fuel flow rate of 0.116g/s with different equivalence ratio, for serial numbers 1 – 12 respectively.

With the flame confinement, the fuel flow rate of 0.116g/s reaches its flame flashback limit at 1.740g/s air flow rate with an equivalence ratio of 1.16, compared to the zero g/s of air for the open flame condition. Figure 5.2 (1) gives a turbulent and vigorous flame propagating within the nozzle annulus, beyond which the flame moves upstream to the premixing chamber. With an increased air flow rate, the flame starts to elongate as the CRZ moves downstream of the flame zone. At an air flow rate of 1.940g/s and the equivalence ratio of 1.04, Figure 5.2 (4), the flame becomes well stabilized with an enlarged CRZ whose position was further away from the dump plane. It should be

noted that the reddish portion of the flame is as a result of the flame reflection on the painted side of the quartz tube, as the flame remains bluish.

Table 5.2: Fuel – air composition for confined flames: S=1.50(Serial Number 1-12); S=1.05(Serial Number 13-21)

S/N	Fuel(l/min)	Fuel (g/s)	Air(l/min)	Air (g/s)	Equ. Ratio	Power (kW)
1	10.5	0.116	85.22	1.745	1.16	5.83
2	10.5	0.116	85.22	1.745	1.16	5.83
3	10.5	0.116	90.12	1.845	1.09	5.83
4	10.5	0.116	95.02	1.945	1.04	5.83
5	10.5	0.116	99.91	2.045	0.98	5.83
6	10.5	0.116	104.81	2.145	0.94	5.83
7	10.5	0.116	110.2	2.255	0.86	5.83
8	10.5	0.116	115.1	2.355	0.86	5.83
9	10.5	0.116	119.02	2.435	0.82	5.83
10	10.5	0.116	124.89	2.555	0.79	5.83
11	10.5	0.116	129.79	2.655	0.76	5.83
12	10.5	0.116	134.69	2.755	0.73	5.83
S/N	Fuel(l/min)	Fuel (g/s)	Air(l/min)	Air (g/s)	Equ. Ratio	Power (kW)
13	12	0.133	59.75	1.224	1.88	6.66
14	12	0.133	90.12	1.843	1.25	6.66
15	12	0.133	99.91	2.045	1.13	6.66
16	12	0.133	110.2	2.252	1.02	6.66
17	12	0.133	120	2.453	0.94	6.66
18	12	0.133	129.79	2.654	0.87	6.66
19	12	0.133	140.08	2.861	0.8	6.66
20	12	0.133	149.87	3.062	0.75	6.66
21	12	0.133	160.16	3.273	0.7	6.66

With further increase in air flow rate, the width of the flame gradually reduces and becomes detached from its anchorage, Figure 5.2 (7). At an air rate of 2.650g/s, Figure 5.2 (11), the flame shape is scattered as the blue flame spreads around the entire flame tube with strong oscillations and finally reaches its blowoff limit at an air flow rate of 2.750g/s and equivalence ratio of 0.73. Beyond this condition, the flame disappears from the tube.

Table 5.2 serial numbers 13 – 21 gives the fuel-air mixture of the combustion as the fuel flow rate was increased to 0.133g/s and remained constant at this value while the air flow rate was varied between the flashback and blowoff limits. The blue – yellowish turbulent flame at the flashback limit has a strong flame root whose width covers the entire nozzle diameter with a CRZ region which is close to the nozzle dump plane. An increase in the air flow rate reduces the width of the flame root but increases the size of the CRZ as it moves downstream of the flame zone. The flame becomes fully stabilised at an equivalence ratio of 1.02 with 2.250g/s air flow rate, where the CRZ becomes fully developed with a strong recirculation. The fresh inlet gases mix with the burnt gases and ensure the anchorage of the flame and efficient combustion. This mechanism is common to most swirl flames as reported in many literatures [53][201].

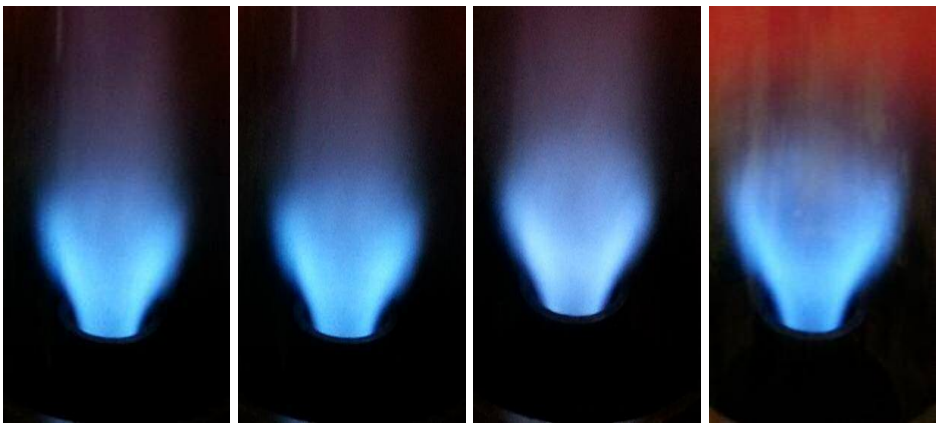

1 2 3 4

Figure 5-2 (a): Confined flames at various equivalence ratios for a fuel mass flow rate of 0.116g/s

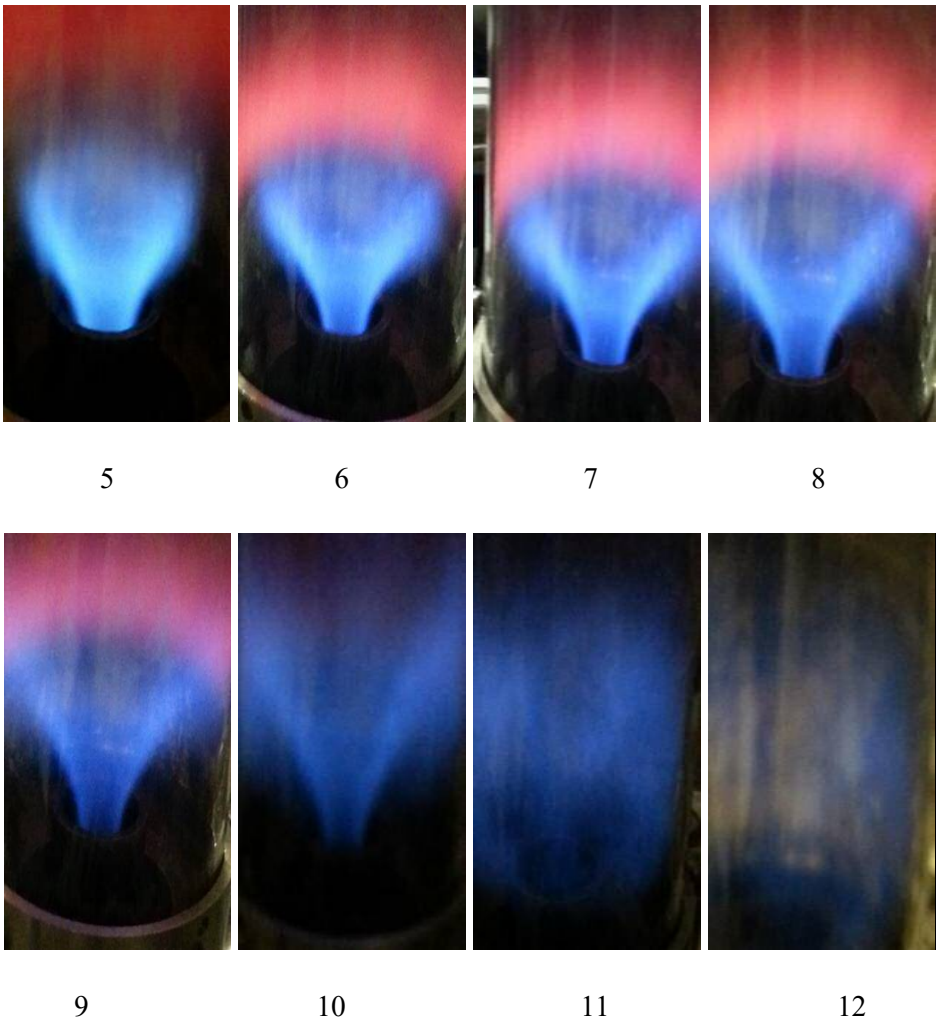

(b)

Figure 5. 2 Confined flames at various equivalence ratios for a fuel mass flow rate of 0.116g/s

[The numbering follows the serial number (1-12) of Table 5.2)]

The flame stability continued to an equivalence ratio of 0.75 at an air flow rate of 3.06g/s, beyond which the flame root became thin and long as its width leaves the boundaries of the nozzle and moves to the centre. Further increase in air flow rate widened the downstream side of the flame before being reduced to a long and thin blue flame with strong oscillation. The flame structure scattered and covered the entire flame tube with a reduced temperature at an air flow rate of 3.270g/s, beyond which further increase in air flow rate saw the flame disappeared from the tube, thus reaching its blowoff limit.

5.1.3 Confined Versus Open Flame

Table 5.3 compares the stability limits of the two flame conditions for a constant fuel flow rate of 0.133g/s, plotted in Figures 5.3. The flashback for the open flame occurred at an equivalence ratio of 3.55 with a total mass flow rate of 0.820 g/s. For the confined condition, the flashback occurred at a lower equivalence ratio of 1.82 at a total mass flow rate of 1.530 g/s.

Table 5.3: Flame flashback – blowoff limits for open and confined flames

	Flame Conditions			
	Flashback		**Blowoff**	
	Eq. Ratio	Total mass flow(g/s)	Eq. Ratio	Total mass flow (g/s)
Open Flame	3.55	0.82	0.93	2.56
Confined Flame	1.82	1.53	0.6	3.92

This implies that, about 0.710g/s ambient air was used when the burner was in open flame condition, thus less air was supplied, and the equivalence ratio remained at 3.55. In the confined condition, because the ambient air was not used by the flame, more air was supplied to the flame thus reducing the equivalence ratio to 1.82. In the blowoff regime, the same scenario was observed, as more air (3.92g/s) was supplied with a reduced equivalence ratio from 0.60 in the confined condition as compared to 0.93 in the open condition. Thus it could be observed that an open flame condition has a wider stability margins due to the ambient effects while a confined flame has a relatively shorter range of stability limits.

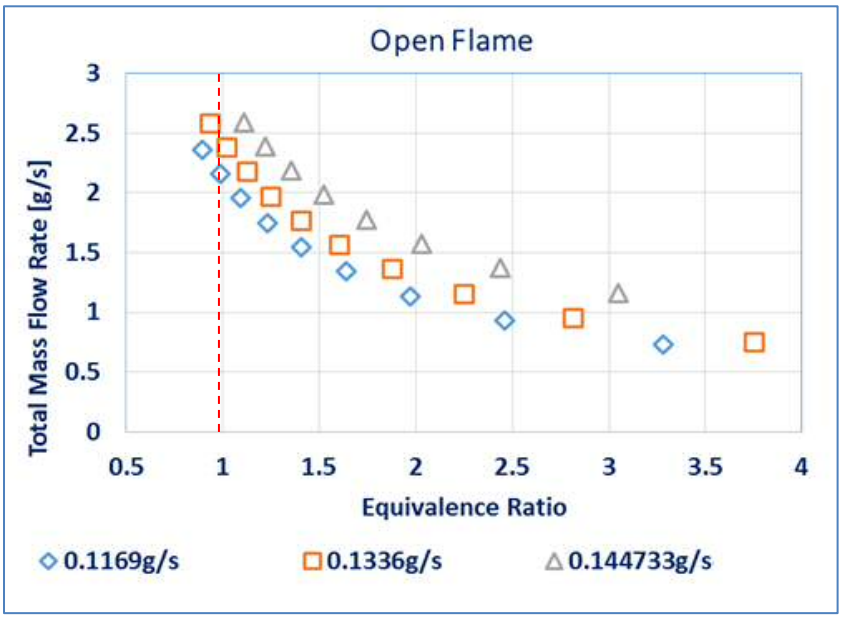

(a)

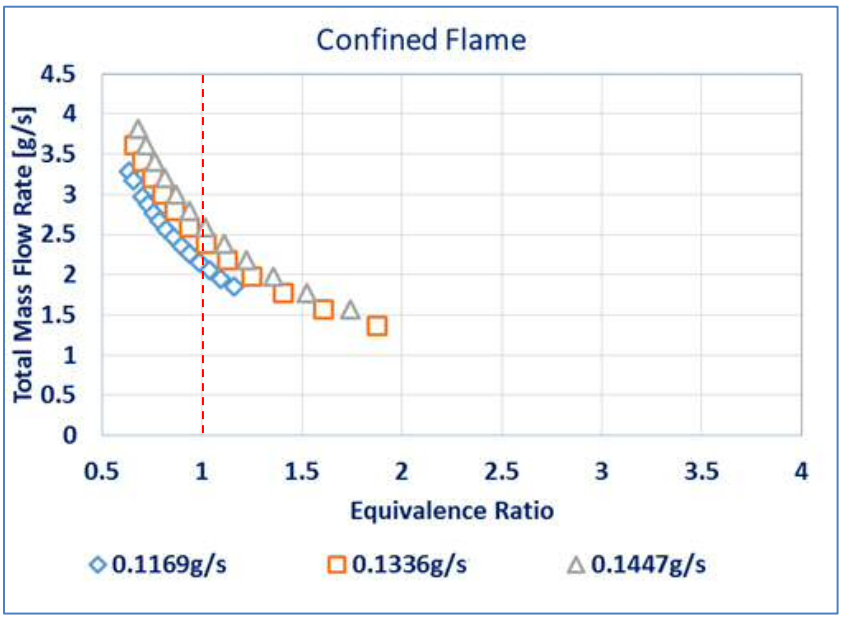

(b)

Figure 5. 3 Flame blowoff and flashback limits

[(a) Open Flame and (b) Confined Flame]

However, a confined flame has a longer blowoff range, due to the shield from the ambience. Because most practical systems use confined flame conditions, the rest of this study is based on this condition.

5.2 Lean Blowoff Limit Characterization and Optimization

Currently, most industrial lean premixed burners run at a blow-off limit range of 0.80 to 0.70 equivalence ratio. The quest is ongoing to extend this limit to much lower equivalence ratio, say 0.50 in order to further reduce NOx emissions to the barest minimum. This could be achieved by varying the injection geometries to change the flow structures or by altering the flow mixture composition to change the chemical time scale. This section seeks to characterise and optimise the blow-off limit of the burner with different geometric and flame conditions.

5.2.1 Stability Limit Variations with Swirl Number

Combustion was carried out with two swirl geometries to compare their blowoff boundaries in a confined flame condition. The inlet flow temperature was kept constant at 300K, the pressure at 1 bar and with swirl numbers of 1.05 and 1.50. The lower swirl number has four and the higher swirl number nine tangential inlets respectively, all symmetrically distributed, Figure 5.4.

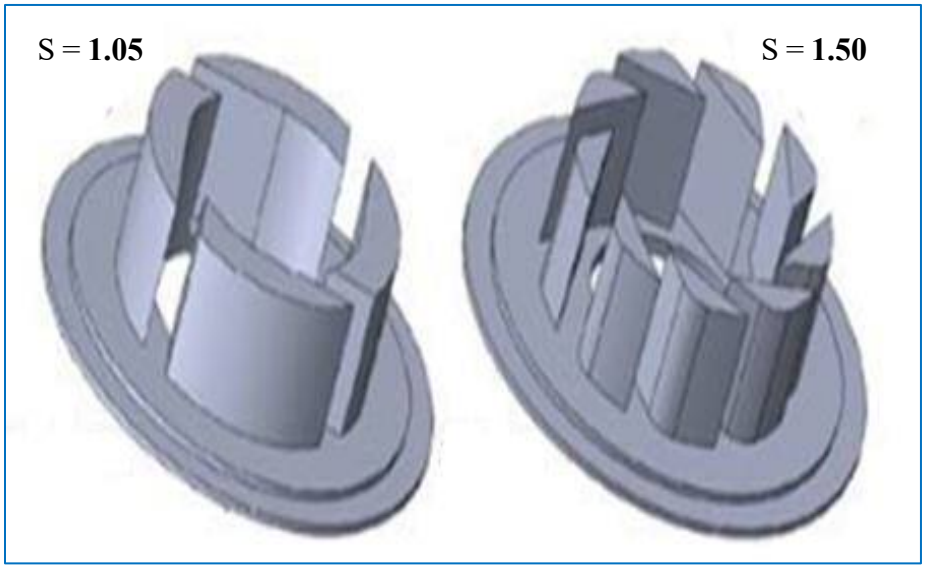

Figure 5. 4 Swirl Vanes with specific Swirl Numbers

The 1.05 swirl was first inserted, and combustion was performed with the fuel flow rate of 0.100g/s to 0.144g/s. The 1.50 swirl was thereafter inserted, and the same conditions were repeated to assess the impact of the swirl geometry and strength on the flame blowoff limits under these experimental conditions. The results showed significant differences with the change in swirl geometry as well as the flow rates. Figure 5.5 plots the equivalence ratio against the total mass flow rate (air and fuel) of the flame to show the blowoff limits for the two swirl numbers using two fuel flow rates: 0.111g/s and 0.133g/s, with the air flow rate varied in each case.

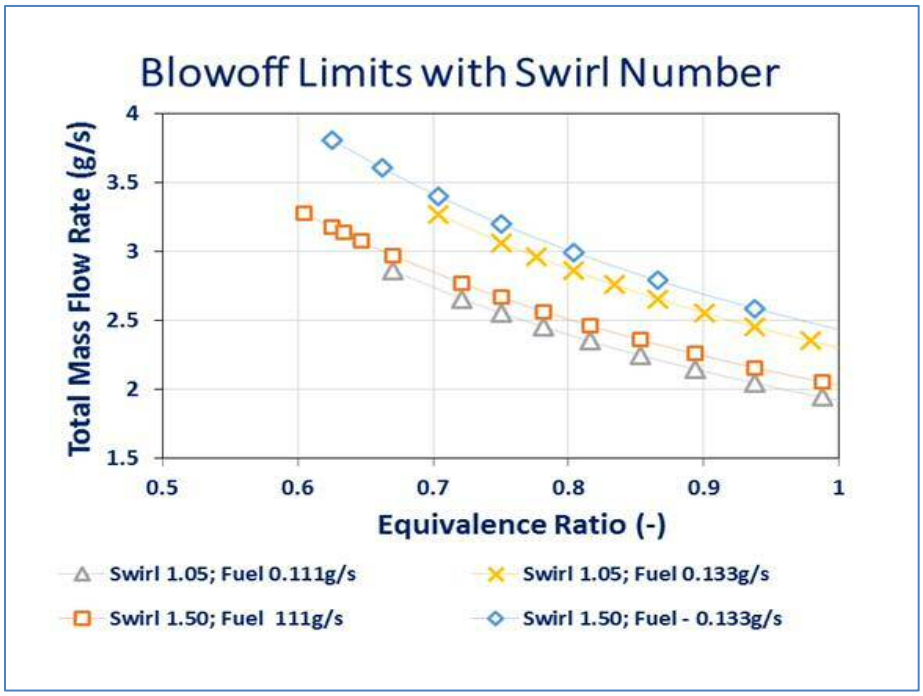

Figure 5. 5 Flame blowoff limit variation with swirl and fuel mass flow rate

From the plot, it can be observed that the 0.133g/s fuel flow has a higher total mass flow than the lower fuel flow rate of 0.111g/s in both swirl conditions. This is because the 0.022g/s extra fuel needs more air to burn within the stoichiometric and lean conditions. The effects of the swirl strength are also evident in the higher swirl number extending its blowoff limit to 0.60 equivalence ratio for the fuel flow rate of 0.111g/s at a total mass flow of 3.300g/s. The blowoff limit for a higher fuel flow of 0.133g/s for the same high swirl number is at equivalence ratio of 0.67 with a total mass flow rate of 3.800g/s. Whereas the blowoff limits of the lower swirl number reduce to an equivalence ratio of 0.67 at a total mass flow rate of 2.800g/s for the lower fuel flow rate of 0.111g/s. For the higher flow rate of 0.133g/s, the blowoff limit reduces slightly

to an equivalence ratio of about 0.71 at a total mass flow rate of 3.300g/s. These show that with the increased swirl strength, the blowoff limit moved by 11 % in the high flow rate and 13 % in the lower flow rate down the lean region.

This enhancement of the blowoff limits with increased swirl number could be attributed to many mechanisms as follows. The increased swirl number increases the turbulent burning velocity of the flame, especially at the base, as the local velocity oscillation is increased. The increased swirl strength increases also the CRZ, thus creating a larger domain for thorough mixing of the fuel and air. Also, the enlarged hot recirculation region increases the residence time, an important factor which stabilizes the flame.

5.2.2 Stability Limit Variations with Divergent Nozzles

The effect of divergent nozzles on the blowoff limits was also examined using three nozzle angles of 45, 60 and 90 degrees, Figure 5.6 (a). The length and diameter of the nozzle were kept constant at 30mm and 28mm respectively. The blowoff limit across the equivalence ratios was measured to assess the various changes in the flame stability limits.

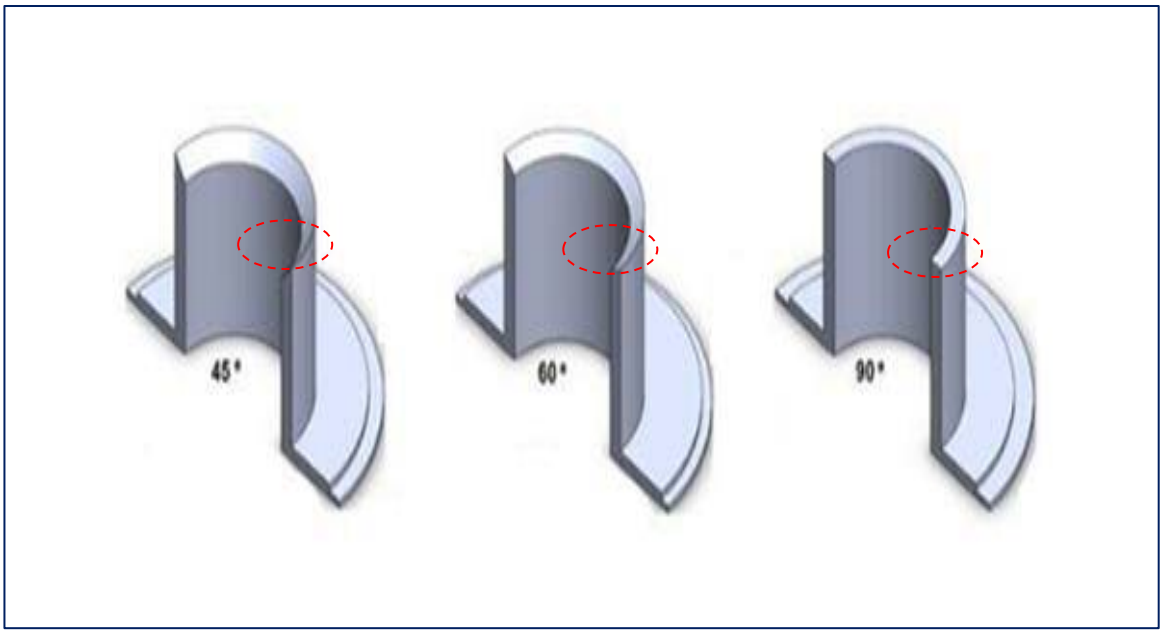

(a)

Figure 5. 6 Swirl nozzles with different divergent angles

(b)

Figure 5. 7 Swirl nozzles with different divergent angles

[(a) angles: 45, 60 and 90 degrees; (b) nozzle – swirl insert assembly]

Two fuel flow rates of 0.111 and 0.133g/s were used with each case kept constant, while the air flow rate was varied. Figure 5.7 indicates that there is a significant shift in the blowoff boundaries of the straight 90-degree from the 60 and 45-degrees divergent angles.

At the low fuel flow rate of 0.111g/s, the blowoff limit of the 90 degrees divergent angle has an equivalence ratio of 0.64 whereas the blowoff limits of 60 and 45 degrees increase to 0.58 and 0.61 which represents an increment of 9 and 4 % respectively. Using the 90-degree nozzle as the baseline, the 60-degree nozzle has a slightly lower total mass flow rate while the 45 degrees nozzle increased the mass flow rate significantly. With increased fuel flow rate to 0.133g/s, the blowoff limit of the 90-degree divergent nozzle reduces to an equivalence ratio of 0.67. Also, the blowoff limits of the 60 and 45-degree nozzles both showed a slight increase in the blowoff limits with about 1 % with a higher total mass flow rate than the 90 degrees nozzle. These changes in the blowoff limits with changes in the geometry of the nozzle are attributed to the corresponding changes in the shape, size and location of the vortical structures of the flow field. The divergence of the nozzle angle enhances the recirculation intensity of the flame zone, by increasing the width of the CRZ and the turbulent intensity, resulting in increased mixing of the flow mixture and flame anchorage and by extension increased flame stability.

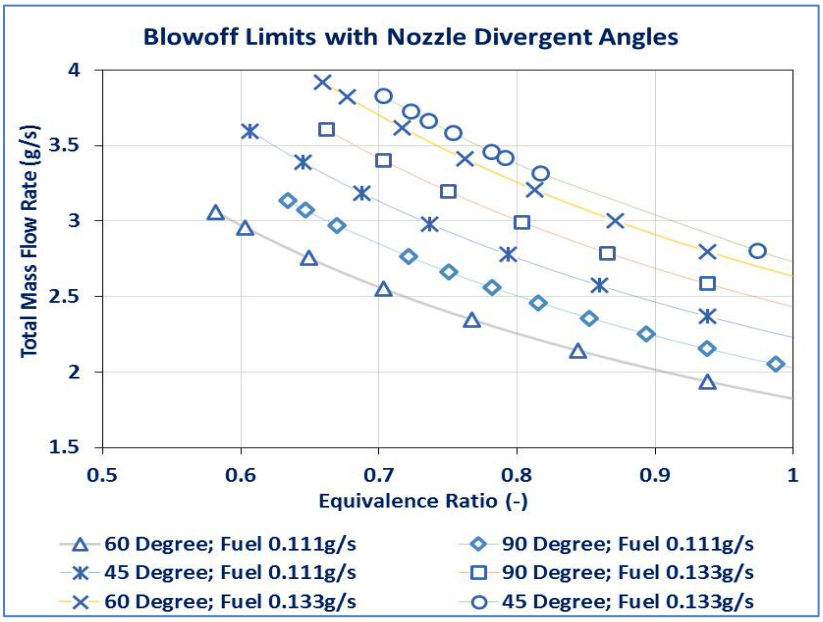

Figure 5. 8 Flame blowoff limits for different divergent angles of the nozzle

[45 degree; 60 degree; 90 degree]

The 90-degree nozzle angle had an elongated CRZ and became lifted away from the nozzle exit, while in the 60-degree nozzle angle, the CRZ became larger and lowered down towards the nozzle exit. In the 45-degree nozzle angle, the CRZ became very broad and lowered further touching the nozzle exit. It was therefore observed that an improved swirling, a strong recirculation and a more stable flame, was achieved as the divergent angle was varied from 90 to 45 degrees. For the purpose of uniformity of this study with other reported studies, the 90-degree angle was used in the rest of the experiment.

5.2.3 Blowoff Limit Variations with Fuel Blend

The effects of fuel composition on the blowoff limit were also examined. The combustion of pure methane, as well as its blend with CO_2, were tested. The conditions were similar, and pure methane was used as the baseline fuel. The use of CO_2, in this case, was motivated by the new EGR technique [141] where CO_2 is recirculated into the air inlet stream to the combustion chamber to increase the concentration of the CO_2 at the exhaust for ease of capturing the CO_2. Also, the use of landfill gases with an average amount of 50% methane and 30% CO_2 is quite promising for gas turbine combustion [202]. A 30% CO_2 and 70% CH4 premixed blend contained in a gas

cylinder was used for this study. Thus as the fuel mass flow rate was increased, the concentration of CO2 in the air- fuel mixture was also increased.

Five fuel flow rates were used with each varied with many air flow rates to give different equivalence ratios. As usual, the increase in fuel rate increases the total mass flow but reduces slightly the equivalence ratio at which the blowoff limit occurs. In all the fuel flow rates, Figure 5.8 (a), the blowoff limit was reached at about 0.63 equivalence ratio at different total mass flow rates. Some differences were observed with the blend of methane with 30%CO2, Figure 5.8 (b). The higher fuel flow rates showed a significant reduction in the equivalence ratio of the blowoff limits to 0.70 and 0.73 equivalence ratios for the 0.133g/s and 0.144 g/s fuel flow respectively. Also, the lower fuel flow rates show the reduction in the blowoff limit when compared to the pure methane baseline. The three lower fuel flow rates of 0.100, 0.111 and 0.122g/s all have their blowoff limits at about 0.67 equivalence ratio with a close range of the total mass flow rate.

The addition of CO_2 to methane-air has a diluent effect due to the relative reduction in the concentrations of the reactive species and direct chemical effects as a result of the breakdown of CO_2 through the reactions of third-body collision and thermal dissociation, [152]. The heat capacity of CO_2 is much higher than air, and its absorption coefficient is quite high. Thus the addition of CO_2 to the fuel mixture is expected to change the flame axial velocity gradient (strain rate). The high density of CO_2 is also assumed to have contributed to the reduction in the turbulence scale in the shear layers, thereby reducing the heat release oscillations. The presence of CO_2 decreased the high momentum flow region velocity drastically while increasing the central recirculation zone velocity since the CO_2's high specific heat increases the pressure differential which drives recirculation with less turbulence, [153], and by extension an enhanced mixing and less heat release oscillation. The above thermodynamics properties of methane –CO_2 fuel reduces the blowoff limit of the fuel blend. On the contrary, other studies [29] [203] have shown that the addition of low density and specific heat, high reactive hydrogen to methane moves the equivalence ratio of the blowoff limit to a leaner region, as the Da Number is decreased as a result of the faster chemical reaction [17].

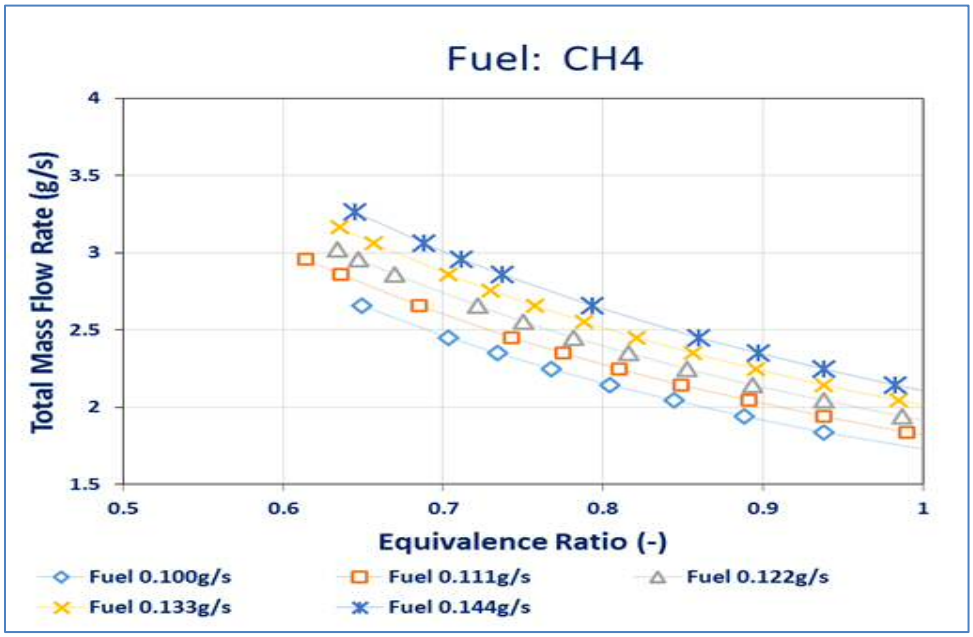

(a)

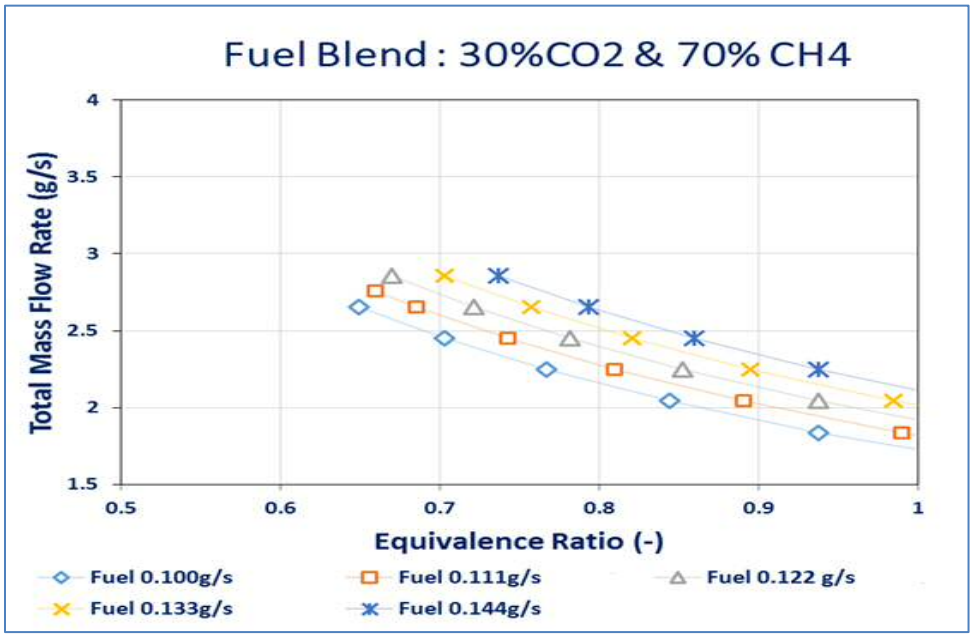

(b)

Figure 5. 9 Flame blowoff limits with fuels

[(a) Methane flame; (b) Methane -30%CO2 flame]

5.2.4 Optimization of LBL by Geometry and Fuel Conditions

The above factors which influence the lean blowoff limits (LBL) of flames were combined in different ways to examine the resultant effect of these factors on the flame, with a view to obtaining an optimal condition for the safe and efficient running of the system. The combination was done in fifteen ways, and three best cases were used to demonstrate the variations in the blowoff limits with the resultant effects of the factors. As given in Table 5.4, case I has a higher swirl strength, a divergent nozzle angle of 60 degrees, a longer nozzle to diameter ratio and pure methane. Case II uses a lower swirl number with a half (45) divergent angle, a longer nozzle length to diameter ratio and pure methane. Finally, case III uses a lower swirl number, a straight nozzle angle, a smaller nozzle length to diameter and a fuel blend of methane and 30% C02. These cases were run one after the other, and the combined effects obtained.

Table 5.4: Combustion conditions with swirl geometry and fuel

Condition	Swirl No.	D. Angle	D/L	Fuel
Case I	1.5	60	0.93	CH4
Case II	1.05	45	0.93	CH4
Case III	1.05	90	1.86	CH4 + 30%C02

From Figure 5.9, Case I reached a blowoff limit at an equivalence ratio of 0.58 followed by case II with an equivalence ratio of 0.67 and finally case III reached the limit at 0.71. Case I, thus becomes the best combination with the lowest equivalence ratio and the most reduced NOx emitter. These indicate that the individual effects of these factors contributed immensely to the resultant effects of the cases.

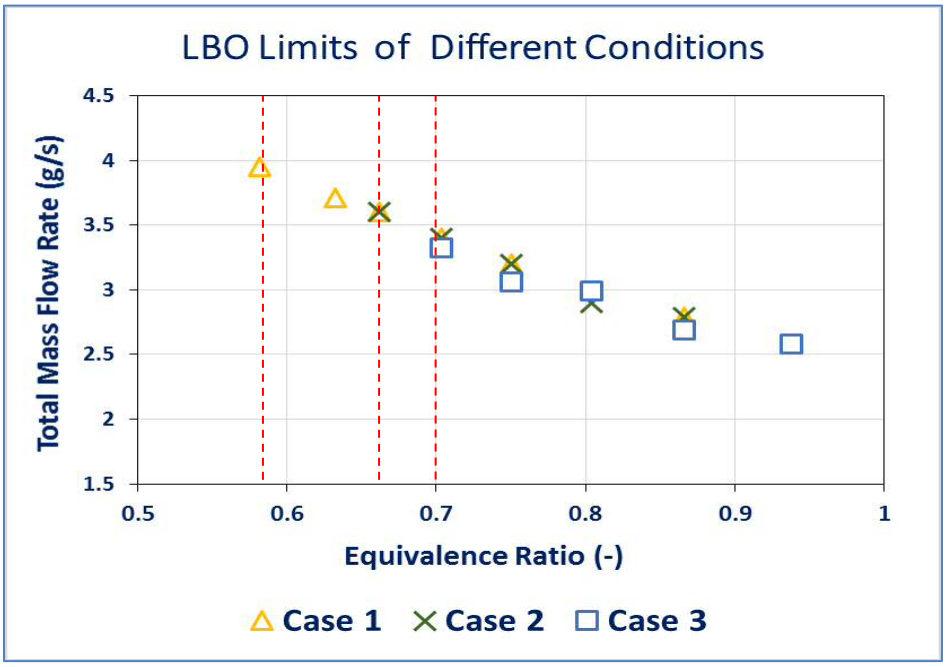

Figure 5. 10 Flame blowoff limits optimization conditions

The above results, therefore, prove that flames could be moved to leaner domains with a proper combination of the swirl and nozzle geometries as well as the fuel composition. From the control point of view, these provide additional capabilities to enhanced clean and efficient combustion.

5.3 Heat Release Fluctuations

As mentioned in chapter two, pressure induced heat release oscillation is attributed to many mechanisms including pulsation of fuel supply resulting from equivalence ratio perturbation, flame front oscillation, vortex induced instabilities etc., [125] [59][134][131]. Swirling flows with various vortical structures are convected to the flame, with the distortion of the flame surface area which results in heat release rate oscillation. To investigate these, high-speed CH* chemiluminescence intensities of the flame were captured and reconstructed to quantify the CH* fluctuations under different flame conditions. This technique has been used in many heat release chemiluminescence studies [204 - 207]. Matlab codes were used for the reconstruction of the CH* chemiluminescence, and the fluctuation rate was used as a measure of the heat release oscillation. Because of the weak nature of the reactive chemiluminescence, an image intensifier was used to measure the light within the UV

range. A CCD camera (Dantec Dynamic Hi sense MKII) with a 1.3-megapixel resolution was coupled to the image intensity (Hamamatsu C9546-031), and a Lens of 78mm focal length was fitted to the intensifier with a bandpass filter cantered at 340nm (FWHM = 10nm), which is approximately the wavelength of the CH* radical as discussed in chapter three.

With a frequency of 125Hz, 682 CH* chemiluminescence images were captured for each test condition using a Photon FASTCAM Viewer Software (PFV Version 3620 (x64)), with a remote control for the modulation of the gain of the heat release intensity. The images were captured about a metre from the flame via the quartz tube flame confinement. Basic Matlab codes, (Appendix B1), were used to obtain the intensity of the chemiluminescence for each image and used as a direct measure of the heat release, where the fluctuations of these values give the heat release fluctuations for the study. The background intensity was first obtained by taking the image of the background without the flame, thus the acquired image intensity was subtracted from the background intensity to give the actual value of the CH* fluctuations. The ratio of the instantaneous CH*' chemiluminescence to the mean value gives the intensity fluctuations.

Figure 5.10 gives the images of the reconstructed CH* chemiluminescence with the corresponding CH* chemiluminescence fluctuation values for the first 16 images of the fuel flow rate of 0.1113g/s (5.50kW) with an equivalence ratio of 0.85 and swirl number of 1.50. The top part of the images represents a region where the vortical flow structures wrap with the flame front. Thus significant fluctuations were observed around this part of the flame at various combustion conditions. The flame surface fluctuation is attributed to the evolution of the flow vortical structures which results in the oscillations of the chemiluminescence.

Table 5.5 gives the CH* fluctuations of various fuel and air flow rates for the two swirl numbers. In each case, the CH*'/CH* values evolve with time within the range of 0.9 and 1.2. A wider range of 0.6 to 1.3 were obtained in many other cases. The heat release fluctuations were then evaluated in many geometric and forcing conditions in the remaining section of this chapter.

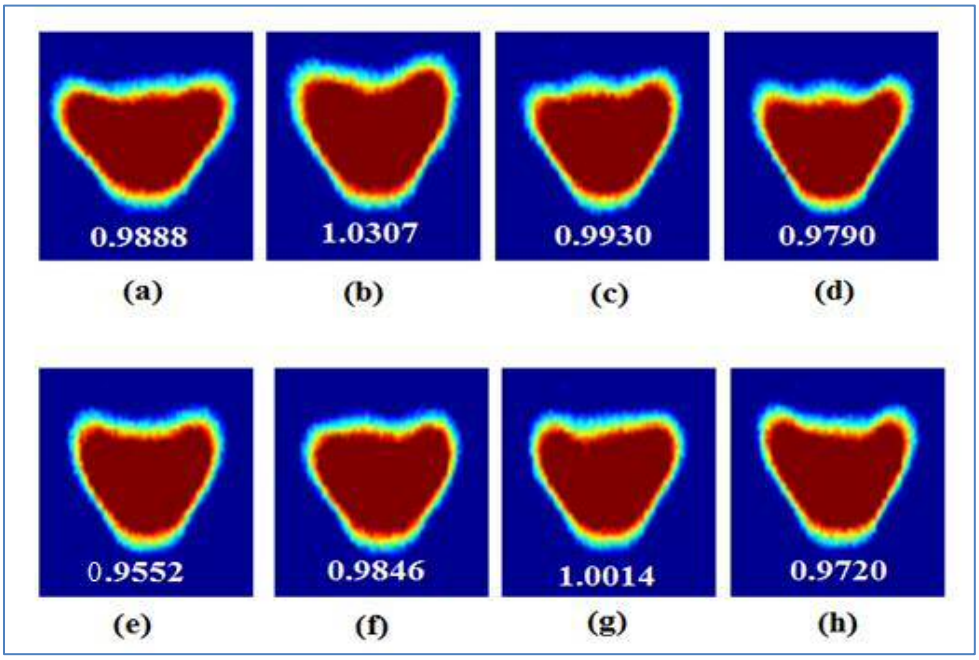

Figure 5.10 (a): Reconstructed images of CH* chemiluminescence fluctuations with corresponding CH*'/CH* values.

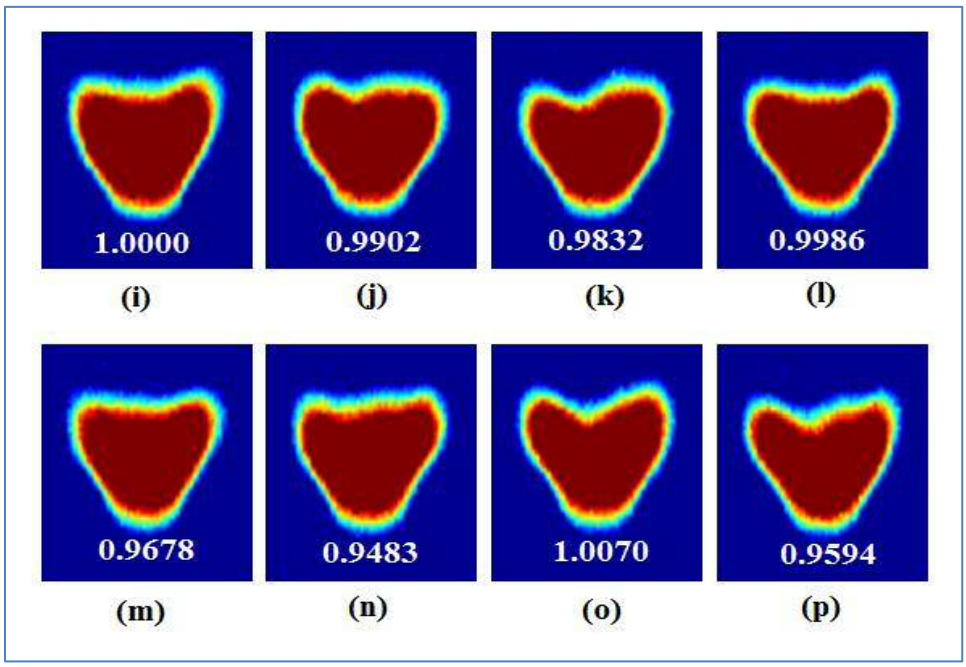

(b)

Figure 5. 11 Reconstructed images of CH* chemiluminescence fluctuations with the corresponding CH*'/CH* values

Table 5.5: CH* chemiluminescence fluctuations with time [Swirl Number – 1.05]

					Fuel = 0.111 g/s			Air = 2.245 g/s			Equi. Ratio 0.85			Power = 5.5kW			
S/N	1	2	3	4	5	6	7	8	9	10	11	12	13	14	15	16	17
TIME (S)	0.008	0.016	0.024	0.032	0.04	0.048	0.056	0.064	0.072	0.08	0.088	0.096	0.104	0.112	0.12	0.128	0.136
Background Intensity	0.002	0.002	0.002	0.002	0.002	0.002	0.002	0.002	0.002	0.002	0.002	0.002	0.002	0.002	0.002	0.002	0.002
Mean value of each image	0.533	0.542	0.545	0.538	0.535	0.536	0.548	0.544	0.536	0.536	0.529	0.537	0.525	0.548	0.535	0.543	0.537
Actual (CH*)' Intensity	0.531	0.54	0.543	0.536	0.533	0.534	0.546	0.542	0.534	0.534	0.527	0.535	0.523	0.546	0.533	0.541	0.535
Mean	0.543	0.543	0.543	0.543	0.543	0.543	0.543	0.543	0.543	0.543	0.543	0.543	0.543	0.543	0.543	0.543	0.543
(CH*)'/(CH*)	0.978	0.994	1	0.9871	0.982	0.983	1.006	0.9982	0.983	0.983	0.971	0.985	0.963	1.0055	0.982	0.996	0.985
					Fuel = 0.122 g/s			Air = 2.449 g/s			Equi. Ratio = 0.85			Power = 6.10kW			
S/N	1	2	3	4	5	6	7	8	9	10	11	12	13	14	15	16	17
TIME (S)	0.008	0.016	0.024	0.032	0.04	0.048	0.056	0.064	0.072	0.08	0.088	0.096	0.104	0.112	0.12	0.128	0.136
Background Intensity	0.002	0.002	0.002	0.002	0.002	0.002	0.002	0.002	0.002	0.002	0.002	0.002	0.002	0.002	0.002	0.002	0.002
Mean value of each image	0.522	0.817	0.606	0.566	0.569	0.651	0.592	0.601	0.57	0.591	0.595	0.582	0.814	0.653	0.589	0.628	0.574
Actual (CH*)' Intensity	0.52	0.815	0.604	0.564	0.567	0.649	0.59	0.599	0.568	0.589	0.593	0.58	0.812	0.651	0.587	0.626	0.572
Mean	0.612	0.612	0.612	0.612	0.612	0.612	0.612	0.612	0.612	0.612	0.612	0.612	0.612	0.612	0.612	0.612	0.612
(CH*)'/(CH*)	0.85	1.332	0.9869	0.9216	0.926	1.06	0.964	0.9788	0.928	0.962	0.969	0.948	1.327	1.0637	0.959	1.023	0.935
					Fuel = 0.133 g/s			Air = 2.65 g/s			Equi. Ratio = 0.86			Power = 6.66kW			
S/N	1	2	3	4	5	6	7	8	9	10	11	12	13	14	15	16	17
TIME (S)	0.008	0.016	0.024	0.032	0.04	0.048	0.056	0.064	0.072	0.08	0.088	0.096	0.104	0.112	0.12	0.128	0.136
Background Intensity	0.002	0.002	0.002	0.002	0.002	0.002	0.002	0.002	0.002	0.002	0.002	0.002	0.002	0.002	0.002	0.002	0.002
Mean value of each image	0.75	0.755	0.732	0.738	0.736	0.741	0.737	0.746	0.744	0.729	0.73	0.746	0.754	0.757	0.757	0.75	0.739
Actual (CH*)' Intensity	0.748	0.753	0.73	0.736	0.734	0.739	0.735	0.744	0.742	0.727	0.728	0.744	0.752	0.755	0.755	0.748	0.737
Mean	0.737	0.737	0.737	0.737	0.737	0.737	0.737	0.737	0.737	0.737	0.737	0.737	0.737	0.737	0.737	0.737	0.737
(CH*)'/(CH*)	1.015	1.022	0.9905	0.9986	0.996	1.003	0.997	1.0095	1.007	0.986	0.988	1.009	1.02	1.0244	1.024	1.015	1

Table 5.6: CH* chemiluminescence fluctuations with time [Swirl Number – 1.50]

					Fuel = 0.111 g/s			Air = 2.245 g/s			Equi. Ratio 0.85			Power = 5.5kW			
S/N	1	2	3	4	5	6	7	8	9	10	11	12	13	14	15	16	17
TIME (S)	0.008	0.016	0.024	0.032	0.04	0.048	0.056	0.064	0.072	0.08	0.088	0.096	0.104	0.112	0.12	0.128	0.136
Background Intensity	0.002	0.002	0.002	0.002	0.002	0.002	0.002	0.002	0.002	0.002	0.002	0.002	0.002	0.002	0.002	0.002	0.002
Mean value of each ima	0.709	0.739	0.712	0.702	0.685	0.706	0.718	0.697	0.717	0.71	0.705	0.716	0.694	0.68	0.722	0.688	0.702
Actual (CH*)' Intensity	0.707	0.737	0.71	0.7	0.683	0.704	0.716	0.695	0.715	0.708	0.703	0.714	0.692	0.678	0.72	0.686	0.7
Mean	0.715	0.715	0.715	0.715	0.715	0.715	0.715	0.715	0.715	0.715	0.715	0.715	0.715	0.715	0.715	0.715	0.715
(CH*)'/(CH*)	0.989	1.0308	0.993	0.97902	0.955	0.985	1.001	0.972	1	0.99	0.983	0.999	0.968	0.948	1.007	0.9594	0.979
					Fuel = 0.122 g/s			Air = 2.449 g/s			Equi. Ratio = 0.85			Power = 6.10kW			
S/N	1	2	3	4	5	6	7	8	9	10	11	12	13	14	15	16	17
TIME (S)	0.008	0.016	0.024	0.032	0.04	0.048	0.056	0.064	0.072	0.08	0.088	0.096	0.104	0.112	0.12	0.128	0.136
Background Intensity	0.002	0.002	0.002	0.002	0.002	0.002	0.002	0.002	0.002	0.002	0.002	0.002	0.002	0.002	0.002	0.002	0.002
Mean value of each ima	0.669	0.653	0.68	0.663	0.688	0.679	0.666	0.66	0.664	0.65	0.672	0.683	0.679	0.688	0.673	0.665	0.696
Actual (CH*)' Intensity	0.667	0.651	0.678	0.661	0.686	0.677	0.664	0.658	0.662	0.648	0.67	0.681	0.677	0.686	0.671	0.663	0.694
Mean	0.663	0.663	0.663	0.663	0.663	0.663	0.663	0.663	0.663	0.663	0.663	0.663	0.663	0.663	0.663	0.663	0.663
(CH*)'/(CH*)	1.006	0.9819	1.0226	0.99698	1.035	1.021	1.002	0.992	0.998	0.977	1.011	1.027	1.021	1.035	1.0121	1	1.047
					Fuel = 0.133 g/s			Air = 2.65 g/s			Equi. Ratio = 0.86			Power = 6.66kW			
S/N	1	2	3	4	5	6	7	8	9	10	11	12	13	14	15	16	17
TIME (S)	0.008	0.016	0.024	0.032	0.04	0.048	0.056	0.064	0.072	0.08	0.088	0.096	0.104	0.112	0.12	0.128	0.136
Background Intensity	0.002	0.002	0.002	0.002	0.002	0.002	0.002	0.002	0.002	0.002	0.002	0.002	0.002	0.002	0.002	0.002	0.002
Mean value of each ima	0.735	0.729	0.695	0.711	0.725	0.687	0.722	0.702	0.711	0.716	0.702	0.699	0.728	0.739	0.723	0.732	0.743
Actual (CH*)' Intensity	0.733	0.727	0.693	0.709	0.723	0.685	0.72	0.7	0.709	0.714	0.7	0.697	0.726	0.737	0.721	0.73	0.741
Mean	0.714	0.714	0.714	0.714	0.714	0.714	0.714	0.714	0.714	0.714	0.714	0.714	0.714	0.714	0.714	0.714	0.714
(CH*)'/(CH*)	1.027	1.0182	0.9706	0.993	1.013	0.959	1.008	0.98	0.993	1	0.98	0.976	1.017	1.032	1.0098	1.0224	1.038

5.3.1 Heat Release Oscillation: Swirl Number Dependence

The effects of swirl strength on the vortical structures especially the CRZ were quite significant in chapter four. Thus this sub-section examines the corresponding effects of these changes on the flame heat release fluctuation. Two swirl numbers of 1.05 and 1.50 as well as three fuel flow rate of 0.111, 0.122 and 0.133g/s were used with

different air flow rate to maintain a constant equivalence ratio of 0.85 as given in table 5.6.

Figure 5.11 and 5.12 compare the magnitude of heat release fluctuation for the two swirl numbers. The plots indicate an increase in the magnitude of the heat release fluctuation in the higher swirl number of 1.50 especially for a fuel flow rate of 0.122 g/s. Whereas the heat release oscillation in most cases stays below the limits of 0.95 and 1.05 (indicated by the dotted lines) in the lower swirl strength of 1.05, the oscillation in the higher swirl strength of 1.50 goes beyond both limits thus showing the influence of the swirl strength on the heat release rate. Figure 5.13 with a similar low swirl number but with the nozzle length reduced by half also shows a reduced heat release oscillation as compared to the higher swirl strength.

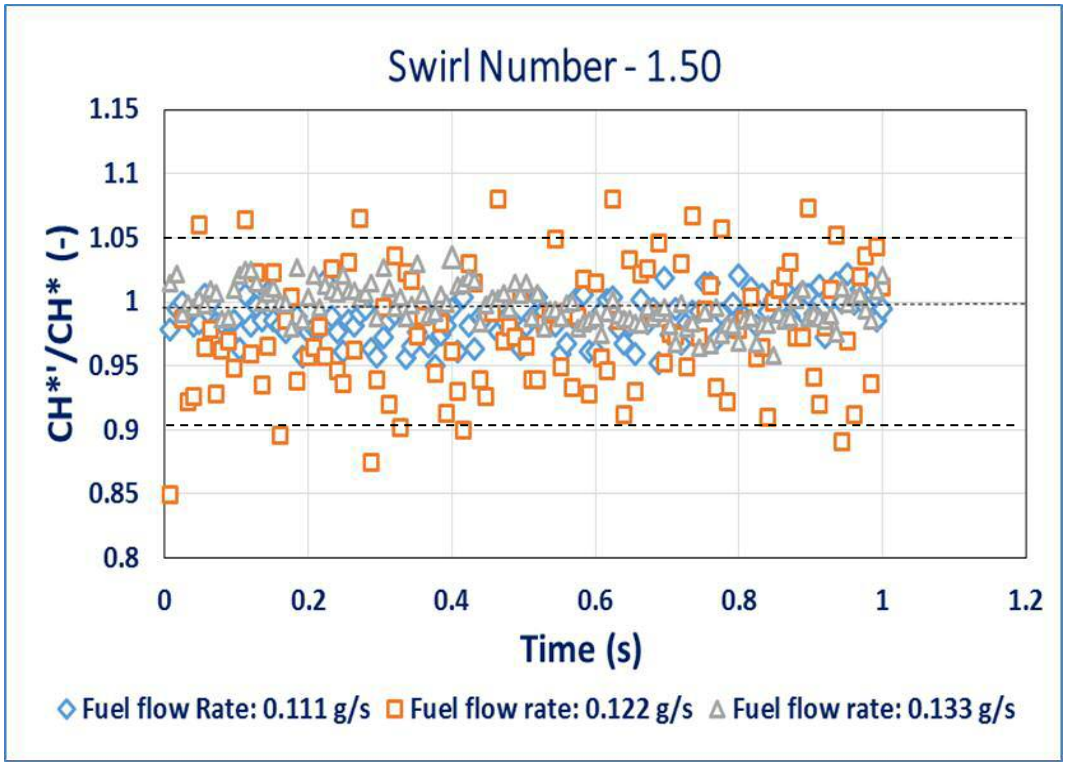

Figure 5. 12 Heat release oscillation [S=1.50]

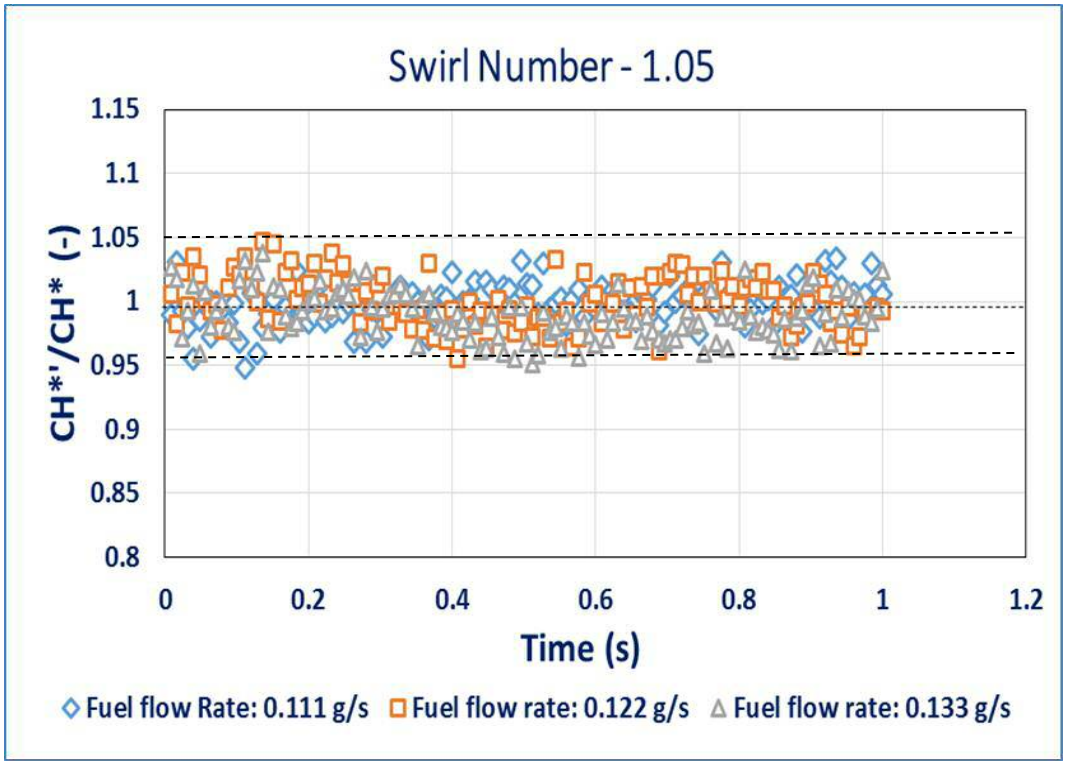

Figure 5. 13 Heat release oscillation [S=1.05]

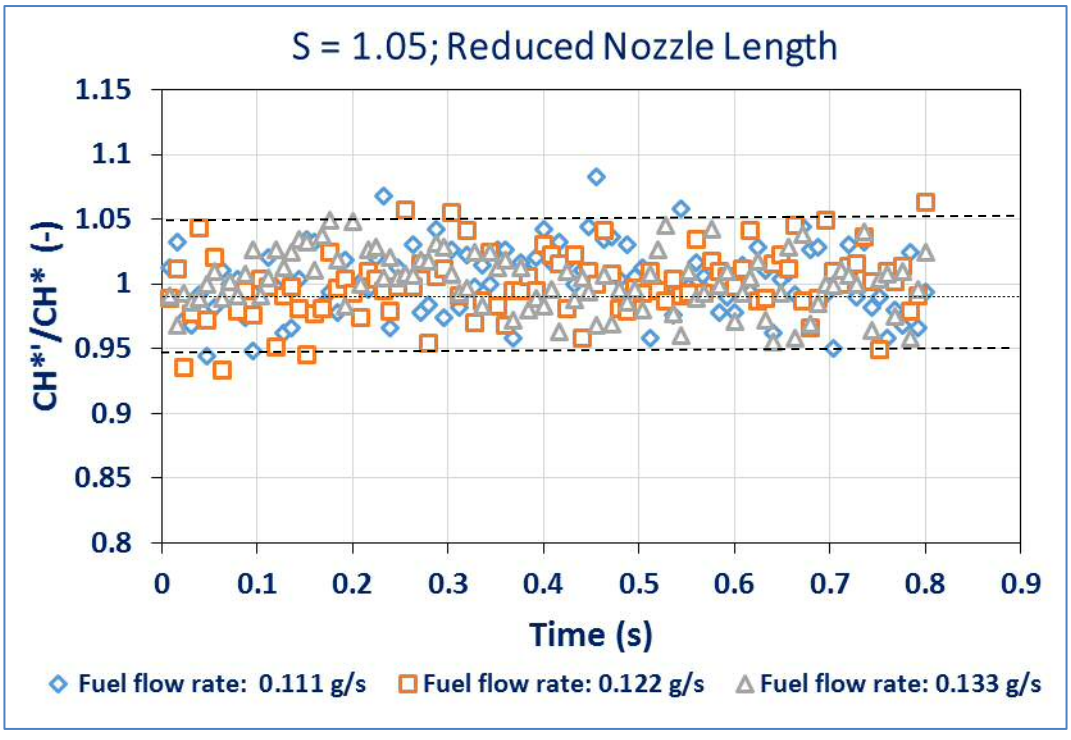

Figure 5. 14 Heat release oscillation [S = 1.50; Reduced Nozzle Length]

The heat release fluctuation rate with changes in swirl number is attributed to the contortion and convolution of the flame by the vortex structures of different swirling

flows. There are many mechanisms responsible for this behaviour. The vortical structures of the shear layer when convected downstream dissipate into small eddies. The increased in swirl strength further distorts the sizes of the vortices and breaks them further into smaller pieces due to the strong recirculation of the flow, which might generate vortex shedding whose frequency is far apart with different swirl numbers. The PVC starts evolving from the shear layer as it originates at the back-facing step, as a result of the Kelvin- Helmholtz instabilities in axial and azimuthal planes. It turns severally, before being split. However, the increased swirl makes the spiral more complicated with alternating frequencies. Also, the increased swirl enhances the flame stiffness and makes the flame less sensitive to the structural fluctuation of the flow field. Although the swirl number has less influence on the oscillation frequency of heat release, the wave amplitude becomes highly influenced.The work of Huang [208] [209] shows that heat release fluctuations are directly linked to the fluctuations in the flame surface area, which is a function of the swirl number. As the swirl number gets to an extreme value of 1.50 further complexities are introduced which could widen the heat release rate disparity between these swirl strength. The vortices generated within the edge of the backward-facing step which could also lead to the creation of new flame pocket as the flame moves downstream.

5.3.2 Heat Release Oscillation Rate: Fuel Dependence

The changes in the physical, chemical and thermodynamic properties of the combustion system as a result of the blend of methane with CO_2 was tested with 30 and 15% of CO_2. Figures 5.14 show the plots of heat release rate oscillations of methane and a blend of methane with 30% of CO_2 for three fuel mass flow rates, while other parameters were kept constant. Whereas the heat release oscillation for the methane flame (Figure 5.14a) goes beyond both limits of 0.95 and 1.05 (indicated by the dotted lines), especially for the fuel flow rate of 0.122 g/s, the heat release oscillation for the methane – 30% CO_2 flame (Figure 5.14b) stays below the limits, thus showing a reduced heat release oscillation for the methane- CO_2 flame. A similar reduced heat release oscillation was observed in Figure 5.15 with methane – 15% CO_2 with similar fuel flow rates. The oscillation goes further below both limits and

demonstrates that a lower percentage of CO_2 blended with methane gives the least heat release oscillation.

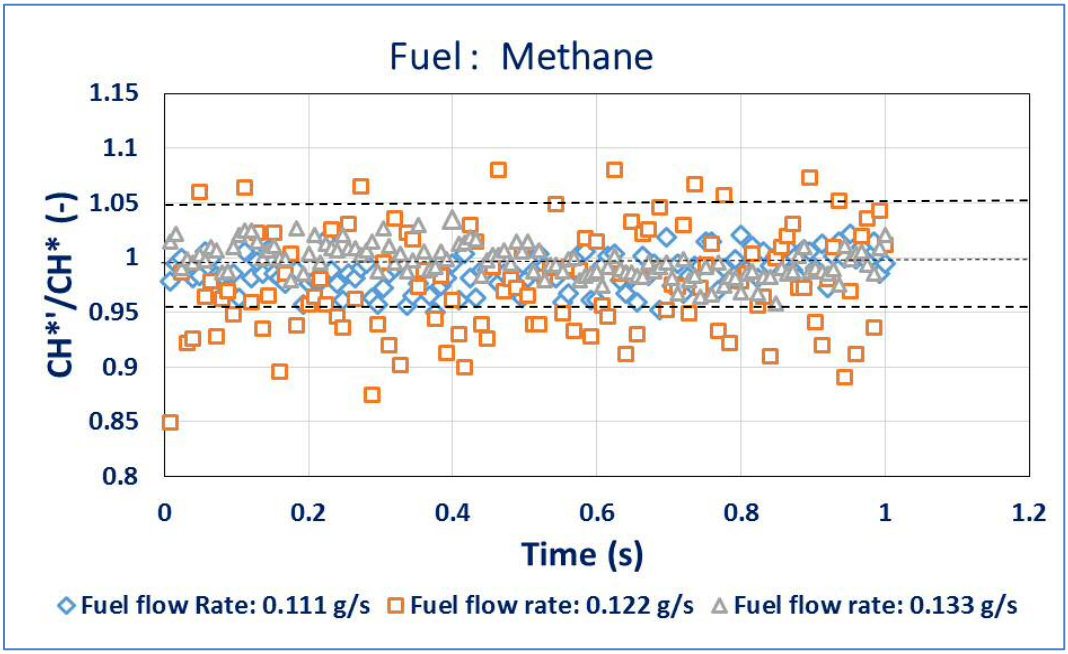

(a)

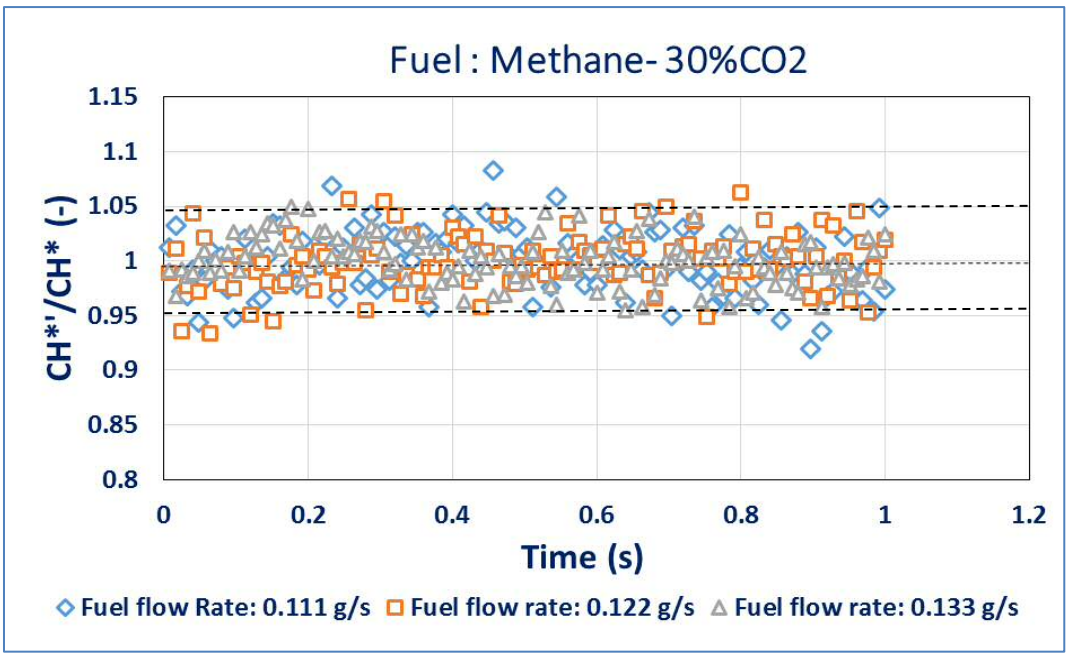

(b)

Figure 5. 15 Heat release oscillation: (a) Methane (b) Methane - 30% CO_2

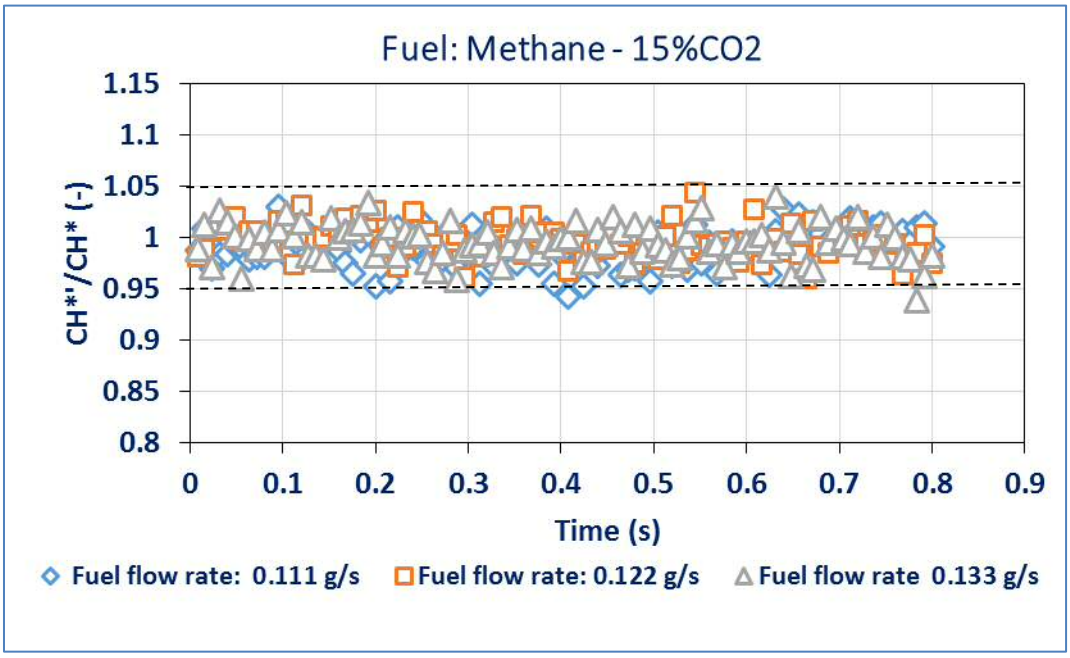

Figure 5. 16 Heat release oscillation Methane – 15% CO_2

As described in the literature review, The addition of CO_2 to pure methane reduces the calorific value of the mixture [23], the turbulent flame speed and flame temperature as well as the NOx formation, [147 - 151]. The general view is that CH4/air- CO_2 flame has a reduced flame temperature compared to the CH4/air flame with corresponding strain rate especially when radiant effects are considered. The addition of CO_2 to methane-air has a diluent effects due to the relative reduction in the concentrations of the reactive species and direct chemical effects as a result of the breakdown of CO_2 through the reactions of third-body collision and thermal dissociation, [152]. The heat capacity of CO_2 is much higher than air, and its absorption coefficient is quite high. Thus the addition of CO_2 to the fuel mixture is expected to change the flame axial velocity gradient (strain rate). The high density of CO_2 is also assumed to have contributed to the reduction in the turbulence scale in the shear layers, thereby reducing the heat release oscillations. The presence of CO_2 decreased the high momentum flow region velocity drastically while increasing the central recirculation zone velocity since the CO_2's high specific heat increases the pressure differential which drives recirculation with less turbulence, [153], and by extension an enhanced mixing and less heat release oscillation. The above thermodynamics properties of methane –CO_2 fuel reduces the heat release fluctuations, which is a critical component to suppressing combustion instabilities.

The flame power also affects the rate of heat release oscillation. As was observed in Figures 5.11, 5.12 and 5.13 with two swirl strength and Figures 5.14 and 5.15, with two fuel blends all indicated that the fuel flow rate of 0.122g/s with a flamee power of 6.10Kw generated the higest heat release oscillation than the two extreme flow rates of 0.111g/s and 0.133 g/s with flame powers of 5.50 and 6.66Kw respectively, all having the same equivalence ratio of 0.85, Table 5.5 and 5.6. In this case, the changes in the heat release oscillation with fuel flow rate (flame power) is attributed to the CH4-CO_2- air variations, which depends largely on the mass-based additive to fuel ratio, [146].

5.3.3 Forcing Frequency Effects on Heat Release Fluctuation

The effect of forcing frequency on the heat release fluctuations was assessed by subjecting the flame to many frequencies at a constant amplitude of A = 0.3, and the flame response was measured. Figures 5.16 plot the heat release rate evolution with changes in forcing frequencies from 60 to 500 Hz, at a forcing amplitude of A= 0.3, for a swirl number of 1.05. As shown in the figures, the frequency range of 60 – 200 Hz has many colour bands (which represent the specific CH*'/CH* intensities). These colour bands mix with each other regularly from a CH*'/CH* ratio of 0.60 to 1.36. The frequency range of 200 to 350Hz presents heat release fluctuation domain whose colour bands are fewer. The colour bands in this location individually occupy large portions of the domain which signifies a reduction in the rate at which these fluctuations switch from one value to another. Further reduction in heat release perturbation is observed as the frequency range is increased from 350 to 500Hz with further reduction in the colour bands and the rate of the switch from one value to another.

Similar trends were also observed at a higher swirl number of 1.50. Figures 5.17 present the Tecplots of the heat release rate with similar frequencies at the same forcing amplitude of 0.3. The range of 60 – 200Hz again presents many colour bands which are regularly mixed with values ranging from 0.60 to 1.50, but with a reduction in the fluctuation rate when compared to the fluctuations generated by a swirl number of 1.05, for the same frequency range. The corresponding reduction in the heat release fluctuations is also observed with further increase in frequencies for

the ranges of 200 to 350Hz and 350 to 500Hz respectively. These results show that low-frequency acoustics generate high heat release fluctuations as a result of the high impact of the surface area oscillation of the flame. High frequencies generate lesser heat release fluctuations since they have less influence on the flame surface area. However, they could affect the flame propagation significantly. These results are in agreement with the findings of many authors [119][122][210], which show the saturation of the gain of heat release oscillation at high frequencies of excitation.

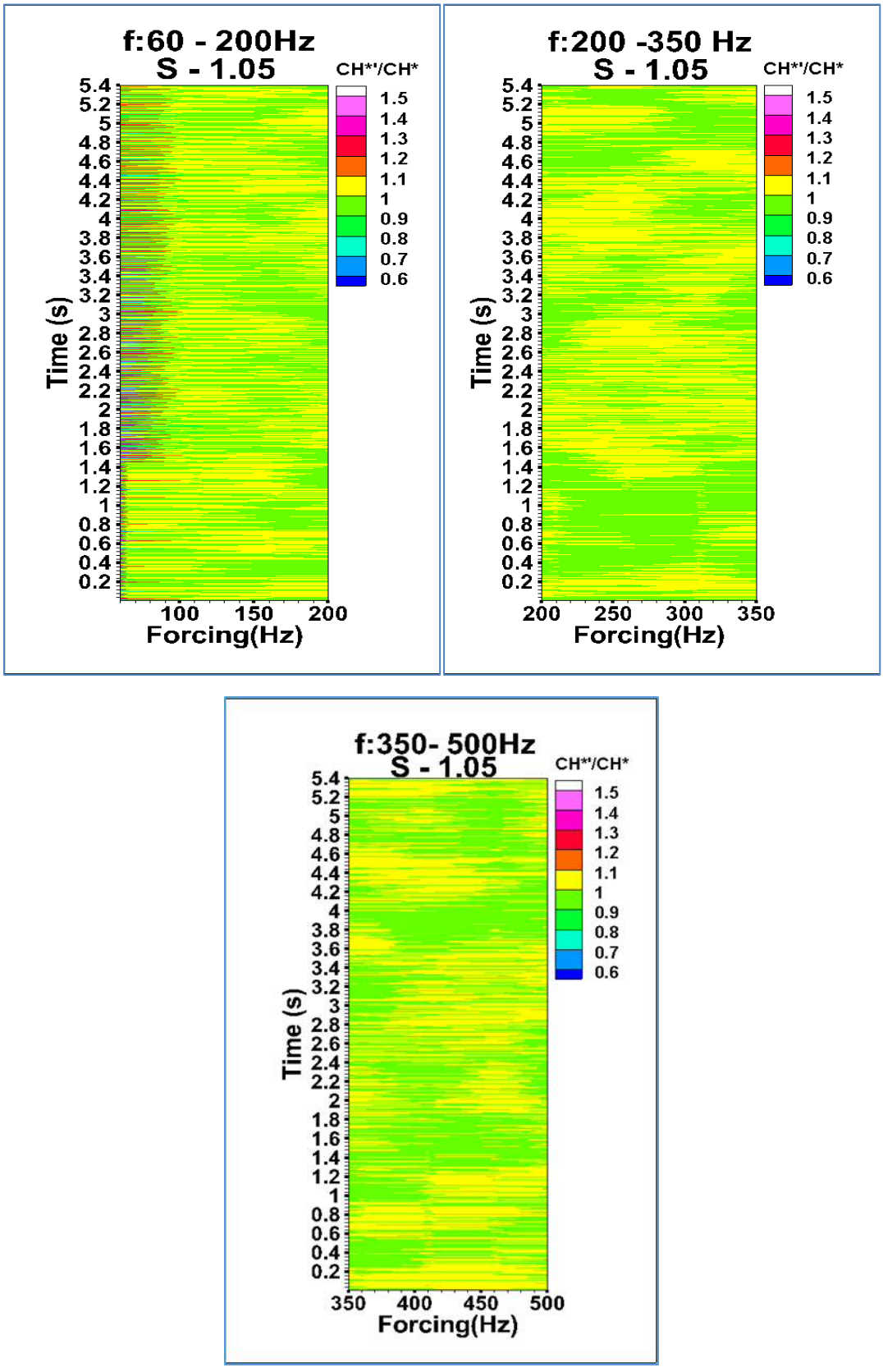

Figure 5. 17 Heat release fluctuation rate with forcing frequencies [S = 1.05]

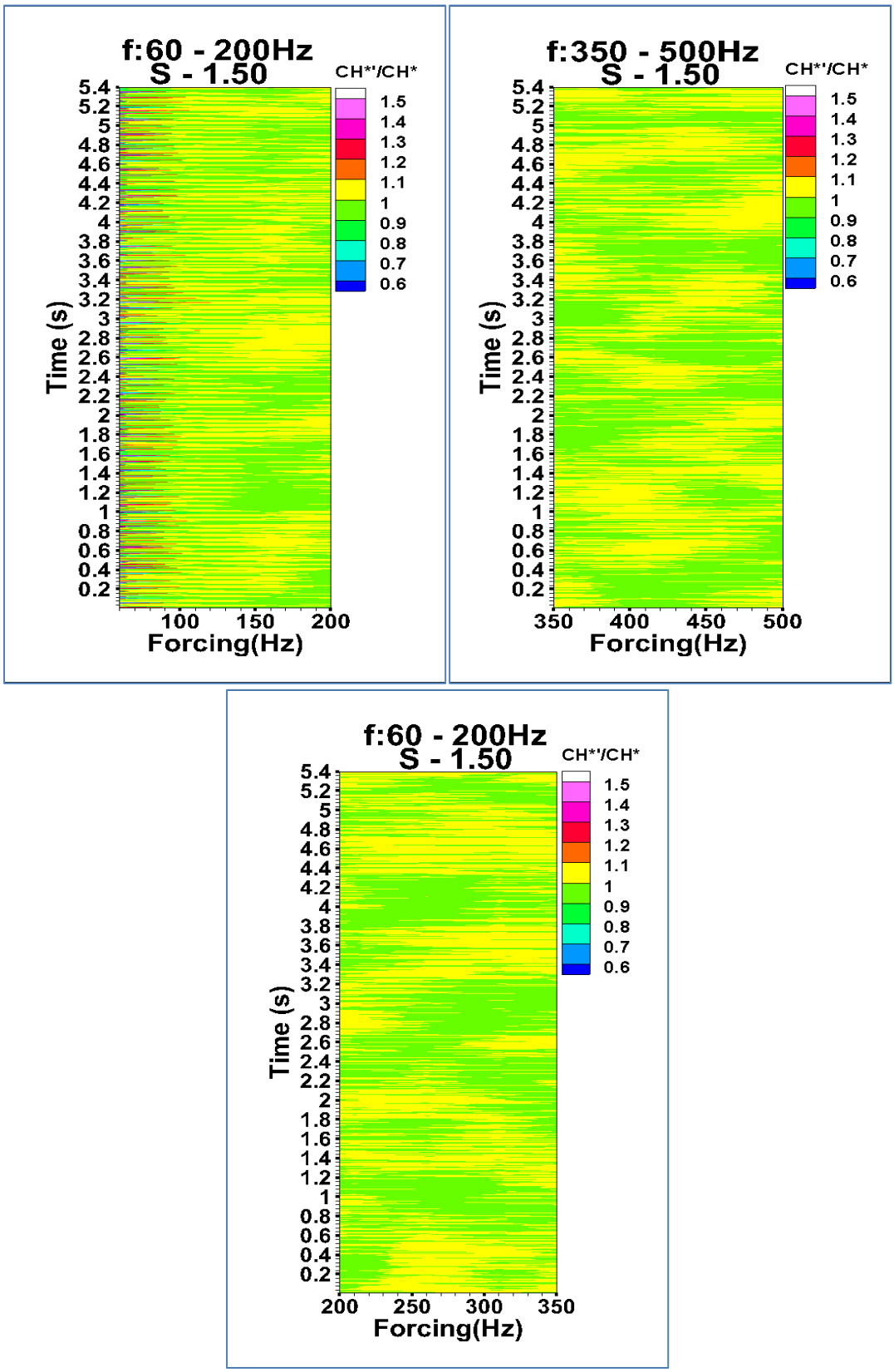

Figure 5. 18 Heat release fluctuation rate with forcing frequencies [S = 1.50]

5.3.4 Forcing Amplitude Effects on Heat Release Fluctuation

The heat release fluctuations in response to the forcing amplitudes were also observed. Forcing introduces sinusoidal wrinkles on the flame which envelopes it linearly in low amplitude but nonlinearly as the forcing amplitude rises. The flame also responds to the frequency of forcing as a result of the growth and decay in the flow vortical structures which are convected to the flame.The background turbulence brings further corrugation on the flame over a range of length scales. Thus the dominant features of the vortical structure oscillation on the flame are the flame anchorage oscillation, flame area fluctuation and the flame propagation normal to itself at the local flame speed. These result in a symmetric distortion on the flame surface area with amplitude as a function of the forcing magnitude.

Figure 5.18 shows the effects of the forcing amplitude on the heat release fluctuations, for (a) A= 0.2, (b) A= 0.3 and (c) A= 0.4 with similar frequency range of 60 – 500Hz. In all the three cases, heat release fluctuations became saturated for high frequencies (200 – 500Hz) but increases with increased amplitude at lower frequencies of 60 – 200Hz, which is in agreement with the reported work of X. Han et al., [119]. The contortion of the flame by the flow vortices is damped within a short duration of time, but the corrugations on the flame sheet persist as the flame moves downstream. Santosh, [211][212] observed that when flames are excited, the convective wave length of the flame front disturbance is equal to the distance that a disturbance propagates at the mean flow velocity travelling in one acoustic period, as the formation of the vortical structures shares the same period with the forcing. Thus at a higher forcing amplitude, the flame starts to cusp indicating the nonlinear flame response to the forcing. A transfer function which should relate this heat release fluctuations to the incident amplitude changes was not obtained at this point, due to the low repetition rate of the high speed camera that was used, however these trends in heat release and flow vortical structures at different conditions were used as the bases for the evaluation of the flame dynamics and its resultant effects on the combustor acoustics.

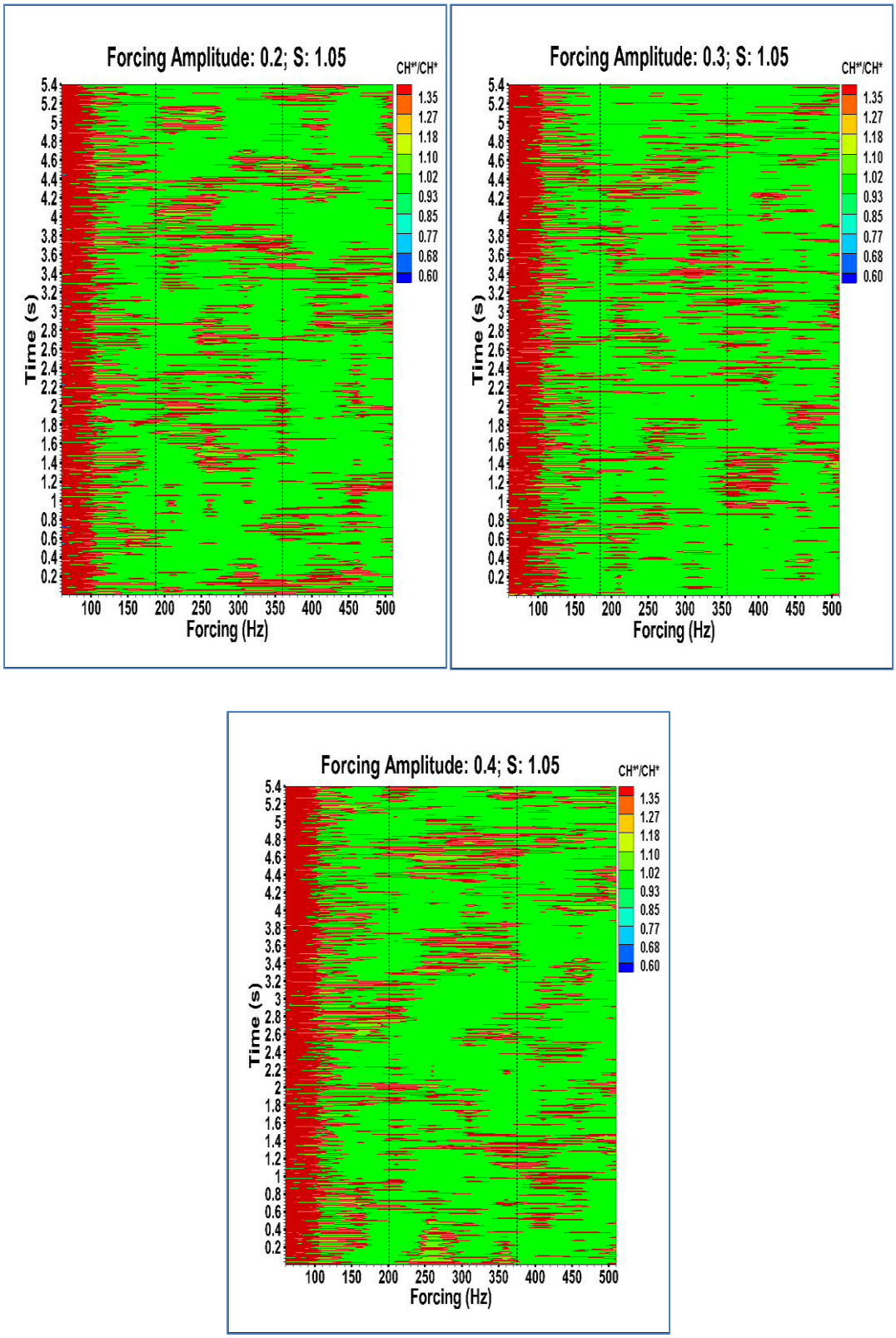

Figure 5. 19 Flame heat release response to forcing amplitude [S = 1.05]

5.4 Summary

The first step was to characterise the flame operational limits of the rig, being a newly designed and manufactured burner. The system was run with methane and air as oxidant with a swirl number of 1.05 and 1.50 under open and confined flame conditions. The aim was to ascertain the flame behaviour and to determine the operational limits of the burner.

The results revealed that an open flame has a wider operating range with a long flashback range up to an equivalence ratio of about 3.00 and a short blowoff limit at an equivalence ratio of 0.93 in most flow rates for both swirl strength. Confined flames were observed to have a relatively short operating limit with the flashback at an equivalence ratio of about 1.50, while the blow-off limit went as far as the equivalence ratio of 0.56. The differences in these operating limits between the open and confined flame are attributed to the influence of the ambient air in the open flame so that more fuel is required to burn the additional air. Because most practical systems use confined flame conditions, the rest of the study was based on confined flame condition.

Three conditions: swirl strength, divergent nozzle angle and fuel blend were used to assess their effects on the blowoff limit of the burner, with a view to optimising them using these conditions.The result revealed that an increased swirl strength moved the blowoff limits in both the high and low flow rates to leaner regions. This enhancement of the blowoff limits with increased swirl strength is attributed to many mechanisms including increased turbulence burning velocity of the flame, especially at the base, as the local velocity oscillation is increased. The increased swirl strength also increased the CRZ, thus creating a larger domain for thorough mixing of the fuel and air, with good anchorage and stability.

The changes in the divergent nozzle angle also showed a significant influence on the blowoff limits. At a lower fuel flow rate, the change in the divergent nozzle from 90 to 60 and 45 degrees showed an increased blowoff limits towards a leaner equivalence ratio by about 9.3 and 4.6% respectively. At a higher fuel flow rate, the reduced divergent angle only showed a marginal increase in the blowoff limits by about 1 % in both cases. These changes in the blowoff limits with a change in the geometry of

the nozzle are also attributed to the corresponding changes in the shape, size and location of the vortical structures of the flow field.

The heat release oscillation was also reduced significantly with the blend of methane baseline fuel with 30% of CO_2. This reduction is attributed to the diluent effects of CO_2 as the concentration of the reactive species are relatively reduced. Its high density is also assumed to have suppressed the turbulence scale in the shear layers, with enhanced recirculation. Other contributory characteristics of CO_2 to the reduction in the heat release oscillation include the reduction in the calorific value of the mixture, reduced flame speed and temperature etc.

The results also revealed that low-frequency forcing generates high heat release fluctuations as the oscillation rate saturates at high frequencies. Heat release oscillation was also affected by forcing amplitude as heat release oscillation increases with increased forcing amplitude at lower frequencies but with little or no effect at higher frequencies. This variation is linked to the impact of the forcing on the flame surface area oscillation. These scenarios show the capability of the combustor geometry and fuel conditions to control the flame stability especially near the blowoff domain and to influence the heat release fluctuation rate being a key component of combustion instabilities in premixed combustors.

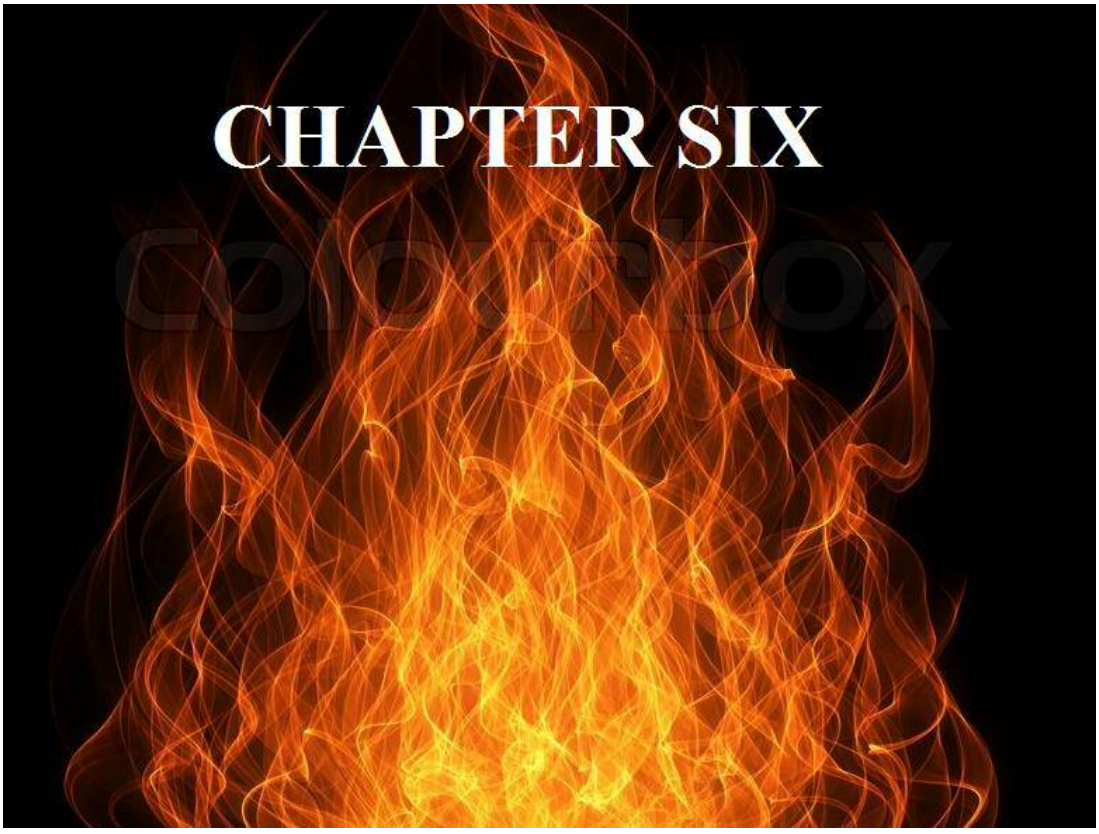
CHAPTER SIX

CHAPTER SIX:

ACOUSTICS AND STABILITY

A theory is a supposition which we hope to be true, a hypothesis is a supposition which we expect to be useful…
-George Stoney

Having demonstrated the effectiveness of controlling the flow and flame fields using inherent parameters, this chapter assesses the corresponding effects of these parameters (swirl, fuel and forcing) on the stability of the combustor dynamic pressure (acquired by pressure transducers) using spectral analysis. The stability criterion is based on the amplitude of the pressure power spectrum, where a reduction in the amplitude corresponds to the damping of the acoustic modes, thus a decrease in the level of instabilities. This technique has been used in many published studies [213 - 217][201]. The prospects of using the combined effects of the above parameters to suppress combustion instabilities are envisaged. Adequate understanding of the acoustic response to these factors could open new frontiers in the control of combustion instabilities in lean premixed burners both open and closed loop active control. This seems quite realistic as all the parameters involved could be numerically controlled, the latest being the reported work of Durox [89] on the variable swirl strength during combustion.

Section 6.1 spectrally examines the acoustic modes of the combustion chamber with methane and its blend with CO_2, without the application of external excitation. Its response to inlet velocity fluctuations, swirl strength and equivalence ratio are also studied. Section 6.2 takes an empirical study on the overall acoustic modes of the combustor when externally excited with low frequency range, different swirl and equivalence ratios. The effect of flame forcing is examined by comparing the forced and unforced flames. Section 6.3 extends the study to the excitation of methane-CO2

flames with several swirl and forcing conditions, and section 6.6 summarises the chapter.

6.1 CAM Characterization of Methane; Methane-CO_2 Flames

This section examines the natural acoustic modes of the flame confined with a 400mm length and 84mm diameter cylindrical combustor with the end open to the atmosphere, as described in section 3.1.2. The acoustic modes obtained were used as baseline values from which the response of the system to external excitation was measured in other sections. This analysis was done by evaluating the combustor's dynamic pressure using the Fast Fourier Transform (FFT), a mathematical algorithm which calculates the discrete Fourier transform of a signal by decomposing it into different frequencies with corresponding spectral power. The dominant resonant frequency during combustion was obtained as well as the evolution of its power spectrum with changes in swirl strength, fuel and equivalence ratio. The computation was done using Matlab codes with the time series pressure signals as input data, details in Appendix B3. This analysis was done for the swirl number of 1.05 and 1.50, the equivalence ratio of 0.7 and 0.8 at different inlet velocity ratios as shown in Figure 6.1. The velocity ratio was obtained as the ratio of the RMS to the bulk flow velocity, controlled by the fuel and air flow rate as well as the inlet pressure of the air, as read off online by the LDA.

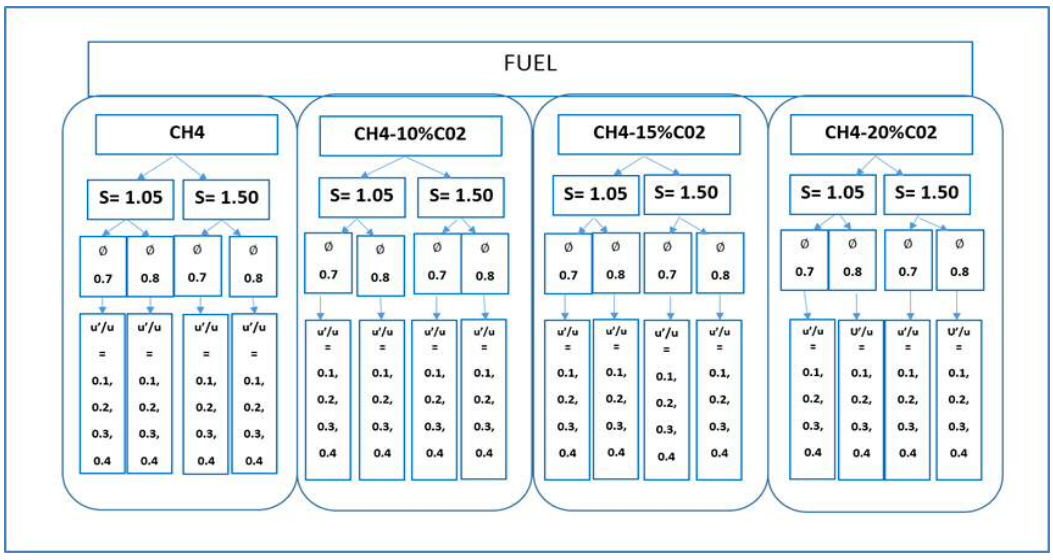

Figure 6. 1 Combustion cases with different fuel mixtures and swirl strength

6.1.1 Methane Flame

Figures 6-2, show the acoustic modes of the combustor for methane flame with a swirl number of 1.05; equivalence ratio of 0.7 and 0.8 at an inlet velocity ratio of u'/u= 0.3. A dominant frequency mode of 150Hz in both cases with a spectral power of 0.46E-3 KPa^2 at the equivalence ratio of 0.7, Figure 6.2a, and 0.53E-3 KPa^2 at 0.8, Figure 6.2b, equivalence ratio. Other acoustic modes with insignificant amplitudes were observed. These weak acoustic modes are attributed to the ambient noise and were discarded in the analysis. The plots show that in some swirl and velocity conditions, a change in equivalence ratio has a minor effect on the amplitude of the resonant frequency. As the swirl number was increased to 1.50, Figures 6.3, the dominant frequency remained at 150Hz but with about 40% increase in power spectrum in the leaner condition of = 0.7, Figure 6.3a, while the amplitude remains same at = 0.8, Figure 6.3b.

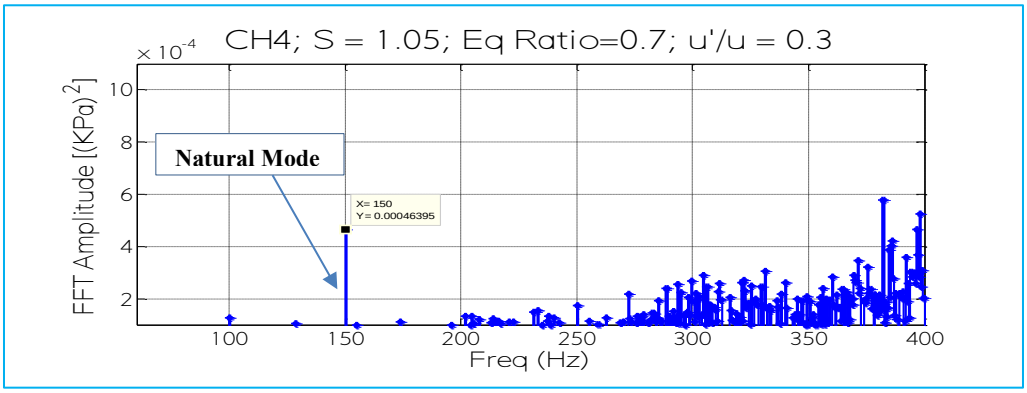

(a)

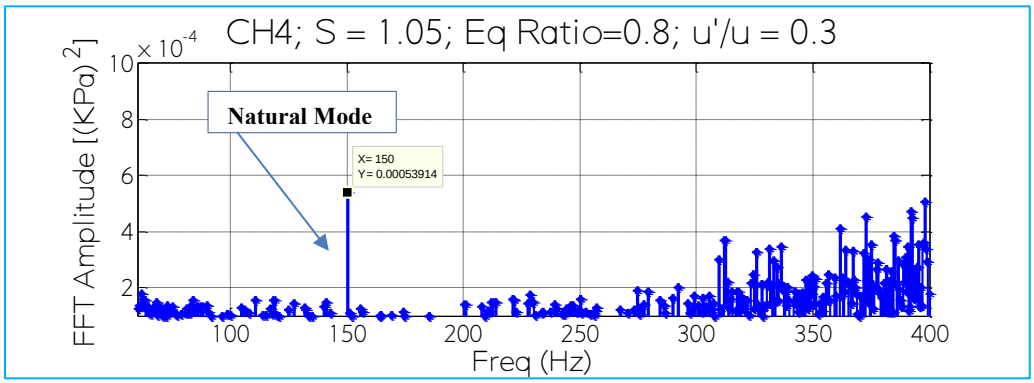

(b)

Figure 6. 2 Acoustic modes of methane flame: CH4; S= 1.05; = 0.7, 0.8; u'/u = 0.3

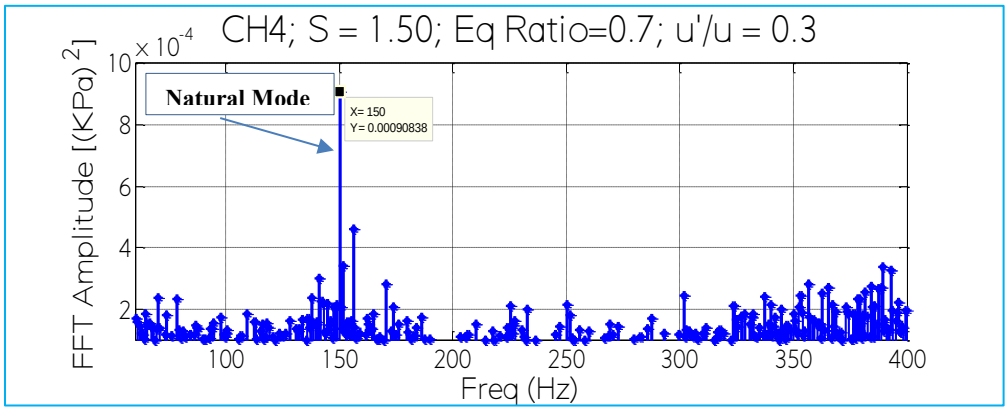

(a)

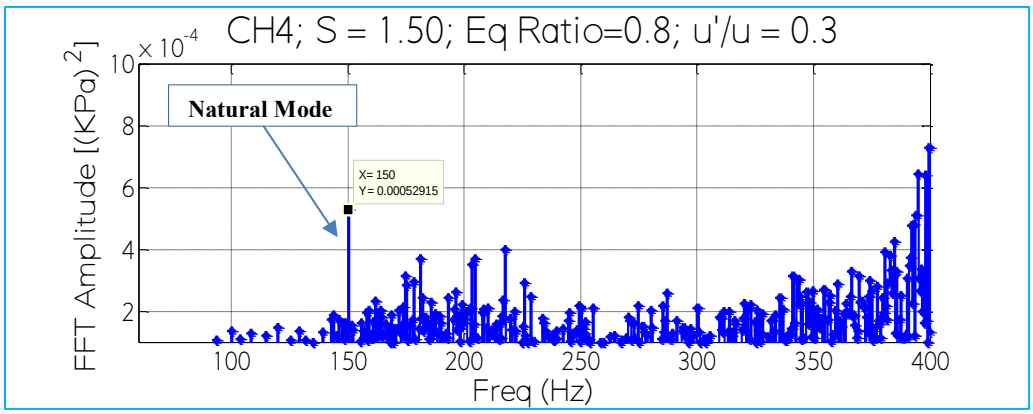

(b)

Figure 6. 3 Acoustic modes of methane flame: CH4; S= 1.50; = 0.7, 0.8; u'/u = 0.3

With this higher swirl strength, a change in inlet velocity amplitude to 0.1 reduced the power spectrum to 0.53E-3 KPa^2, in both equivalence ratios Figure 6.4. The increase in power spectrum with increased equivalence ratio at a higher swirl strength is attributed to increased size of the CRZ as illustrated in Figure 4.16 and the corresponding increased in heat release fluctuation rate as illustrated in Figures 5.11 to 5.13. The increased leaness in this condition creats more pockets of rich and weak mixtures in the flame zone, However, this behaviour needs to be validated with many velocity ratios.These results show that acoustic intensity could be altered with a trade-off between the flow swirl strength and the amplitude of the inlet flow velocity oscillation.

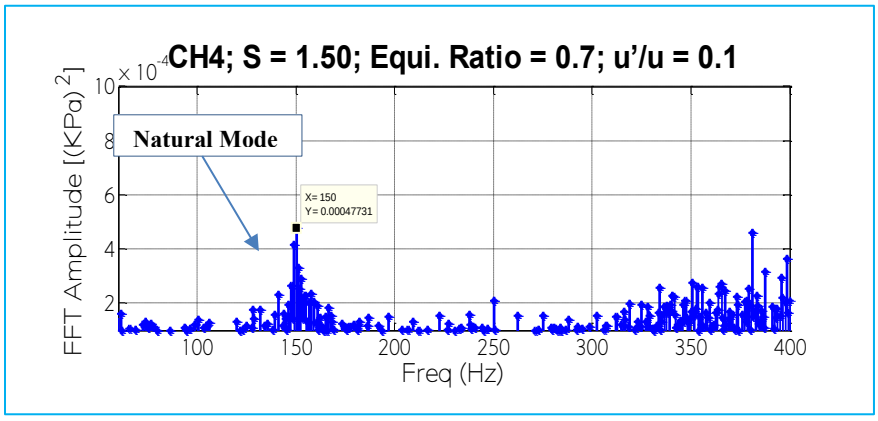

(a)

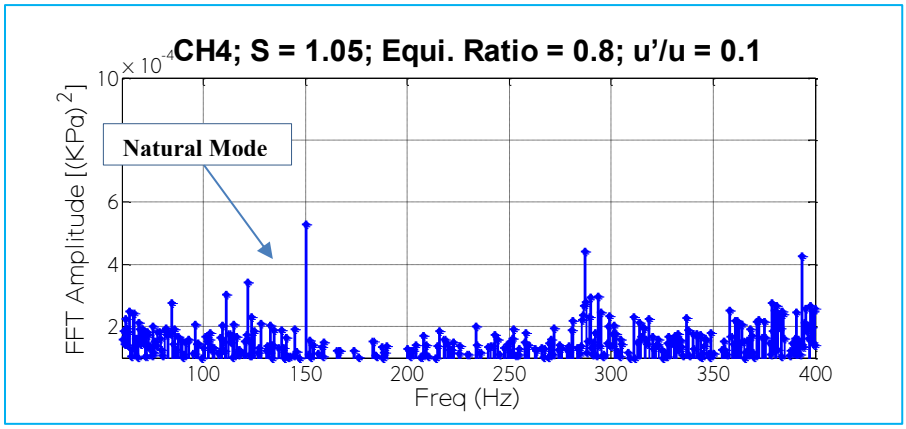

(b)

Figure 6. 4 Acoustic modes of methane flame: CH4; S= 1.50, 1.05; = 0.7, 0.8; u'/u = 0.1

Thus the changes in the flow field are convected to the flame with corresponding changes in the heat release fluctuation rate, which interacts with the inherent dynamic pressure of the system resulting in the growth or damping of the acoustic modes depending on their relative phase. It is also evident that while equivalence ratio variation has little influence on the acoustic mode at a swirl number range within unity, acoustic mode fluctuation becomes very significant at a higher swirl number, with specific values of inlet velocity ratio. This shows that a better combination of the swirl strength, equivalence ratio, and inlet velocity perturbation could provide a degree of control of the disturbance in the combustor without the modulation of the fuel flow rate or the use of external excitation.

6.1.2 Methane – CO_2 Flame

Figures 6.5 compare the acoustic modes of four conditions (two swirl conditions with two equivalence ratios each) of methane flame with a 10% CO_2 blend with methane. Figure 6.5a shows the acoustic amplitude evolution of pure methane flame in all the four-velocity amplitudes. In all the cases except u'/u = 0.3, the equivalence ratio of 0.8 at a higher swirl number shows a higher spectral power above the 0.005E-3 KPa ^2 thresholds in the three cases followed by the leaner mixture of = 0.7.

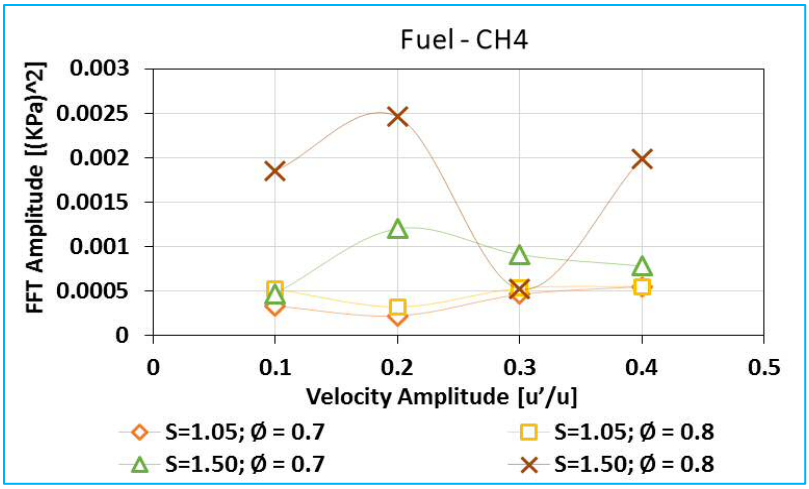

(a)

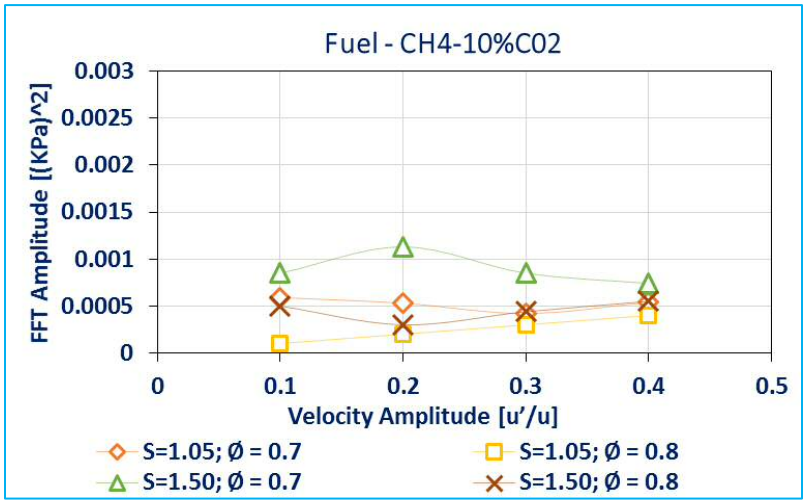

(b)

Figure 6. 5 Amplitudes of 150Hz modes of: (a) Methane flame and (b) its blends with 10%CO_2

The plot demonstrates that a flame could be more stable at leaner fuel condition with a high swirl strength. This is attributed to the fact that, with the increased size of the

CRZ and the flame lift from its anchorage due to increased swirl strength, the increased equivalence ratio results in a more homogenous mixture with minimum heat release fluctuations and a reduced acoustic modes.The acoustic modes of S= 1.05 for the two equivalence ratios have low amplitudes as they fall within the low baseline. With the blend of 10% of CO_2 with methane, the spectral power of = 0.8 at S= 1.50 dropped significantly but with a marginal reduction for = 0.8, Figure 6.5b, while the acoustic modes of the other two low remained the same.

As the percentage of CO_2 was increased to 15%, Figure 6.6a, the amplitudes of all the acoustic modes fell within the baseline, except for S= 1.50, = 0.8 with an increased amplitude at higher velocity ratios. With 20% CO_2 blend, Figure 6.6b, the acoustic amplitudes of the high swirl conditions increased at some velocity ratios. In most of the cases considered, the equivalence ratio of 0.7 at a higher swirl number, showed a relatively lower amplitude of the power spectrum signifying that a leaner mixture could operate in a stable acoustic state at a higher swirl strength with appropriate velocity amplitudes.

Most importantly, it has been shown that acoustic power could be reduced significantly with the blend of methane with CO_2, especially with a low percentage. This is being attributed to the enabling thermodynamic properties of the CO_2 mixed with methane. CO_2 has a higher heat capacity than methane and a high absorption coefficient capable of damping the acoustic energy through thermal dissipation [153]. The high density of the CO_2 also changes the flame axial velocity gradient (strain rate) [29] with an effect on the fluctuation of the chemical time scale of the combustion system. The convective time scale is also altered by the blend, as the high density of CO_2 increases the strength of the recirculation zone due to the high tangential force which enhances the width of the CRZ. It thus takes a longer time for the perturbation at nozzle exit to reach the flame centre of mass. The combination of these characteristics could serve as the basis to reduce the acoustic amplitude of the combustor and by extension reduce the instabilities of the system. However more experimental runs are needed to validate these scenarios.

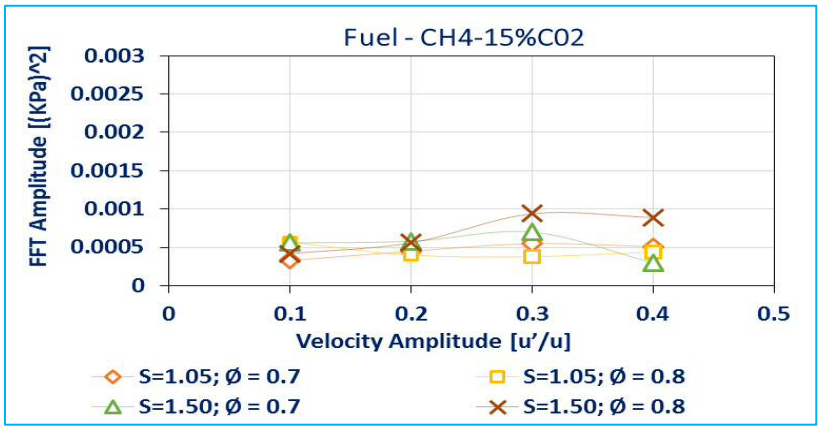

(a)

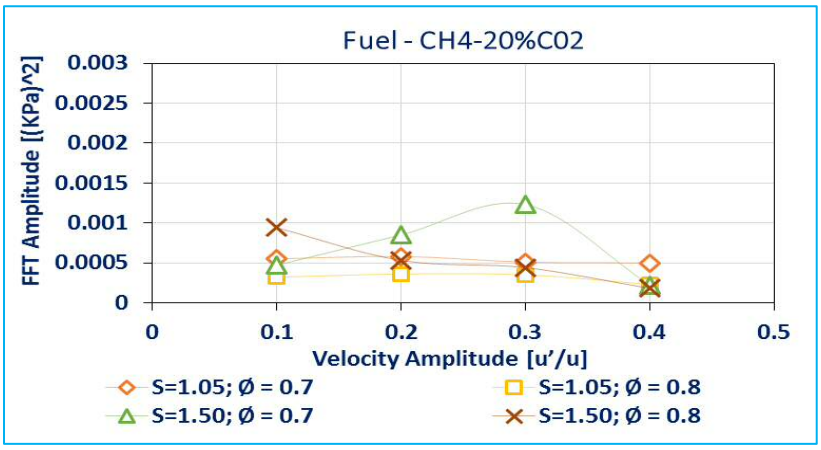

(b)

Figure 6. 6 Amplitudes of 150Hz modes of: (a) Methane- 15 %CO_2 and (b) Methane- 20 %CO_2

6.2 CAM Characterization of Excited Methane Flame

This section takes an empirical study of the overall acoustic modes of methane flame externally excited with low frequencies, different swirl and equivalence ratio. The main aim of this section is to compare the forced and unforced acoustic modes of the combustor. The forcing was done with a loudspeaker placed at the bottom of the plenum as described in chapter three. In many combustion cases [218][219], the length of the combustor is chosen to keep the natural resonant frequency of the combustor out of the chamber so that the forcing frequency becomes the dominant acoustic mode. But in industrial burners with adequate confinement, the same forcing technique keeps both the forced and natural modes interacting within the combustor.

The length of the combustor was consistently maintained at 400mm, to keep the two signals (natural and forced) within the combustion chamber to examine their interactions and the corresponding effects on the system stability. This section considers 16 cases of pure methane-air flame, with two swirl numbers, two equivalence ratios each with four velocity amplitudes. Each of the 16 cases was forced with nine frequencies from 100 to 500Hz with a step of 50Hz as illustrated in Figure 6.7. This frequency range was chosen since known combustion instabilities studies [119][52][210] have shown that acoustic instability modes occur around this low-frequency spectrum. It should be noted that the velocity ratio u'/u of the gas mixture exiting the nozzle was controlled by the voltage of the forcing signal, the flow rate as well as the inlet pressure of air, as read off online by the LDA.

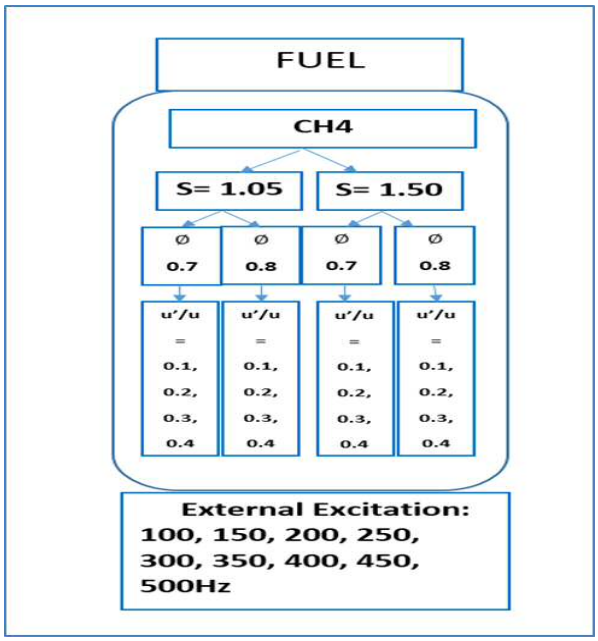

Figure 6. 7 Combustion cases of methane- air flames with forcing conditions

6.2.1 Excited Flame: Swirl Number of 1.50

Figures 6.8 show the acoustic modes of the combustor with a swirl number of 1.50, the equivalence ratio of 0.7, forcing amplitude of 0.3 with forcing frequencies of 100, 150 and 200Hz respectively. For the forcing frequency of 100Hz, there appear two frequency modes: 100Hz with a spectral amplitude of 1.79E-3 KPa ^2 and 150Hz with an amplitude of 0.932E-3 KPa ^2, with their harmonics. As the forcing frequency was

increased to 150Hz, a single mode was observed at 150Hz with a power of 1.026E-3 KPa ^2. This implies that the forced and the natural frequencies are fused up to form a single mode with a particular amplitude.

The forcing frequency was further increased to 200Hz, and there was a reappearance of the two modes at frequencies of 150 and 200Hz, with amplitudes of 0.93E-3 KPa ^2 and 3.13E-3 KPa ^2 respectively. In all these, the frequency of 150Hz which was common in the cases earlier considered without external excitation confirms the frequency as the natural acoustic mode of the combustor. The second acoustic mode observed is that of the forced signal. The harmonics of the two acoustic modes were insignificant, considering their weak magnitudes in most cases. The three figures reveal that the forced flame possesses two acoustic modes (forced and the natural) within the combustor when forced with a frequency other than the natural mode, but with a single acoustic mode when forced with the natural mode frequency of 150Hz.

It is also observed that, with these conditions, the forced signal has a higher power spectrum than the natural mode but the spectral power of the forced mode is reduced when the two modes fuse together at the same frequency. From the figures, the fusion of the two modes at a forcing frequency of 150Hz shows a reduction in spectral power by about 80% of the 100Hz excitation and about 300% with the 200Hz forcing condition. Similar acoustic trends were also observed in Figures 6.9 with a richer mixture of = 0.8. The 100Hz forced frequency has an amplitude similar to its harmonic at 200Hz which is a 50% increase in the amplitude of the natural acoustic mode at 150Hz.

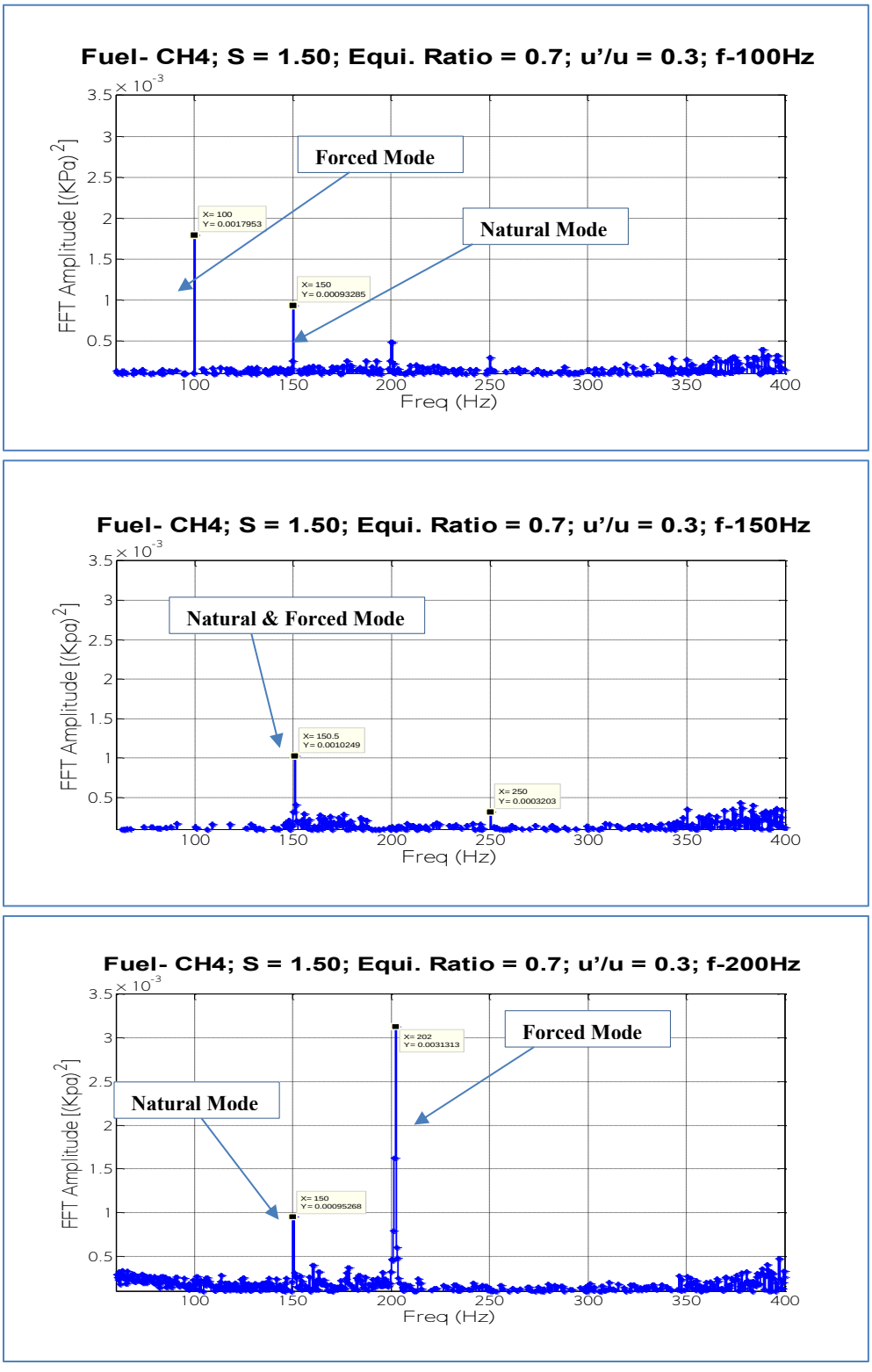

Figure 6. 8 Acoustic modes of methane flame with different swirl, equivalence ratio, velocity and forcing conditions: CH4; S= 1.50; = 0.7; f=100, 150, 200Hz

In the second case with 150Hz forcing, the forced and natural acoustic mode also merged as a single signal with an amplitude almost similar to that of the natural mode

in the first instance. This implies a reduction in the forced acoustic amplitude. In the third case, with a forcing frequency of 200Hz, the natural acoustic mode increases in amplitude by about 75% while the forced mode possesses an extreme amplitude of about 100% higher than the natural mode. These results demonstrate the response of the combustor acoustic modes to the forcing frequencies, equivalence ratio and velocity amplitudes with a high swirl strength of 1.50 swirl number. This implies that the instabilities of the system could be increased or suppressed by the combination of these parameters. Most importantly, it shows the possibility of reducing acoustic instability in a combustor when the flame is forced with a similar frequency to the natural acoustic mode.

The forcing of 100Hz and the natural acoustic mode at 150Hz generate their harmonics at 200Hz and 250Hz respectively. While the forced mode has similar amplitude with its harmonic, the harmonic of the natural frequency has a reduced amplitude of about 50%. These multi-acoustic modes could increase the susceptibility of the system to instabilities as some could couple with other oscillation frequencies such as PVC, hydrodynamic, flow fluctuation, to energise the acoustic modes. In contrast, the fusion of the two frequencies with a reduced amplitude does not have any harmonic, which makes it easy to control in relation to other prevailing oscillation frequencies.

As was also observed in the leaner mixture of = 0.7, the forced flame with a frequency of 200Hz generates a higher amplitude which indicates increased instabilities of the system. In this particular condition, it has been observed that the acoustic amplitude of the forced frequency increases as the frequency goes higher than the natural acoustic mode. However, this needs to be observed in other inlet velocity amplitudes, as would be seen in subsequent sections of this chapter. In general, it could be observed that forced frequencies in relation to the natural mode at a particular velocity amplitude have a substantial influence on the instability of the system.

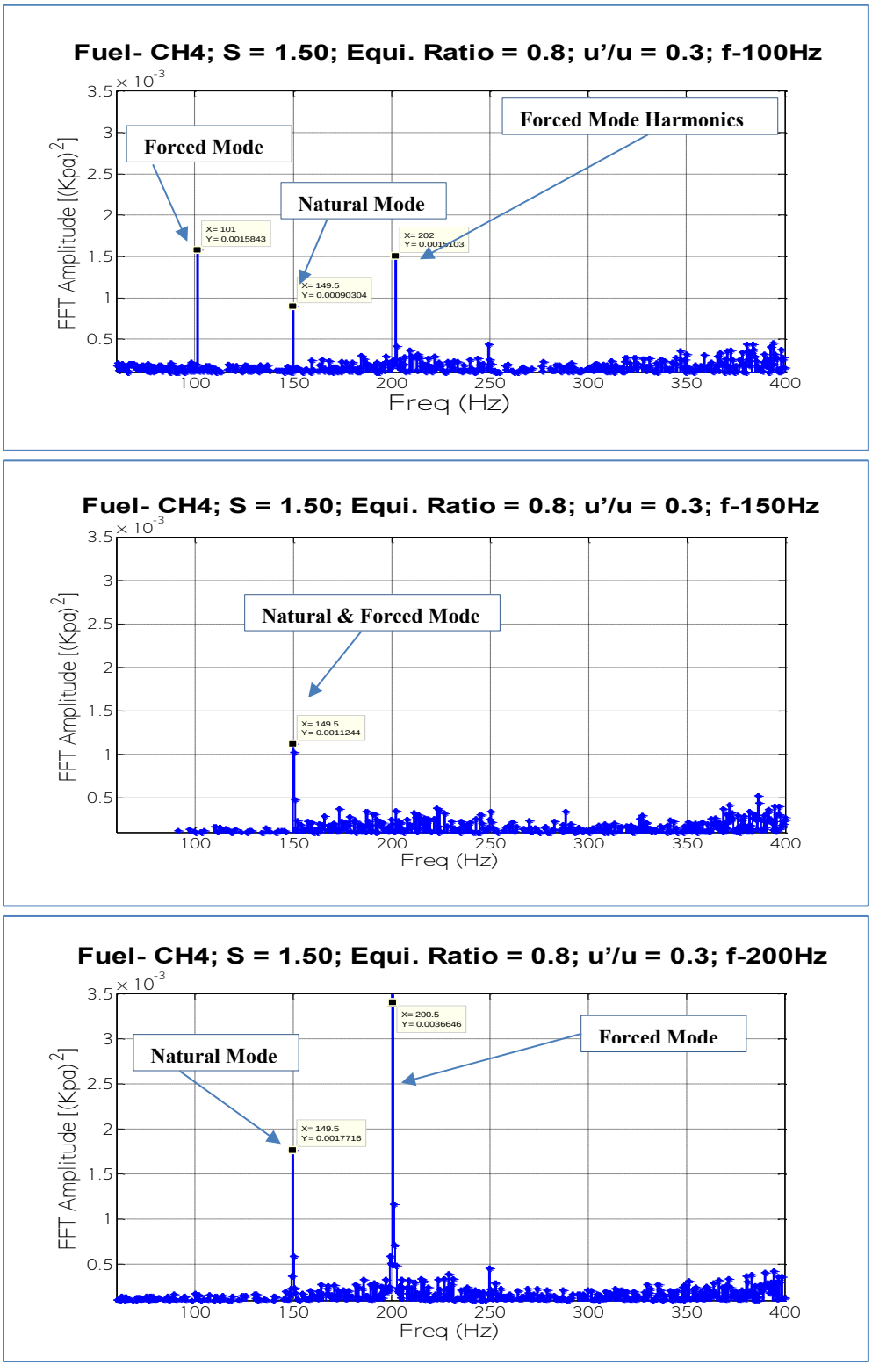

Figure 6. 9 Acoustic modes of methane flame with different swirl, equivalence ratio, velocity and forcing conditions: CH4; S= 1.50; = 0.8; f=100, 150, 200Hz

6.2.2 Excited Flame: Swirl Number of 1.05

Figures 6.10 and 6.11 examine the acoustic modes of the combustor with the forcing frequencies at a reduced swirl number of 1.05. In the first case, the system was forced with a frequency of 150Hz, Figures 6.10, similar to the natural mode of the combustor. The magnitude of this combined modes remained similar to those of the higher swirl number of 1.50. As the forcing frequency was increased to 200Hz, Figures 6.11, the amplitudes of the forced and natural modes were reduced by about 111% and 254% respectively, when compared to the similar conditions in the higher swirl strength in Figure 6.9. With further increased forcing to 250Hz, an increased amplitude of the forced signal by about 21% was observed, while the amplitude of the natural mode remained the same.

It could, therefore, be deduced that the amplitude of both the forced and natural acoustic mode of the combustor was reduced at specific inlet velocity amplitudes when the swirl strength of the flow field was reduced. However, further velocity amplitudes are required to confirm the evolution of these signal amplitudes.

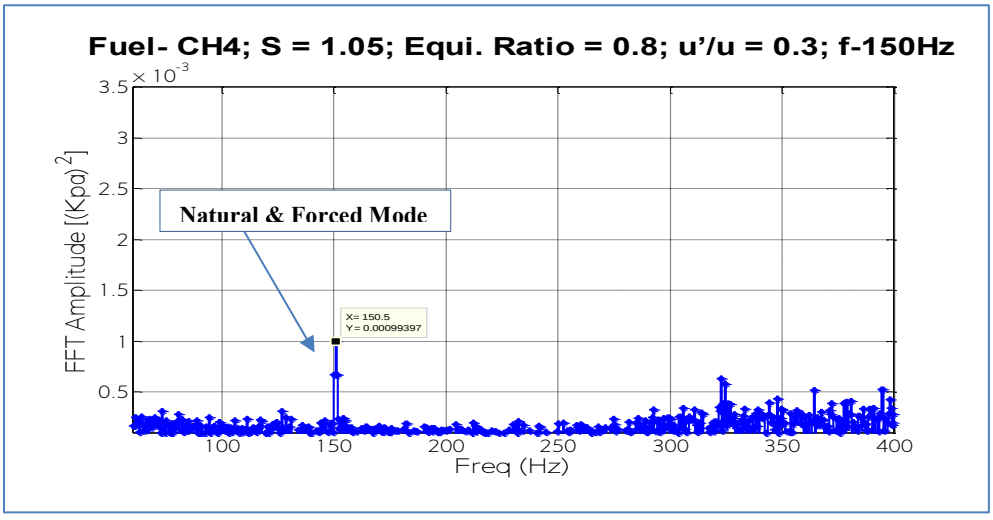

Figure 6. 10 Acoustic modes of methane flame with forcing: S= 1.05; = 0.8; f=150Hz

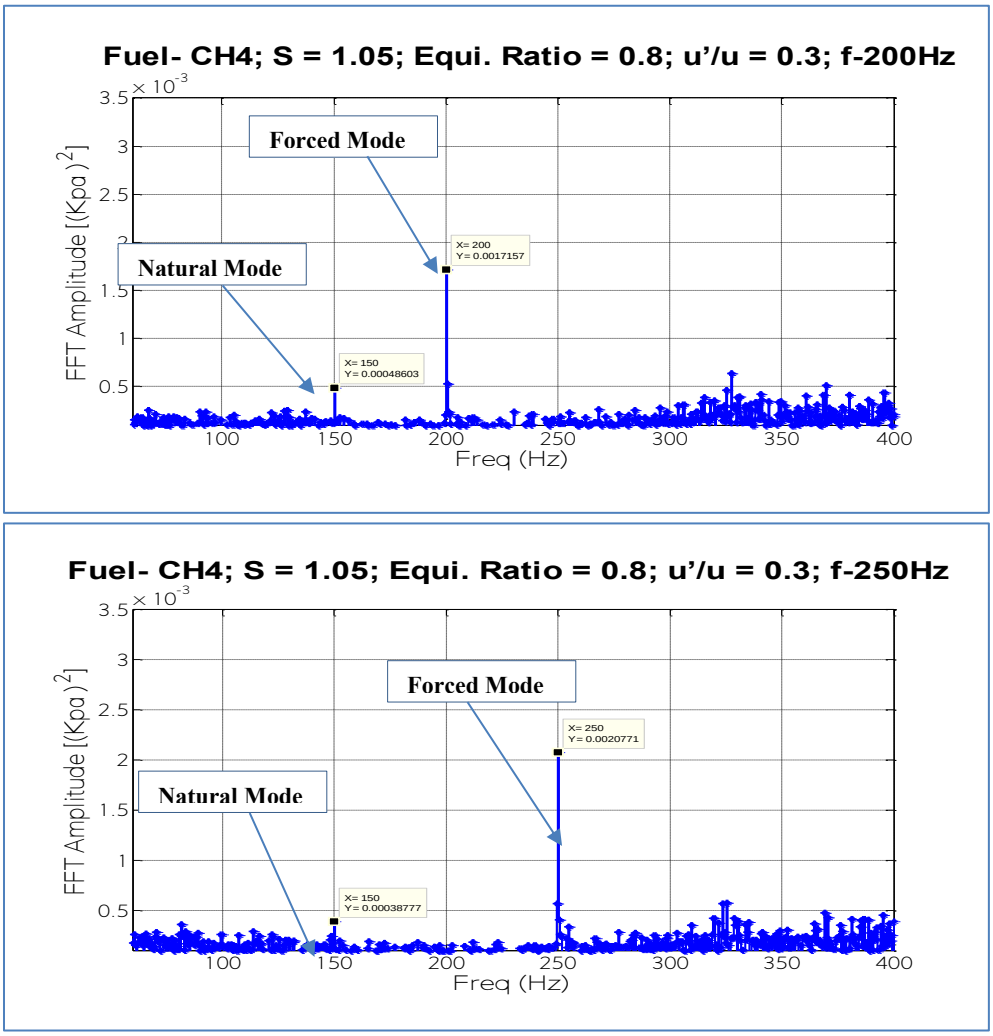

Figure 6. 11 Acoustic modes of methane flame with forcing: S= 1.05; = 0.8; f= 200, 250Hz

The remaining part of this section discusses the plots of the acoustic mode evolution of the 16 test cases, with each plot showing the natural and excited modes for two velocity ratios. At each forcing (excitation) frequency, the amplitude of the forced frequency mode and the corresponding amplitude of the natural mode of 150Hz were measured and plotted at different velocity and equivalence ratios.

Figure 6.12a plots the acoustic amplitude evolution of the lower swirl number of 1.05 with an equivalence ratio of 0.7, each with two inlet velocity ratios. The forced acoustic mode at u'/u = 0.1, remained low within 1.0E-3 KPa^2 except at 150Hz where it merges with the natural mode with a significant increased amplitude. As the velocity ratio was increased to 0.2, the amplitude of the forced mode remained low except for three frequencies of 150, 250 and 450Hz, where it rises to about 4.0E-3 KPa^2 for 150Hz and 2.0E-3 KPa^2 for the other two frequencies. Remarkably these frequencies

are the natural mode and its harmonics. The natural mode remained high in most of the frequencies at u'/u = 0.1 and increased further as the velocity amplitude was increased to u'/u = 0.2, with a maximum amplitude of 5.2E-3 KPa^2 at 300Hz, beyond which the amplitudes reduce significantly towards the benchmark.

Figure 6.12b plots the behaviour of the acoustic dynamics with similar conditions but with increased velocity amplitudes to 0.3 and 0.4. At the velocity amplitude of u'/u= 0.3, the acoustic amplitude of the forced signal remained low within 1.0E-3 KPa^2 except at 250 and 450Hz, where both rise by about 100% above the threshold value. Similar behaviour was also observed with the forced mode as the velocity ratio was increased to u'/u = 0.4. There was a reduction in the magnitude of the natural acoustic mode at u'/u = 0.3 as six of the nine points fell below the 2.0E-3 KPa^2 threshold. When the velocity ratio was moved to 0.4, the amplitude of the natural mode increased by about 100% above the benchmark and fell below the margin at higher frequencies of 450 and 500Hz.

Figure 6.13 examines the acoustic mode evolution with similar conditions as in Figure 6.12 but with an equivalence ratio of 0.8. In Figure 6.13a, both the forced and natural modes at u'/u = 0.1 have very low acoustic amplitudes in all the frequencies below 1.0E-3 KPa^2 except at 450Hz, where the amplitude of the forced mode increases marginally. The amplitudes of the forced mode at u'/u = 0.2 all fell below the 2.0E-3 KPa ^2 threshold except at 450Hz where the amplitude moved up by about 50% above the benchmark. The natural acoustic mode at similar velocity ratio have the amplitudes at 100,150 and 450Hz below the threshold, but the rest of the frequencies are about 65% above the threshold. As the velocity ratio was increased to 0.3 and 0.4, Figure 6.13b, the power spectrum of the natural acoustic mode in both cases fell significantly below the 2.0E-3 KPa^2 threshold in all the frequencies. The forced mode in both cases also show a significant reduction in the amplitude as all the points either fell within or below the margin.

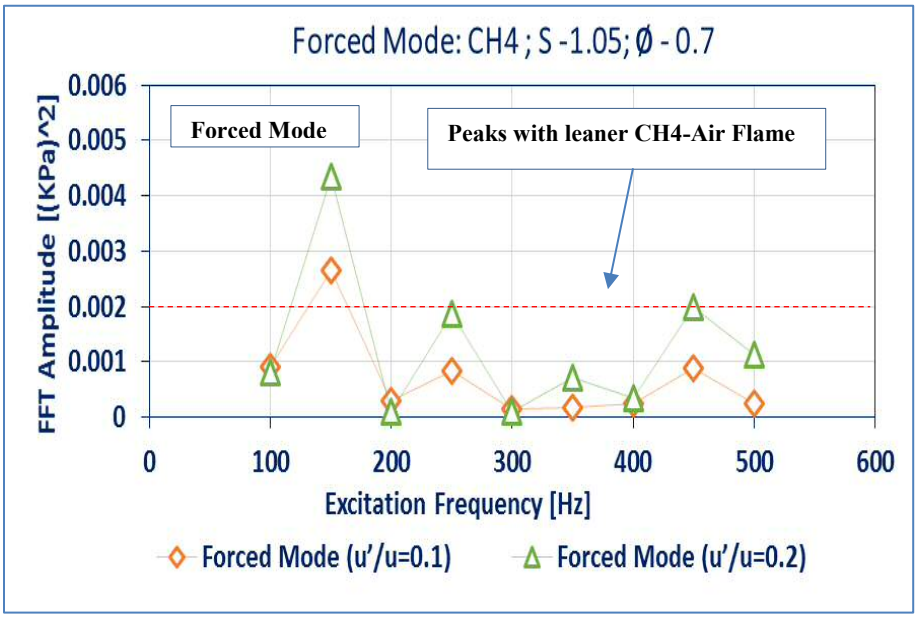

(i)

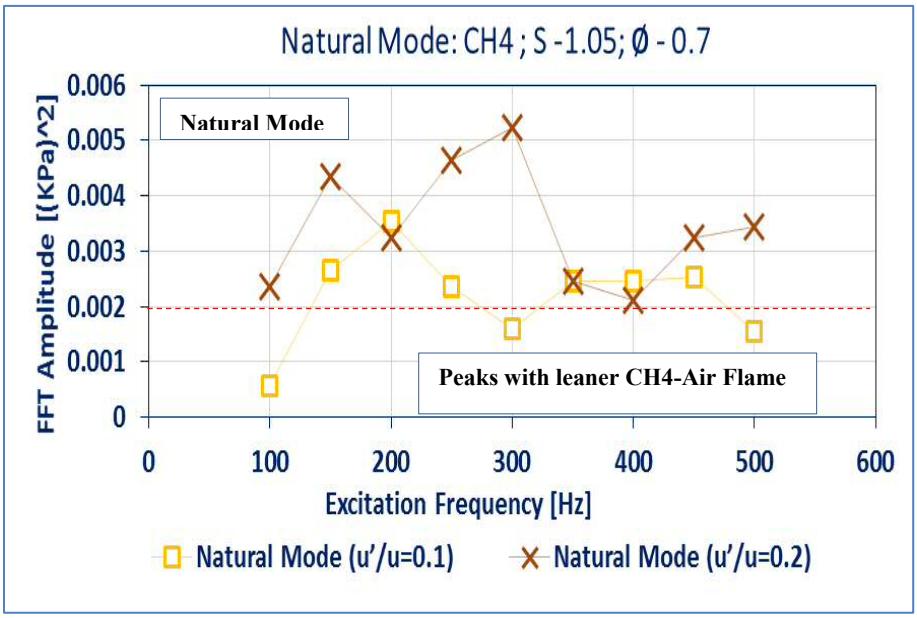

(ii)

Figure 6-12a: Acoustic modes of methane flame with external excitation: S= 1.05; = 0.7; u'/u = 0.1, 0.2.

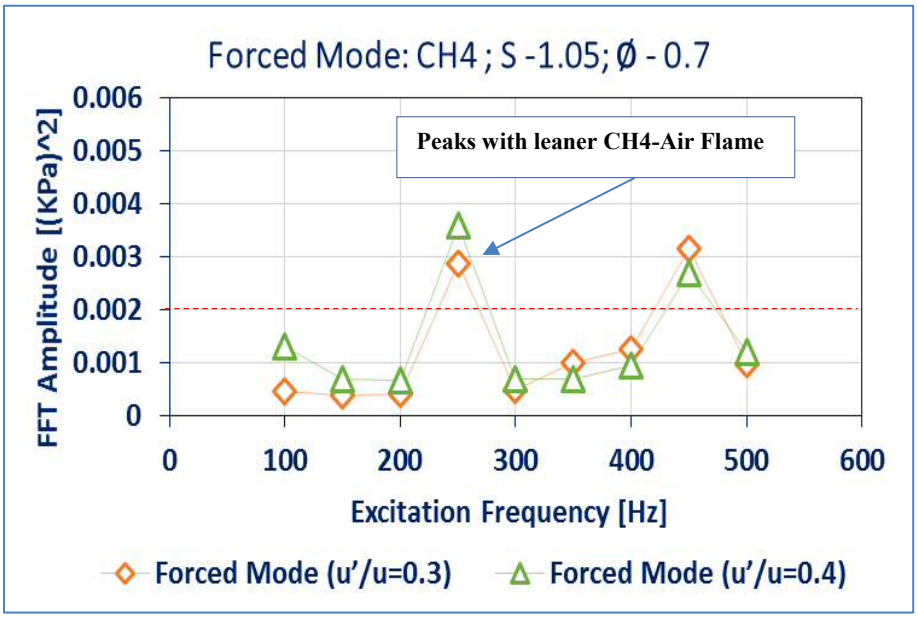

(i)

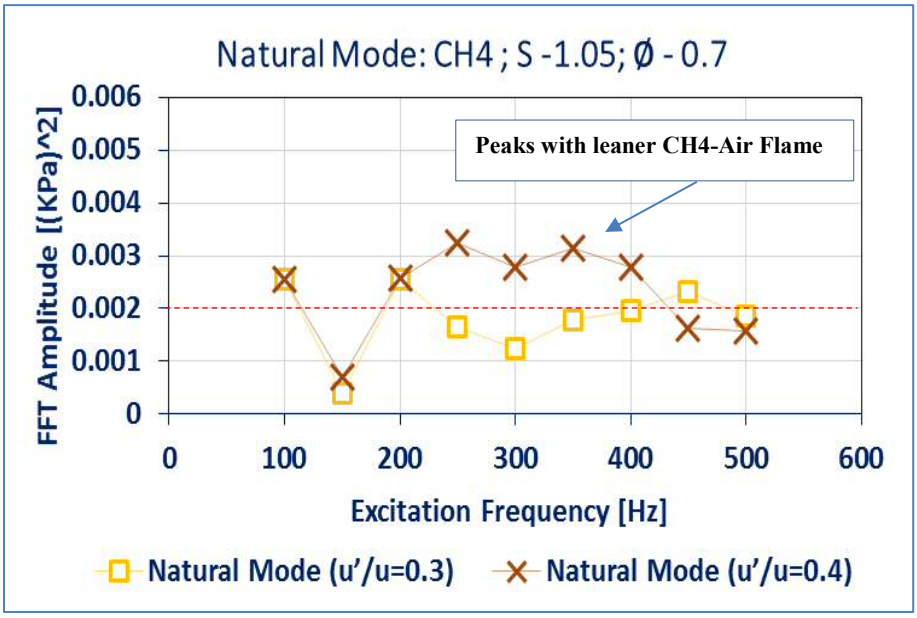

(ii)

(b)

Figure 6. 12 Acoustic modes of methane flame with external excitation: S= 1.05; = 0.7; u'/u = 0.3, 0.4

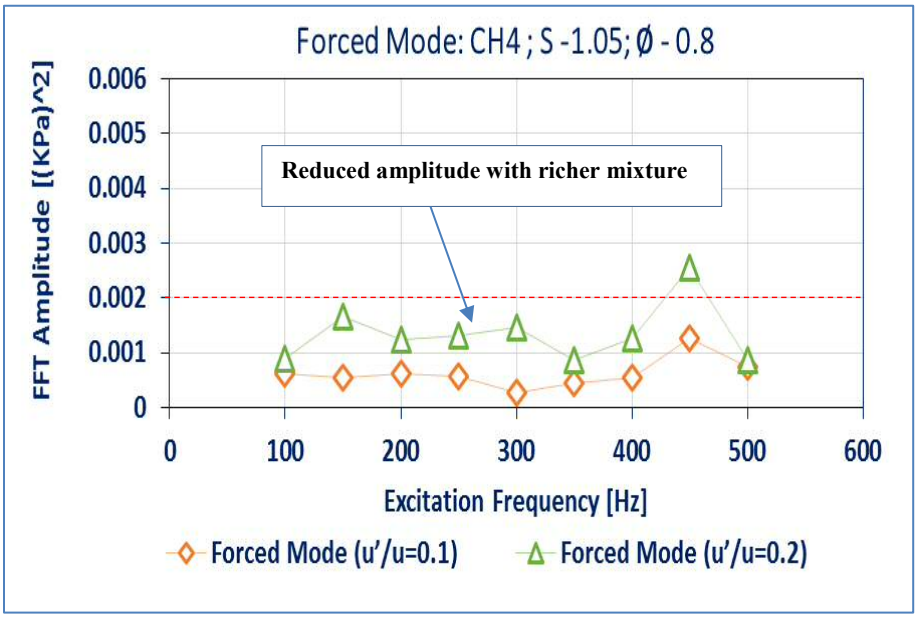

(i)

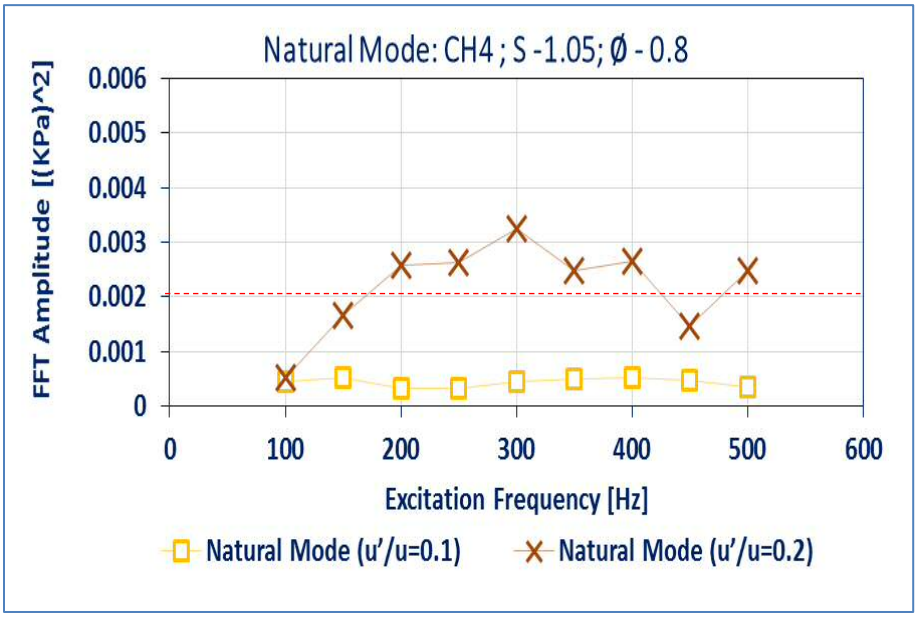

(i)

Figure 6-13a: Acoustic modes of methane flame with external excitation: S= 1.05; = 0.8; u'/u = 0.1, 0.2.

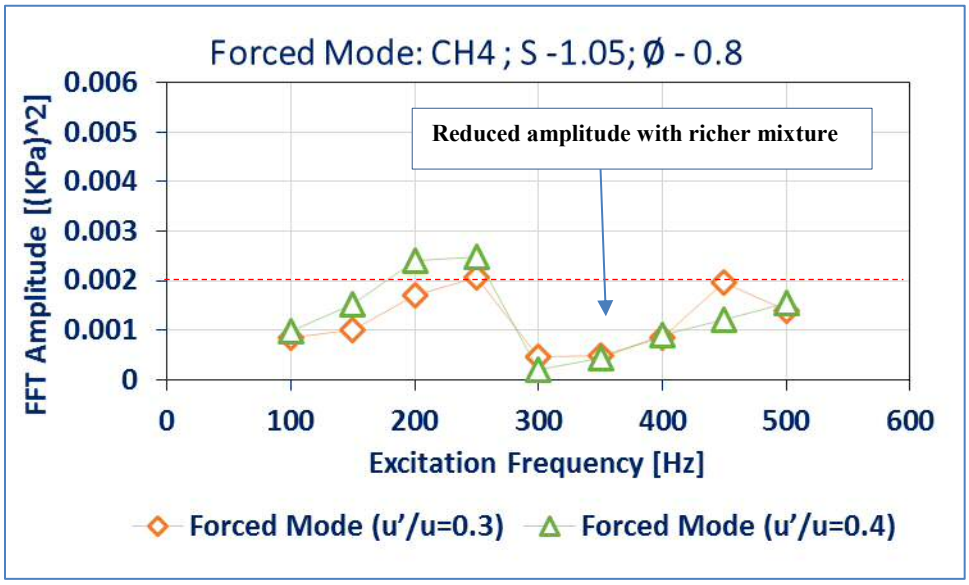

(i)

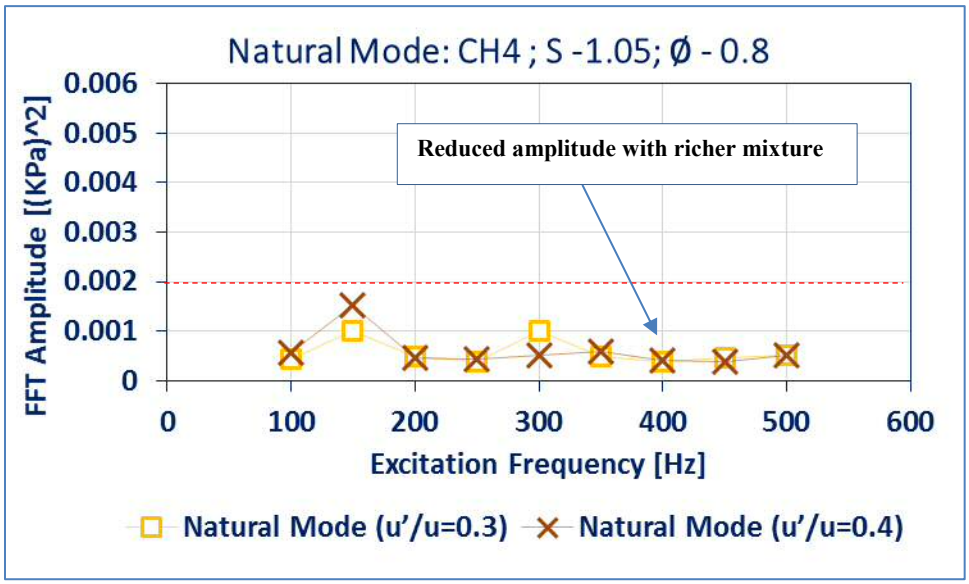

(ii)

(b)

Figure 6. 13 Acoustic modes of methane flame with external excitation: S= 1.05; = 0.8; u'/u = 0.3, 0.4

For the two equivalence ratios with a lower swirl strength, an improved stability of the combustor oscillation with increased inlet velocity amplitude especially at higher forcing frequencies was evident. This is because, at higher velocity ratios and forcing frequencies; the heat release fluctuation saturates and the acoustic driving process is also saturated whereas the acoustic damping process keeps increasing. By Rayleigh

criterion, the overall acoustic instability is reduced as it reaches the limit cycle. The saturation of the heat release oscillation by the forcing and velocity conditions have been reported in other published studies [119][122].

Next, the swirl number was increased to 1.50, and the acoustic evolutions with two equivalence ratios, velocity ratios as well as forcing frequencies were assessed. In this swirl condition, the amplitudes of acoustic modes were observed to be very high when compared to the acoustic modes of the lower swirl number. At = 0.7, Figure 6.14a, the power of the natural mode at u'/u = 0.1 increases almost linearly with the forcing frequencies to a maximum value of 5.0E-3 KPa^2 at 500 Hz. As the velocity ratio was increased to u'/u = 0.2, the power of the natural mode remained quite close to 6.0E-3 KPa^2. The amplitude of the forced signal remained at 1.0E-3 KPa^2 for u'/u = 0.1 and increases to 2.0E-3 KPa^2 at u'/u = 0.2.

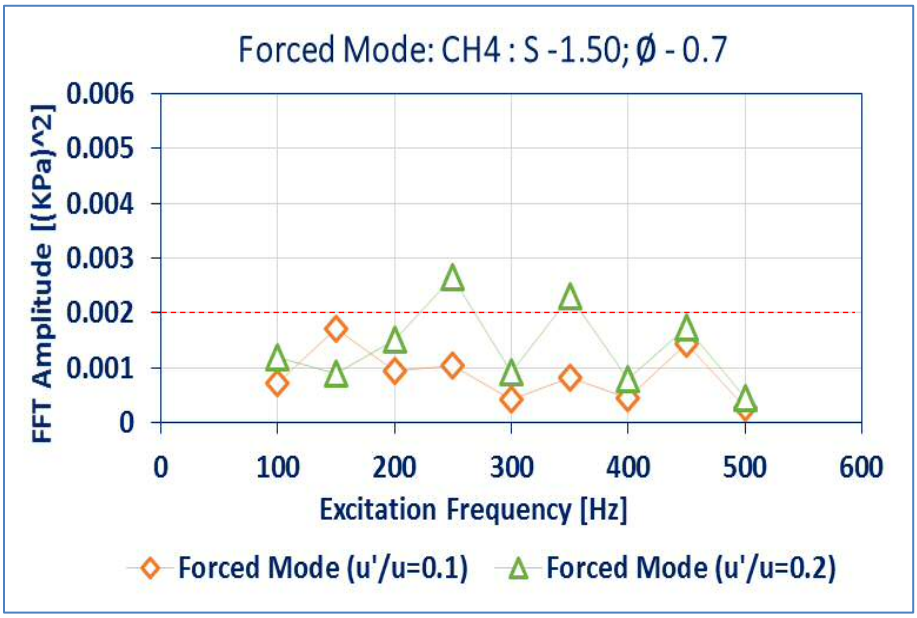

(i)

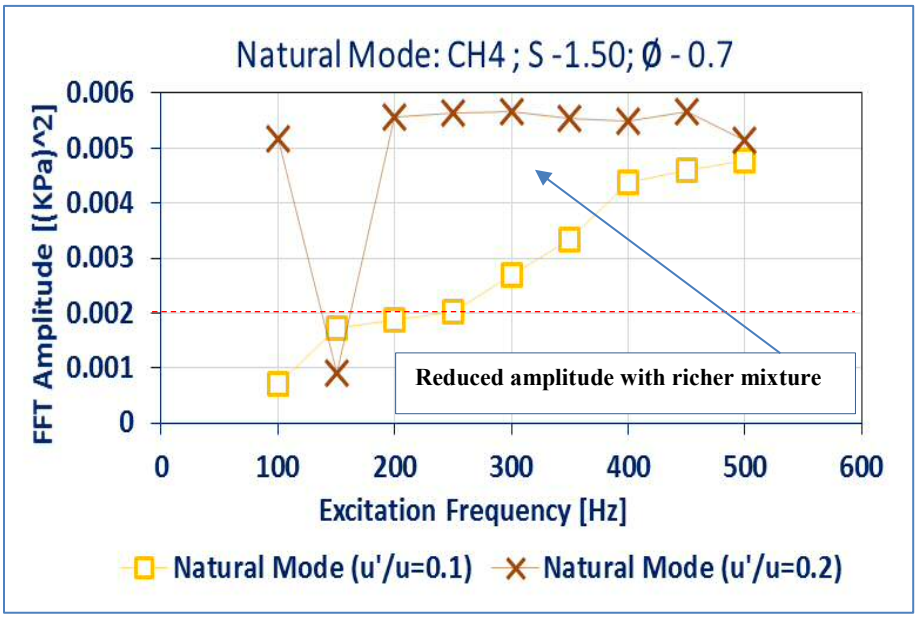

(ii)

Figure 6-14a: Acoustic modes of methane flame with external excitation: S= 1.50; = 0.7; u'/u= 0.1, 0.2.

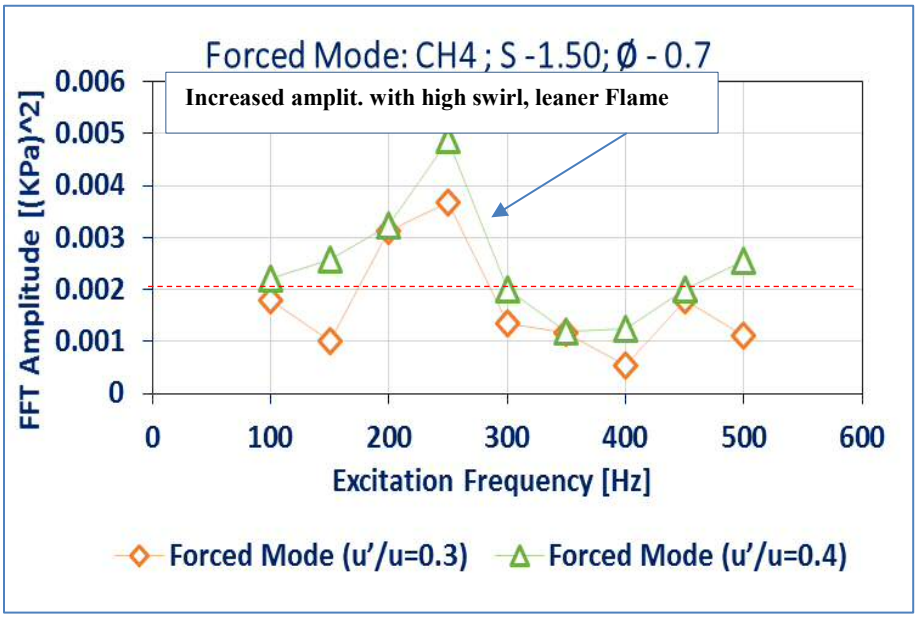

(i)

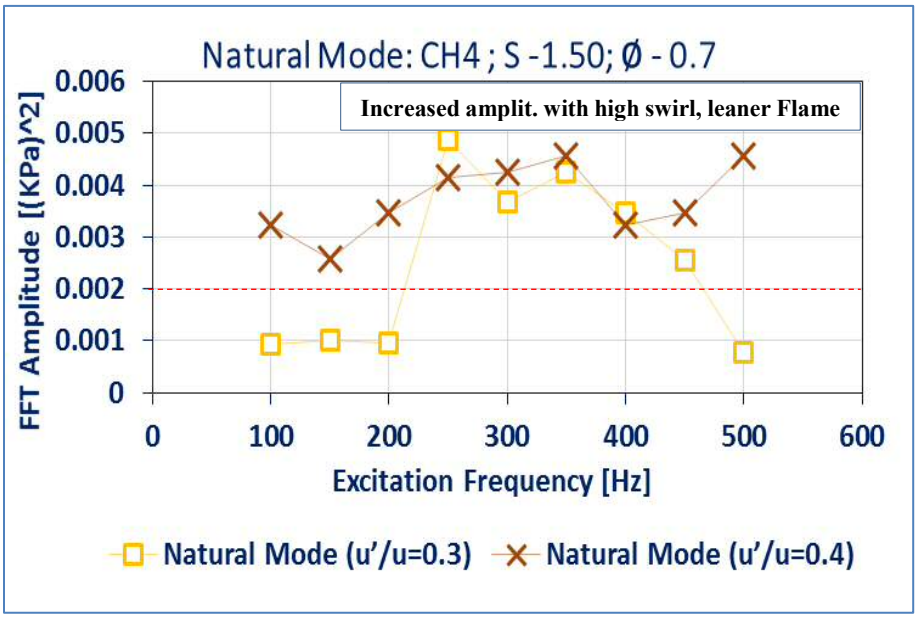

(ii)

(b)

Figure 6. 14 Acoustic modes of methane flame with external excitation: CH4; S= 1.50; = 0.7; u'/u= 0.3, 0.4

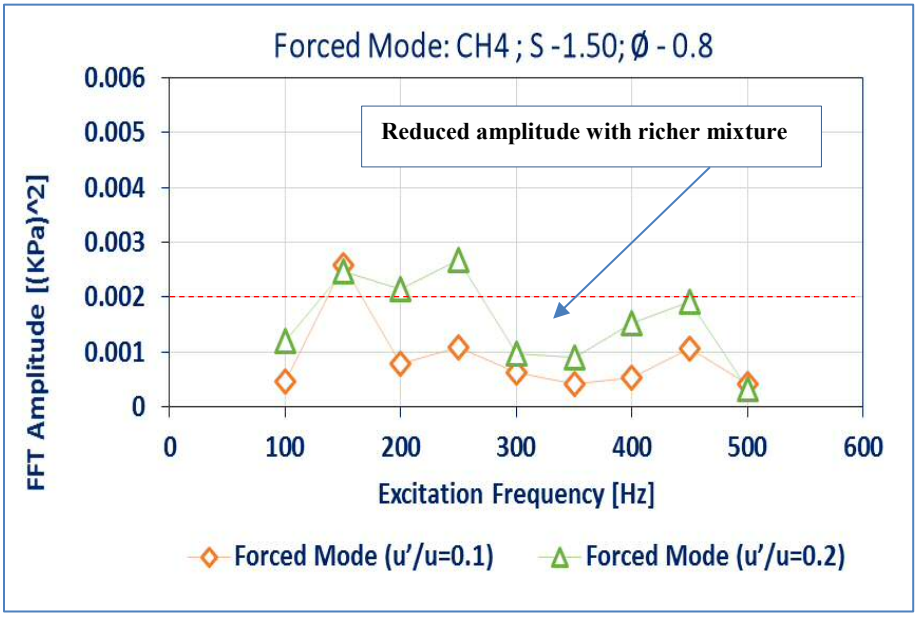

(i)

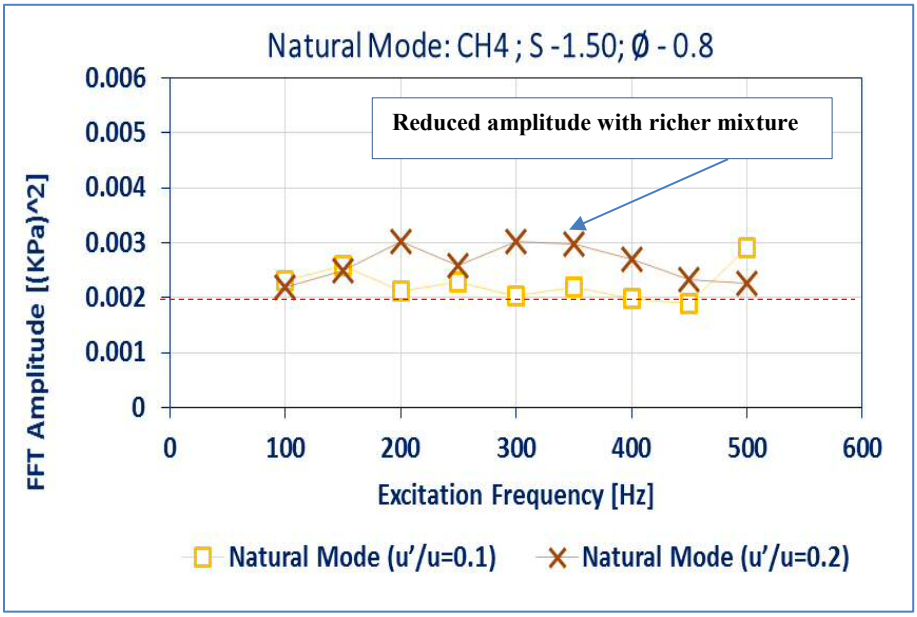

(ii)

Figure 6-15a: Acoustic modes of methane flame with external excitation: S= 1.50; = 0.8; u'/u = 0.1, 0.2.

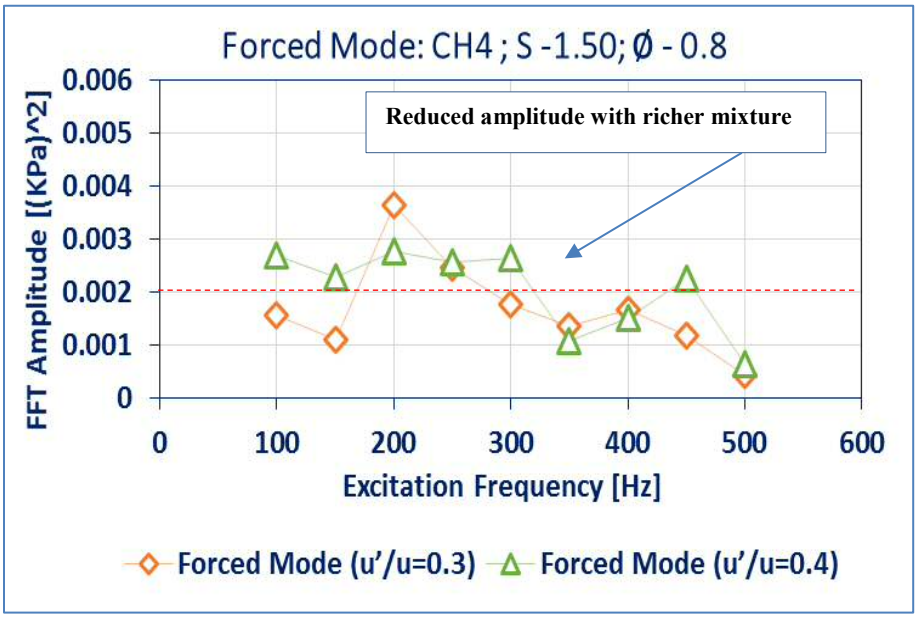

(i)

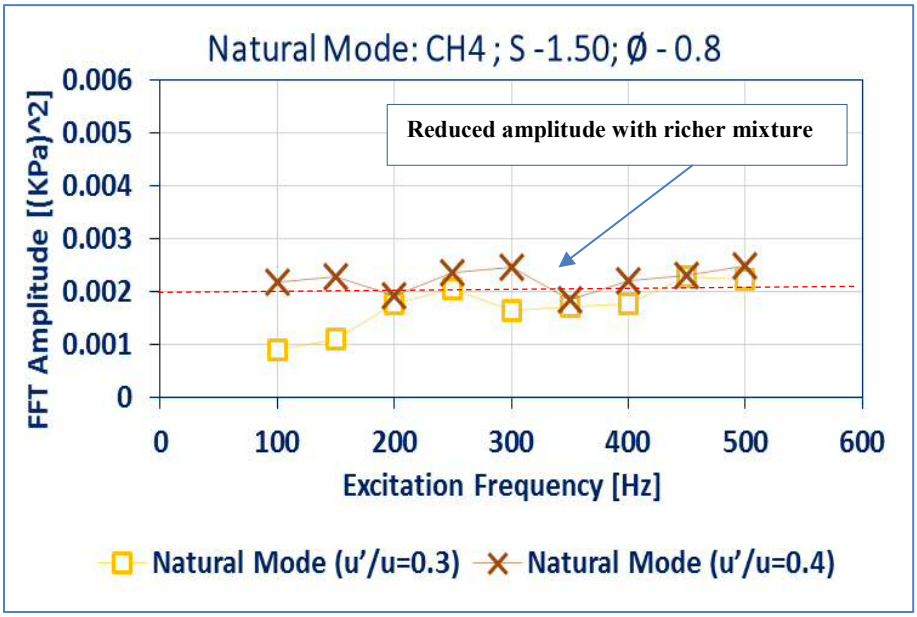

(ii)

(b)

Figure 6. 15 Acoustic modes of methane flame with external excitation: S= 1.50; = 0.8; u'/u = 0.3, 0.4

As the velocity ratio was increased to 0.3 and 0.4, Figure 6.14b, the amplitudes of both the forced and natural modes show a slight reduction, although most of the amplitudes

still stay above the 2.0E-3 KPa^2 benchmark. Next, the equivalence ratio was decreased to 0.8. Figure 6.15a shows a substantial reduction in amplitudes of the acoustic modes of the richer mixture. Nearly all the amplitudes of the forced signal in the two velocity ratios fall below the threshold value while the natural mode amplitudes stay within the threshold value throughout the forcing frequencies at u'/u = 0.1 and rise by about 75% as the velocity ratio rises to u'/u = 0.2.

A similar improved stable acoustic condition was also observed as the velocity ratio was increased to 0.3 and 0.4, Figure 6.15b. In comparison, it has been shown that unforced methane-air flames have acoustic modes with relatively low spectral power across most velocity ratios. In figures 6.5a the four cases of CH4-plots give low spectral amplitudes of the acoustic modes in the four velocity ratios. The amplitudes fell within 1.0E-3 KPa^2, except for S= 1.50, = 0.8, where they revolve around 2 and 2.5E-3 KPa^2. But in the 16 cases of forced methane-air flame, Figures 6.12 to 6-15, the acoustic spectral power rose significantly at different forcing conditions, to maximum values of 5 to 6.0E-3 KPa^2 at higher swirl number. The two results indicate about 250% rise in acoustic amplitude when a flame is excited externally. These acoustic modes include both the forced and natural modes of the system as well as their harmonics. The increased magnitude could be attributed to the multi-coupling of these signals with other oscillations within the flow, flame and pressure fields. Thus the use of signal forcing as flow and flame modulation technique in active control could energise the acoustic modes, resulting in high amplitudes in some swirl and forcing conditions.

It, therefore, suggests that there might be some forcing conditions which could generate acoustic modes that are worse than those of the unforced flames. These dangerous conditions need to be recognised and avoided during instability control processes. As observed in this section, some cases like forcing the flame with frequencies similar to the harmonics of the natural acoustic mode of the combustor are capable of amplifying the power of the acoustic modes. In contrast, forcing the flame with a frequency similar to the natural acoustic mode of the combustor in some cases tends to generate a single acoustic mode with a low spectral amplitude.

6.3 CAM Characterization of Excited Methane –CO_2 Flames

Instability control could also be enhanced by heat release modulation by varying the fuel characteristics. An earlier study conducted by this research group [29][153] revealed that the blend of methane with CO_2 results in a decrease in the HMFR velocity but increases the CRZ velocity sharply due to the increased pressure differential as a result of the high specific heat of the CO_2. The effects of the swirl strength variation on the CRZ, shear layers and the HMFR were also discussed in chapter four. Chemically, it is known that the blend of CO_2 with methane during combustion has a substantial impact on the chemical kinetics of the flame. The CO_2 with high specific heat reduces both the flame temperature and the reaction rate due to its radiative absorption. In this section, the interaction of the two main frequency modes is properly examined with respect to swirl strength and fuel blend variations. Methane flame is used as the baseline to evaluate the acoustic mode evolution with its blends with CO_2. Sixty-four cases were considered to examine the evolution of the acoustic modes' spectral power with respect to the fuel blends. As shown in Figure 6.16, the 64 cases are each forced with nine forcing frequencies.

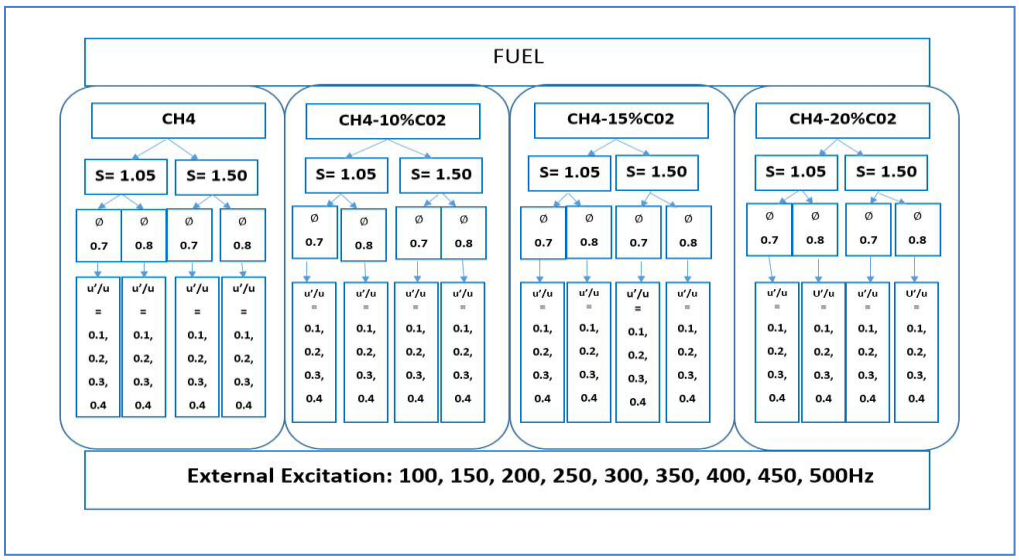

Figure 6. 16 Combustion cases with different fuel mixtures, swirl strength and forcing conditions

6.3.1 CAM Characterization of Excited Methane – CO_2 Flame: S - 1.05

This section compares the acoustic amplitudes of methane-air flames with those methane-CO_2- air flames at various conditions to assess the response of acoustic modes to the two fuels. Figures 6.17 to 6.20 present different plots for the interactions of the natural and forced acoustic modes in the combustor for a swirl number of 1.05 and both equivalence and velocity ratios. Figures 6.17 consider the equivalence ratio of 0.7 for two velocity ratios of u'/u = 0.1 and 0.2. As described in the previous section, the excitation of methane-air flame energises its acoustic mode resulting in high spectral powers of both the forced and natural modes, Figure (6.12a i-ii). There are changes in the acoustic modes when 10% of CO_2 was added to the fuel as the spectral powers of all the acoustic modes were drastically reduced to about 0.5E-3 KPa^2 across all the forcing frequencies, representing a significant reduction in most cases. Similar reductions in acoustic amplitude were also seen when the CO_2 was increased to 15 and 20%.

Figures 6.18 consider the remaining velocity ratio of u'/u = 0.3 and 0.4 with all other conditions kept constant. The acoustic spectral power of pure methane was reduced due to the increased velocity ratio to between 2.0E-3 KPa^2 to 3.0E-3 KPa^2 across most forcing frequencies while the forced modes remain lower than this margin except for forcing frequencies of 250 and 450Hz with higher spectral powers Figure (6.12b i-ii). For the blends of CO_2, the spectral powers show a reduction of about 120% when compared to the pure methane. Almost all the points in the fuel blend fall below the benchmark of 2.0E-3 KPa^2.

In Figures 6.19, the equivalence ratio is reduced to 0.8. The amplitude of the natural acoustic mode of methane flame at u'/u = 0.2 rises from less than 1.0E-3 KPa^2 at 100Hz to about 3.0E-3 KPa^2 at 250Hz and stays at this range for most of the remaining forcing frequencies. The forced mode at u'/u = 0.2 remains at 1.0E-3 KPa^2 while the natural and the excited modes at the velocity ratio of u'/u = 0.1 are below these values throughout the entire forcing Figure (6.13a i-ii). In contrast, the spectral amplitudes of the acoustic modes of the CO_2 blends are reduced by about 200% even with the reduced amplitudes of the pure methane flames. As shown, the amplitudes of the fuel blends are below the red dotted-line benchmark. Figures 6.20 show the acoustic amplitudes with an increased velocity ratio of u'/u = 0.3 and 0.4. The acoustic

amplitudes of both the pure methane, Figure (6.13b i-ii) and its blends with CO_2 remain same at lower forcing frequencies, however, at higher forcing frequencies, the blend showed a reduction of about 70% particularly in the least percentage of CO_2. The low-swirl flame in all conditions has demonstrated the effectiveness of the blend of CO_2 with methane to suppress combustion instabilities. The percentage of the reduction of the instabilities with fuel blend becomes high at leaner mixture but reduces with rich mixtures. The reduction is also seen to be more effective at high-velocity ratios and forcing frequencies due to the saturation of the heat release rate.

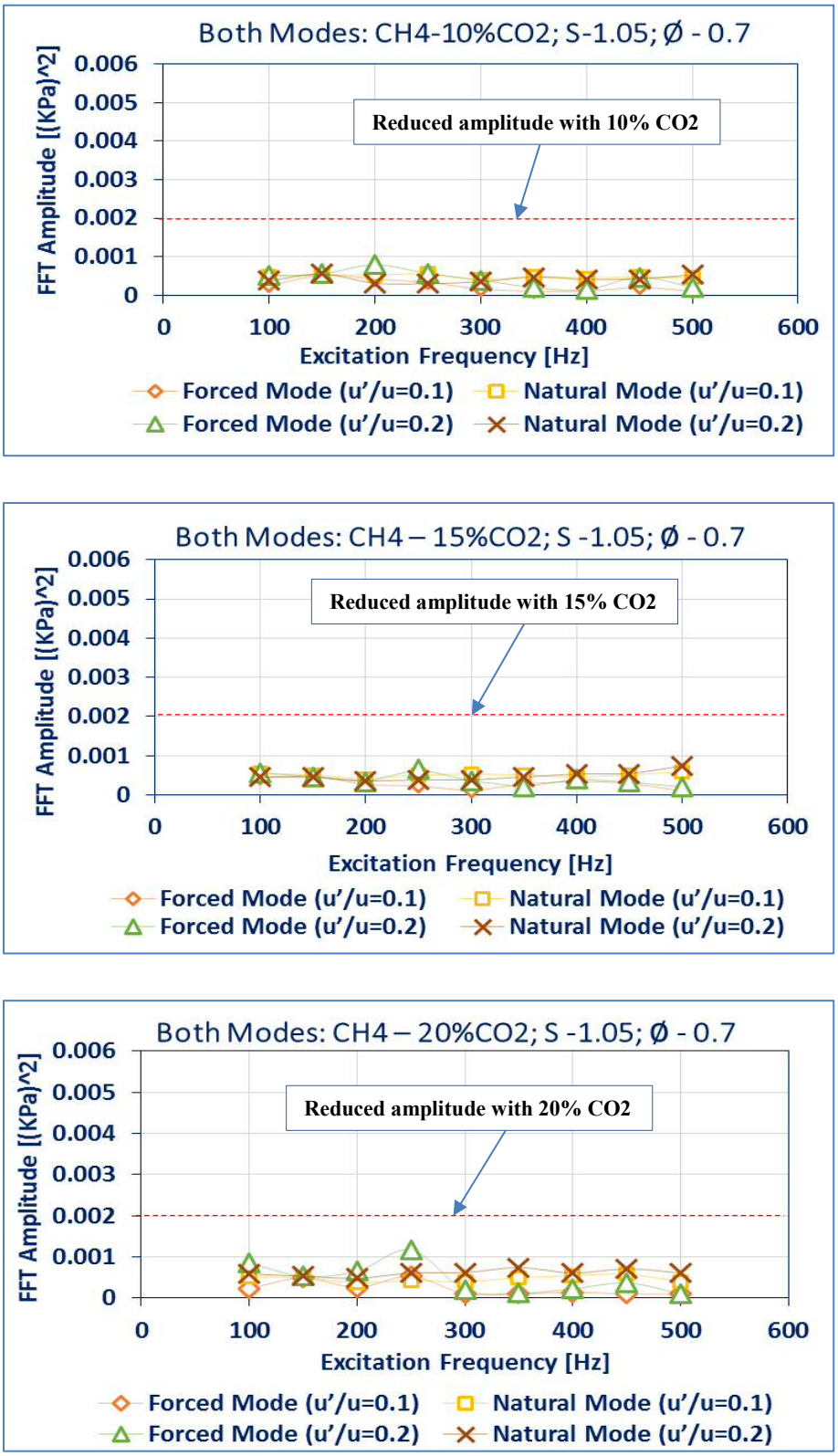

Figure 6. 17 Acoustic modes of Methane –CO_2 flames [10%, 15% and 20%; S=1.05; = 0.7; u'/u = 0.1, 0.2]

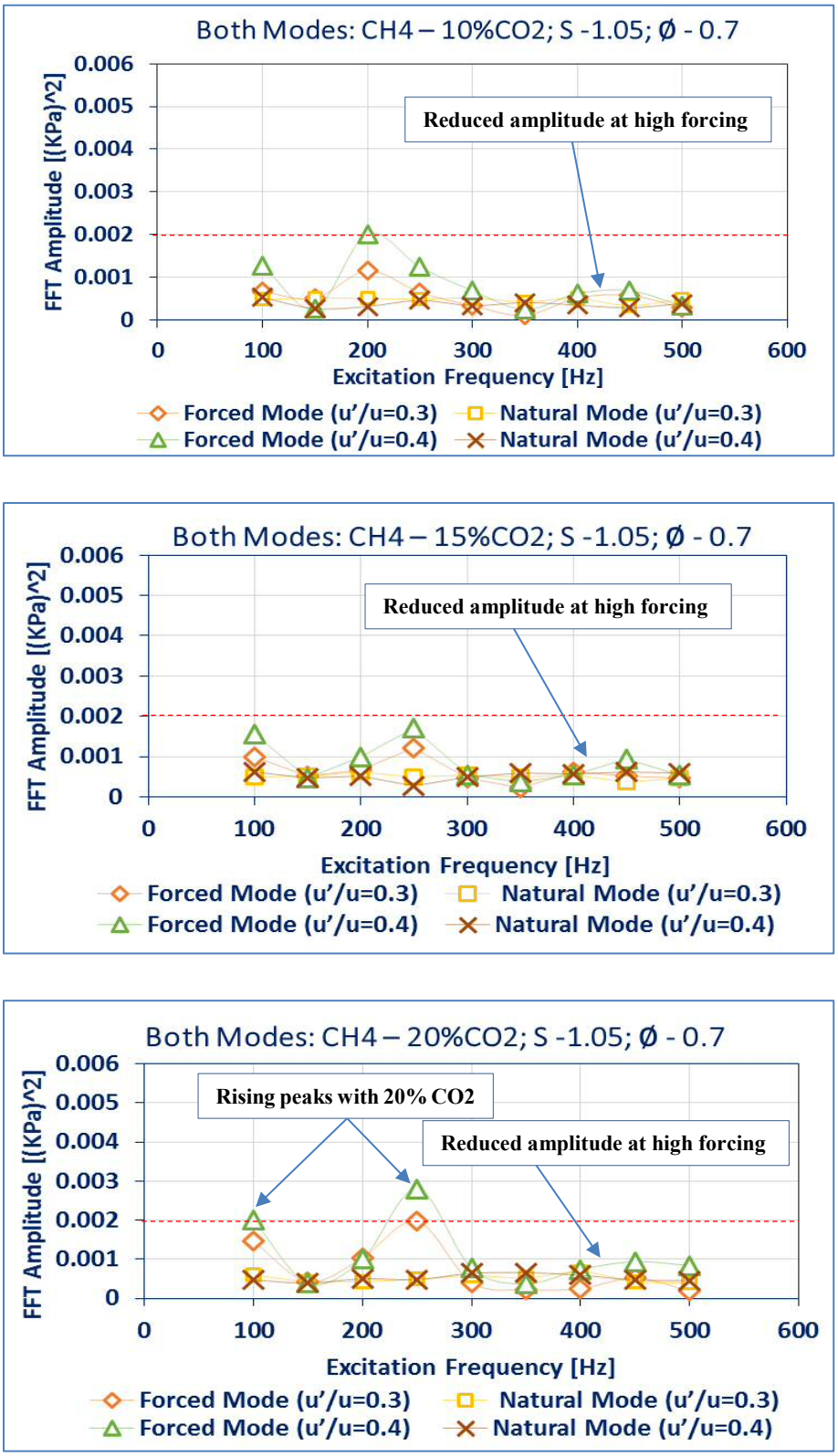

Figure 6. 18 Acoustic modes of Methane –CO2 flames [10%, 15% and 20%; S=1.05; = 0.7; u'/u = 0.3, 0.4]

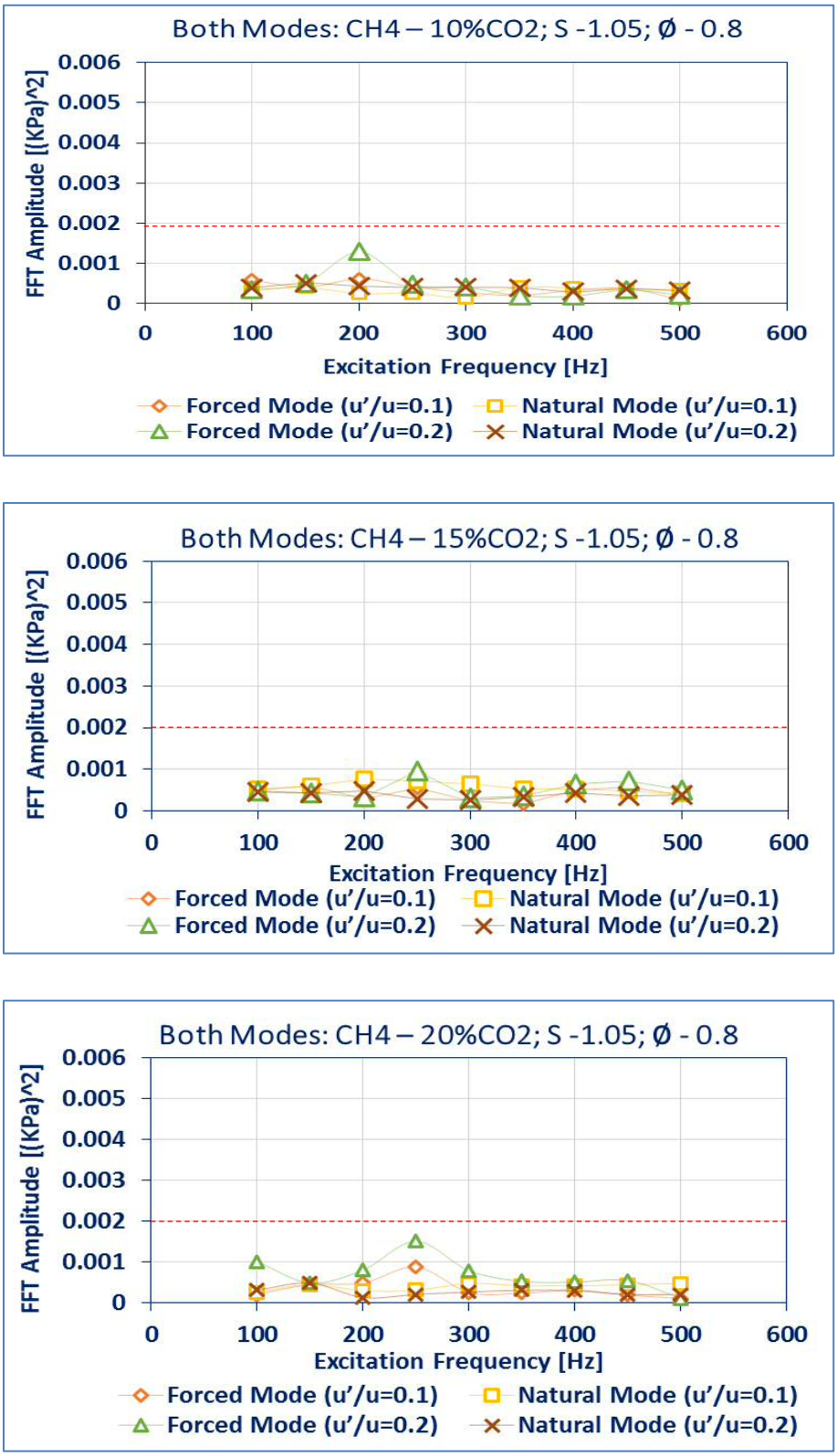

Figure 6. 19 Acoustic modes of Methane –CO_2 flames [10%, 15% and 20%; S=1.05; = 0.8; u'/u = 0.1, 0.2]

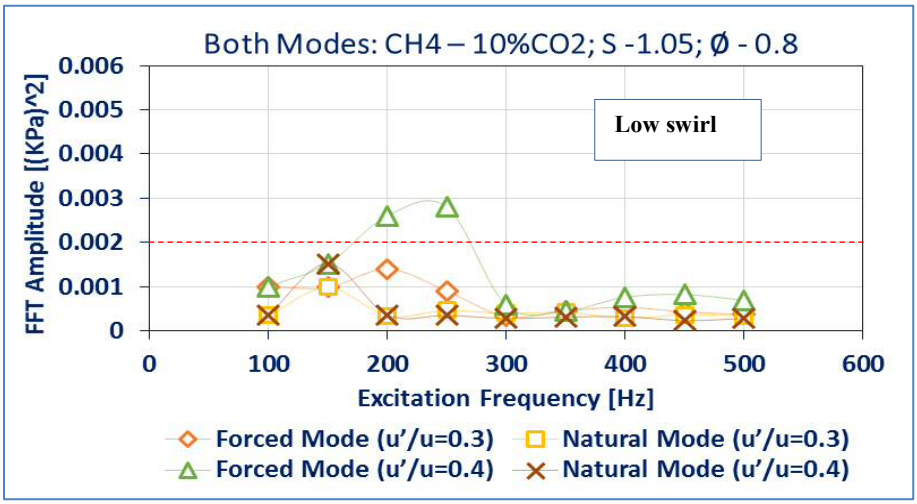

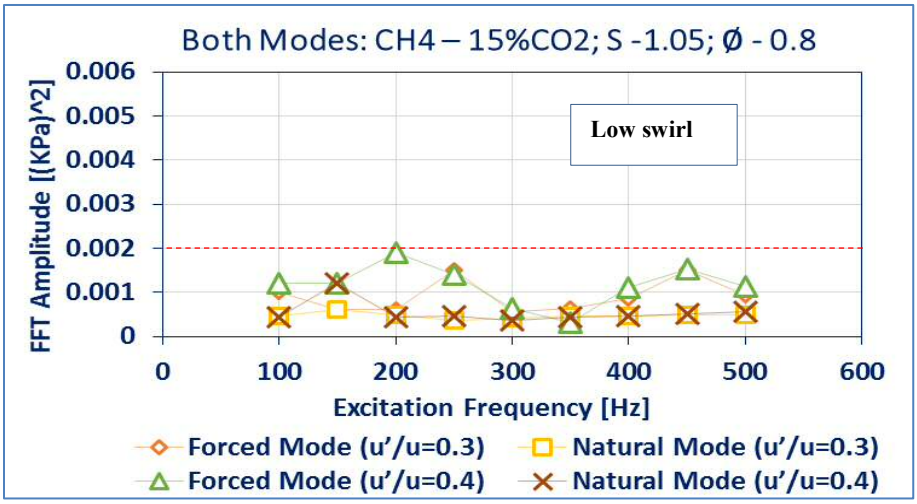

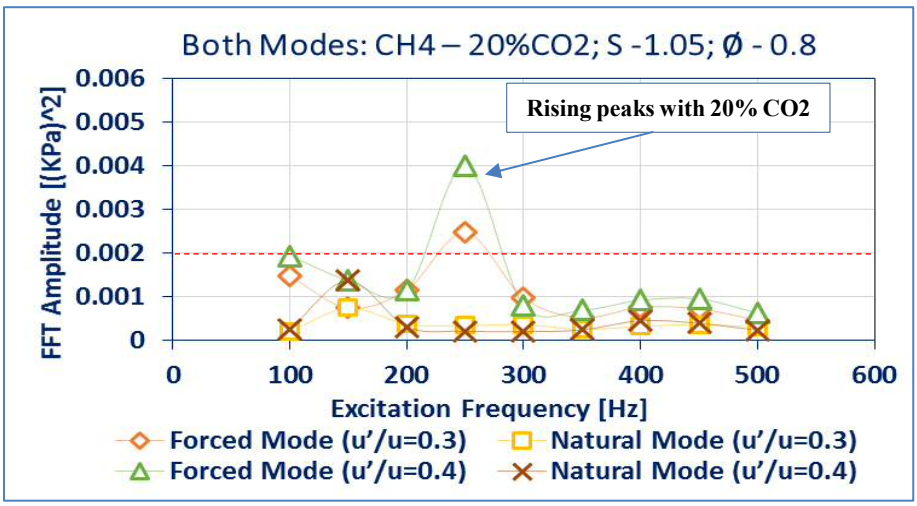

Figure 6. 20 Acoustic modes of Methane –CO_2 flames [10%, 15% and 20%; S=1.05; = 0.8; u'/u = 0.3, 0.4]

6.3.2 CAM Characterization of Excited Methane - CO_2 Flame: S - 1.50

The effects of methane- CO_2 blend to reduce combustion instabilities was also tested with high swirl flames. This section considers similar cases with section 6.3.1, but with an increased swirl number of 1.50. Figures 6.21 to 6.24, therefore, present different plots comparing the acoustic amplitudes of methane flame and its blends with CO_2, at a high swirl number.

Figures 6.21 show the interactions of the natural and forced signals at an equivalence ratio of 0.7, velocity ratios of 0.1 and 0.2 for pure and its mixtures with CO_2. The CH4 flame shows very high amplitudes of the power spectra of the natural acoustic modes in both velocity ratios. While the amplitudes of the forced signal in both velocity ratios remain within the 2.0E-3 KPa^2 benchmark, the amplitudes of the natural mode rise extremely to about 5.0E-3 KPa^2, Figure (6.14a i-ii). The amplitudes of the fuel blends in both velocity ratios reduced drastically below the benchmark to as low as 1.0E-3 KPa^2 E for both the forced and natural modes. It is also observed that the lowest acoustic amplitudes were obtained by the least percentage of CO_2 in methane as the instability increases marginally with increased proportion of CO_2.

When the velocity ratio was increased to 0.3 and 0.4, Figure 6.22, the amplitudes of the forced mode remained within the benchmark except for the frequencies of 200 and 250Hz, where the amplitudes rise higher. The amplitudes of the natural modes remained high in both velocity ratios across all the forcing frequencies, Figure (6.14b i-ii). The reduction in amplitudes with the blends with CO_2 was also evident. The amplitudes of the natural acoustics of the 10% CO_2 blend reduced by about 70% below the benchmark in both velocity ratios in all forcing frequencies. The amplitudes of the forced signals increase marginally in the lower forcing frequencies. The amplitudes of the forced signals rise further with the increment of the percentage of CO_2 to 15%. In this condition, the amplitudes of the natural mode remained low in all conditions. At 20% increase in CO_2, the amplitudes of the natural mode rise by about 80% above the baseline at a velocity ratio of 0.3 and further rise extremely at the velocity ratio of 0.4. The amplitudes of the forced signals maintain their low values.

The spectral evolution was further investigated with a change in equivalence ratio to 0.8. Figures 6.23 present the evolution of the spectral power of the natural and forced acoustic modes of the combustor for a swirl number of 1.50 but with an equivalence ratio of 0.8. The methane-air flame has a spectral range of 0 to 3E-3 KPa^2 for the signals in both velocity ratios across all forcing frequencies, Figures 6.15a (i) and (ii). A drastic reduction in spectral power for all the acoustic modes was also seen at the 10% CO_2 fuel blend. The amplitudes of all the four signals saturated around 0 and 0.5 E-3 KPa^2 from the forcing frequency of 300 to 500Hz. Increase in acoustic amplitudes was only observed at a forcing frequency of 200 and 250Hz. Similar behaviour was seen with the 15% of CO_2 blend, but some changes were observed when the percentage of CO_2 was increased to 20. The natural acoustic mode of the chamber at u'/u= 0.2, rose extremely between the forcing frequency range of 250Hz to 500Hz.

At a higher velocity amplitude of u'/u =0.3, and 0.4, Figure 6.24, The amplitudes of the forced and natural modes of the pure methane still stayed at a maximum limit of about 3.0E-3 KPa^2 for the two velocity ratios across all the forcing frequencies, Figure (6.15b i-ii). In the 10% CO_2 blend, the forced acoustic spectra at a velocity ratio of 0.4 experienced a further increase in amplitude for the forcing range of 200Hz to 300Hz but saturated across the remaining forcing frequencies. The natural acoustic modes in the two velocity ratios remained very low across all the frequencies. With the 15% CO_2 blend the amplitudes of the forced modes were reduced to 3.0E-3 KPa^2 in the two velocity cases. While in the 20% CO_2 blend the forced modes remained at a range of 4.0E-3 KPa^2 for the first four forcing frequencies and reduced to 2.5E-3 KPa^2 in the remaining forcing frequencies for the higher velocity amplitude of 0.4. At a reduced velocity ratio of 0.3, the amplitudes of the signals reduced drastically across the entire forcing frequencies.

These results have also proven the efficacy of methane CO_2 blend to reduce acoustic amplitude, and by extension combustion instabilities. The high power spectrum of acoustic modes of both forced and natural signals of the high swirl flows was significantly reduced when the fuel blend was introduced. The effects of the velocity amplitude were more significant in a leaner equivalence ratio of 0.7 with slight

differences at an equivalence ratio of 0.8. This shows the possibility of running leaner flames in a stable condition using this technique.

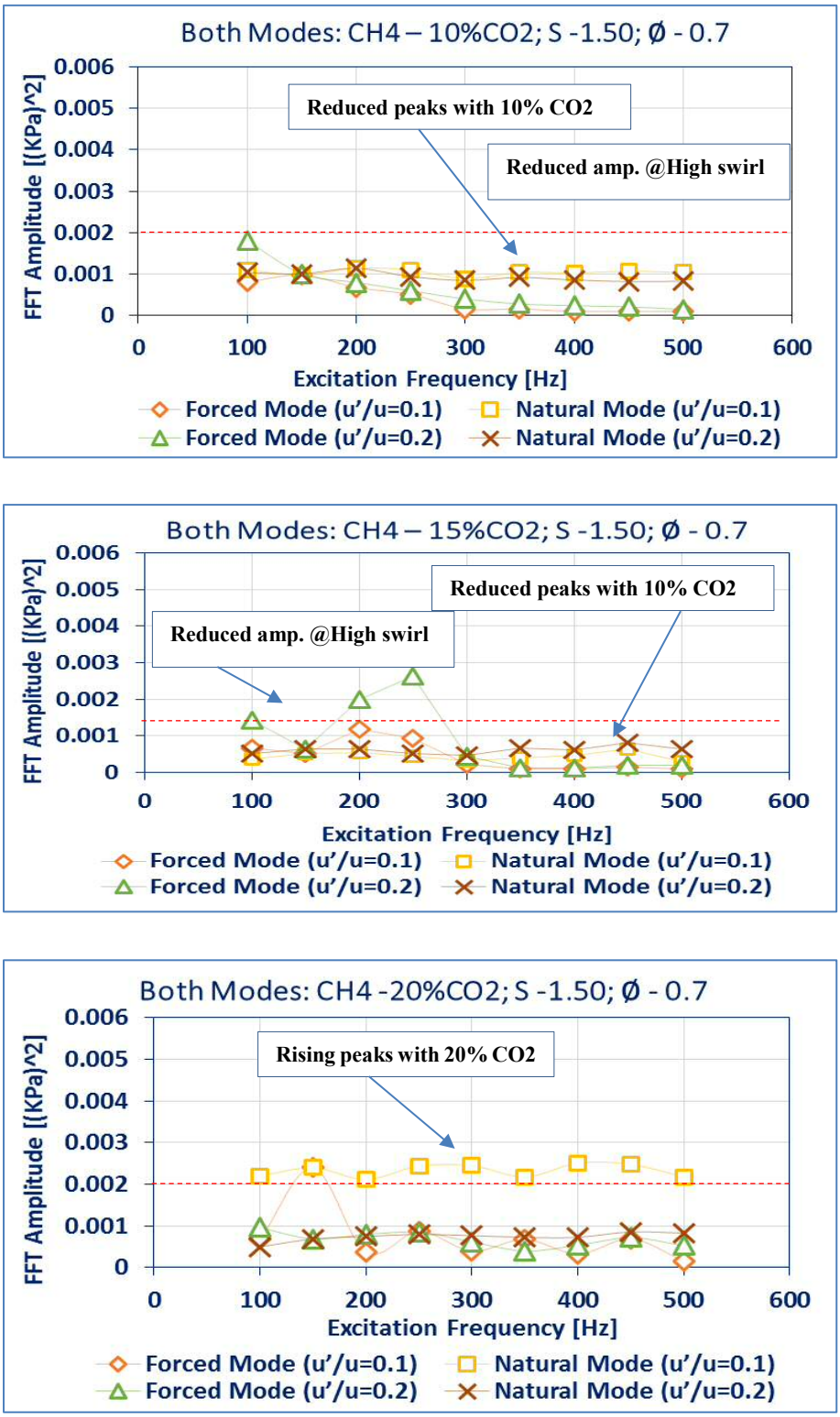

Figure 6. 21 Acoustic modes of Methane –CO2 flames [10%, 15% and 20%; S=1.50; = 0.7; u'/u = 0.1, 0.2]

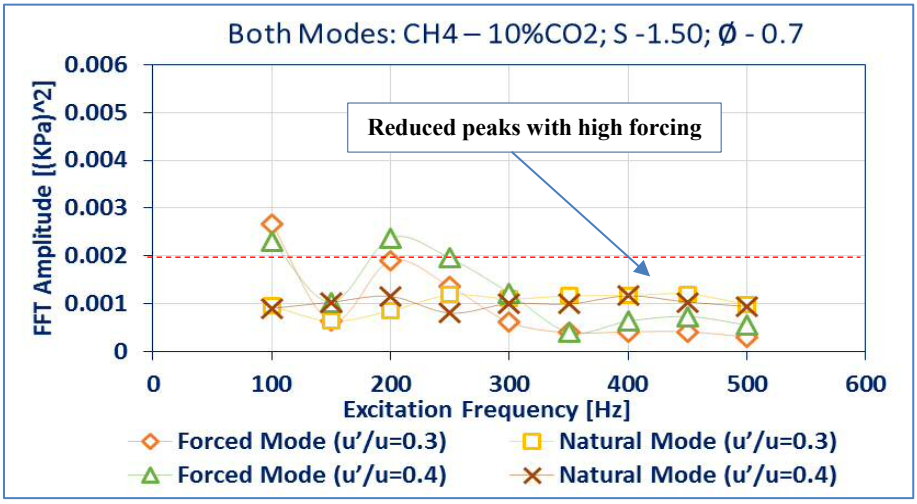

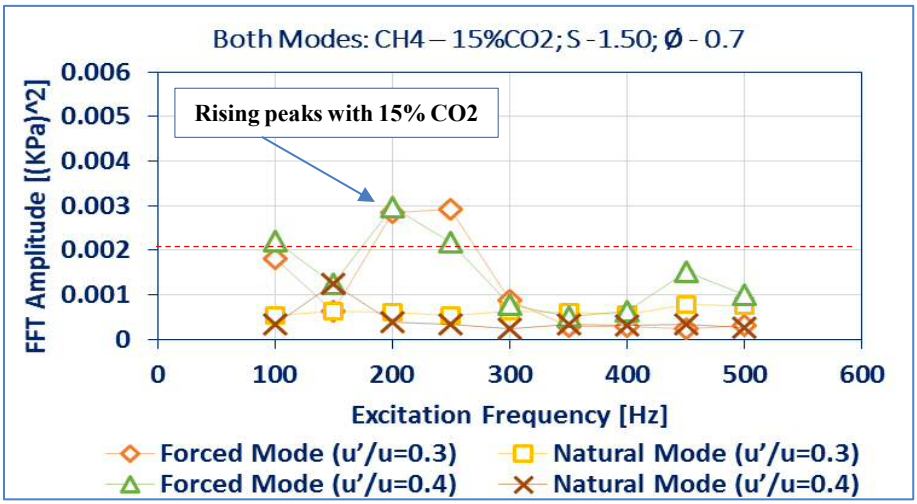

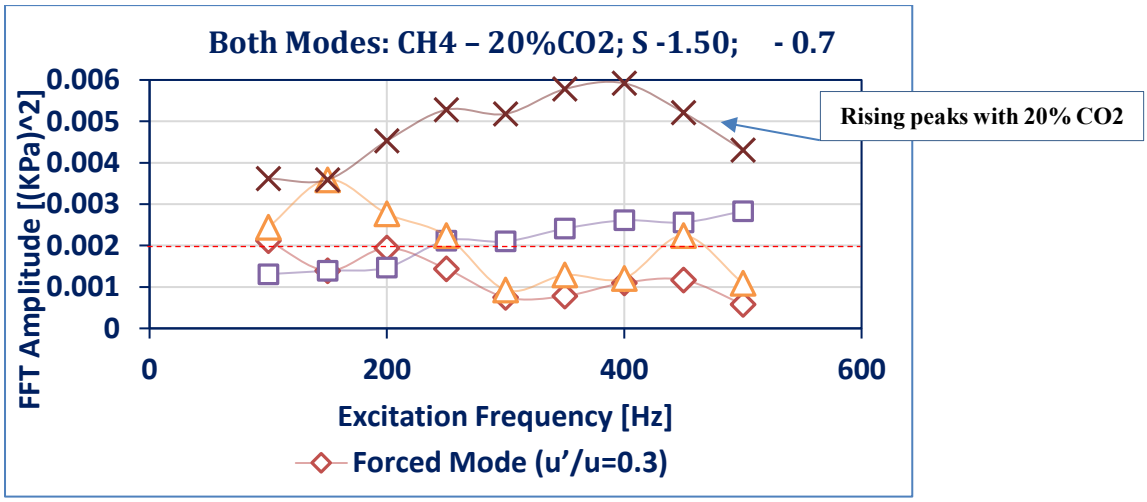

Figure 6. 22 Acoustic modes of Methane –CO2 flames [10%, 15% and 20%; S=1.50; = 0.7; u'/u = 0.3, 0.4]

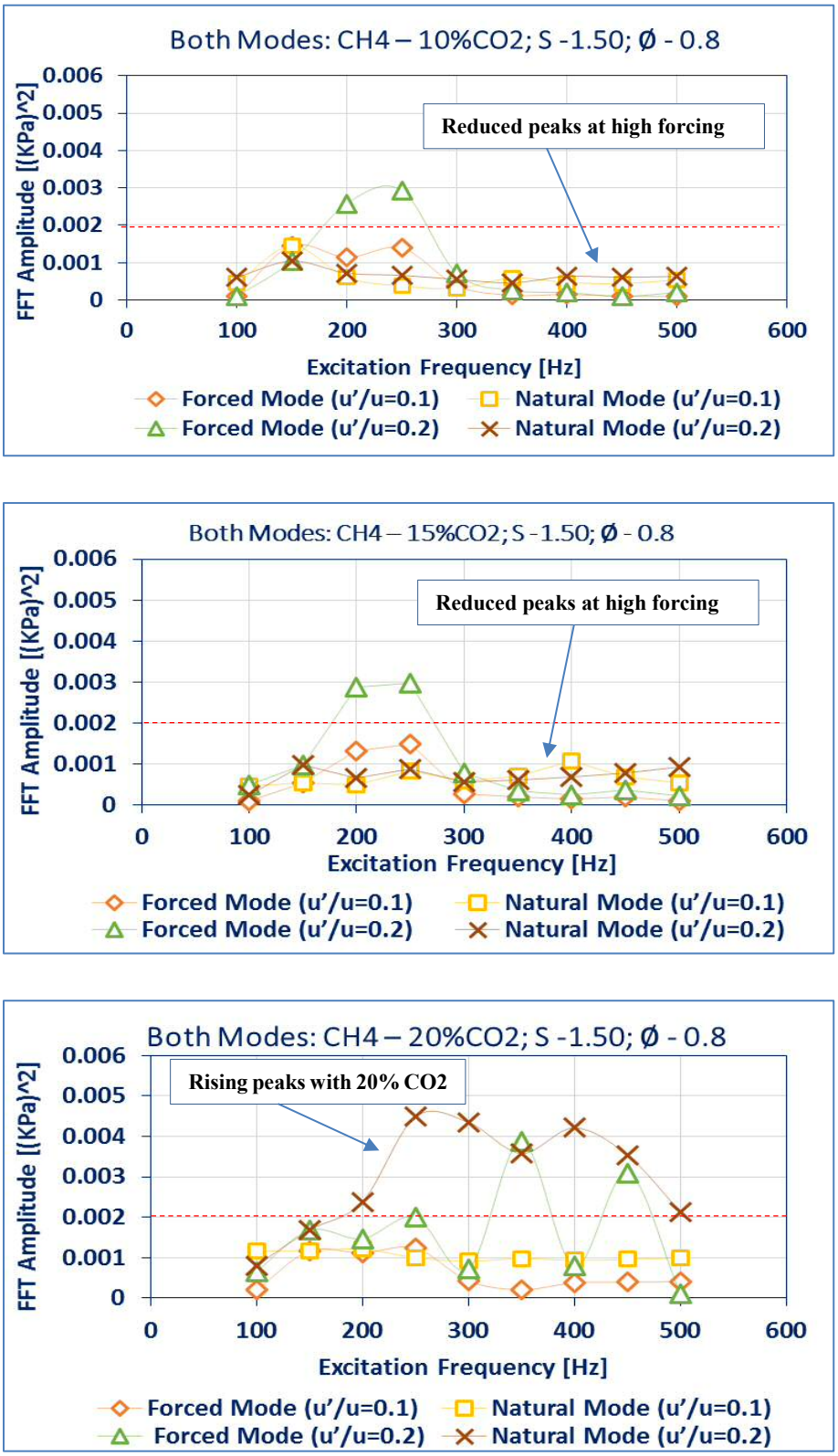

Figure 6. 23 Acoustic modes of Methane –CO2 flames [10%, 15% and 20%; S=1.50; = 0.8; u'/u = 0.1, 0.2]

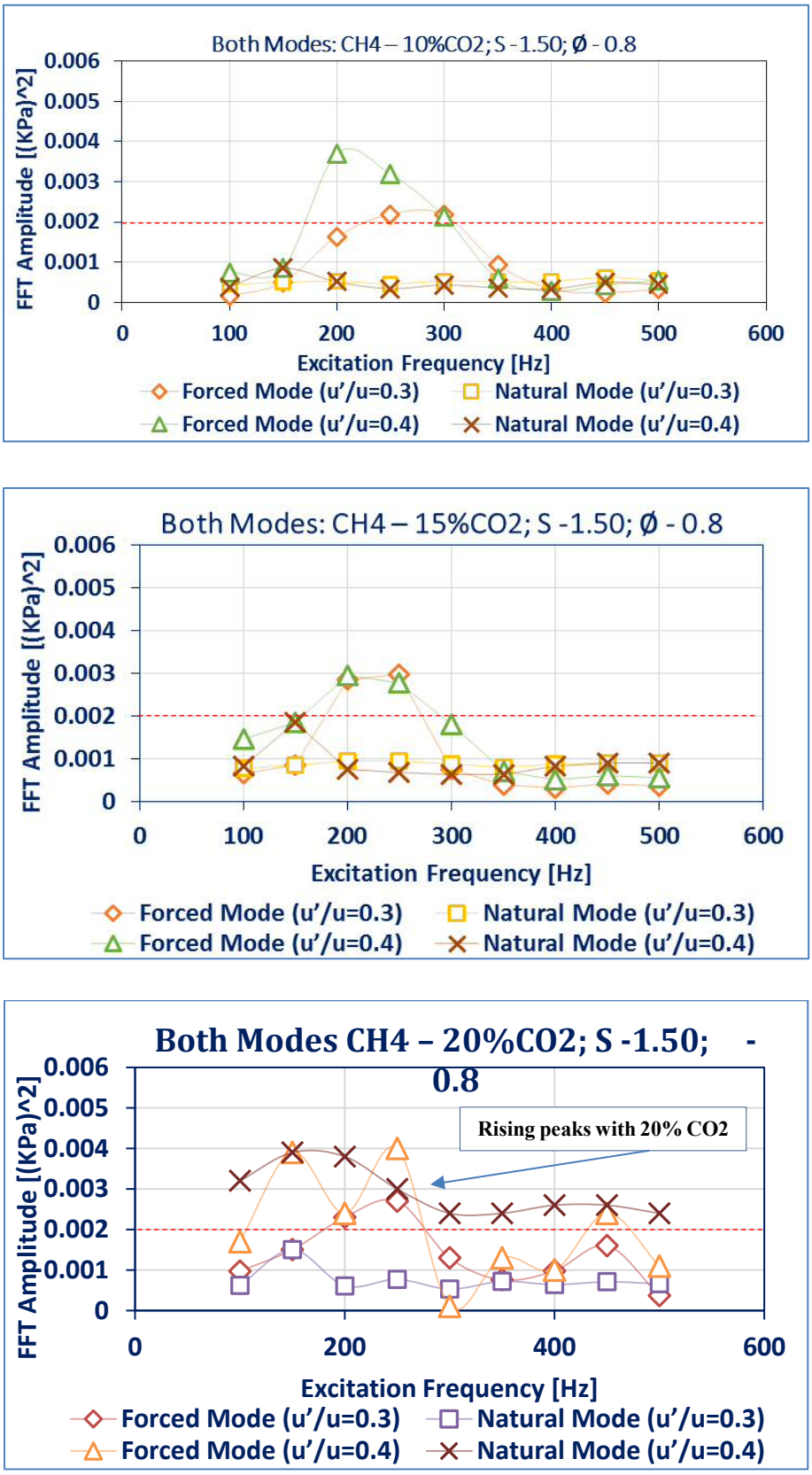

Figure 6. 24 Acoustic modes of Methane –CO2 flames [10%, 15% and 20%; S=1.50; = 0.8; u'/u = 0.3, 0.4]

6.4 Summary

This chapter measured the real-time acoustic modes of the combustor using the FFT analysis of the time series of the dynamic pressure. The modes were examined under three categories of the confined flames: methane-air and methane-CO_2- air flames without forcing; methane-air flame with external excitation and finally, methane-CO_2-air flame with external excitation. In each case, two swirl numbers of 1.05 and 1.50, as well as two equivalence ratios of 0.7 and 0.8, were used. The results showed significant variations in the amplitudes of the acoustic modes which were the basis for the measurement of the instabilities of the combustor. High amplitude acoustic modes signify combustion instability whereas reduced amplitudes denote stable systems.

In all the unforced flames, the dominant acoustic mode was 150Hz, and with external excitation, its frequency was also observed. The amplitudes of the modes varied, depending on the forcing, swirl strength and fuel mixtures. It was observed in most cases that the amplitudes of the acoustic modes of the forced flames were higher than those of the unforced flames, although in most cases, the stability of the system was improved at higher forcing frequencies. Increased forcing was seen to split the turbulent regions leading to a reduced heat release fluctuations, however, the interaction of the forced and natural modes, as well as their harmonics with other oscillations within the combustor in some cases, could further enhance the turbulence intensity of the regimes resulting in increased heat release fluctuations and instabilities.

Increased swirl strength showed an increase in acoustic amplitudes, a similar condition in the flame field with high heat release oscillation caused by the increased turbulence as seen in the previous chapter. The reduced heat release oscillation also corresponds to a reduced amplitude with low swirl strength. Also, the amplitudes were reduced with increased rich mixture, a mechanism which could be linked to the mass-based additive to fuel ratio. Above all, the reduced heat release oscillation with the blend of methane with CO_2 presented a corresponding effect of reducing the acoustic amplitudes at both high and low swirl strength as well as rich and lean mixtures. The reduced amplitude with CO_2 blend was linked to the enhanced thermodynamic properties of CO_2 which were mentioned earlier. However, the blend with the lowest

percentage of CO_2 showed the most stable condition in most cases. With these conditions, a leaner mixture with low emissions could run in a more stable condition. Therefore the control of the flow and flame fields with swirl strength, forcing and fuel conditions responded accordingly to the suppression of the high acoustic modes.

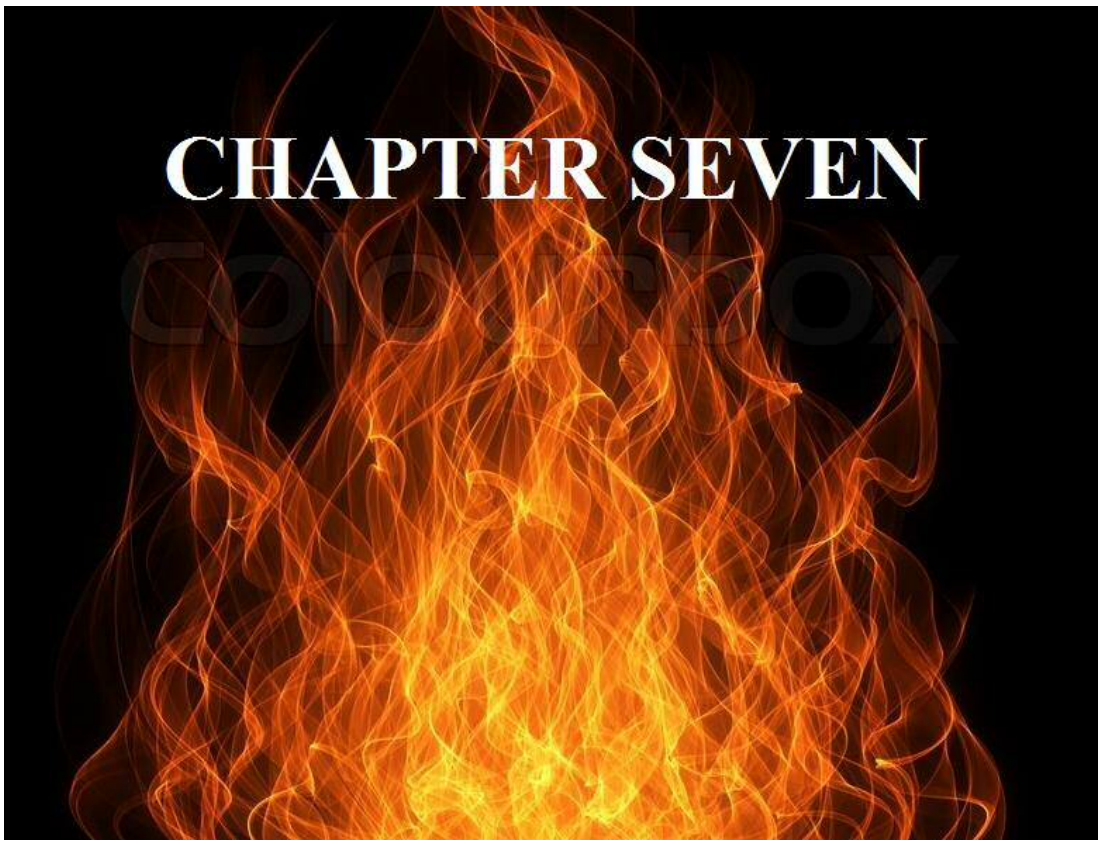
CHAPTER SEVEN

CHAPTER SEVEN:

VALIDATION OF ACOUSTIC MODES AND STABILITY

The great problem of the concert hall is that the shoebox
is the ideal shape for acoustics but that no architect
worth their names wants to build a shoebox.
- Rem Koolhaas

This chapter examines the results of chapter six by simulating an acoustic network model to obtain the chamber acoustic frequencies with the aim of comparing them with the experimental acoustic characteristics. Also, two statistical tools are deployed to evaluate the stable state of the acoustic modes in the combustion chamber so as to compare with the stability behaviour of the spectral analysis in chapter six. Section 7.1 commences with the low order combustion instability simulation using OSCILOS as described in chapter three to obtain the eigen frequencies of acoustic oscillation for comparison with the experimental values. Section 7.2 evaluates the stable states of the acoustic modes at different swirl, fuel and forcing conditions by examining the Autocorrelation Decay of the time series pressure signals. 7.3 performs similar validations using another statistical tool: Probability Density Function. Section 7.4 finally summarises the chapter.

7.1 Combustion Instability Low Order Simulation

The geometry of the mixing and combustion chambers of the experimental rig was captured on the user interface of the Low Order Combustion Instability software (OSCILOS), Figure 7.1, as described in chapter three. With the prescription of the thermodynamic properties of the system and the flame model, the resonant frequencies of the combustor were predicted, as discussed in section 3.5. The flame heat release fluctuation was prescribed by an *n-* model, filtered by a second order model. This analytical flame model was used in this case since the process of obtaining the experimental flame describing function was still ongoing in the research group. With

the analytical model, the thermodynamic properties of the experimental combustor were well captured in the software and the simulation was performed so as to obtain the eigen frequencies at different conditions to give a level of accuracy of the frequency modes obtained experimentally.

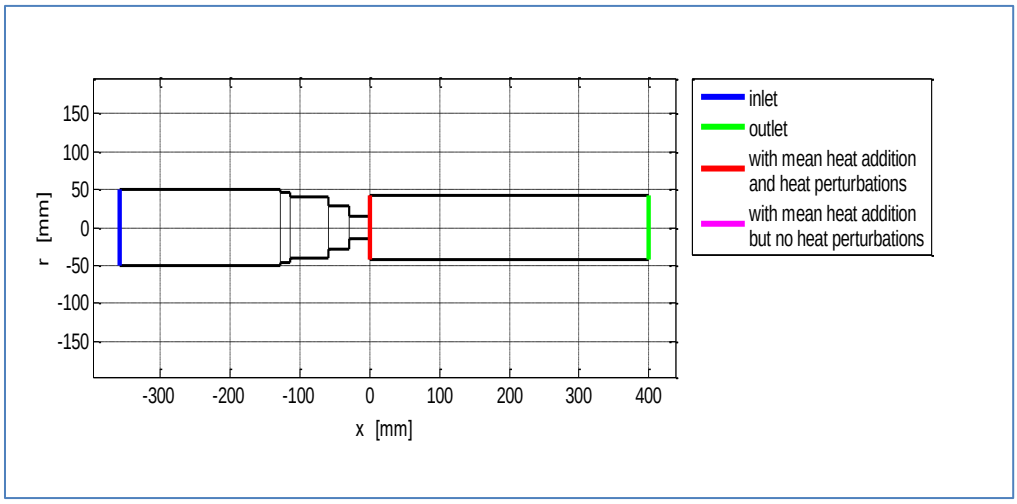

Figure 7. 1 Combustor geometry captured in the software (OSCILOS)

7.1.1 Thermodynamic Properties and Flame Model

Table 7.1 presents the mean flow and thermal properties of the combustion system. It uses a heating grid in place of fuel combustion, with different thermodynamic properties. These properties are temperature before the heating grid Tu, temperature after the heating grid Tb, mean pressure P, mean flow velocity into the premixed chamber u1, mean flow velocity of the mixture into the flame zone u2, mean heat release Q and temperature ratio Tb/Tu. Three cases with different temperature ratios were considered for the simulation. The flame model relates the response of normalised heat release rate fluctuation to the normalised inlet velocity fluctuation . The linear regime of the model was prescribed using an model filtered by a second order filter, where a_F is the gain, f_c- cut-off frequency, - damping ratio and - time delay, as given in table 7. 2. The nonlinear regime was modeled based on the saturation of the heat release rate with velocity oscillation prescribed by Li et al, [93], where are the coefficients which shape the nonlinear regime while is the time delay. The boundary conditions which represent the link between

the outward and inward propagating waves were assigned "closed end" and "open end" for the inlet and outlet configurations respectively.

Table 7.1: Fluid thermal properties for simulation

Case	Pm	T1 [K]	T3 [K]	U1 [m/s]	U2 [m/s]	Tb/Tu	Q [KW]
1	101325	293.15	800	1	4.3	2.7	5.11
2	101325	293.15	1600	1	8.2	5.4	14.2
3	101325	293.15	2500	1	12.4	8.4	25.02

where T1 = Tu for x 0 and T3 = Tb for x 0 in Figure 7-1

Table 7.2: Analytical flame model characteristic values for simulation

Linear Regime				Nonlinear Regime			Boundary Condition	
af	fc						Inlet	Outlet
1.5	250	0.3	3	0.8	25	3	choked	open end

7.1.2 Computed Flame Describing Function

The flame describing function was computed as presented in Figure 7.2, where the gain begins with 1.5 (for the lowest velocity ratio of 0.1) at low frequencies and rises exponentially to a peak value of 2.6 at 250Hz. The gain reduces across the velocity ratio and then saturates at 500Hz. The phase remains constant across the velocity ratio at lower frequencies but varies at higher velocity ratios. This plot shows similar features in terms of the values of the gain and phase at certain positions with many published studies [119] [122][210][136]. This flame model was then fitted into the acoustic wave network model, and the eigenvalues (frequency, growth rate) were simulated.

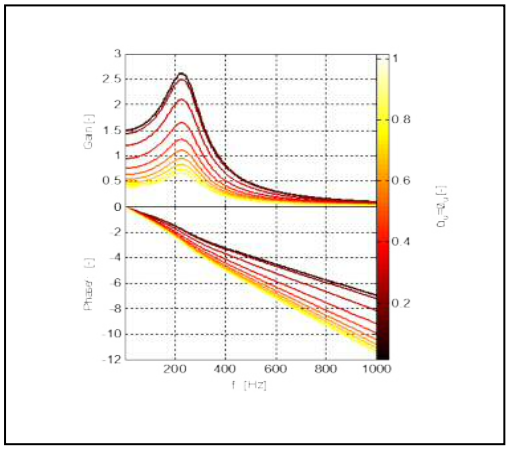

Figure 7. 2 Computed flame describing function

7.1.3 Resonant Frequency Modes

Figures 7.3 give the Contour plots of 20log10 in the s-plane for the normalised velocity ratios of 0.1 (a), 0.4 (b) and 0.8 (c) of case 1. They all show two main acoustic modes designated by the white stars. As earlier mentioned, a positive growth rate signifies an unstable mode while a negative growth rate denotes a stable condition. This analysis focuses on the unstable mode, which oscillates at a growth rate of 73 rad/s with a frequency of 156Hz for the velocity ratio of 0.1 for case 1, Figure 7.3a. At a velocity ratio of 0.4, the growth rate reduces to 23 rad/s with a frequency of 131Hz, Figure 7.3b, and as the velocity ratio increases further to 0.8, the mode became stable at -17 rad/s growth rate with a frequency of 119Hz, Figure 7.1 c. These eigenvalues were also computed for all the velocity ratios in the three cases. The evolution of the acoustic modes from unstable states at lower velocity ratios to stable mode at higher velocity ratios was observed in all the cases.

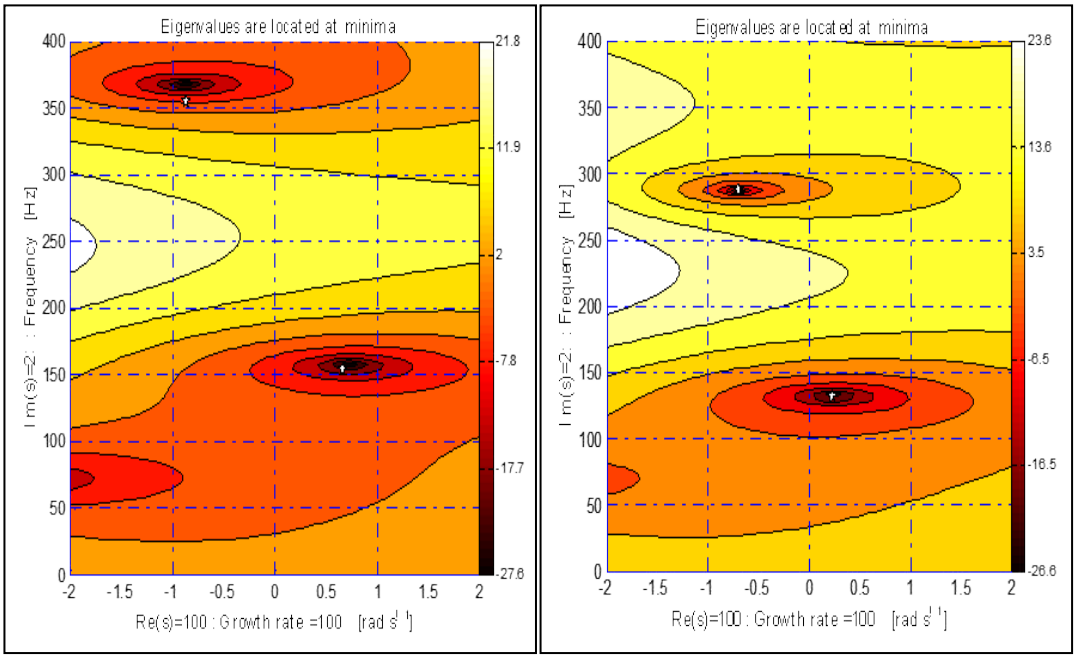

(a) (b)

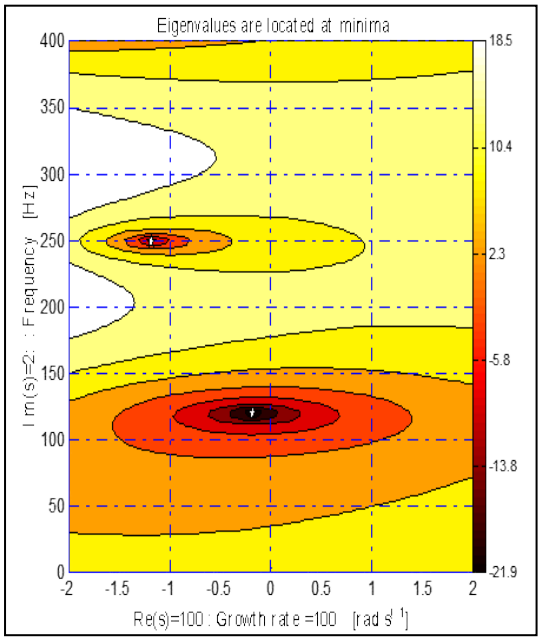

(c)

Figure 7. 3 Contour plot of 20log10 |δe(s)| in the s-plane for the normalised velocity ratios of 0.1 (a), 0.4 (b) and 0.8 (c) of case 1

.

7.1.4 Acoustic Mode Evolution with Temperature Ratio Variations

Figure 7.4a compares the evolution of the growth rate with the velocity ratios in the three cases, with the least temperature ratio in case 1 and the highest temperature ratio in case 3. In Case 1 (temperature ratio of 2.7), the unstable acoustic mode has a growth rate of 73 rad/s at a velocity ratio of 0.1, it then reduces successively with increased velocity ratio and reaches the limit cycle (zero growth rate) between the velocity ratios of 0.5 (8.8 rad/s) and 0.6 (-2 rad/s). In case 2, with a temperature ratio of 5.4, which is a real condition for a methane-air flame, the unsteady mode exhibits a higher growth rate of 128 rad/s at a velocity ratio of 0.1 and reduces successively until it reaches the limit cycle at 0.8 velocity ratio. In case 3, where the temperature ratio is increased further to 8.4, the growth rate of the unstable mode moves further to 148 rad/s at a velocity ratio of 0.1, and reduces with increase in velocity ratio, however the mode still remains unstable at a velocity ratio of 0.8 and requires more increase in the velocity ratio to reach its limit cycle. It is evident that in all these cases, the growth rate decreases as the velocity ratio increases until the zero value is reached, where the flame saturates, and the system becomes stable.

Figure 7.4b compares the evolution of the growth rate with the frequency of the unstable mode in all the cases. The frequency of the unstable acoustic mode also reduces with a decrease in growth rate. In case 1, the growth rate of 73 rad/s has a frequency of 156 Hz, and as the growth rate reduces to 23 rad/s, the frequency moves to 131 Hz. The mode then became stable at a rate of -17 rad/s, with a frequency of 119Hz. In case 2 with increased temperature ratio, the growth rate of 128 rad/s exhibits a frequency of 159 Hz for a velocity ratio of 0.1. As the rate reduces to 58 rad/s, the frequency reduces to 135Hz and reduces further to 124Hz at a growth rate of 0 rad/s. Similar trends were found in case 3 with a higher temperature ratio. Thus in all the cases, the frequency decreases with a decrease in growth rate. The growth rate increases with increase in temperature ratio from case 1 to 3.

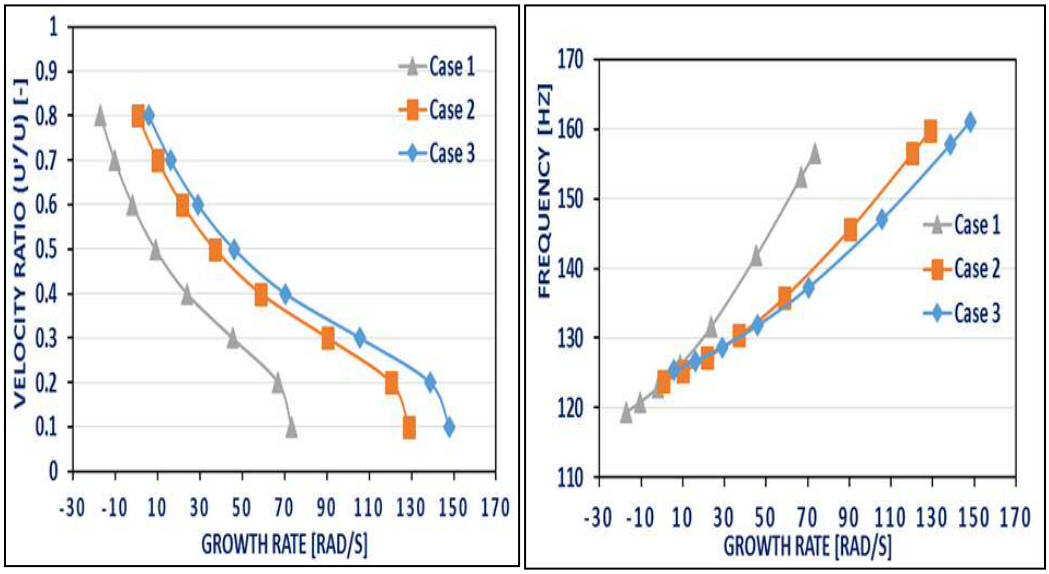

(a) (b)

Figure 7. 4 Eigenvalues evolution with velocity ratio for the three cases

[Case 1: T3/T1 = 2.7; Case 2: T3/T1 = 5.4; Case 3: T3/T1 = 8.4]

Figure 7.5 links the evolution of the Eigen frequency and its corresponding growth rate to the velocity ratio in order to obtain the limit cycle frequency and amplitudes for the three cases. The frequency of the unstable acoustic mode (left-hand side) and its corresponding growth rate (right-hand side) was plotted against the eight velocity ratios (= 0.1, 0.2, 0.3, 0.4, 0.5, 0.6, 0.7 and 0.8). In case 1 the plot indicates that the unstable mode reaches the zero value growth rate between 0.50 and 0.60 velocity perturbations. By linear interpolation (dotted green lines), the limit cycle velocity amplitude is determined as 0.58 at a corresponding frequency of 124 Hz. Case 2, shows that as the temperature ratio increases to 5.4, the 124 Hz acoustic mode shifts its limit cycle amplitude to 0.8 and as the temperature ratio increases to 8.4 (Case 3), the eigen frequency remains at 124Hz but the limit cycle velocity goes beyond the maximum 0.8 velocity perturbation (the maximum limit of this simulation) and is assumed to go as far as 0.9. In all the three cases, even with the changes in flame temperature ratio, the limit cycle frequency remains at 124Hz, but the limit cycle amplitude varies from 0.58 in case 1, 0.8 in case 2 and presumably 0.9 in case 3. It thus shows that the flame temperature could be used as an important tool to control combustion instabilities.

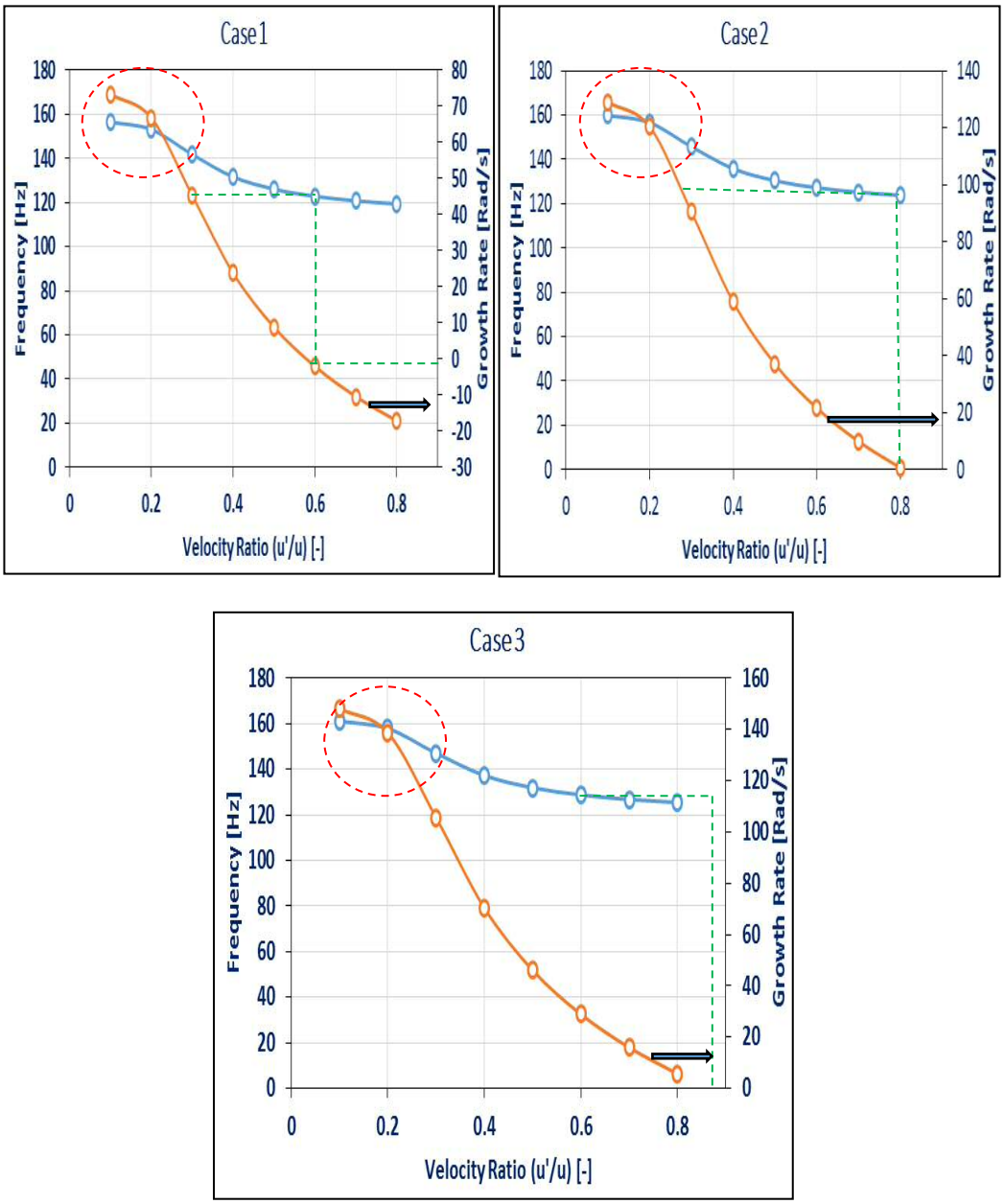

Figure 7. 5 Acoustic mode evolution with velocity ratio

From these three cases, it is clear that the unstable acoustic modes occur at a frequency of around 150Hz (red broken oval shape rings) at a velocity ratio range of 0.2 to 0.3. When damping sets in, the growth rate of the acoustic modes decreased to its limit cycle at about 124 Hz for different velocity ratios in the three cases depending on the variant parameter which is the inlet temperature ratio.

7.1.5 Experimental and Simulated Results

In comparing the simulated results with those of experiment, Figure 7.6 shows that the experimental unstable acoustic frequencies were obtained at 150Hz within the range of values of the unstable modes in the three simulated cases, illustrated by the red broken oval shape in Figure 7.6. The damping of the acoustic modes decreases with the growth rate with a decrease in mode frequency until the limit cycle was reached at a frequency of 124Hz in the simulation. This is similar to the damping acoustic modes of the experimental technique shown in Figure 7.7, with full detail in the next section. This agreement of the simulation with experimental values gives an indication of the accuracy of the experimental acoustic modes with the use of the theoretical flame function.

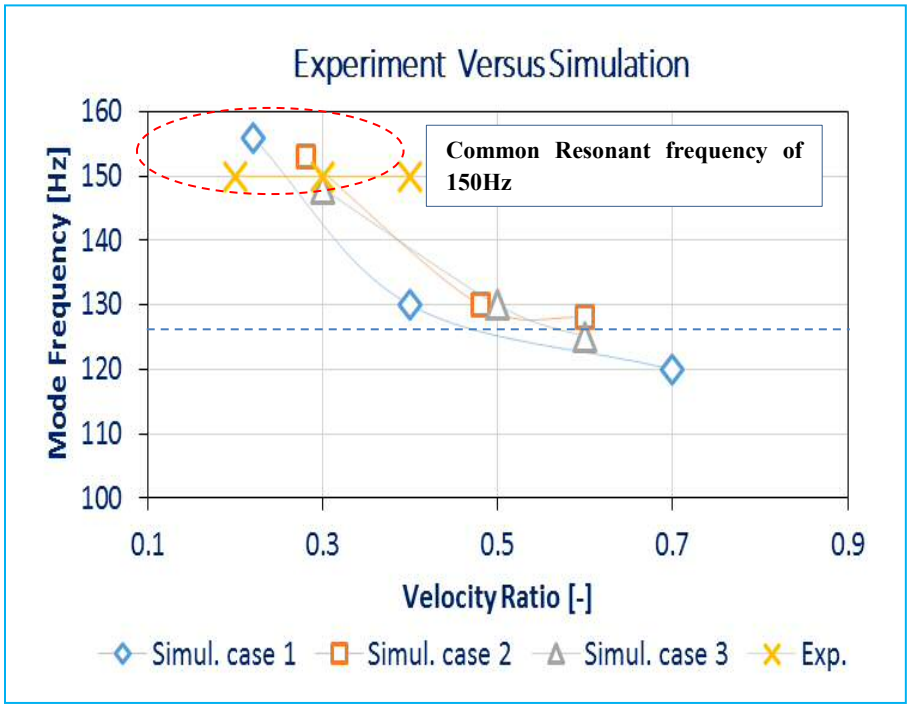

Figure 7. 6 A Comparison of acoustic frequencies of experiment and simulation

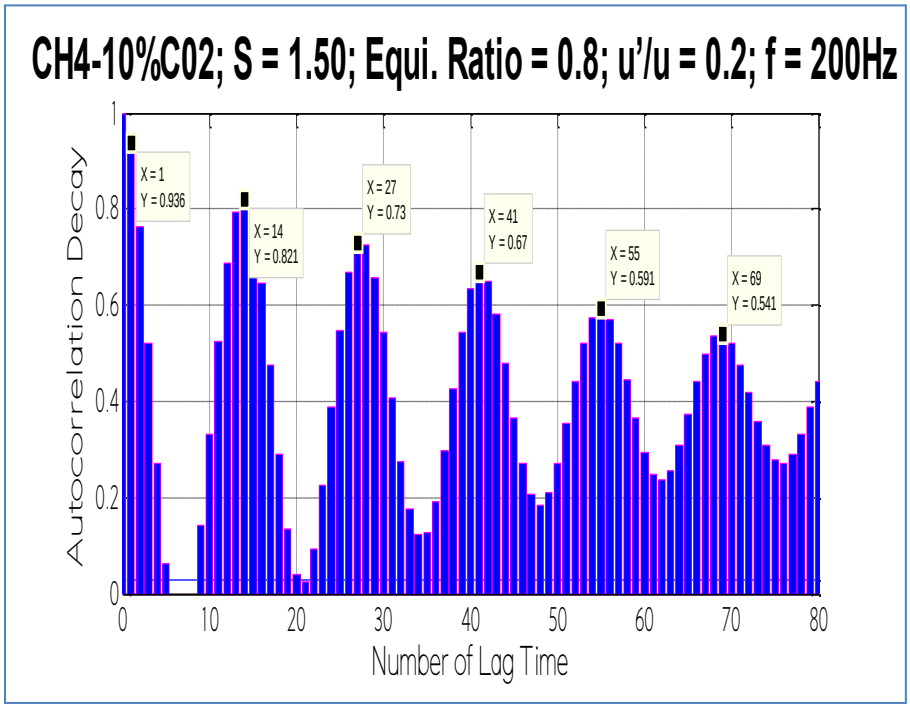

Figure 7. 7 Acoustic autocorrelation decay: CH4; S=1.50; = 0.8, u'/u = 0.2

Table 7.3 summarises the limit cycle values with their corresponding temperature ratios. With a constant limit cycle frequency of 124Hz, the changes in the amplitude was based on the corresponding change in temperature ratio.

Table 7.3: Acoustic oscillation limit cycle values with different temperature ratio

CASE	Temp. Ratio	Limit Cycle Frequency	Limit Cycle Amplitude
1	2.7	124	0.58
2	5.4	124	0.8
3	8.4	124	0.9 (projected)

These results show that an unstable system could be made to reach an early limit cycle (stability) with a low-velocity ratio by reducing the temperature ratio between the inlet fuel-air temperature and the temperature in the flame zone, which could be achieved by preheating the inlet air. However, the temperature ratio must be kept at a value which does not reduce the overall thermal efficiency of the system. The temperature ratio variation thus becomes a potential technique for the control of combustion instabilities in premixed combustors.

7.2 Acoustic Mode Dynamics: Autocorrelation Decay

Autocorrelation decay (ACD) is a mathematical tool which gives the degree of similarity between the original time series signal with its delayed version over several time intervals [220] [221]. This shows how a signal is similar to the original version after a given time interval or lag. In this case, an unstable signal remains at unity or slightly lower over several time lag as the acoustic amplitude grows or remains the same. But a stable mode has a decrease ACD as the amplitude of the oscillation decays over time. This technique has been used in published studies to examine the acoustic stability of dynamic pressure signals in swirl premixed combustors [158] [213]. The ACD analysis was done using Matlab functions with the time series of the dynamic pressure signals at different conditions as input values. The first part of this section compares the stability modes of forced and unforced methane flame under different conditions while the second part compares the stability conditions of forced methane flames with the blend of methane with different proportions of CO2.

7.2.1 CAM of Unexcited and Excited Methane Flames

This section compares the acoustic instability of the forced and unforced flame with different flame conditions. The first case of Figure 7.8, presents the autocorrelation of the dynamic pressure of the combustor with methane fuel at a higher swirl number of 1.50, the equivalence ratio of 0.7 and inlet velocity amplitude of 0.1 without external excitation. The decrease in the autocorrelation envelope of the pressure signal from unity, ACD =1 to 0.6 shows the decay in the oscillation amplitude over a period as a result of the damping acoustic amplitude caused by the dissipative processes within the combustor [213].

In the second case with the same variable but with a forcing frequency of 100Hz, the ACD remains around unity throughout the entire time evolution. The same behaviour was also observed with a further increase in forcing frequency of 300Hz, where the ACD remains at about 0.93 throughout the 80 lag time. At a higher swirl number of 1.50, the amplitudes of acoustic modes became very high. These signify the lack of acoustic damping in the oscillation which suggests that the system was unstable. This acoustic behaviour agrees with the spectral analysis in chapter six that external excitation of flame at certain condition could move a stable acoustic combustor to

instability. In the spectral analysis of this particular condition in Figure 6.11, the power spectrum of the acoustic frequency was found to rise excessively for all the forcing frequencies.

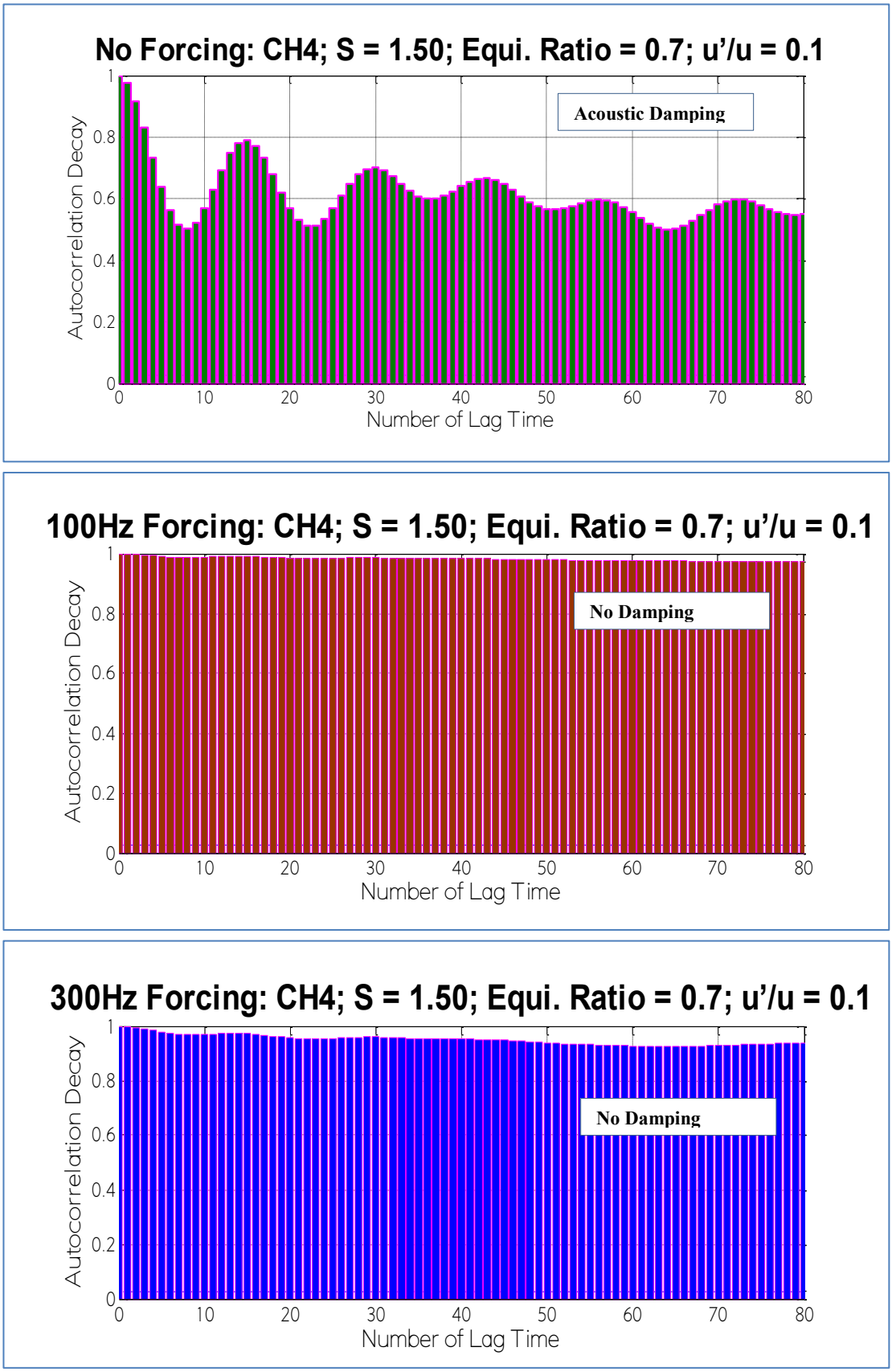

Figure 7. 8 Acoustic autocorrelation decay: CH4; S=1.50; = 0.7, u'/u = 0.1

The assessment was also carried out with the dynamic pressure signal with similar swirl number of 1.50, an equivalence ratio of 0.8 and an increased inlet velocity amplitude of 0.3 as presented in Figures 7.9. In the first case without forcing, the autocorrelation decay dropped further from ACD = 1 to 0.40, representing a 60% damping with the time lag. In the reaming two cases, where forcing frequencies of 100Hz and 250Hz were applied, a corresponding damping of 9 and 7% respectively were observed. These again show the impact of excitation on the stability of the combustor acoustic at certain conditions, which suggests that the stability of a system could be reduced when forced. In Figures 7.10 with a reduced swirl number of 1.05, the equivalence ratio of 0.8 and inlet velocity of 0.2, the crest of the oscillation was reduced from ACD =0.9 to 0.52 which is about 48% decay over the time lack. In the remaining two cases with forcing frequencies of 200 and 400Hz, a slight increase in acoustic damping by 17 and 8% respectively were observed. The increase in damping, in this case, is attributed to the reduction in the swirl strength which aggress with the spectral analysis illustrated in Figure 6.10.

The above scenarios confirm the earlier observation in the spectral analysis that at a particular swirl and forcing conditions, increase in oscillation amplitude could result when the flame is forced. The question that might arise could be why the system was forced if running it without forcing could keep the system in a stable condition. In real combustors with a more compact confinement of the flame, the acoustic stability may not be guaranteed in all conditions and thus requires forcing to control the flow field coherent structures and its convection to the flame. Because the forced signal interacts with other frequencies such as the resonant frequency of the burner, PVC, heat release frequency etc., depending on their time scales, the interactions could increase or decrease the acoustic stability of the system.

The effect of the inlet velocity amplitude and swirl strength on the acoustic amplitude damping were also evident in all the cases considered. The unforced flame in Figure 7-9 with u’/u = 0.3 showed a high percentage of damping, followed by the unforced flame in Figure 7-10 with a reduced u’/u = 0.2. The swirl strength was also crucial in this regard, as observed in the spectral analysis, where forcing in a lower swirl strength showed a reduced instability of the burner.

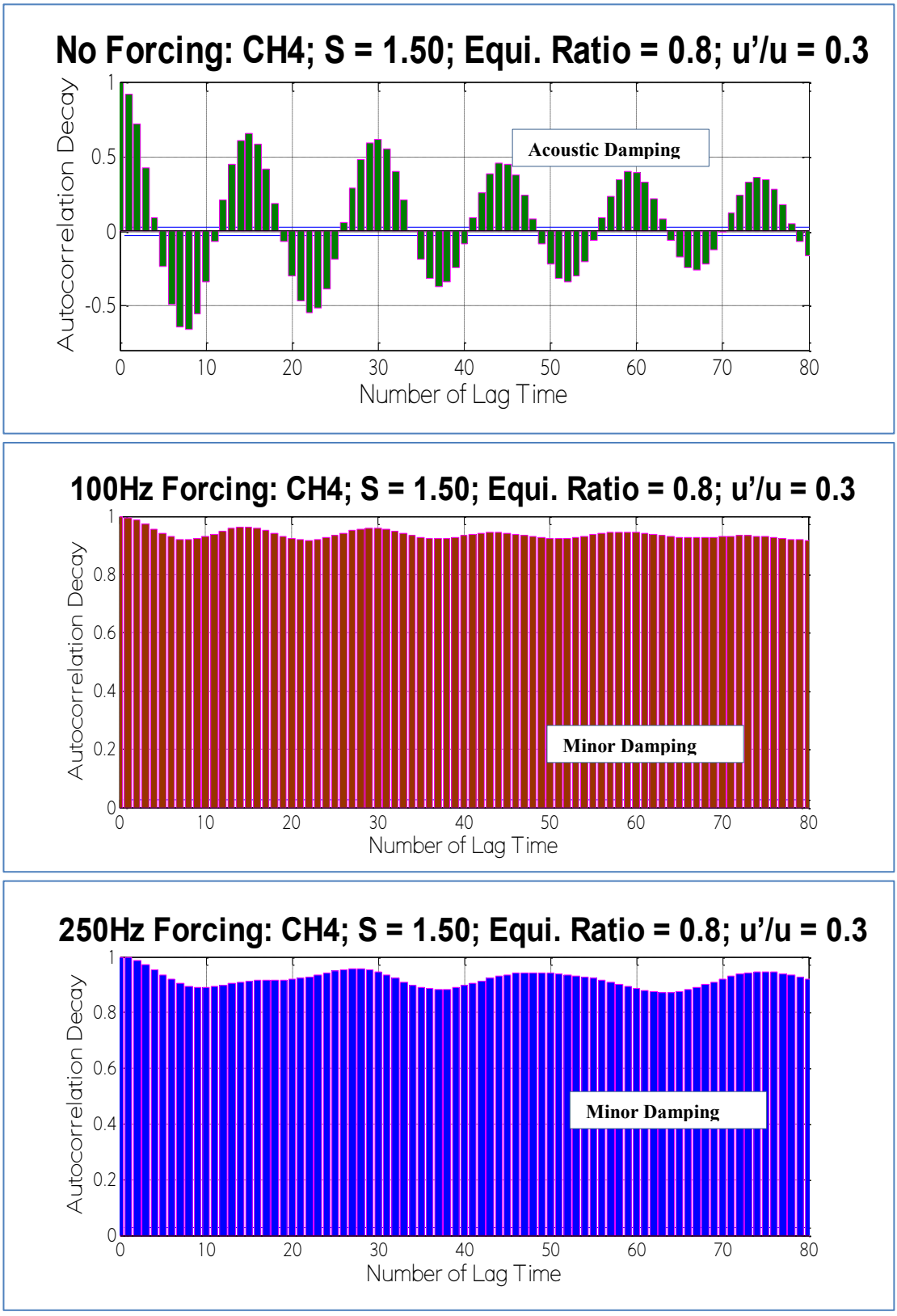

Figure 7. 9 Acoustic autocorrelation decay: CH4; S=1.50; =0.8, u'/u = 0.3

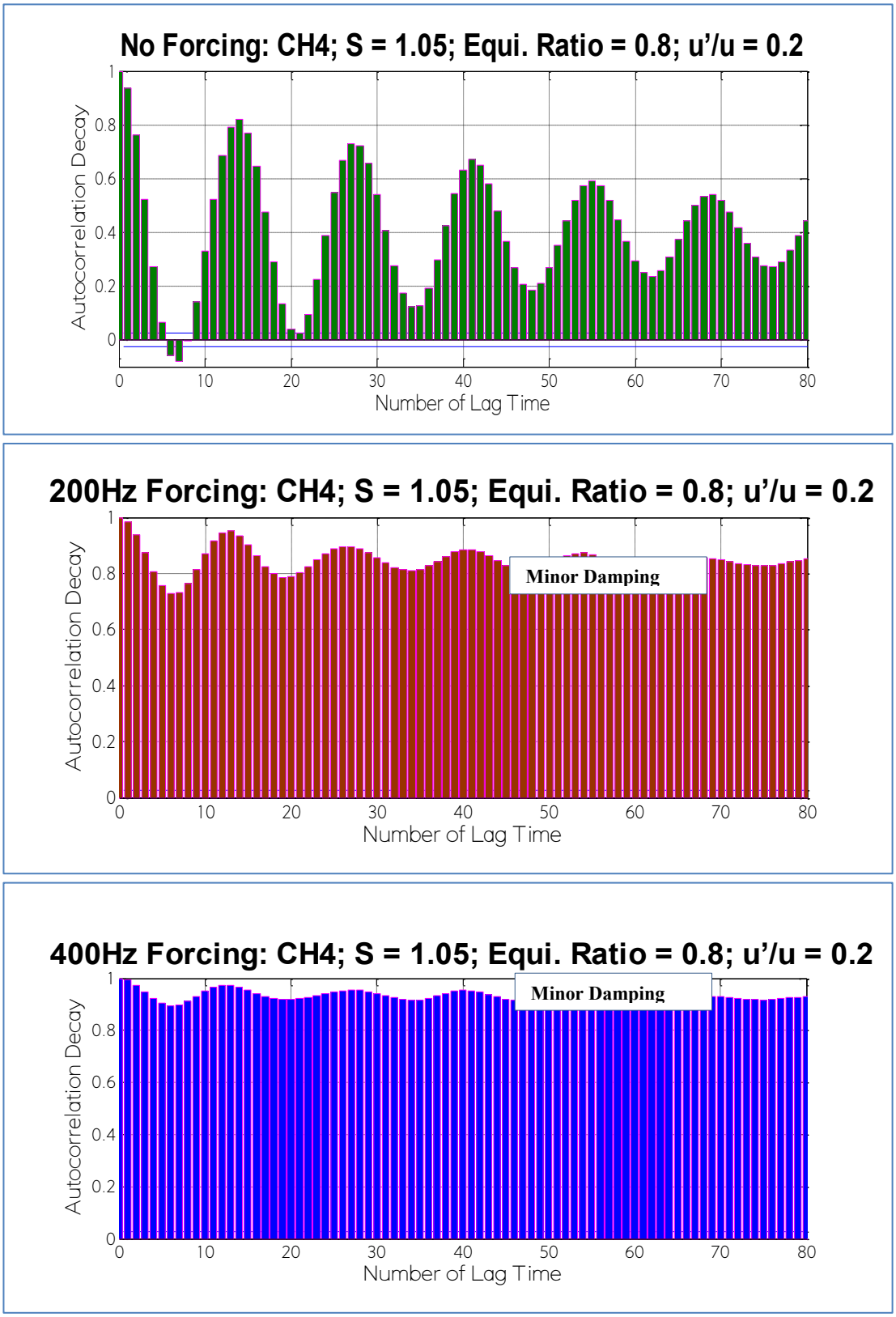

Figure 7. 10 Acoustic autocorrelation decay: CH4;S=1.05; = 0.8, u'/u = 0.2

7.2.2 CAM of Unexcited and Excited Methane – CO2 Flames

This section samples the stability conditions of the combustor pressure oscillation of 32 cases using Autocorrelation Decay (ACD). The sampled cases cut across different fuels, swirl, and velocity amplitudes. In each case, nine forcing frequencies (100-500Hz with a step of 50Hz) were applied to assess the chamber acoustic stability response to the combined effects of these parameters. The main aim here is to compare the stability of the methane-air flame with its blends with different proportions of CO2. Because of the numerous cases considered, a bar chat is used in each case, where the length of the bar represents the lowest value of the acoustic mode decay when the Autocorrelation function is run with Matlab with each input data, as illustrated in Figure 7.11. At a forcing frequency of 200Hz, the lowest Autocorrelation decay is 0.54, which is indicated by the red bar.

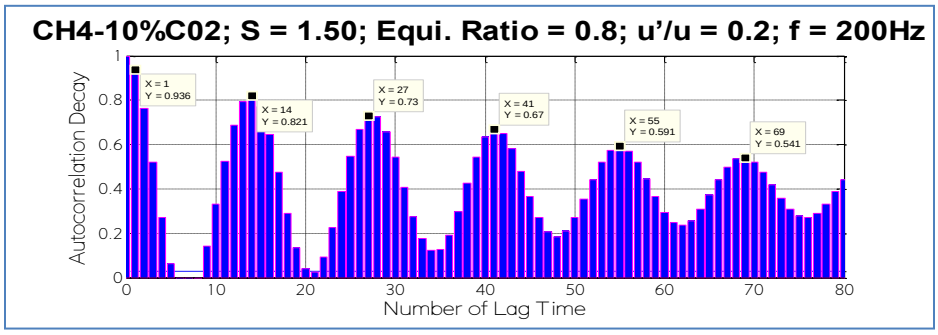

(a) f=200Hz

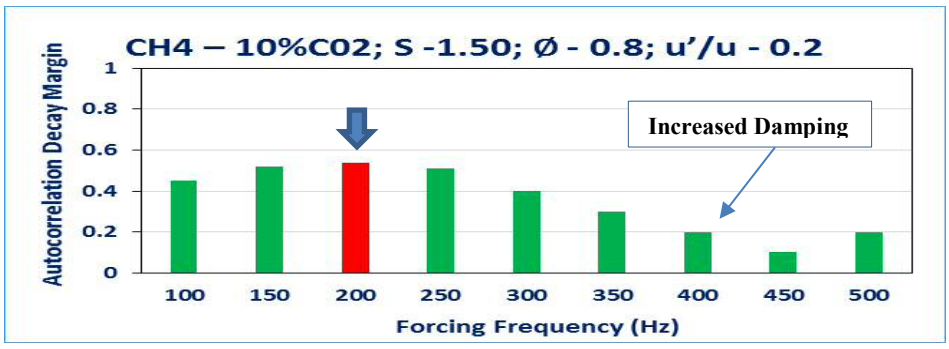

(a) f=100 – 500Hz

Figure 7. 11 Acoustic autocorrelation decay: CH4-10%CO2; S=1.50 = 0.8

Figures 7.12 consider the oscillation characteristics of 8 cases of methane-air flame, with both swirl numbers, the equivalence ratio of 0.7 and 0.8, velocity ratios of 0.2 and 0.4 for nine forcing frequencies. The length of the bars represents the drop in the acoustic envelopes of the ACD. The first case (a) has a maximum decay of 0.54 at a forcing frequency of 500Hz and a minimum level of 0.9 at a forcing frequency of 200Hz, with the rest above the 0.6 damping arbitrary margin (red dotted line). In the second case with a richer mixture, (= 0.8), the level of damping increases as five of the nine bars have their damping levels within the 0.6 margin. In case (c) and (d), with increased velocity amplitude to 0.4, the richer mixture again showed a higher level of acoustic damping than (c), while a comparison between (b) and (d) shows an increased damping with increased velocity amplitude. Case (a) and (c) become relatively nonlinear in terms of damping with increased velocity ratio which could be attributed to the increased leanness of the mixture, as observed in previous cases. Cases e to h present the acoustic damping behaviours as the swirl strength was increased to S= 1.50. Here a decrease in acoustic damping level (which implies an unstable system) were observed as none of the forcing levels fell below the 0.6 arbitrary margin. As earlier observed, the forced conditions with high swirl strength present a high level of instabilities, especially at high equivalence ratio.

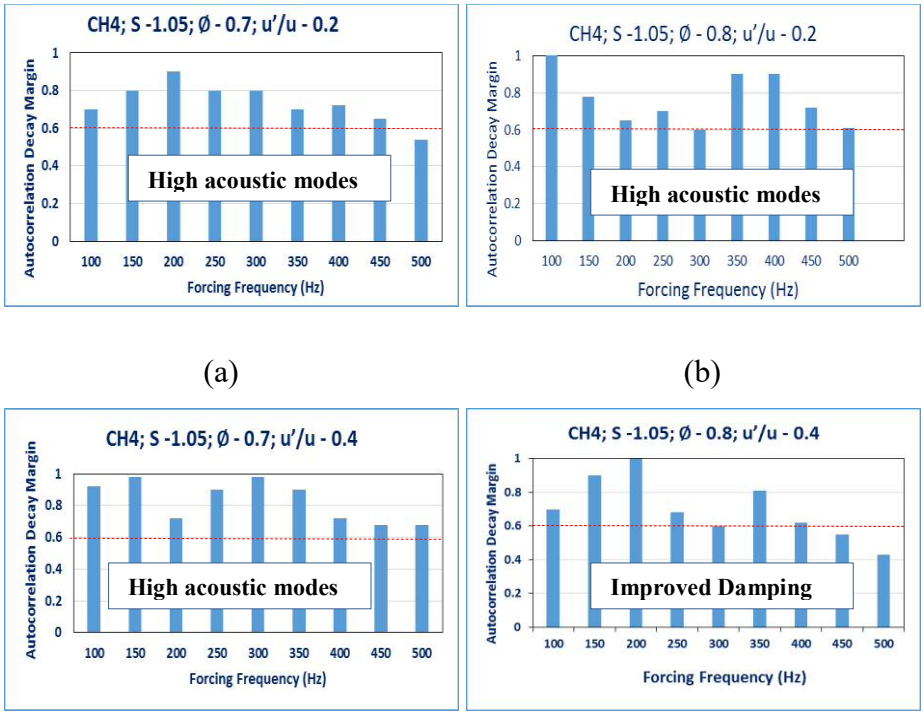

(c) (d)

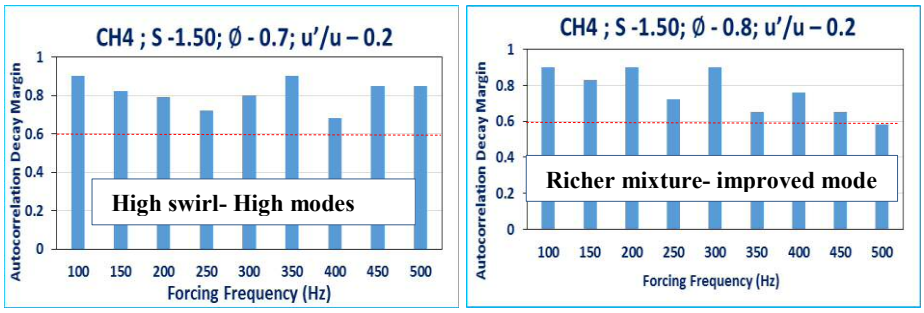

(e) (f)

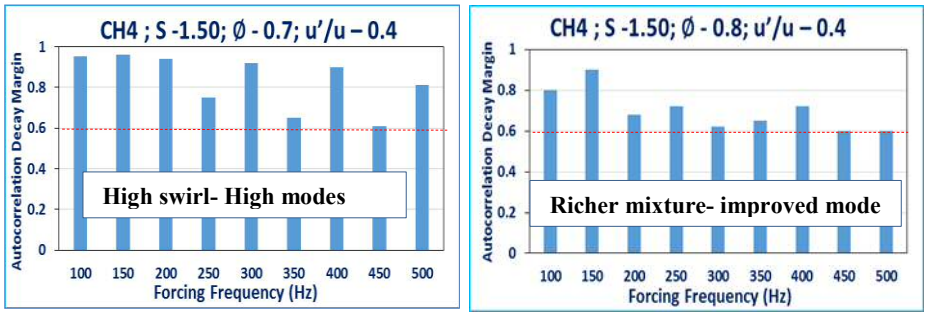

(g) (h)

Figure 7. 12 Acoustic oscillation autocorrelation decay: CH4; S= 1.05, 1.50

Figures 7.13 examine the oscillation characteristics of 8 cases of methane blended with 10% of CO2, with both swirl numbers, the equivalence ratio of 0.7 and 0.8, velocity ratios of 0.2 and 0.4 for nine forcing frequencies. In all the cases, almost all the bars fell below the 0.6 damping margin, representing a sharp decrease in acoustic envelopes and by extension a more stable system with the blend of 10% CO2 with methane. Because of this high damping rate, another arbitrary margin was created at 0.3 oscillation margin for ease of evaluating the oscillations, since most of them fall within this region. The first four cases of Figure 7.13 are of lower swirl number of 1.05, with most of the bars within the 0.3 margin especially with richer mixtures and higher velocity amplitudes. Similar behaviours are observed in the remaining four cases even with increased swirl number of 1.50. It thus confirms the capability of this fuel blend to suppress the acoustic oscillations at leaner and higher swirl and velocity ratios.

Figures 7.14 consider the oscillation characteristics of another 8 cases with an increased percentage of CO2 blend to 15%, with both swirl numbers, the equivalence ratio of 0.7 and 0.8, velocity amplitudes of 0.2 and 0.4 for nine forcing frequencies. The increased in the percentage of CO2 shows similar behaviour with the 10% CO2 blend, although there is a slight decrease in the level of oscillation damping. Case (a) has 2 bars below the 0.3 margin while the remaining 6 cases are above. The last four cases with higher swirl strength show a greater degree of oscillation damping than the lower swirl strength similar to the 10% CO2. Case (g) with an equivalence ratio of 0.7, swirl number of 1.50, velocity amplitude of 0.4 has all the bars from 250Hz forcing frequency within the 0.3 margin, thus having the most stable acoustic mode among the eight cases considered. In the lower swirl number regimes, most of the bars are above this margin, thus showing an enhanced stability with leaner mixtures at high swirl strength.

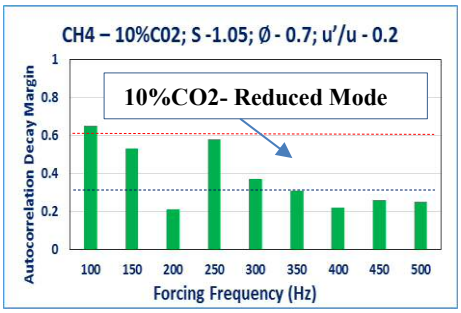

(a)

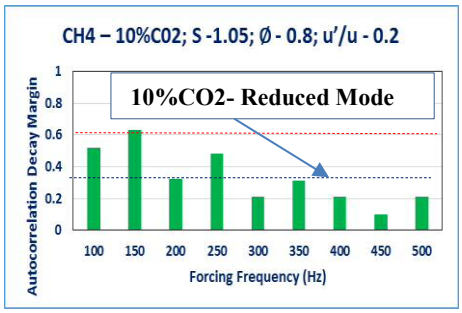

(b)

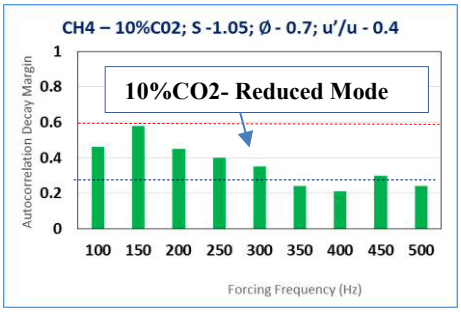

(c)

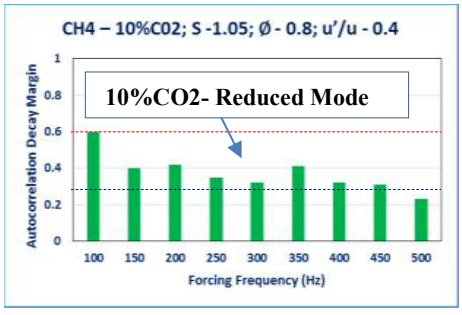

(d)

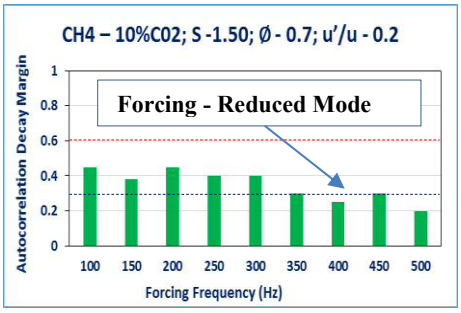

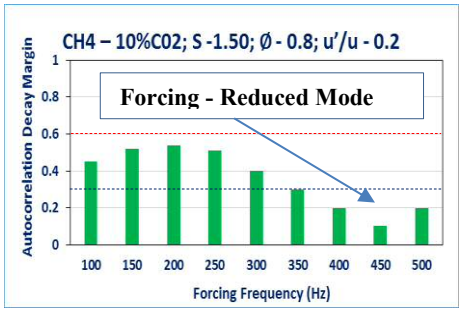

(e) (f)

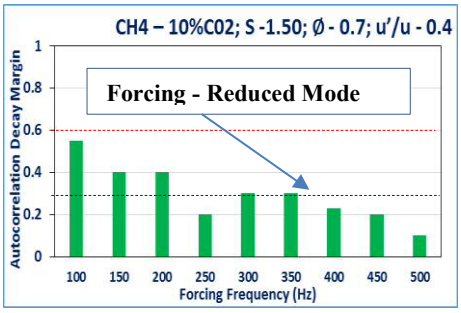

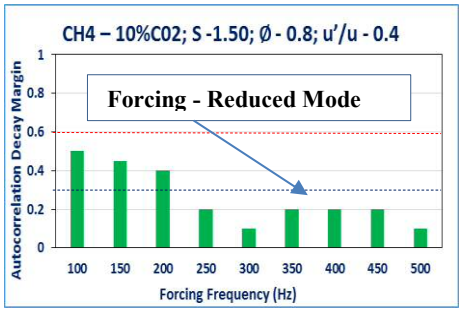

(g) (h)

Figure 7. 13 Acoustic autocorrelation decay: CH4 – 10%CO2; S-1.05, 1.50

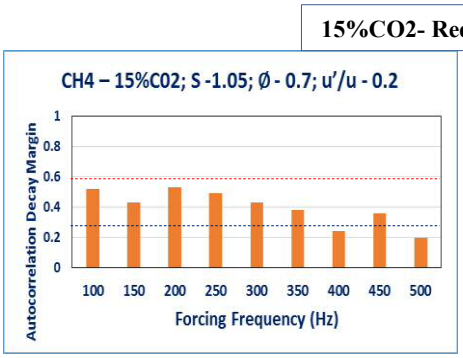

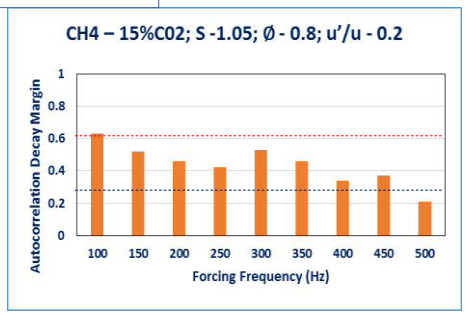

(a) (b)

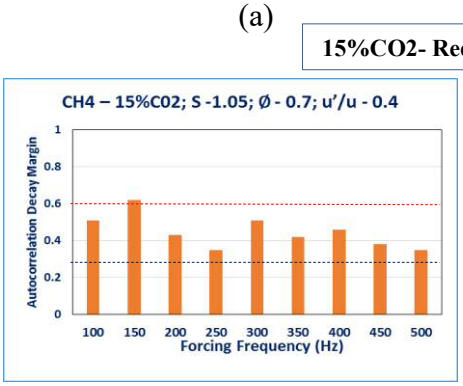

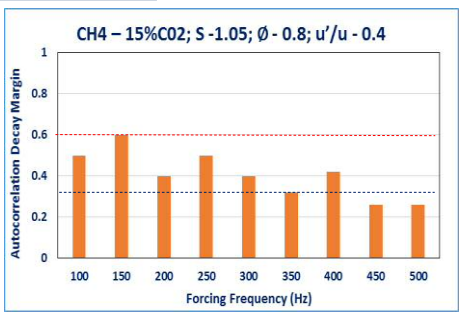

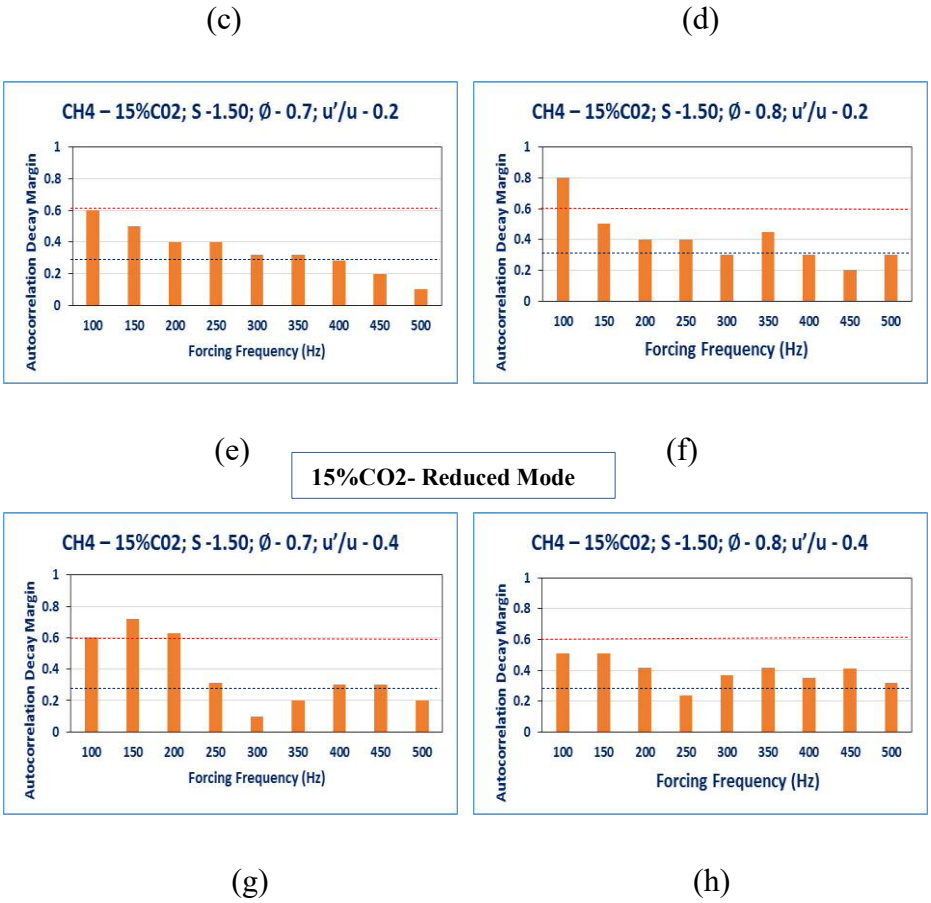

Figure 7. 14 Acoustic autocorrelation decay: CH4 – 15%CO2; S-1.05, 1.50

Figures 7.15 present the oscillation characteristics of another 8 cases with an increased percentage of the CO2 blend to 20%, with both swirl numbers, the equivalence ratio of 0.7 and 0.8, velocity amplitudes of 0.2 and 0.4 for nine forcing frequencies. In this case, the damping level of most of the cases stands between the upper and lower margins. The lower swirl strength oscillations show more damping than the high swirl strength, especially at high-velocity ratios. The lean flame shows an improved oscillation stability than the richer mixture in the high swirl strength. However, the level of acoustic damping is reduced as the percentage of CO2 was increased. Also in most cases, the high swirl flows have improved stability states with leaner equivalence ratio, because of the improved mixing as the size of the CRZ increases and the enhancement of the heat release rate due to the diluent and density effects of CO2.

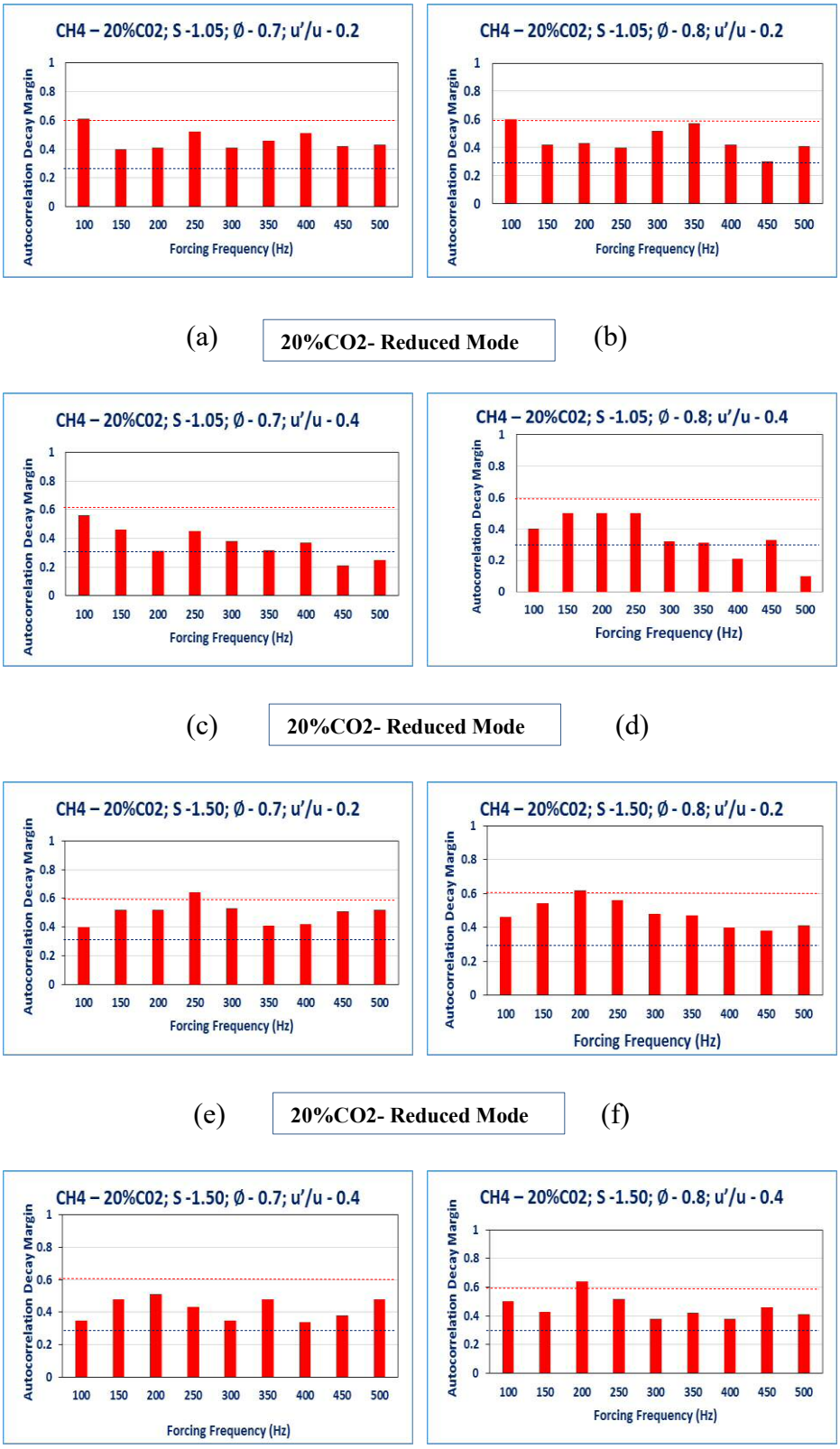

Figure 7. 15 Acoustic autocorrelation decay: CH4 – 20%CO2; S-1.05, 1.50

7.3 Dynamic Pressure Distribution: PDF

The stability of the oscillations within the combustor was further examined using the Probability Density Function (PDF), a statistical tool which provides the likelihood that a randomly sampled data falls within a particular sample space. The distributions were obtained using Matlab functions with the time series of the dynamic pressure signals at different conditions as input values. Depending on the relative phasing of the heat release perturbations and dynamic pressure, the amplitude of oscillations grows exponentially to limit cycle or decays towards a zero amplitude margin. The conditions for the stability of the system in this technique is that a system is considered to be stable if the pressure distribution reaches its peak value at zero pressure amplitude [P' (t) = 0], with a Gaussian distribution about the mean. The peak zero amplitude denotes the decay of the dynamic pressure towards the zero amplitude thus damping the oscillations, but an unstable system is characterised by the multimodality of the pressure distributions. This technique has been used in the reported studies of Lieuwen [158][213].

7.3.1 Stability Mode of Methane- Air Flame: S = 1.05; 1.50

Figures 7.16 present the cases for pure methane-air flame, lower swirl number of 1.05, two equivalence ratios and four velocity ratios with specific forcing frequencies. In all the cases, the pressure distributions spread across different pressure amplitudes with peak values away from the zero margin. In the first case the pressure amplitudes spread between 0.8 and 0.93 Kpa with a multimodality distribution, the second case peaks at about 0.065 Kpa, the third case has a bimodal distribution with one of the peaks at zero value, the fifth case peaks at -0.05 while the eighth case has its peak at 0.165 Kpa. According to the stability conditions, these cases are characterised by unstable pressure oscillations although the level of instabilities varies, with some having low-pressure amplitudes at peak points. Figures 7.17 consider similar cases but with an increased swirl number of 1.50. Here, the increased level of instability is evident in most of the cases with multimodality distributions. The first case has three peaks at 0.01, 0.025 and 0.035 Kpa respectively; the second case has the pressure amplitude between -0.04 and 0.04 Kpa with a uniform distribution around zero with a higher peak at -0.02 and a lower peak at 0.03 Kpa.

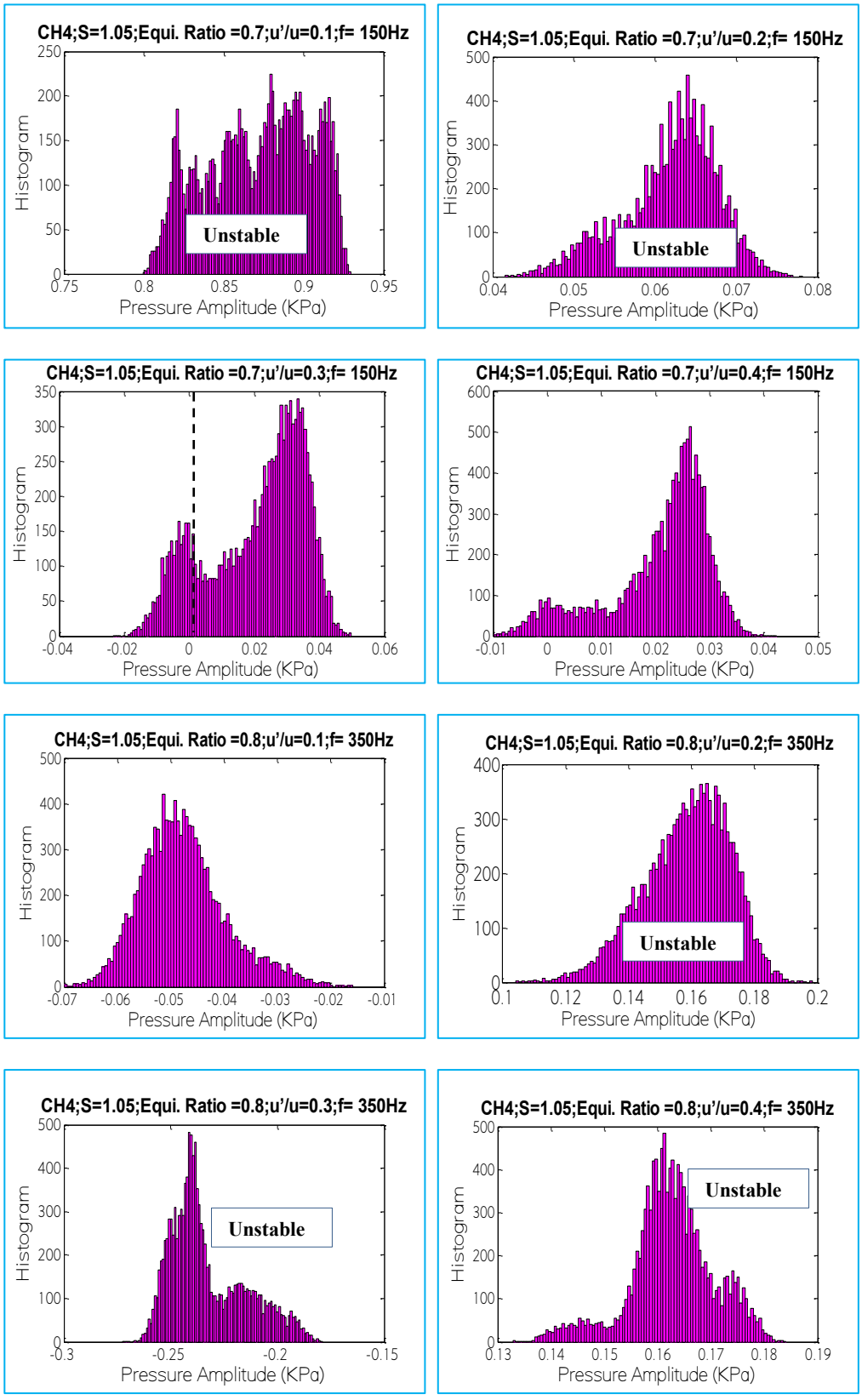

Figure 7. 16 Dynamic pressure Amplitude distribution of methane-air flames S=1.05

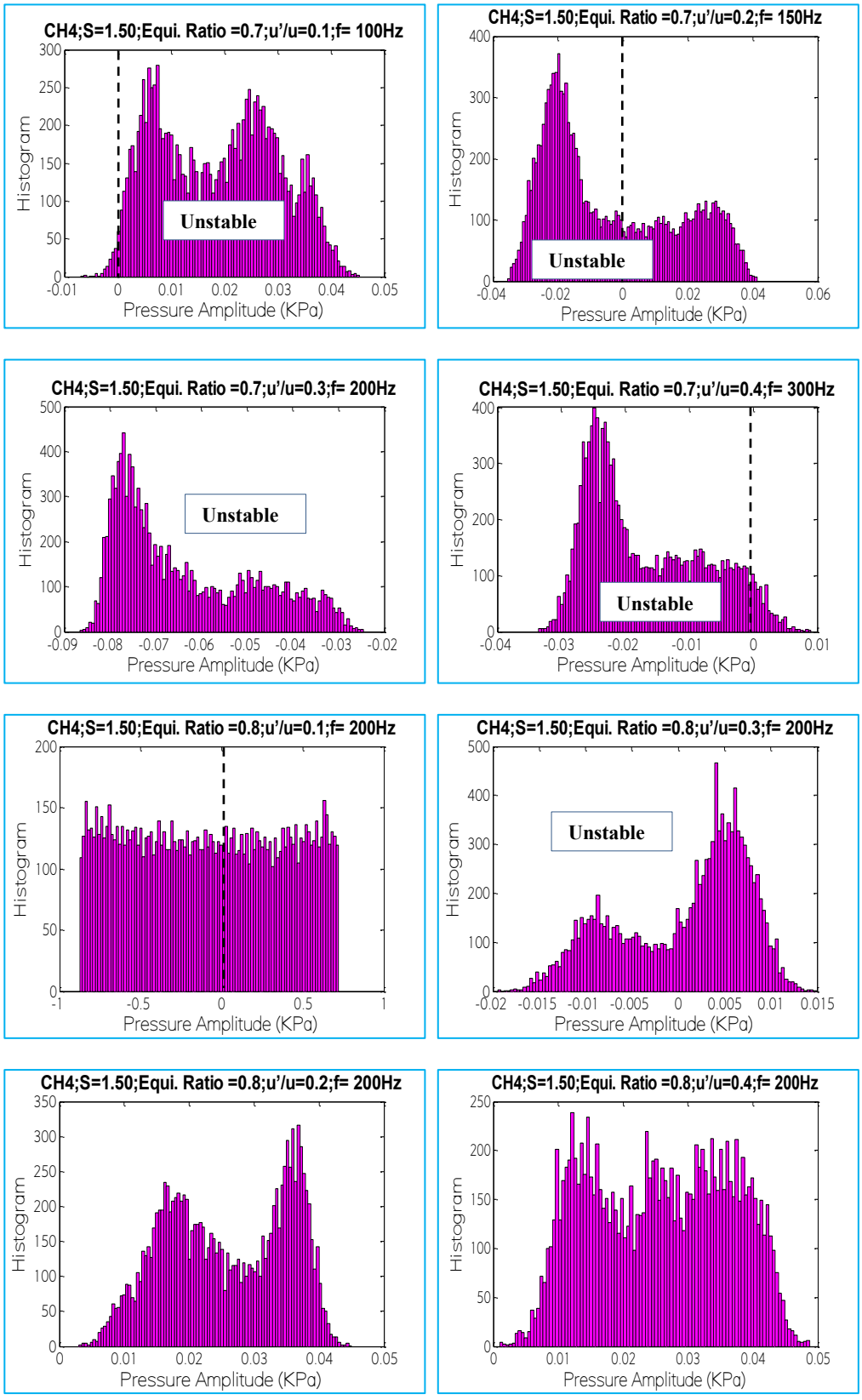

Figure 7. 17 Dynamic pressure Amplitude distribution of methane-air flames S=1.50

The third case peaks at -0.08 Kpa, the fourth spreads across zero point with a peak value of -0.025. The fifth and seventh cases also spread across the zero value while others are characterised by extreme multimodality of the distributions. This increased instability with increased swirl strength especially at high equivalence ratio, is common in all the analysis so far. It is attributed to the variation of the CRZ leading to mixture inhomogeneity with attendant increased heat release fluctuation.

7.3.2 Stability Mode of Methane-10CO2 –Air Flame: S = 1.05; 1.50

Figures 7.18 present the distribution for cases with a blend of methane with 10% of CO2, a lower swirl number of 1.05, the equivalence ratio of 0.7 and 0.8 and similar velocity amplitudes and forcing with the two previous cases (Figures 7.16 and 7.17). As observed, most of these cases either peak at or very close to the zero pressure amplitude. The first case peaks at a very low-pressure amplitude of -0.005 next to zero, the second case centralises at the zero value, but the peak moves slightly away from it. Cases 3, 4 and 5 also have their peak values around zero and cases 6 and 8 peak at zero with only one odd case (7) with a peak value of -0.01 Kpa. Similar pressure behaviours are also observed with increased swirl number of 1.50 as plotted in Figure 7.19. Out of the eight cases considered, five of them have their peak dynamic pressure amplitude at zero. These are cases 1, 3, 6, 7 and 8. Out of the remaining two cases, one peaks quite close to zero (0.015) while the other peaks further away at 0.065Kpa. Thus the relative stability of the pressure oscillation with 10% blend of CO2 with methane in all the forcing conditions has again been proven.

7.3.3 Stability Mode of Methane-20%CO2-Air Flame: S = 1.05; 1.50

Figures 7.20 present the pressure amplitude distribution cases with a blend of methane with 20% of CO2, a lower swirl number of 1.05, the equivalence ratio of 0.7 and 0.8 with various velocity ratios and forcing conditions. Many cases here reveal the multimodality of the dynamic pressure amplitudes away from the centre zero margin. The first case has two main peak points at 0.01and 0.02, the second case peaks away from zero, the third is also away from zero. In case four, although one of the two peaks falls around zero margin, the other which is away has a higher magnitude. Out of the four remaining conditions, only the last case has its peak around 0 and -0.01 Kpa; others are far of this margin.

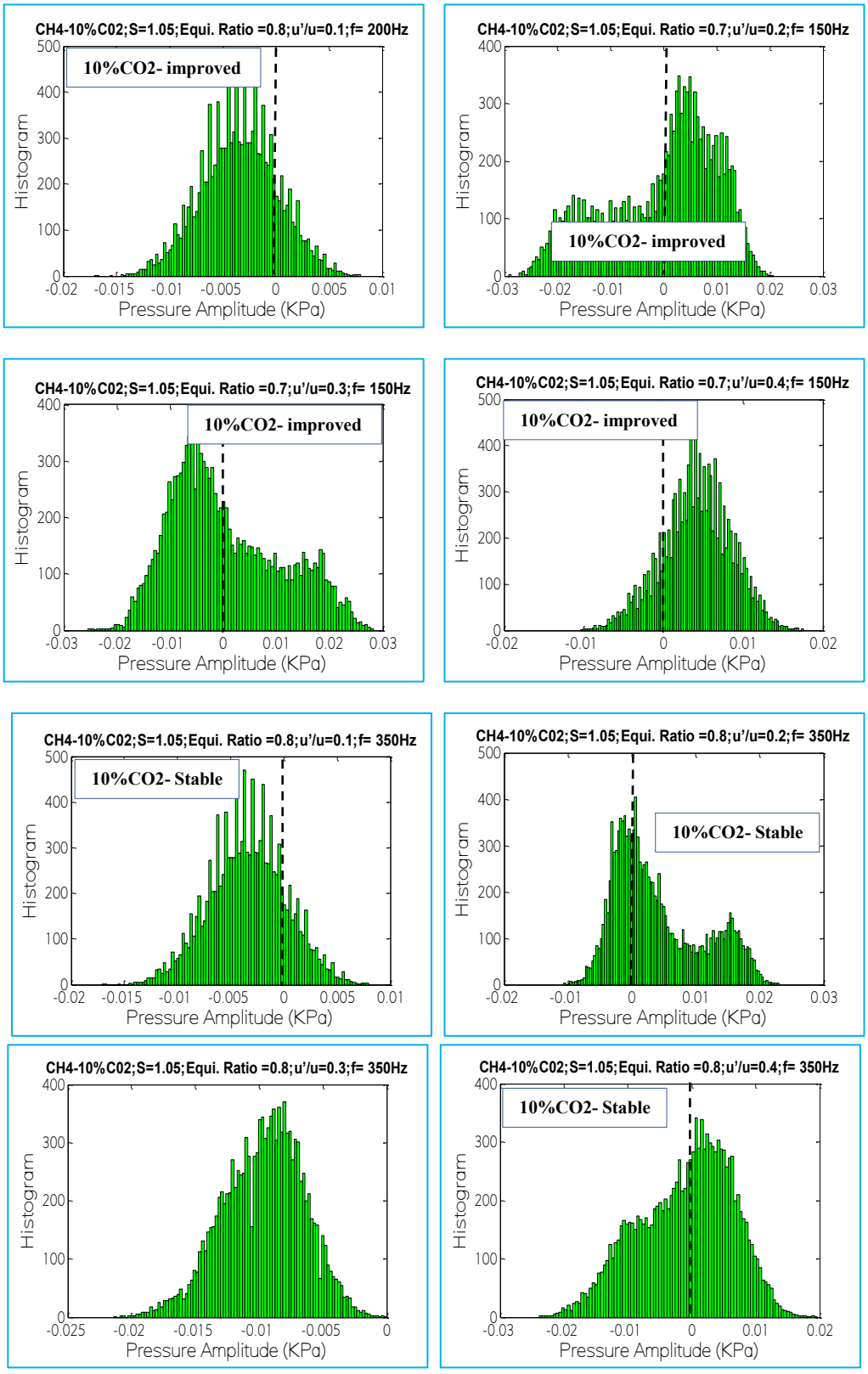

Figure 7. 18 Dynamic pressure Amplitude distribution of methane- 10%CO2-air flames S=1.05

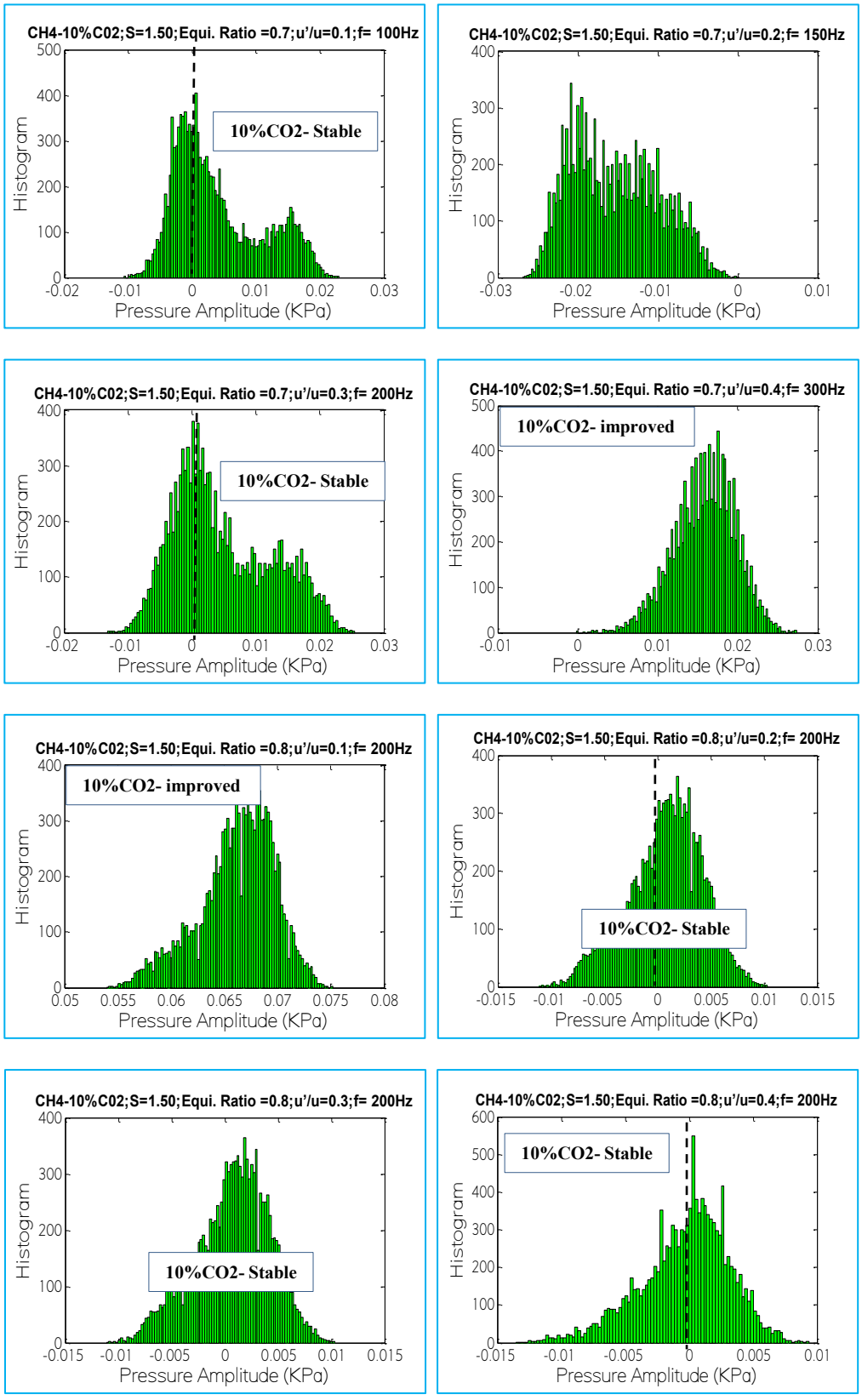

Figure 7. 19 Dynamic pressure Amplitude distribution of methane- 10%CO2-air flames S=1.50

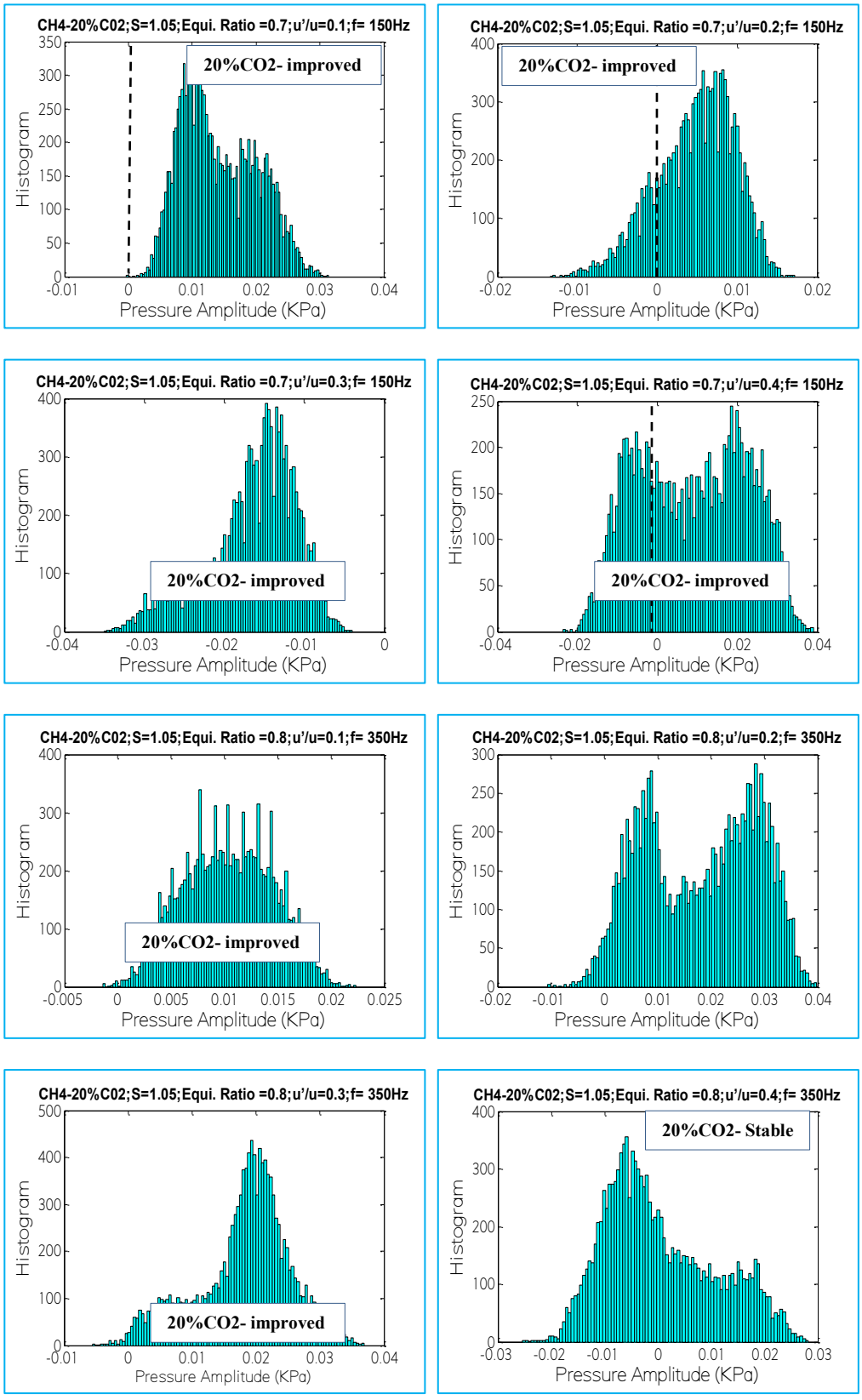

Figure 7. 20 Dynamic pressure Amplitude distribution of methane- 20%CO2-air flames S=1.05

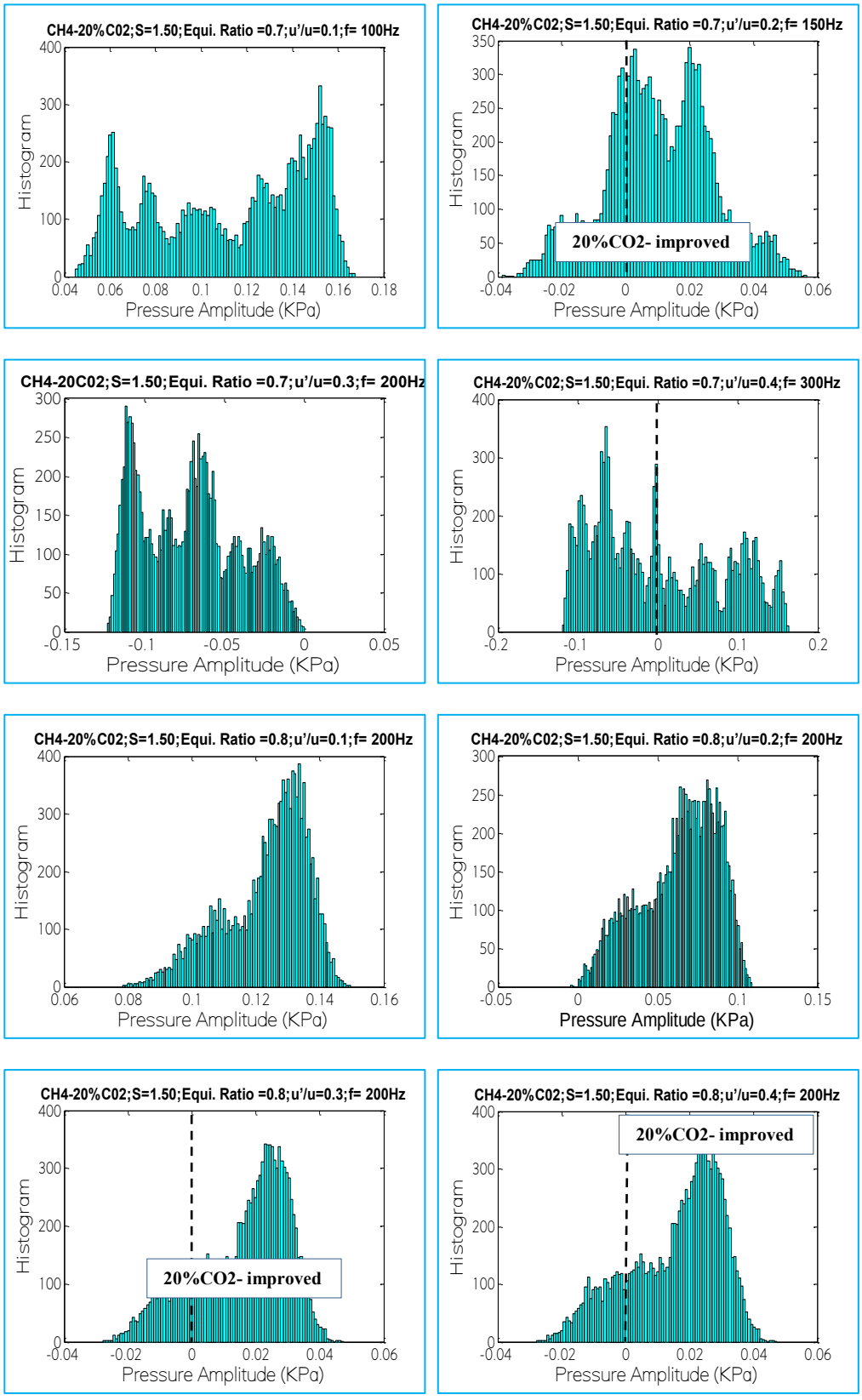

Figure 7. 21 Dynamic pressure Amplitude distribution of methane- 20%CO2-air flames S=1.50

Figures 7.21 plot the behaviour of the pressure oscillations with increased swirl number to 1.50, with a further spread of the pressure amplitudes. The first four cases show the existence of multimodal distributions even though two of them have zero value within the pressure spread. The remaining four cases peak at 0.13, 0.05, 0.02 and 0.02 Kpa which are away from the margin respectively, though relatively close. This shows that the level of dynamic pressure stability observed in the 10% CO_2 blend gradually returns to unstable acoustic modes in some cases with an increased percentage of CO_2. This is in agreement with the results obtained from the spectral and autocorrelation decay analysis of the dynamic pressure at various conditions.

Therefore this statistical tool has also shown the efficacy of the blend of methane with CO_2 in suppressing combustion instabilities in lean premixed combustion. According to the stability criteria, most of the cases considered in the forcing of pure methane showed the existence of multimodality in the pressure distribution with peak values away from the zero margin. The low swirl number with richer mixture cases showed improved stability states, as most of the pressure distributions have Gaussian distribution about the mean. The distribution of the blend of methane with 10% CO_2 showed a very stable condition with most of the pressure distribution at zero peak value with Gaussian distribution about the mean. A higher swirl number of 1.50 shown a better stability relatively to the lower swirl number cases, which proves that a leaner fuel mixture can operate in a stable condition with a combined effect of high swirl strength and a low percentage of CO_2 blend with methane. In 20% CO_2 blend cases, the distribution showed unstable conditions in some cases, thus showing increased instability with increased percentage of CO_2.

7.4 Summary

The accuracy of the spectral analysis of the combustor's dynamic pressure in chapter six was proved in this chapter. Two approaches were used, firstly the simulation of the combustor acoustic modes using a low order acoustic simulator (OSCILOS) to compare its eigen frequencies with those of the experiment. Secondly, two statistical tools: Autocorrelation Decay (ACD) and Probability Density Function (PDF) were deployed to validate the stability of the acoustic modes in the combustion chamber,

using the experimental pressure time series data. The eigen frequencies of the unstable acoustic modes in three simulated cases were around 150Hz which is in agreement with the natural mode of the combustor obtained experimentally. The acoustic mode decay to a limit cycle frequency and amplitude of 124Hz and 0.58 respectively by simulation was linked to the autocorrelation decay of the experimental acoustic modes.

The ACD results showed significant decay in the acoustic modes of the unforced flames relative to the forced flames at different swirl, velocity and equivalence ratios. The high acoustic modes of the forced flames were substantially damped with the blend of methane with CO_2. The lowest percentage of 10% CO_2 in methane showed the highest damping of the acoustic modes significantly with minor variations as the swirl strength, and velocity amplitudes were altered.

PDF results also demonstrated that, in many cases of forced methane-air flames, the pressure distributions spread across different pressure amplitudes with peak values away from the zero margin which indicates the unstable nature of the system. With a reduction in the swirl strength, the stability was a bit improved with peak values of the pressure amplitudes close to zero. With the blend of methane with various percentages of CO_2, the pressure distribution showed stable conditions in most cases with zero peak value and Gaussian distribution about the mean. A higher swirl number showed a better stability relative to the lower swirl cases at leaner fuel mixture, which further confirms that a leaner fuel mixture can operate in a stable condition with an appropriate combination of fuel, swirl, and forcing and velocity ratio conditions. This results, therefore, confirm the accuracy of the pressure modes obtained experimentally as well as the accuracy of the acoustic stability obtained at various swirl, forcing and fuel conditions.

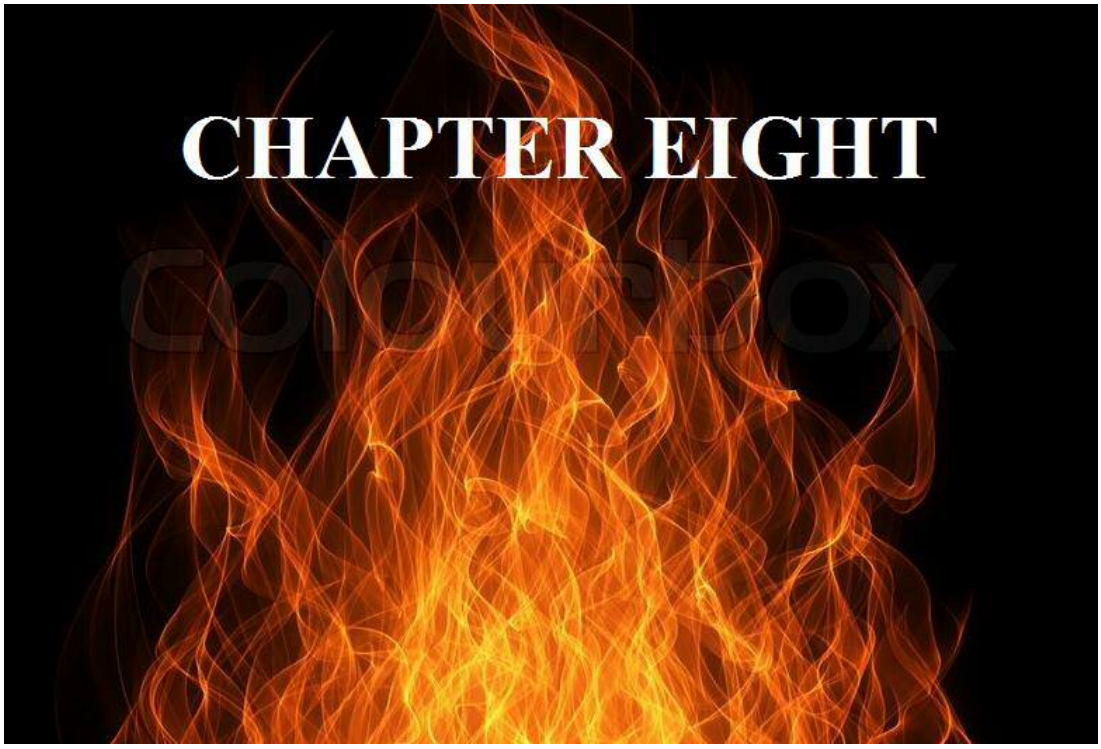
CHAPTER EIGHT

CHAPTER EIGHT

DISCUSSION

The important thing in science is not so much to obtain new facts as to discover new ways of thinking about them" – William Lawrence Bragg.

Modern gas turbines use natural gas which is known to be the purest among the fossil fuels with fewer pollutants to the environment. With the expected dominance of natural gas in the global fuel mix, gas turbines will contribute tremendously to power generation in the coming future. A low emission combustion technique, lean premixed combustion (Dry low NOx), ensures that low pollutant emissions mainly NOx are reduced to the barest minimum thus maintaining a clean and efficient combustion. However, running a gas turbine in this condition subjects it to serious operability challenges, the most prominent being combustion instabilities where the acoustic modes of the combustor are excited by the unsteady heat release forming high-pressure waves in the combustor. These instabilities are detrimental both to the performance as well as the structural makeup of the system, due to the advanced heat transfer, thermal stress on the walls of the combustor and mechanical load oscillation, which could shatter the system in extreme cases. The major challenges currently facing combustion experts are adequate knowledge of the operating conditions that cause combustion instability, accurate prediction and control of the instability modes.

Factors such as fuel-air mixture and injection, fuel composition, flow structures, flame dynamics play crucial roles in lean premixed combustion. In swirling flows, the coherent flow structures produce flow rotation with inherent flow pressure gradient which causes flow reversal resulting in the formation of the central recirculation zone, (CRZ). This region of high flame stretch enhances the recirculation of hot gases with the cold flow, reduces NOx formation, anchors and stabilizes the flame. Other flow structures include the Processing Vortex Core, (PVC), a three-dimensional asymmetric flow structure which is formed when the central vortex core starts

precessing around the axis of symmetry at a well-defined frequency; and shear layers which are formed as a result of the velocity differential between the jets and ambient flows. A very important parameter of this flow structures is the swirl number (S) which relates the axial flux of tangential momentum to the axial momentum flux. A change in this number alters the flow mean velocity and turbulence as well as the flow structures which are convected to the flame resulting in heat release fluctuations. The coupling of the heat release oscillation with the dynamic pressure of the combustor energises or damps the acoustic energy depending on their relative phase.

This study commenced with the design and manufacture of a 100kW combustor for combustion studies in the research group. It is made up of the plenum for fuel-air premixing, injection section and an external flame confinement. A loudspeaker placed at the bottom of the plenum provides an excitation of the flow mixture. The system uses gaseous fuel only and could be used for various fundamental studies in efficient and clean combustion. Highly sensitive instruments were used for the study. Key areas of measurement were the velocity of the flow field, flame heat release rate (chemiluminescence) and the dynamic pressure field. The flow and flame dynamics were used as the basis for the evaluation of the dynamics and stability of the acoustic field of the combustor.

8.1 Flow Field Dynamics

The experimental results showed the influence of the flow field by two major parameters being the swirl number and external excitation. The increased swirl number increased the swirl strength by increasing both the length and width of the CRZ and aligned it with the flow axis. In contrast, a reduced swirl number reduced the swirl strength by reducing the length of the CRZ and drew it away from the flow axis. The increased swirl strength also reduced the size of the HMFR as it pushes it away from the flow axis while increasing the turbulence within the region and down the shear layers.

The flow structures were also influenced by external excitation, as increased forcing increased the width of the CRZ slightly and moved the entire structure closer to the dump plane. At a higher forcing frequency, the high turbulence region in the HMFR

became split into small domains. In general, the velocity profiles of the flow field were altered by the swirl and forcing conditions, which were then convected to the flame zone resulting in variation of the combustion length scale.

The chemical time scale was also varied by changes in the mean axial velocities and turbulence intensity, as the turbulent flame speed relies solely on the turbulence intensity of the flow. According to Lieuwen [92][213][158], the intensity of an acoustic period of a combustor is a function of the convective time and chemical time scale delays, with a constant which is related to the combustor chamber acoustics. Thus, the control of the flow field controls the flame heat release oscillations and the acoustic instability modes.

8.2 Burner Operational Limit

Being a newly designed and manufactured burner, the system was run with methane and air as oxidant with two swirl numbers under open and confined flame conditions to characterise the flame behaviour and the operational limit of the burner. The results revealed that the open flame had a wider operating range with a long flashback range at an equivalence ratio of 3.00 and a short blowoff limit at an equivalence ratio of 0.93 in most flow rates for both swirl numbers. Confined flames were observed to have a relatively shorter operating limit with the flashback at an equivalence ratio of about 1.50, while the blow-off limit went as far as the equivalence ratio of 0.56. The differences in these operating limits between the open and confined flame were attributed to the ambient air in the open flame so that more fuel was required to burn the additional ambient air. However in most practical systems confined flame are used. Therefore the focus of this study was on confined flames.

The results also revealed that an increased swirl strength moved the blowoff limit by about 11 % in the high flow rate and 13 % in the lower flow rate into the lean region. This enhancement of the blowoff limits with increased swirl strength is attributed to many mechanisms including increased turbulence burning velocity of the flame, especially at the base, as the local velocity oscillation was increased. The increased swirl strength also widened the CRZ, thus creating a larger domain for thorough mixing of the fuel and air.

Some differences were observed with the blend of methane with 30% CO_2. The higher fuel flow rates showed a significant reduction in the equivalence ratio of the blowoff limits to 0.70 and 0.73 for the 0.1336 g/s and 0.1447g/s fuel mass flow rate respectively. Also, the lower fuel flow rates showed the reduction in the blowoff limit when compared to the methane-air flame baseline. This reduction was attributed to the diluent effects of CO_2 as the relative concentration of the reactive species was reduced. Also CH4/air- CO_2 flame showed a relatively reduction in the flame temperature with a corresponding effect on the strain rate especially when with radiant effects ,[152].

The changes in the divergent nozzle angle also showed a significant influence on the blowoff limit. At a lower fuel flow rate, the change in the divergent nozzle from 90 to 60 and 45 degrees showed an increased blowoff limit towards a leaner equivalence ratio by about 9.3 and 4.6% respectively. At a higher fuel flow rate, the reduced divergent angle only showed a marginal increased in the blowoff limit by about 1 % in both cases. These changes in the blowoff limits with a change in the geometry of the nozzle were also attributed to the corresponding increase in the CRZ. Therefore a high swirl strength and a divergent nozzle angle of about 60 degrees gave an enhanced blowoff limit for clean and efficient combustion. Therefore the appropriate combination of these factors, (swirl geometry and fuel) could enhance the combustion of leaner fuel with a corresponding emissions reduction.

8.3 Flame Field Dynamics with Swirl, Fuel and Forcing

The changes in the flow structures with variations in flow swirl strength and forcing showed corresponding effects on the flame heat release fluctuations. The flame was influenced by three key factors, namely: swirl strength, fuel blend and forcing frequencies.The increased swirl strength with increased size of the CRZ and turbulence intensities showed a corresponding increased in heat release fluctuation rates. Although this condition was characterised by a strong recirculation of the hot and cold flow with high homogeneous combustion mixture, the increased turbulence down the shear layers increased the heat release fluctuations. The heat release oscillation was reduced with the blend of methane fuel with 30% of CO2. This

reduction was attributed to the diluent effects of CO_2 as the relative concentration of the reactive species was reduced.

There was a reduction in heat release fluctuations with increased forcing frequencies. As was found in the flow field, increased forcing lowered the CRZ to the dump plane thereby reducing the flame lift and turbulence intensities in the HMFR. This is in agreeement with the reported transfer functions of forced flames, where the flame heat release saturates at extreme forcing frequencies,[122] [119]. Heat release oscillation was also affected by forcing amplitude as heat release oscillation increased with increased forcing amplitude at lower frequencies but with little or no effect at higher frequencies.

Therefore with high swirl strength, blend of methane with CO_2, forcing conditions, heat release fluctuation could be controlled. The heat release saturation causes the driving process to saturate and intersect with the damping process at the limit cycle amplitude of the instability curve, where the time average driving mode equals the damping mode and no net energy is supplied to the oscillations, [106][107]. These show the capability of certain flow and flame conditions to control the heat release fluctuation rate as a key component of combustion instabilities.

8.4 Swirl Strength and Acoustic Dynamics

By analysing the dynamic pressure of the combustor using Fast Fourier Transform (FFT), the dominant resonant frequency during combustion was obtained at 150Hz as well as the evolution of its Power spectrum at different swirl strength, fuel and equivalence ratio. Minor acoustic modes attributed to the ambient noise were also observed and discarded. For methane flame, high spectral powers were observed at high swirl strength especially at the leaner mixture which were attributed to the increased flow recirculation and turbulence that were observed in the flow field. These resulted in increased pockets of rich and weak mixtures with the lean mixture which were convected to the flame with a corresponding response to heat release fluctuation and high acoustic amplitude. In the flame field, this was evident by the increased heat release fluctuations. Increased velocity ratio of the inlet flow field was also observed

to influence the acoustic mode with a reduced power spectrum which was linked to the saturation of heat release fluctuation.

8.5 Flame Forcing and Acoustic Dynamics

As the use of acoustic forcing for the actuation of the system for instability closed loop control is becoming more promising. The combustor acoustic mode response to external forcing at different frequencies and velocity ratio was also examined with methane-air flames. The aim here was to compare the acoustic modes of the forced and unforced flames in terms of the power spectrum of the natural and forced acoustic signals and to examine the interactions of the two signals at different forcing and velocity conditions. In all the cases considered, two dominant acoustic modes were observed, one being the natural acoustic mode at 150Hz and the second being the forcing frequency. But when it was forced with 150Hz, both the forcing and natural mode fused together to form a single mode with a specific spectral power whose magnitude depended on factors like swirl strength, equivalence ratio and flow inlet velocity ratio.

The harmonics of the two signals were also observed but their spectral magnitudes were relatively low, thus they were discarded in the evaluation. It was observed in most cases that the forced signals had a higher power spectrum than the natural acoustic modes but with a reduced power at a single frequency at 150Hz. In contrast, the spectral power became magnified when it was forced with the harmonics of the natural acoustic mode of the combustor. This indicates a better forcing conditions of the system although the velocity amplitude must also be taken into consideration. In lower swirl strength, the acoustic power in most of the cases was reduced as the velocity ratio was increased from 0.1 to 0.4, across all the forcing frequencies. At a higher swirl number of 1.50, the acoustic power increased in larger proportions at a high lean condition for all forcing frequencies and velocity ratios except at an extreme velocity ratio of 0.4 where the acoustic power of the leaner mixture became reduced with increased forcing frequencies. At a rich mixture of 0.8, the acoustics were reduced with increased velocity ratio across the forcing frequencies. Considering the two swirl strength and equivalence ratio, the lower swirl had the acoustic modes with

the lowest spectral power for both equivalence ratios. This shows that the higher swirl strength in this case generates high acoustic powers due to high turbulence. In comparison, the unforced methane-air flame had acoustic modes with relatively low spectral power across most velocity ratios. It, therefore, means that there might be some forcing conditions with acoustic modes that are worse than those of the unforced methane –air flames. These conditions need to be recognised and avoided during the control processes.

8.6 Methane –CO2 Blend and Acoustic Dynamics

The reduced heat release fluctuation with the blend of methane with CO_2 also showed a corresponding effects on the acoustic mode of the combustor. The high spectral amplitudes of methane-air flame, especially at high swirl strength, for both forced and unforced flames were drastically reduced with the blend of CO_2. A significant reduction in acoustic amplitude was obtained with leaner equivalence ratio of 0.7 with a high swirl strength and the fuel blend. It was further evident that the instability reduction was very effective at a lower percentage of CO_2. With increased percentage of CO_2 in the blend to about 20%, the instabilities started setting in, due to its high mass-based additive to fuel ratio with further complexities to the chemical time scale.

8.7 Combined Effect of Parameters on Acoustic Suppression

The high swirl strength increased the size of the CRZ with improved fuel-air mixing and thermal efficiency but with high turbulence within the HMFR and the shear layers, resulting in heat release fluctuations. The forcing of the flow field lowered the CRZ to the dump plane thus reducing the flame lift, and the interaction of the flame front with the CRZ. However, the interaction of the excitation signals such as PVC, natural acoustic modes and the hydrodynamics within the combustor increased the flow turbulence with a corresponding heat release fluctuation. The introduction of CO_2 blend reduced the flow turbulence with increased flow recirculation.

The addition of CO_2 to methane-air has a diluent effects due to its relative reduction in the concentrations of the reactive species and direct chemical effects as a result of the breakdown of CO_2 through the reactions of third-body collision and thermal

dissociation,[152]. The heat capacity of CO_2 is much higher than air, and its absorption coefficient is quite high, so that the addition of CO_2 to the fuel mixture changes the flame axial velocity gradient (strain rate). The presence of CO_2 decreased the high momentum flow region velocity drastically while increasing the central recirculation zone velocity since the CO_2's high specific heat increases the pressure differential which drives recirculation,[153].

Thus the high recirculation, lower flame lift and high heat capacity collectively resulted in high thermal efficiency with the saturated heat release fluctuation and a stable acoustic mode. The combination of these characteristics has more tendency to keep the heat release fluctuation rate off-phase with the dynamic pressure of the system in order to damp the acoustic energy.

8.8 Validation of Experimental Results

The natural frequency mode of 150Hz obtained experimentally was in agreement with the simulation using a low order combustion instability simulator. The decay of the acoustic mode to limit cycle in the simulation was equivalent to the autocorrelation decay of the experimental acoustic modes. Also the probability density function demonstrated the increased instability at high swirl and forcing but a drastic reduction of the acoustic amplitudes with the addition of CO2 which agrees with the spectral analysis, thus validating the accuracy of this study.

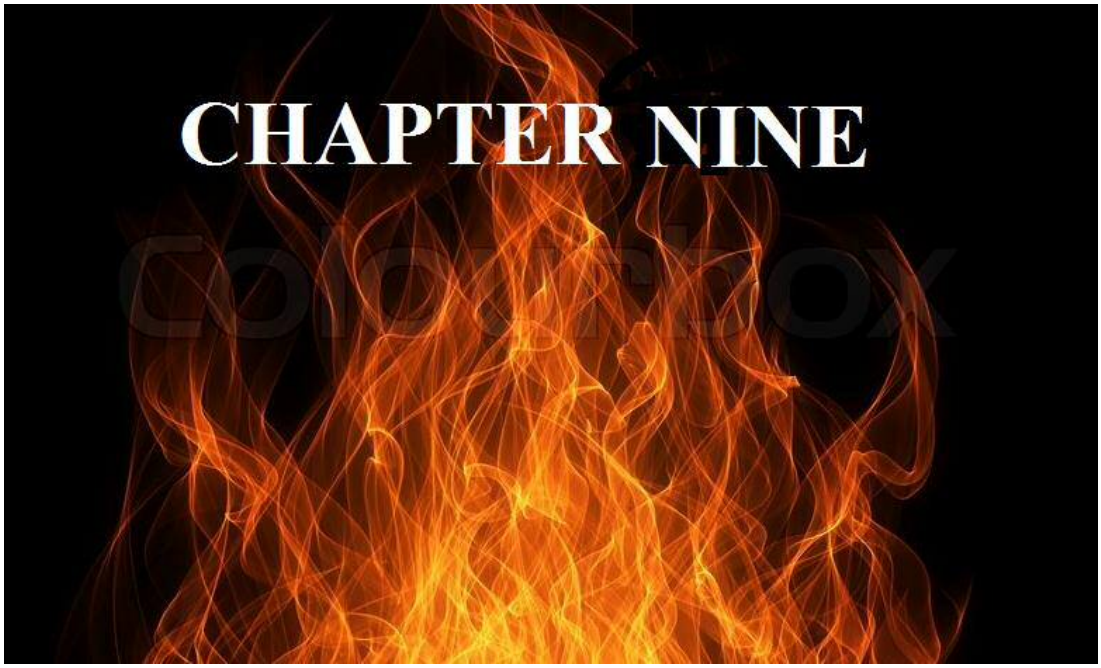
CHAPTER NINE

CHAPTER NINE

CONCLUSION AND FUTURE WORK

A story really isn't truly a story until it reaches its climax and conclusion
Ted Naifeh

9.1 Conclusion

This study has provided a novel approach to combustion instabilities control. It has revealed that appropriate combination of the combustion parameters like swirl geometry, external excitation and fuel composition could suppress the acoustic oscillation of the combustor to a level that is not destructive to the system. From the system control point of view, this technique seems quite realistic as the three parameters considered in this study could be varied numerically. For aero engines with limited space for a complicated close loop control system, this approach could be an effective tool to reduce combustion instabilities in the system and keep it in a stable running condition. It can also serve as a potential approach for close loop design.

The major findings of this study are summarised thus:

- The increased in the swirl strength via the swirl number, increases the size of the CRZ; flow reversal intensity; enhanced mixing and turbulence scale around the shear layers.
- The level of the reversed flow could be further altered by forcing the flow with discrete sinusoidal frequencies. Therefore the used of variable swirl geometry and forcing could provide a wide range of the magnitude of the reversed flow.
- High forcing frequencies increases the size of the CRZ and draws the high-velocity regimes further upstream of the flow closer to the nozzle dump plane and becomes split with extreme forcing.

- With increased forcing, the regions with higher mean velocities are drawn towards the exit nozzle with enlarge width of the CRZ. Also with increased forcing, the axis of the CRZ which was initially away from the centerline of the nozzle gradually aligns with the flow axes especially in the lower flow field.
- In all the swirl strength, the size of the HMFR was reduced while the shear layers expanded with increased turbulence increased forcing frequency.

- The evolution of the flow structures as a result of the variation in the swirl number causes fluctuation in the flow oscillation frequency which agrees with the Strouhal number.
- The interaction of this frequency with other oscillation frequencies like PVC, heat release or dynamic pressure leads to the amplification of the resultant acoustic mode of the system.
- The change in the position of the CRZ with a reduced swirl strength is capable of reducing the combustion convective time scales, as the distance between the flow exit from the nozzle and the flame centre of mass is reduced.

- An increase in the swirl strength enhances the blowoff limits due to increased turbulence burning velocity; an enlarger domain for thorough mixing; increased residence time as a result of increased flame length scale.
- The excessive increase of the swirl strength could result in the destabilization and reduction in the blowoff limit of the flame.
- The blowoff limits of 60 and 40 degrees divergent angles were increased substantially over the 90 degrees flat nozzle.
- The divergence of the nozzle angle enhances the recirculation intensity of the flame zone, by increasing the width of the CRZ and the turbulent intensity, resulting in increased mixing of the flow mixture and flame anchorage.
- Blowoff limit was reduced with the blend of methane with CO2 due to the enabling physical and thermodynamics properties of CO2 such as the diluent effects of CO2; high heat capacity; high absorption coefficient; the reduction in the calorific value of the mixture, decreased flame speed and temperature etc.

- Increased swirl strength increases the heat release fluctuations due to increase turbulence in the high momentum flow regions.
- The blend of methane with CO2 reduces the heat release oscillation due to the enabling physical and thermodynamic properties of CO2 earlier mentioned.
- Heat release perturbation is also affected by forcing amplitude as heat release oscillation increases with increased forcing amplitude at lower frequencies but with little or no effect at higher frequencies. In all the unforced flames, the dominant acoustic mode was 150Hz, and with external excitation, an additional mode was observed, with variations in the amplitudes of the modes depending on the forcing, swirl strength and fuel mixtures.

- The amplitudes of the acoustic modes of the forced flames were higher than those of the unforced flames, although in most cases, the stability of the system was improved at higher forcing frequencies.

- The interaction of the forced and natural modes, as well as their harmonics with other oscillations within the combustor in some cases, could further enhance the turbulence intensity of the regimes resulting in increased heat release fluctuations and instabilities.

- Increased swirl strength showed an increased acoustic amplitudes, a similar condition in the flame field with high heat release oscillation, caused by the increased turbulence.

- The reduced heat release oscillation also corresponds to a reduced amplitude with low swirl strength.

- The amplitudes were reduced with the increased rich mixture, a mechanism which could be linked to the mass-based additive to fuel ratio.

- The reduced heat release oscillation with the blend of methane with CO2 presented a corresponding effect of reducing the acoustic amplitudes significantly at both high and low swirl strength as well as rich and lean mixtures.

- Therefore the control of the flow and flame fields with swirl strength, forcing and fuel conditions responded accordingly to the suppression of the high acoustic modes.

9.2 Future Work

In continuation of this study, the following are suggested for further work:

- A better resolution of the heat release fluctuation of both the CH* and OH* chemiluminescence should be acquired simultaneously with the inlet velocity fluctuations with a high acquisition rate, say 20 KHz. With this, the flame describing function of the flame could be obtained for each of the flame conditions for the prediction of instability modes in all the cases.

- The blend of hydrogen with methane as well as methane-CO2-hydrogen flame should also be tested to obtain the flame describing function as well as the instability characteristics. The low-density hydrogen could enhance the stability characteristics of the system. This is motivated by the fact that a potential fuel for gas turbines: syngas is composed of these fuel constituents.

- The predicted acoustic characteristics via the flame describing functions should be compared with the experimental acoustic behaviours so as to validate the capabilities of acoustic simulators to capture intricate acoustic characteristics.

- The predicted acoustic modes should be implemented in an active control using variable swirl angle, fuel composition and forcing characteristics as the main control parameters.

References:

[1] EIA, "EIA - Annual Energy Outlook 2015," 2015.
[2] IEA, "WEO 2012 Executive Summary - International Energy Agency," 2012.
[3] EIA, "International Energy Outlook 2013 - US Energy Information," 2013.
[4] REN, "Renewables 2015 Global Status Report - REN21," 2015.
[5] U. S. E. I. A. (EIA), "Annual Energy Outlook 2012 - US Energy Information Administration," 2012.
[6] U. S. E. I. A. (EIA, "Annual Energy Outlook 2013 - US Energy Information Administration," 2013. [Online]. Available: https://www.eia.gov/forecasts/aeo/pdf/0383(2013).pdf.
[7] "Open-cycle constant pressure gas turbine engine," Encyclopedia Britannica. [Online]. Available: http://www.britannica.com/EBchecked/topic-art/187279/19424/Open cycle constant-pressure-gas-turbine-engine.
[8] "A cut section of gas turbine." [Online]. Available: https://www.quora.com/How-does-continously-fuel-burn-in-combustion-chamber-of-gas-turbine-engine.
[9] B. Combuster, "Combuster - Burner," 2015.
[10] A. H. Lefebvre and D. R. Hallal, "Gas Turbine Alternative Fuels and Emissions," CRC, Boca Raton, FL, 2010.
[11] C. Wilkes and B. Gerhold, "NOx reduction from a Gas turbine Combustor using Exhaust gas recirculation," Am. Soc. Mech. Eng.,(Pap.);(United States), vol. 80, no. CONF-8009102-, 1980.
[12] M. B. Hilt and J. Waslo, "Evolution of NOx abatement techniques through combustor design for heavy-duty gas turbines," J. Eng. gas turbines power, vol. 106, no. 4, pp. 825–832, 1984.
[13] D. J. White, A. Batakis, R. T. LeCren, and H. G. Yacobucci, "Low NOx Combustion Systems for Burning Heavy Residual Fuels and High-Fuel-Bound Nitrogen Fuels," J. Eng. Power, vol. 104, no. 2, pp. 377–385, 1982.
[14] T. Poinsot and D. Veynante, Theoretical and numerical combustion. RT Edwards, Inc., 2005.
[15] N. Syred, A. Giles, J. Lewis, A. Valera-Medina, P. Bowen, and A. Griffiths, "Tangential Velocity Effects and Correlations for Blow-Off and Flashback in a Generic Swirl Burner and the effect of a Hydrogen containing Fuel."
[16] M. Abdulsada, N. Syred, A. Griffiths, and P. J. Bowen, "Effect of swirl number and fuel type upon the flashback in swirl combustors," in AIAA conference paper, Orlando, Florida, 2011, pp. 4–7.
[17] H. Baej, A. Valera-Medina, P. Bowen, N. Syred, T. O'Doherty, and R. Marsh, "Impacts on Blowoff by a variety of CRZs using various gases for Gas Turbines," Energy Procedia, vol. 61, pp. 1606–1609, 2014.
[18] S. Daniele, P. Jansohn, and K. Boulouchos, "Flashback Phenomena Associated with Lean Premixed Syngas Combustion at Gas Turbine Like Conditions."
[19] A. P. Dowling and A. S. Morgans, "Feedback control of combustion oscillations," Annu. Rev. Fluid Mech., vol. 37, pp. 151–182, 2005.
[20] T. C. Lieuwen, "Investigation of Combustion Instability Mechanisms in Premixed Gas Turbines," 1999.
[21] A. Fluent, "Ansys Fluent 12.0 Theory Guide," Fluent Inc., Lebanon, NH, 2009.
[22] P. N, Turbulent Combustion. Germany: Cambride University Press, 2000.
[23] M. Abdulsada, "Flashback and blowoff characteristics of gas turbine swirl combustor," Cardiff University, 2011.
[24] A. H. Lefebvre, Gas turbine combustion. CRC press, 1998.
[25] E. Ranzi et al., "Hierarchical and comparative kinetic modeling of laminar flame speeds of hydrocarbon and oxygenated fuels," Prog. Energy Combust. Sci., vol. 38, no. 4, pp. 468–501, 2012.
[26] G. Yu, C. K. Law, and C. K. Wu, "Laminar flame speeds of hydrocarbon+ air mixtures with hydrogen addition," Combust. Flame, vol. 63, no. 3, pp. 339–347, 1986.
[27] S. A. Klein, On the acoustics of turbulent non-premixed flames. Universiteit Twente, 2000.
[28] X. Han, J. Yang, and J. Mao, "LES investigation of two frequency effects on acoustically forced premixed flame," Fuel, 2016.
[29] H. Baej, "Effects of geometry and gas composition on swirling flow," Cardiff University, 2015.
[30] J. F. Driscoll and J. Temme, "Role of swirl in flame stabilization," in 49thAIAA Aerospace Sciences Meeting including the New Horizons Forum and Aerospace Exposition, AIAA, 2011, vol. 108, pp. 1–11.
[31] S. Candel, D. Durox, T. Schuller, J.-F. Bourgouin, and J. P. Moeck, "Dynamics of swirling flames," Annu. Rev. Fluid Mech., vol. 46, pp. 147–173, 2014.

[32] J. Wan, A. Fan, K. Maruta, H. Yao, and W. Liu, “Experimental and numerical investigation on combustion characteristics of premixed hydrogen/air flame in a micro-combustor with a bluff body,” Int. J. Hydrogen Energy, vol. 37, no. 24, pp. 19190–19197, 2012.
[33] S. M. Correa and A. Gulati, “Measurements and modeling of a bluff body stabilized flame,” Combust. Flame, vol. 89, no. 2, pp. 195–213, 1992.
[34] A. Valera-Medina, “Coherent structures and their effects on processes occurring in swirl combustors,” Cardiff University, 2009.
[35] D. R. Noble, Q. Zhang, A. Shareef, J. Tootle, A. Meyers, and T. Lieuwen, “Syngas mixture composition effects upon flashback and blowout,” in ASME Turbo Expo 2006: Power for Land, Sea, and Air, 2006, pp. 357–368.
[36] S. Nair and T. Lieuwen, “Acoustic Characterization of Premixed Flames under Near Blowout Conditions,” AIAA Pap. 2002, vol. 4011, 2002.
[37] A. A. Chaparro and B. M. Cetegen, “Blowoff characteristics of bluff-body stabilized conical premixed flames under upstream velocity modulation,” Combust. Flame, vol. 144, no. 1, pp. 318–335, 2006.
[38] T. C. Lieuwen, “Static and Dynamic Combustion stability,” Gas Turbine Handbook. Natl. Energy Technol. Lab., pp. 197–203, 2006.
[39] S. G. Turtle, S. Chaudhri, S. Kostka, M. Kulakhmetov, B. M. Cetegen, and M. M. Renfro, “Transitional blow off behaviour of wake stabilized flames in vitiated flow,” in AIAA aerospace sciences meeting including the new horizons forum and aerospace, Orlando, Florida, 2010.
[40] C. J. Goy, S. R. James, and S. Rea, “Monitoring combustion instabilities: E. ON UK’s experience,” Prog. Astronaut. Aeronaut., vol. 210, p. 163, 2005.
[41] A. Nauert, P. Petersson, M. Linne, and A. Dreizler, “Experimental analysis of flashback in lean premixed swirling flames: conditions close to flashback,” Exp. Fluids, vol. 43, no. 1, pp. 89–100, 2007.
[42] Y. Huang and V. Yang, “Bifurcation of flame structure in a lean-premixed swirl-stabilized combustor: transition from stable to unstable flame,” Combust. Flame, vol. 136, no. 3, pp. 383–389, 2004.
[43] Y. Huang and V. Yang, “Effect of swirl on combustion dynamics in a lean-premixed swirl-stabilized combustor,” Proc. Combust. Inst., 2005.
[44] E. L. Petersen, J. M. Hall, S. D. Smith, J. de Vries, A. Amadio, and M. W. Crofton, “Ignition of fuel-lean natural gas blends at gas turbine pressures,” ASME Turbo EXPO 2005, 2005.
[45] G. A. Richards, M. M. McMillian, R. S. Gemmen, W. A. Rogers, and S. R. Cully, “Issues for low-emission, fuel-flexible power systems,” Prog. Energy Combust. Sci., vol. 27, no. 2, pp. 141–169, 2001.
[46] J. De Vries and E. L. Petersen, “Autoignition of methane-based fuel blends under gas turbine conditions,” Proc. Combust. Inst., vol. 31, no. 2, pp. 3163–3171, 2007.
[47] E. L. Petersen and J. de Vries, “Measuring the ignition of fuel blends using a design of experiments approach,” AIAA Pap., vol. 1165, pp. 10–13, 2005.
[48] T. C. Lieuwen, “Physics of premixed combustion-acoustic wave interactions,” in Combustion instabilities in gas turbine engines operational experience, fundamental mechanisms and modeling, T. C. Lieuwen and V. Yang, Eds. Reston -USA: American Institute of Aeronautics and Astronautics, Inc., 2005, pp. 315–366.
[49] S. V Alekseenko, V. M. Dulin, M. P. Tokarev, and D. M. Markovich, “A swirling jet with vortex breakdown: three-dimensional coherent structures,” Thermophys. Aeromechanics, vol. 23, no. 2, pp. 301–304, 2016.
[50] A. M. Annaswamy, M. Fleifil, J. W. Rumsey, R. Prasanth, J. P. Hathout, and A. F. Ghoniem, “Thermoacoustic instability: model-based optimal control designs and experimental validation,” IEEE Trans. Control Syst. Technol., 2000.
[51] D. K. Winter G, Eickhoff He, “Fuel injectors. Chapter 3,” in Design of modern gas turbine combustion, San Diego: Academic Press, 1990, pp. 229–341.
[52] P. Palies, D. Durox, T. Schuller, and S. Candel, “Experimental study on the effect of swirler geometry and swirl number on flame describing functions,” Combust. Sci. Technol., vol. 183, no. 7, pp. 704–717, 2011.
[53] N. Syred, “A review of oscillation mechanisms and the role of the precessing vortex core (PVC) in swirl combustion systems,” Progress in Energy and Combustion Science. 2006.
[54] V. M. Rodriguez-Martinez, J. R. Dawson, N. Syred, and T. O’Doherty, “The effect of expansion plane geometry on fluid dynamics under combustion instability in a swirl combustor,” AIAA Pap., no. 2003–116, 2003.

[55] J. M. Beér and N. A. Chigier, “Combustion aerodynamics,” New York, 1972.
[56] C. N. A. Beer J. M, Combustion Aerodynamics. Krieger Publishing Company, 1983.
[57] H. J. Sheen, W. J. Chen, S. Y. Jeng, and T. L. Huang, “Correlation of swirl number for a radial-type swirl generator,” Exp. Therm. fluid Sci., vol. 12, no. 4, pp. 444–451, 1996.
[58] W. Leuckel, Swirl intensities, swirl types and energy losses of different swirl generating devices. 1973.
[59] Y. Huang and V. Yang, “Dynamics and stability of lean-premixed swirl-stabilized combustion,” Prog. Energy Combust. Sci., vol. 35, no. 4, pp. 293–364, 2009.
[60] P. Iudiciani and C. Duwig, “Large eddy simulation of the sensitivity of vortex breakdown and flame stabilisation to axial forcing,” Flow, Turbul. Combust., vol. 86, no. 3–4, pp. 639–666, 2011.
[61] C. O. U. Umeh, Z. Rusak, and E. J. Gutmark, “Experimental study of reaction and vortex breakdown in a swirl-stabilized combustor,” in ASME Turbo Expo 2009: Power for Land, Sea, and Air, 2009, pp. 935–950.
[62] C. Duwig, L. Fuchs, A. Lacarelle, M. Beutke, and C. O. Paschereit, “Study of the vortex breakdown in a conical swirler using LDV, LES and POD,” in ASME Turbo Expo 2007: Power for Land, Sea, and Air, 2007, pp. 1–10.
[63] C. O. U. Umeh, Z. Rusak, E. Gutmark, R. Villalva, and D.-J. Cha, “Experimental and computational study of nonreacting vortex breakdown in a swirl-stabilized combustor,” AIAA J., vol. 48, no. 11, pp. 2576–2585, 2010.
[64] H. B. Squire, Analysis of the vortex breakdown phenomenon. Imperial College of Science and Technology, Aeronautics Department, 1960.
[65] T. B. Benjamin, “Theory of the vortex breakdown phenomenon,” J. Fluid Mech., vol. 14, no. 4, pp. 593–629, 1962.
[66] S. Leibovich and K. Stewartson, “Sufficient condition for the instability of columnar vortices,” J. Fluid Mech., vol. 126, pp. 335–356, 1983.
[67] J. P. Jones, “On the explanation of vortex breakdown,” in IUTAM Symposium on Vortex Motions, Ann Arbor, 1964.
[68] H. Ludwieg, Vortex breakdown. 1970.
[69] T. Sarpkaya, “On stationary and travelling vortex breakdowns,” J. Fluid Mech., vol. 45, no. 3, pp. 545–559, 1971.
[70] T. Sarpkaya, “Vortex breakdown in swirling conical flows,” AIAA J., vol. 9, no. 9, pp. 1792–1799, 1971.
[71] X. Lu, S. Wang, H.-G. Sung, S.-Y. Hsieh, and V. Yang, “Large-eddy simulations of turbulent swirling flows injected into a dump chamber,” J. Fluid Mech., vol. 527, pp. 171–195, 2005.
[72] S. Wang, S.-Y. Hsieh, and V. Yang, “Unsteady flow evolution in swirl injector with radial entry. I. Stationary conditions,” Phys. Fluids, vol. 17, no. 4, p. 45106, 2005.
[73] J. P. Moeck, J.-F. Bourgouin, D. Durox, T. Schuller, and S. Candel, “Nonlinear interaction between a precessing vortex core and acoustic oscillations in a turbulent swirling flame,” Combust. Flame, vol. 159, no. 8, pp. 2650–2668, 2012.
[74] D. Froud, T. O’doherty, and N. Syred, “Phase averaging of the precessing vortex core in a swirl burner under piloted and premixed combustion conditions,” Combust. Flame, vol. 100, no. 3, pp. 407–412, 1995.
[75] S. Candel, D. Durox, T. Schuller, J.-F. Bourgouin, and J. P. Moeck, “Dynamics of Swirling Flames CRZ: central recirculation zone,” Annu. Rev. Fluid Mech, vol. 46, pp. 147–73, 2014.
[76] N. Syred and J. M. Beer, “Damping of precessing vortex cores by combustion in swirl generators,” Astronaut. Acta, vol. 17, no. 4–5, p. 783, 1972.
[77] N. Syred, “A review of oscillation mechanisms and the role of the precessing vortex core (PVC) in swirl combustion systems,” Prog. Energy Combust. Sci., vol. 32, no. 2, pp. 93–161, 2006.
[78] S. Wang, V. Yang, G. Hsiao, S.-Y. Hsieh, and H. C. Mongia, “Large-eddy simulations of gas-turbine swirl injector flow dynamics,” J. Fluid Mech., vol. 583, pp. 99–122, 2007.
[79] W. Fick, “Ph.D Thesis,” Cardiff University, 1968.
[80] D. Froud, “Ph.D Thesis,” University of Wales, Cardiff, 1996.
[81] V. M. Rodriquez-Martinez, “Ph.D Thesis,” Cardiff University, 2003.
[82] T. Ivanic, E. Foucault, and J. Pecheux, “Dynamics of swirling jet flows,” Exp. Fluids, vol. 35, no. 4, pp. 317–324, 2003.
[83] F. Gallaire, S. Rott, and J.-M. Chomaz, “Experimental study of a free and forced swirling jet,” Phys. Fluids, vol. 16, no. 8, pp. 2907–2917, 2004.
[84] D. W. Lim and L. G. Redekopp, “Absolute instability conditions for variable density, swirling jet flows,” Eur. J. Mech., vol. 17, no. 2, pp. 165–185, 1998.

[85] F. Gallaire and J.-M. Chomaz, “Instability mechanisms in swirling flows,” Phys. Fluids, vol. 15, no. 9, pp. 2622–2639, 2003.
[86] S. McIlwain and A. Pollard, “Large eddy simulation of the effects of mild swirl on the near field of a round free jet,” Phys. Fluids, vol. 14, no. 2, pp. 653–661, 2002.
[87] M. R. Ruith, P. Chen, E. Meiburg, and T. Maxworthy, “Three-dimensional vortex breakdown in swirling jets and wakes: direct numerical simulation,” J. Fluid Mech., vol. 486, pp. 331–378, 2003.
[88] H. Liang and T. Maxworthy, “An experimental investigation of swirling jets,” J. Fluid Mech., vol. 525, pp. 115–159, 2005.
[89] D. Durox et al., “Flame dynamics of a variable swirl number system and instability control,” Combust. Flame, vol. 160, no. 9, pp. 1729–1742, 2013.
[90] F. Nicoud and T. Poinsot, “Thermoacoustic instabilities: Should the Rayleigh criterion be extended to include entropy changes?,” Combust. Flame, 2005.
[91] A. P. Dowling, “The calculation of thermoacoustic oscillations,” J. Sound Vib., vol. 180, no. 4, pp. 557–581, 1995.
[92] T. Lieuwen, F. A. Leader, and N. Energy, “Recent progress in predicting, monitoring and controlling combustion driven oscillations in gas turbines,” System, 2003.
[93] J. Li, D. Yang, C. Luzzato, and A. S. Morgans, “Open Sounce Combustion Instability Low Order Simulator (OSCILOS--Long) Technical report,” London, 2015.
[94] S. R. Stow and A. P. Dowling, “A Time-Domain Network Model for Nonlinear Thermoacoustic Oscillations.”
[95] C. O. Paschereit, E. Gutmark, and W. Weisenstein, “Control of thermoacoustic instabilities and emissions in an industrial-type gas-turbine combustor,” in Symposium (International) on Combustion, 1998, vol. 27, no. 2, pp. 1817–1824.
[96] Sé, bastien Ducruix, T. Schuller, D. Durox, Sé, and bastien Candel, “Combustion dynamics and instabilities: Elementary coupling and driving mechanisms,” J. Propuls. power, vol. 19, no. 5, pp. 722–734, 2003.
[97] R. Lord and others, “The theory of sound.” Dover, New York, 1945.
[98] B. T. Zinn and T. C. Lieuwen, “Combustion instabilities: Basic concepts,” in Combustion instabilities in gas turbine engines operational experience, fundamental mechanisms and modeling, Reston: American Institute of Aeronautics and Astronautics, Inc., 2005, pp. 3–25.
[99] D. W. Karkow, “Combustion instabilities: an experimental investigation on the effects of hydrogen in a lean premixed combustor.”
[100] K. C. Schadow and E. Gutmark, “Combustion instability related to vortex shedding in dump combustors and their passive control,” Prog. Energy Combust. Sci., vol. 18, no. 2, pp. 117–132, 1992.
[101] U. G. Hegde, D. Reuter, B. R. Daniel, and B. T. Zinn, “Flame driving of longitudinal instabilities in dump type ramjet combustors,” Combust. Sci. Technol., vol. 55, no. 4–6, pp. 125–138, 1987.
[102] S. Candel, “Combustion dynamics and control: Progress and challenges,” Proc. Combust. Inst., vol. 29, no. 1, pp. 1–28, 2002.
[103] D. W. Kendrick, T. J. Anderson, W. A. Sowa, and T. S. Snyder, “Acoustic sensitivities of lean-premixed fuel injectors in a single nozzle rig,” J. Eng. Gas Turbines power, vol. 121, no. 3, pp. 429–436, 1999.
[104] L. Crocco and S.-I. Cheng, Theory of combustion instability in liquid propellant rocket motors, vol. 8. Cambridge Univ Press, 1956.
[105] T. Lieuwen, H. Torres, C. Johnson, and B. T. Zinn, “A Mechanism of Combustion Instability in Lean Premixed Gas Turbine Combustors,” J. Eng. Gas Turbines Power, vol. 123, no. 1, pp. 182–190, 2001.
[106] R. M. Murray et al., “System identification for limit cycling systems: a case study for combustion instabilities,” in American Control Conference, 1998. Proceedings of the 1998, 1998, vol. 4, pp. 2004–2008.
[107] T. C. Lieuwen, Static and dynamic combustion stability. 2013.
[108] D. Durox, T. Schuller, N. Noiray, and S. Candel, “Experimental analysis of nonlinear flame transfer functions for different flame geometries,” Proc. Combust. Inst., vol. 32, no. 1, pp. 1391–1398, 2009.
[109] P. Palies, T. Schuller, D. Durox, and S. Candel, “Modeling of premixed swirling flames transfer functions,” Proc. Combust. Inst., vol. 33, no. 2, pp. 2967–2974, 2011.
[110] A. P. Dowling, “A kinematic model of a ducted flame,” J. Fluid Mech., vol. 394, no. 1, pp. 51–72, 1999.

[111] T. Lieuwen, “Modeling premixed combustion-acoustic wave interactions: A review,” J. Propuls. power, vol. 19, no. 5, pp. 765–781, 2003.
[112] C. A. Armitage, R. Balachandran, E. Mastorakos, and R. S. Cant, “Investigation of the nonlinear response of turbulent premixed flames to imposed inlet velocity oscillations,” Combust. Flame, vol. 146, no. 3, pp. 419–436, 2006.
[113] A. X. Sengissen, J. F. Van Kampen, R. A. Huls, G. G. M. Stoffels, J. B. W. Kok, and T. J. Poinsot, “LES and experimental studies of cold and reacting flow in a swirled partially premixed burner with and without fuel modulation,” Combust. Flame, vol. 150, no. 1, pp. 40–53, 2007.
[114] Y. Huang, H.-G. Sung, S.-Y. Hsieh, and V. Yang, “Large-eddy simulation of combustion dynamics of lean-premixed swirl-stabilized combustor,” J. Propuls. Power, vol. 19, no. 5, pp. 782–794, 2003.
[115] R. Balachandran, B. O. Ayoola, C. F. Kaminski, A. P. Dowling, and E. Mastorakos, “Experimental investigation of the nonlinear response of turbulent premixed flames to imposed inlet velocity oscillations,” Combust. Flame, vol. 143, no. 1, pp. 37–55, 2005.
[116] B. D. Bellows, M. K. Bobba, J. M. Seitzman, and T. Lieuwen, “Nonlinear flame transfer function characteristics in a swirl-stabilized combustor,” J. Eng. Gas Turbines Power, vol. 129, no. 4, pp. 954–961, 2007.
[117] A.-L. Birbaud, D. Durox, S. Ducruix, and S. Candel, “Dynamics of confined premixed flames submitted to upstream acoustic modulations,” Proc. Combust. Inst., vol. 31, no. 1, pp. 1257–1265, 2007.
[118] C. Külsheimer and H. Büchner, “Combustion dynamics of turbulent swirling flames,” Combust. Flame, vol. 131, no. 1, pp. 70–84, 2002.
[119] X. Han, J. Li, and A. S. Morgans, “Prediction of combustion instability limit cycle oscillations by combining flame describing function simulations with a thermoacoustic network model,” Combust. Flame, 2015.
[120] F. Ewald, “On the measurement and modelling of flame transfer function at elevated pressure,” Technische Universitat Munchen, 2009.
[121] A. Cuquel, D. Durox, and T. Schuller, “Theoretical and experimental determination of the flame transfer function of confined premixed conical flames,” in 7th Mediterranean Combustion Symposium, Cagliari, Sardinia, Italy, September, 2011, pp. 11–15.
[122] P. Palies, D. Durox, T. Schuller, and S. Candel, “Nonlinear combustion instability analysis based on the flame describing function applied to turbulent premixed swirling flames,” Combust. Flame, vol. 158, no. 10, pp. 1980–1991, 2011.
[123] C. F. Silva, F. Nicoud, T. Schuller, D. Durox, and S. Candel, “Combining a Helmholtz solver with the flame describing function to assess combustion instability in a premixed swirled combustor,” Combust. Flame, vol. 160, no. 9, pp. 1743–1754, 2013.
[124] A. P. Dowling and S. Hubbard, “Instability in lean premixed combustors,” Proc. Inst. Mech. Eng. Part A J. Power Energy, vol. 214, no. 4, pp. 317–332, 2000.
[125] T. Lieuwen and B. T. Zinn, “The role of equivalence ratio oscillations in driving combustion instabilities in low NO x gas turbines,” in Symposium (International) on Combustion, 1998, vol. 27, no. 2, pp. 1809–1816.
[126] A. P. Dowling, “Modeling and control of combustion oscillations,” Proc. ASME Turbo Expo, 2005.
[127] P. L, Tai-Wo-Chong, T, Komarek, R Kaess , S Foller, W, “Identification of flame transfer functions from LES of a premixed swirl burner,” Proc. ASME Turbo Expo, 2010.
[128] T. Sattelmayer, “Influence of the combustor aerodynamics on combustion instabilities from equivalence ratio fluctuations,” J. Eng. Gas Turbines Power, vol. 125, no. 1, pp. 11–19, 2003.
[129] J. Eckstein, E. Freitag, C. Hirsch, T. Sattelmayer, R. der Bank, and T. Schilling, “Forced low-frequency spray characteristics of a generic airblast swirl diffusion burner,” in ASME Turbo Expo 2003, collocated with the 2003 International Joint Power Generation Conference, 2003, pp. 471–478.
[130] S. R. Stow and A. P. Dowling, “Low-order modelling of thermoacoustic limit cycles,” in ASME Turbo Expo 2004: Power for Land, Sea, and Air, 2004, pp. 775–786.
[131] R. Balachandran, “Experimental Investigation of the Response of Turbulent Premixed Flames to Acoustic Oscillations,” 2005.
[132] N. Noiray, D. Durox, T. Schuller, and S. Candel, “A unified framework for nonlinear combustion instability analysis based on the flame describing function,” J. Fluid Mech., vol. 615, pp. 139–167, 2008.
[133] A. P. Dowling, “Nonlinear self-excited oscillations of a ducted flame,” J. Fluid Mech., vol. 346,

pp. 271–290, 1997.
[134] B. D. Bellows, “Characterization of Nonlinear Heat Release-Acoustic Interactions in Gas Turbine Combustors a Dissertation Presented to The Academic Faculty,” 2006.
[135] B. D. Bellows, M. K. Bobba, A. Forte, J. M. Seitzman, and T. Lieuwen, “Flame transfer function saturation mechanisms in a swirl-stabilized combustor,” Proc. Combust. Inst., vol. 31, no. 2, pp. 3181–3188, 2007.
[136] M. A. Heckl, “Analytical model of nonlinear thermo-acoustic effects in a matrix burner,” J. Sound Vib., vol. 332, no. 17, pp. 4021–4036, 2013.
[137] K. T. Kim and S. Hochgreb, “The nonlinear heat release response of stratified lean-premixed flames to acoustic velocity oscillations,” Combust. Flame, vol. 158, no. 12, pp. 2482–2499, 2011.
[138] X. Han and A. S. Morgans, “Simulation of the flame describing function of a turbulent premixed flame using an open-source LES solver,” Combust. Flame, vol. 162, no. 5, pp. 1778–1792, 2015.
[139] A. Orchini and M. P. Juniper, “Flame Double Input Describing Function analysis,” 2016.
[140] T. Lieuwen, “Nonlinear kinematic response of premixed flames to harmonic velocity disturbances,” Proc. Combust. Inst., vol. 30, no. 2, pp. 1725–1732, 2005.
[141] “UKCCSRC, Gas turbine with exhaust gas recycle – Pilot-scale advanced capture technology,” 2013. [Online]. Available: http://www.pact.ac.uk/facilities/PACT-Core-Facilities/Gas-Turbine/gas-turbine-with-exhaust-gas-recycle-gt-egr/.
[142] H. Li, G. Haugen, M. Ditaranto, D. Berstad, and K. Jordal, “Impacts of exhaust gas recirculation (EGR) on the natural gas combined cycle integrated with chemical absorption CO 2 capture technology,” Energy Procedia, vol. 4, pp. 1411–1418, 2011.
[143] H. Li, M. Ditaranto, and D. Berstad, “Technologies for increasing CO 2 concentration in exhaust gas from natural gas-fired power production with post-combustion, amine-based CO 2 capture,” Energy, vol. 36, no. 2, pp. 1124–1133, 2011.
[144] A. T. Evulet, A. M. Elkady, A. R. Branda, and D. Chinn, “On the performance and operability of GE’s dry low NO x combustors utilizing exhaust gas recirculation for postcombustion carbon capture,” Energy Procedia, vol. 1, no. 1, pp. 3809–3816, 2009.
[145] C. Botero, M. Finkenrath, M. Bartlett, R. Chu, G. Choi, and D. Chinn, “Redesign, optimization, and economic evaluation of a natural gas combined cycle with the best integrated technology CO 2 capture,” Energy Procedia, vol. 1, no. 1, pp. 3835–3842, 2009.
[146] P. E. Røkke and J. E. Hustad, “Exhaust gas recirculation in gas turbines for reduction of CO2 emissions; combustion testing with focus on stability and emissions,” Int. J. Thermodyn., vol. 8, no. 4, pp. 167–173, 2005.
[147] H. Kobayashi, H. Hagiwara, H. Kaneko, and Y. Ogami, “Effects of CO 2 dilution on turbulent premixed flames at high pressure and high temperature,” Proc. Combust. Inst., vol. 31, no. 1, pp. 1451–1458, 2007.
[148] C. Cohé, C. Chauveau, I. Gökalp, and D. F. Kurtulu\cs, “CO 2 addition and pressure effects on laminar and turbulent lean premixed CH 4 air flames,” Proc. Combust. Inst., vol. 32, no. 2, pp. 1803–1810, 2009.
[149] B. E. Gelfand, V. P. Karpov, and others, “Turbulent flames in lean H2-air-CO2 mixtures,” in Mediterranean combustion symposium, 1999, pp. 1000–1006.
[150] H. Kobayashi, T. Tamura, K. Maruta, T. Niioka, and F. A. Williams, “Burning velocity of turbulent premixed flames in a high-pressure environment,” in Symposium (International) on Combustion, 1996, vol. 26, no. 1, pp. 389–396.
[151] C. E. Lee, S. R. Lee, J. W. Han, and J. Park, “Numerical study on effect of CO2 addition in flame structure and NOx formation of CH4-air counterflow diffusion flames,” Int. J. Energy Res., vol. 25, no. 4, pp. 343–354, 2001.
[152] J. L. J, Park K, M Lee E, “Effects of CO2 addition on flame structure in counterflow diffusion flame of H2/CO2/N2 fuel,” Int. J. Energy Res., vol. 25, no. in press, 2000.
[153] J. Lewis, R. Marsh, A. Valera-Medina, S. Morris, and H. Baej, “The use of CO2 to improve stability and emissions of an IGCC combustor,” in ASME Turbo Expo 2014: Turbine Technical Conference and Exposition, 2014, p. V04AT04A029--V04AT04A029.
[154] A. P. Dowling and S. R. Stow, “Acoustic analysis of gas-turbine combustors,” in Combustion instabilities in gas turbine engines: operational experience, fundamental mechanics, and modeling, Raston -USA: American Intstitute of Aeronautics and Astronautics, Inc., 2005, pp. 369–414.
[155] S. R. Stow, A. P. Dowling, and T. P. Hynes, “Reflection of circumferential modes in a choked nozzle,” J. Fluid Mech., vol. 467, pp. 215–239, 2002.

[156] V. Yang and F. E. C. Culick, “Analysis of unsteady inviscid diffuser flow with a shock wave,” J. Propuls. Power, vol. 1, no. 3, pp. 222–228, 1985.
[157] F. E. C. Culick and T. Rogers, “The response of normal shocks in diffusers,” AIAA J., vol. 21, no. 10, pp. 1382–1390, 1983.
[158] T. C. Lieuwen, “Experimental investigation of limit-cycle oscillations in an unstable gas turbine combustor,” J. Propuls. Power, vol. 18, no. 1, pp. 61–67, 2002.
[159] T. Lieuwen, “Combustion driven oscillations in gas turbines,” Turbomach. Int., vol. 44, no. 1, pp. 16–18, 2003.
[160] Y. Huang, “Advanced methods for validating combustion instability predictions using pressure measurements,” Purdue University, 2015.
[161] G. A. Richards, D. L. Straub, and E. H. Robey, “Passive control of combustion dynamics in stationary gas turbines,” J. Propuls. Power, vol. 19, no. 5, pp. 795–810, 2003.
[162] D. Zhao and A. S. Morgans, “Tuned passive control of combustion instabilities using multiple Helmholtz resonators,” J. Sound Vib., vol. 320, no. 4, pp. 744–757, 2009.
[163] N. Noiray, D. Durox, T. Schuller, and S. Candel, “Passive control of combustion instabilities involving premixed flames anchored on perforated plates,” Proc. Combust. Inst., vol. 31, no. 1, pp. 1283–1290, 2007.
[164] C. F. Speich and A. A. Putnam, “Suppression of Pulsations in Oil-Fired Residential Heating Equipment,” in ASHRAE semi-annual Meeting, Chicago, 1961.
[165] J. R. Hibshman, J. M. Cohen, A. Banaszuk, T. J. Anderson, and H. A. Alholm, “Active Control of Combustion Instability in a Liquid--Fueled Sector Combustor,” in ASME 1999 International Gas Turbine and Aeroengine Congress and Exhibition, 1999, p. V002T02A030--V002T02A030.
[166] C. O. Paschereit, E. Gutmark, and W. Weisenstein, “Control of combustion driven oscillations by equivalence ratio modulations,” in ASME 1999 International Gas Turbine and Aeroengine Congress and Exhibition, 1999, p. V002T02A023--V002T02A023.
[167] J. C. DeLaat, G. Kopasakis, J. R. Saus, C. T. Chang, and C. Wey, “Active combustion control for aircraft gas-turbine engines—experimental results for an advanced, low-emissions combustor prototype,” in Proc., 50th American Institute of Aeronautics and Astronautics Aerospace Sciences Meeting, 2012.
[168] K. R. McManus, T. Poinsot, and S. M. Candel, “A review of active control of combustion instabilities,” Prog. energy Combust. Sci., vol. 19, no. 1, pp. 1–29, 1993.
[169] T. Samad and A. M. Annaswamy, “Active control of combustion instability; theory and practice,” 2011. [Online]. Available: www.ieeecss.org.
[170] D. Gorinevsky, N. Overman, and J. Goeke, “Amplitude and phase control in active suppression of combustion instability,” in 2012 American Control Conference (ACC), 2012, pp. 2601–2608.
[171] G. Kopasakis, J. C. DeLaat, and C. T. Chang, “Adaptive instability suppression controls method for aircraft gas turbine engine combustors,” J. Propuls. Power, vol. 25, no. 3, pp. 618–627, 2009.
[172] N. Docquier and S. Candel, “Combustion control and sensors: a review,” Prog. energy Combust. Sci., vol. 28, no. 2, pp. 107–150, 2002.
[173] A. M. Annaswamy and A. F. Ghoniem, “Active control of combustion instability: Theory and practice,” IEEE Control Syst., vol. 22, no. 6, pp. 37–54, 2002.
[174] S. Evesque and A. P. Dowling, “LMS algorithm for adaptive control of combustion oscillations,” Combust. Sci. Technol., vol. 164, no. 1, pp. 65–93, 2001.
[175] R. Blonbou, A. Laverdant, S. Zaleski, and P. Kuentzmann, “Active control of combustion instabilities on a Rijke tube using neural networks,” Proc. Combust. Inst., vol. 28, no. 1, pp. 747–755, 2000.
[176] S. Murugappan, S. Acharya, D. C. Allgood, S. Park, A. M. Annaswamy, and A. F. Ghoniem, “Optimal control of a swirl-stabilized spray combustor using system identification approach,” Combust. Sci. Technol., vol. 175, no. 1, pp. 55–81, 2003.
[177] C. E. Johnson, Y. Neumeier, M. Neumaier, B. T. Zinn, D. D. Darling, and S. S. Sattinger, “Demonstration of active control of combustion instabilities on a full-scale gas turbine combustor,” in ASME Turbo Expo 2001: Power for Land, Sea, and Air, 2001, p. V002T02A062--V002T02A062.
[178] J. M. Cohen, N. M. Rey, C. A. Jacobson, and T. J. Anderson, “Active Control of Combustion Instability in a Liquid--Fueled Low--NOx Combustor,” in ASME 1998 International Gas Turbine and Aeroengine Congress and Exhibition, 1998, p. V003T06A020--V003T06A020.
[179] K. Ogata and Y. Yang, “Modern control engineering,” 1970.

[180] M. Fleifil, J. P. Hathout, A. M. Annaswamy, and A. F. Ghoniem, “The origin of secondary peaks with active control of thermoacoustic instability,” Combust. Sci. Technol., vol. 133, no. 4–6, pp. 227–265, 1998.
[181] P. Dines, “Active control of flame noise,” University of Cambridge, 1983.
[182] H. M., “Active control of the noise from a Rijke tube,” J. Sound Vib., vol. 124, pp. 117–33, 1988.
[183] W. Lang, T. Poinsot, and S. Candel, “Active control of combustion instability,” Combust. Flame, vol. 70, no. 3, pp. 281–89, 1987.
[184] T. Poinsot, F. Bourienne, S. Candel, E. Esposito, and W. Lang, “Suppression of combustion instabilities by active control,” J. Prop. Power, vol. 5, pp. 14–20, 1989.
[185] J. P. Hathout, A. M. Annaswamy, M. Fleifil, and A. F. Ghoniem, “A model-based active control design for thermoacoustic instability,” Combust. Sci. Tech., vol. 132, pp. 99–138, 1998.
[186] D. Dynamics, StreamWare Basic Installation and User Guide. Denmark: Dantec Dynamics, 2013.
[187] D. Dynamics, “Probes for Hot-Wire A nemometry.” [Online]. Available: http://www.dantecdynamics.jp/docs/products-and-services/general-literature/Hot-wire_catalog_238.pdf. [Accessed: 15-Jul-2017].
[188] F. E. Jørgensen, How to measure turbulence with hot-wire anemometers: a practical guide. Dantec dynamics, 2001.
[189] D. Dynamics, “Integrated solution in Laser Doppler Anemometry.” [Online]. Available: http://www.dantecdynamics.jp/docs/products-and-services/general-literature/Laser_Doppler_Anemometry_318.pdf. [Accessed: 15-Jul-2017].
[190] J. O. Keller and K. Saito, “Measu rements of the Combusting Flow in a Pulse Combustor,” Combust. Sci. Technol., vol. 53, no. 2–3, pp. 137–163, 1987.
[191] V. K. Khanna, U. Vandsburger, W. R. Saunders, and W. T. Baumann, “Dynamic analysis of swirl stabilized turbulent gaseous flames,” in ASME Turbo Expo 2002: Power for Land, Sea, and Air, 2002, pp. 285–297.
[192] R. Obertacke, H. Wintrich, F. Wintrich, and A. Leipertz, “A new sensor system for industrial combustion monitoring and control using UV emission spectroscopy and tomography,” Combust. Sci. Technol., vol. 121, no. 1–6, pp. 133–151, 1996.
[193] K. I. Corp, “Miniature, High Sensitivity, Voltage Output Pressure Sensor,” 2012. [Online]. Available: http://www.intertechnology.com/Kistler/pdfs/Pressure_Model_211B.pdf. [Accessed: 15-Jul-2017].
[194] Kistler Instrument Corp, “Quartz High Pressure Sensor,” 2014. [Online]. Available: http://www.process-controls.com/intertechnology/Kistler/pdfs/Pressure_Model_701A.pdf. [Accessed: 15-Jul-2017].
[195] Dantec Dynamics, “BSA Flow Software for LDA.” [Online]. Available: https://www.dantecdynamics.com/download-login. [Accessed: 15-Jul-2017].
[196] L. Crocco, “Aspects of combustion stability in liquid propellant rocket motors part i: fundamentals. low frequency instability with monopropellants,” J. Am. Rocket Soc., vol. 21, no. 6, pp. 163–178, 1951.
[197] S. R. Stow and A. P. Dowling, “A time-domain network model for nonlinear thermoacoustic oscillations,” J. Eng. gas turbines power, vol. 131, no. 3, p. 31502, 2009.
[198] D. Rockwell and E. Naudascher, “Self-sustained oscillations of impinging free shear layers,” Annu. Rev. Fluid Mech., vol. 11, no. 1, pp. 67–94, 1979.
[199] T. Lieuwen, V. McDonell, E. Petersen, and D. Santavicca, “Fuel flexibility influences on premixed combustor blowout, flashback, autoignition, and stability,” J. Eng. gas turbines power, vol. 130, no. 1, p. 11506, 2008.
[200] V. Acharya, Shreekrishna, D. H. Shin, and T. Lieuwen, “Swirl effects on harmonically excited, premixed flame kinematics,” Combust. Flame, 2012.
[201] Y. Huang, W. Shanwu, and V. Yang, “Flow and flame dynamics of lean premixed swirl injectors,” in Combustion instabilities in gas turbine engines operational experience, fundamental mechanisms and modeling, Raston -USA: American Institute of Aeronautics and Astronautics, Inc., 2005, pp. 213–276.
[202] V. G. McDonell, M. W. Effinger, and J. L. Mauzey, “Correlation of Landfill and Digester Gas Composition With Gas Turbine Pollutant Emissions,” in ASME Turbo Expo 2006: Power for Land, Sea, and Air, 2006, pp. 565–575.
[203] P. Strakey, T. Sidwell, and J. Ontko, “Investigation of the effects of hydrogen addition on lean extinction in a swirl stabilized combustor,” Proc. Combust. Inst., vol. 31, no. 2, pp. 3173–3180, 2007.

[204] J. P. Moeck, J.-F. Bourgouin, D. Durox, T. Schuller, and S. Candel, "Tomographic reconstruction of heat release rate perturbations induced by helical modes in turbulent swirl flames," Exp. Fluids, vol. 54, no. 4, p. 1498, 2013.
[205] N. A. Worth and J. R. Dawson, "Tomographic reconstruction of OH* chemiluminescence in two interacting turbulent flames," Meas. Sci. Technol., vol. 24, no. 2, p. 24013, 2012.
[206] Y. Ishino and N. Ohiwa, "Three-dimensional computerized tomographic reconstruction of instantaneous distribution of chemiluminescence of a turbulent premixed flame," JSME Int. J. Ser. B Fluids Therm. Eng., vol. 48, no. 1, pp. 34–40, 2005.
[207] B. O. Ayoola, R. Balachandran, J. H. Frank, E. Mastorakos, and C. F. Kaminski, "Spatially resolved heat release rate measurements in turbulent premixed flames," Combust. Flame, vol. 144, no. 1, pp. 1–16, 2006.
[208] Y. Huang and V. Yang, "Effect of swirl on combustion dynamics in a lean-premixed swirl-stabilized combustor," Proc. Combust. Inst., vol. 30, no. 2, pp. 1775–1782, 2005.
[209] Y. Huang, "No Title," The Pennsylvania State University, 2003.
[210] C. F. Silva, F. Nicoud, T. Schuller, D. Durox, and S. Candel, "Combining a Helmholtz solver with the flame describing function to assess combustion instability in a premixed swirled combustor," Combust. Flame, vol. 160, no. 9, pp. 1743–1754, 2013.
[211] S. H. Preetham and T. C. Lieuwen, "Response of turbulent premixed flames to harmonic acoustic forcing," Proc. Combust. Inst., vol. 31, no. 1, pp. 1427–1434, 2007.
[212] S. Shanbhogue, D.-H. Shin, S. Hemchandra, D. Plaks, and T. Lieuwen, "Flame-sheet dynamics of bluff-body stabilized flames during longitudinal acoustic forcing," Proc. Combust. Inst., vol. 32, no. 2, pp. 1787–1794, 2009.
[213] T. Lieuwen, "Online combustor stability margin assessment using dynamic pressure data," Trans. ASME-A-Engineering Gas Turbines Power, vol. 127, no. 3, pp. 478–482, 2005.
[214] J. M. Cohen, W. Proscia, and J. Delaat, "Characterization of aeroengine combustion instability," in Combustion instabilities in gas turbine engines operational experience, fundamental mechanisms and modeling, Reston -USA: American Institute of Aeronautics and Astronautics, Inc., 2005, pp. 113–145.
[215] J. Hermann and S. Hoffmann, "Implementation of active control in a full-scale gas-turbine combustor," Raston -USA: American Institute of Aeronautics and Astronautics, Inc., 2005, pp. 611–634.
[216] J. M. Cohen and A. Banaszuk, "Factors affecting the control of unstable combustors," in Combustion instabilities in gas turbine engines operational experience, fundamental mechanisms and modeling, Raston -USA: American Institute of Aeronautics and Astronautics, Inc., 2005, pp. 581–609.
[217] J. B. Sewell and P. A. Sobieski, "Monitoring of combustion instabilities: Calpine's experience," in Combustion instabilities in gas turbine engines operational experience, fundamental mechanisms and modeling, Raston -USA: American Institute of Aeronautics and Astronautics, Inc., 2005, pp. 147–162.
[218] R. Balachandran, "Experimental investigation of the response of turbulent premixed flames to acoustic oscillations," University of Cambridge, 2005.
[219] P. Palies, D. Durox, T. Schuller, and S. Candel, "Combustion Instabilities Analysis Based on the Flame Describing Function Applied to Swirling Flames."
[220] M. W. Woolrich, B. D. Ripley, M. Brady, and S. M. Smith, "Temporal autocorrelation in univariate linear modeling of FMRI data," Neuroimage, vol. 14, no. 6, pp. 1370–1386, 2001.
[221] J. D. Scargle, "Studies in astronomical time series analysis. III-Fourier transforms, autocorrelation functions, and cross-correlation functions of unevenly spaced data," Astrophys. J., vol. 343, pp. 874–887, 1989.

Appendix A1: Setup of the experimental rig

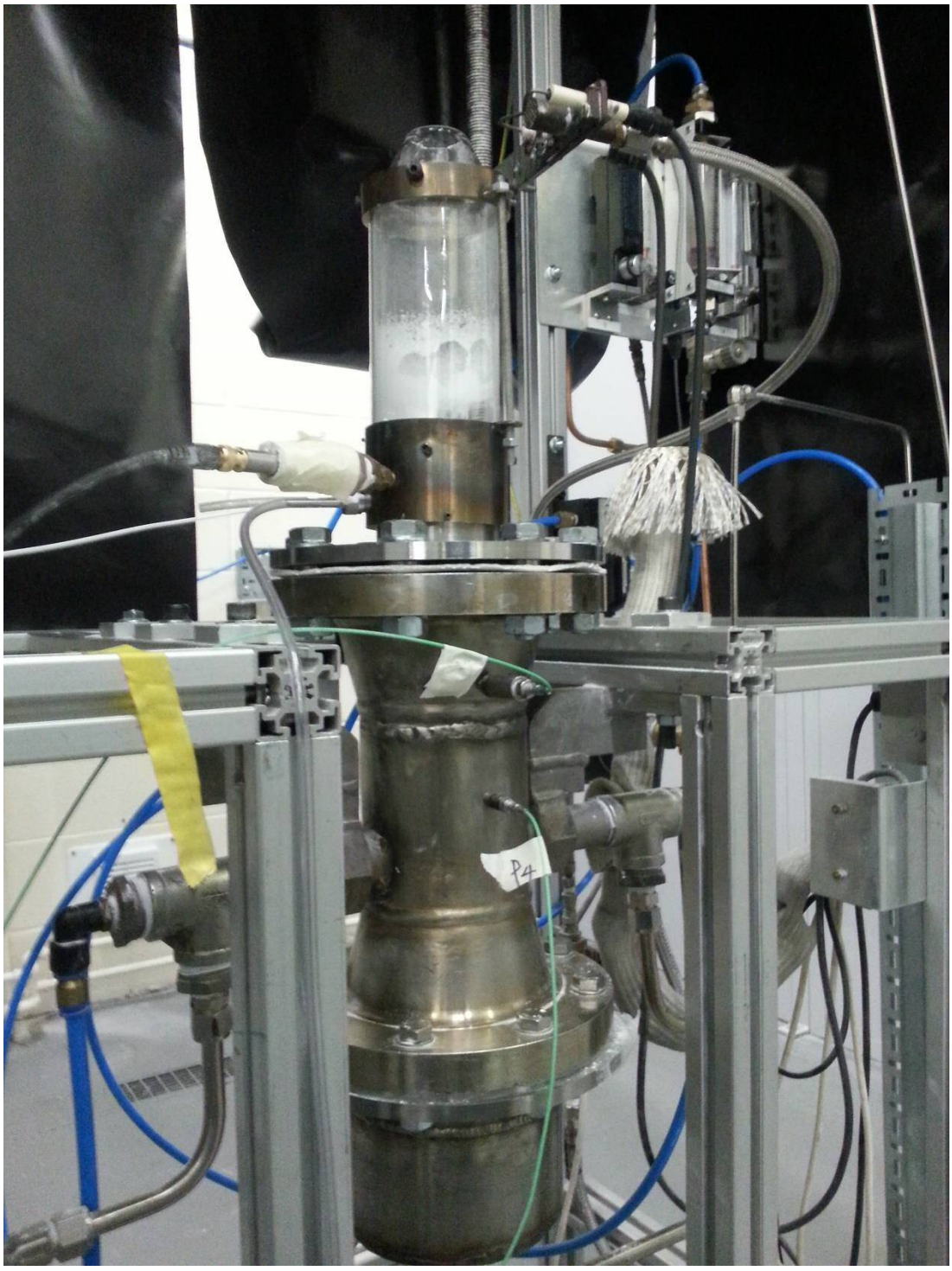

Appendix A2: The flame confinement section of the rig.

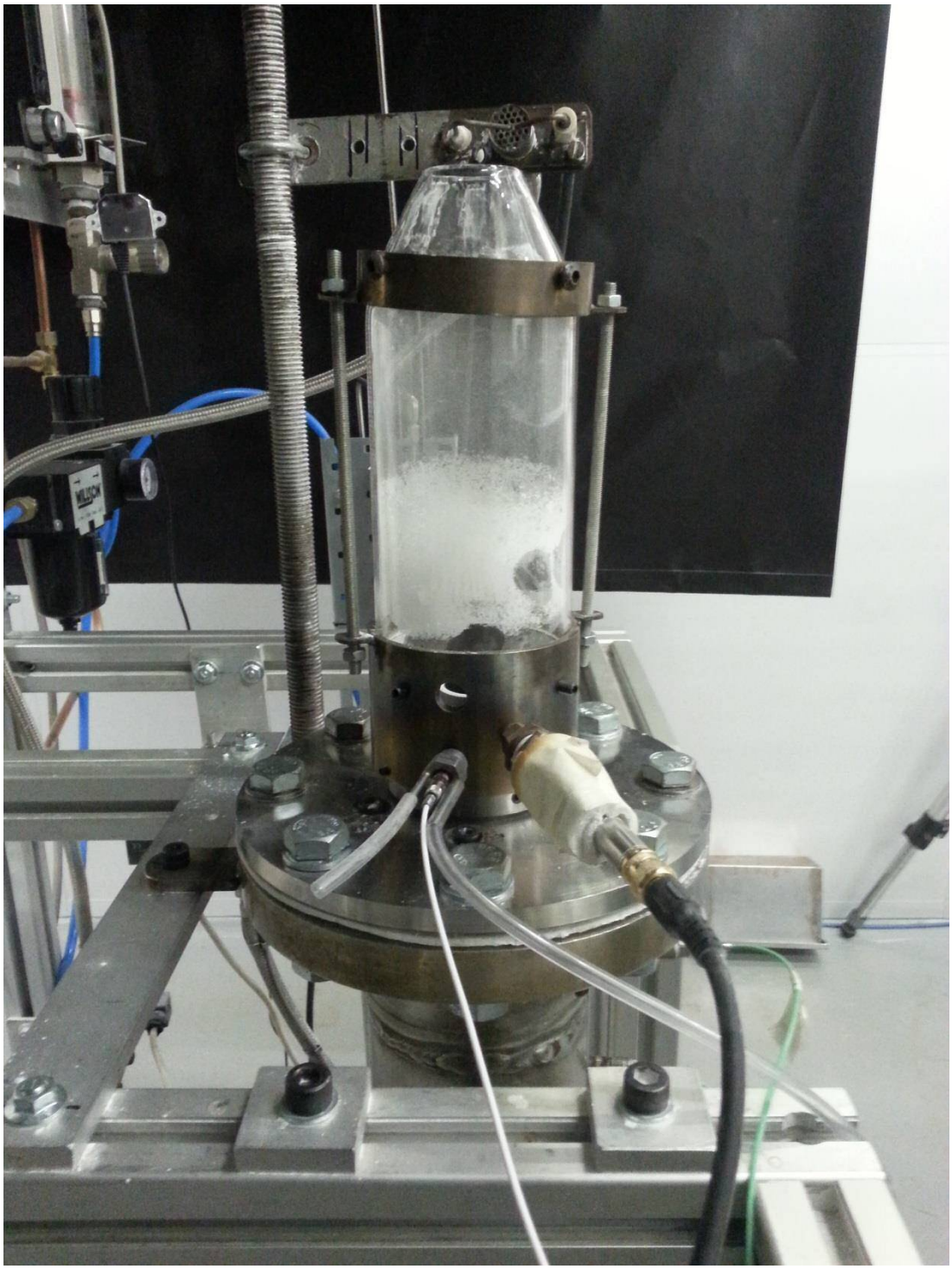

Appendix A3: A Picture of the manufactured Combustor before setup

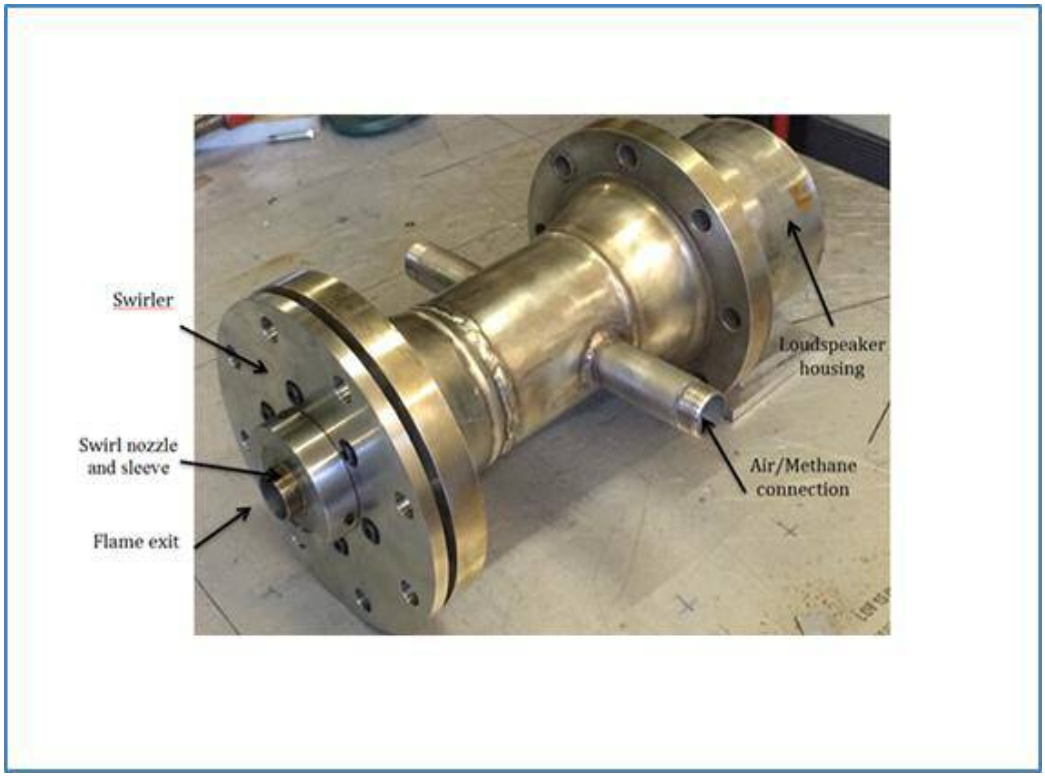

Appendix A4: A Windows Package- BSA Flow Software

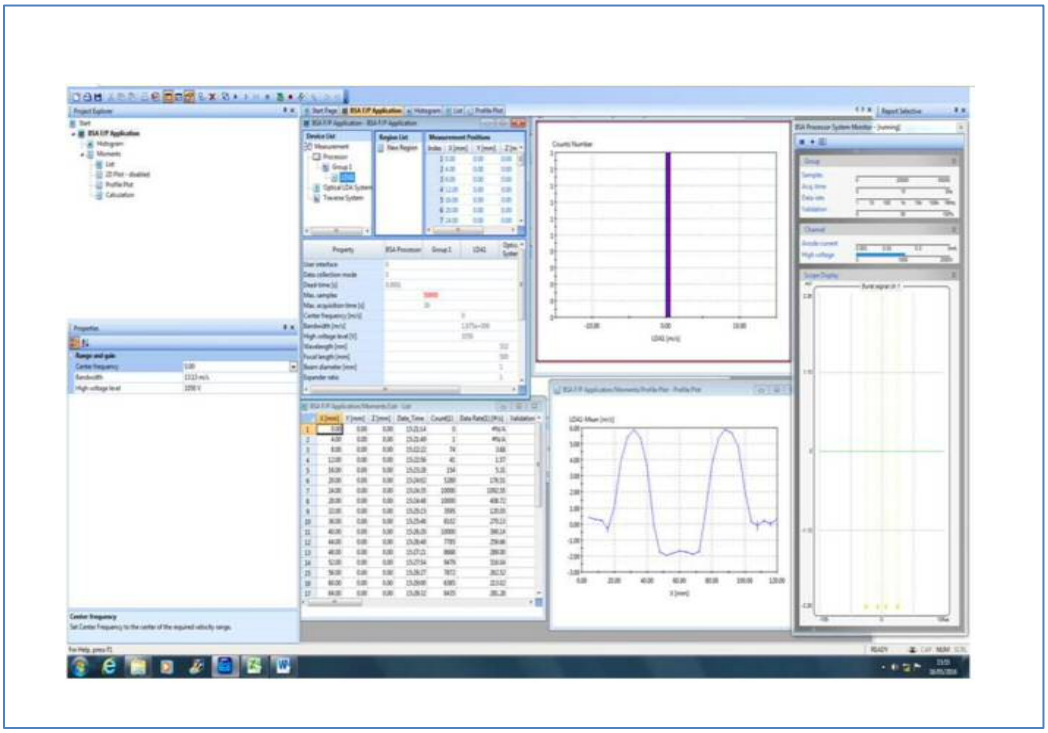

Appendix A5: CTA data acquisition interface

Appendix A6: A Model 5165A – 4- Channel Kistler Labamplifier data acquisition interface

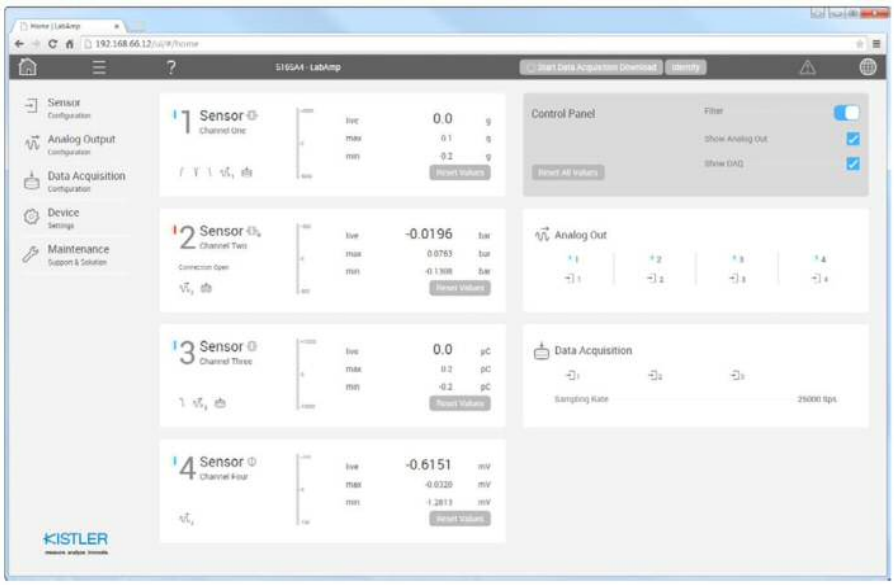

Appendix B1: Imatool software interface for flame CH* quantification

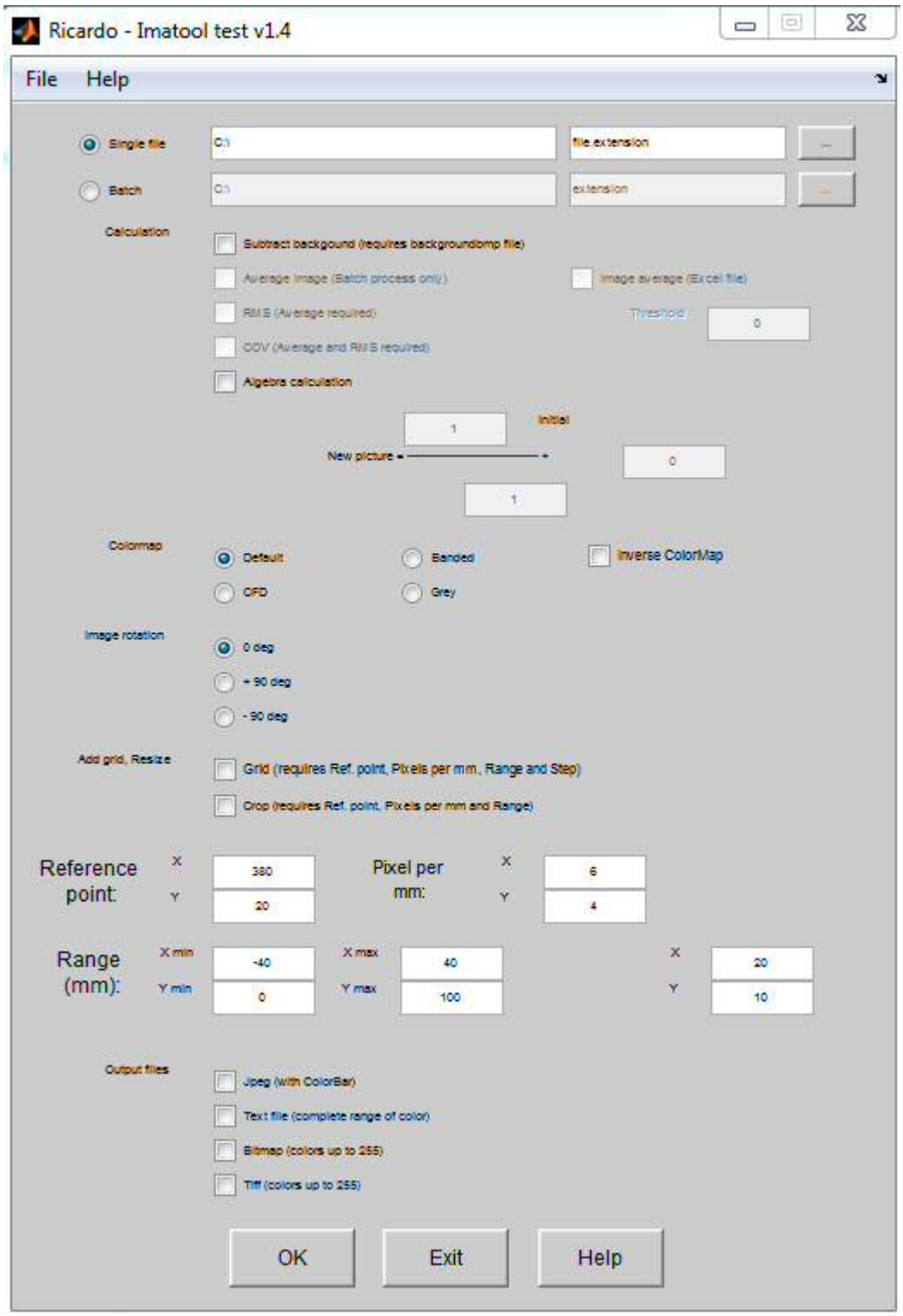

Appendix B2: Matlab Codes for CH* intensity quantification

```
global pic pic1 pic2 sum CoGx CoGy back0 back1 back2 res1
sum = 0;
CoGx = 0;
CoGy = 0;
back0 = imread('emmy.jpg');
back1 = im2double(back0);
back2 = rgb2gray(back1)
pic = imread('emmy.jpg');
pic1 = im2double(pic);
pic2 = rgb2gray(pic1);
res1 = pic2 - back2;
for i=1:288
    for j=1:423
        sum = sum + res1(i,j);
    end
end

for i=1:288
    for j=1:423
        CoGx = CoGx + i*res1(i,j);
        CoGy = CoGy + j*res1(i,j);
    end
end
CoGx
CoGy
sum
```

.....

```
global pic pic1 pic2 sum CoGx CoGy back0 back1 back2 res1

sum = 0;
CoGx = 0;
CoGy = 0;
back0 = imread('t0.jpg');
back1 = im2double(back0);
back2 = rgb2gray(back1);

pic = imread('t10.jpg');
pic1 = im2double(pic);
pic2 = rgb2gray(pic1);

res1 = pic2 - back2;
for i=1:288
    for j=1:423
        sum = sum + res1(i,j);
    end
end
for i=1:288
    for j=1:423
        CoGx = CoGx + i*res1(i,j);
        CoGy = CoGy + j*res1(i,j);
    end
end

CoGx
CoGy
sum
```

Appendix B3: Matlab Codes and runs for FFT Analysis

```
08/06/17 11:05  MATLAB C...   1 of 1

>> %s100 is equivalent to loading s_100 data
>> time=[0:0.00016:2-0.00016]'; %ws = 6250 Hz,↙
Tt = 2 s
>> subplot(2,1,1);plot(time,s100);grid;axis([0↙
2 0 0.12]);xlabel('Time (s)');ylabel('S_100↙
data (unknown units)')
>> y=fft(s100); %Nfft=2*6250 = 12,500
>> subplot(2,1,2);plot(abs(y));grid;axis([2↙
3125 0 20]);xlabel('Index');ylabel('FFT↙
Amplitude(unknown units)')
>> %deltaf=1/2=0.5 Hz, wmax=deltaf*Nfft/2 =↙
3125 Hz
>> %dc value = average = 0.0897
>> %your zoom (by index)
>> subplot(2,1,2);plot(abs(y));grid;axis([50↙
600 0 20]);xlabel('Index');ylabel('FFT↙
Amplitude(unknown units)')
>>
```

```
>> f=fft(s100);
>> F=2*abs(f)/12500; F(1)=F(1)/2; freq=[0:0.5:↙
6249.5]';
>> subplot(2,1,2);stem(freq,F); grid; axis([0↙
500 0 0.003]);xlabel('Freq (Hz)');ylabel('FFT↙
Amplitude(unknown units)')
>>
```

Check F(1) = 0.0897 dc value matches average value

FFT Runs

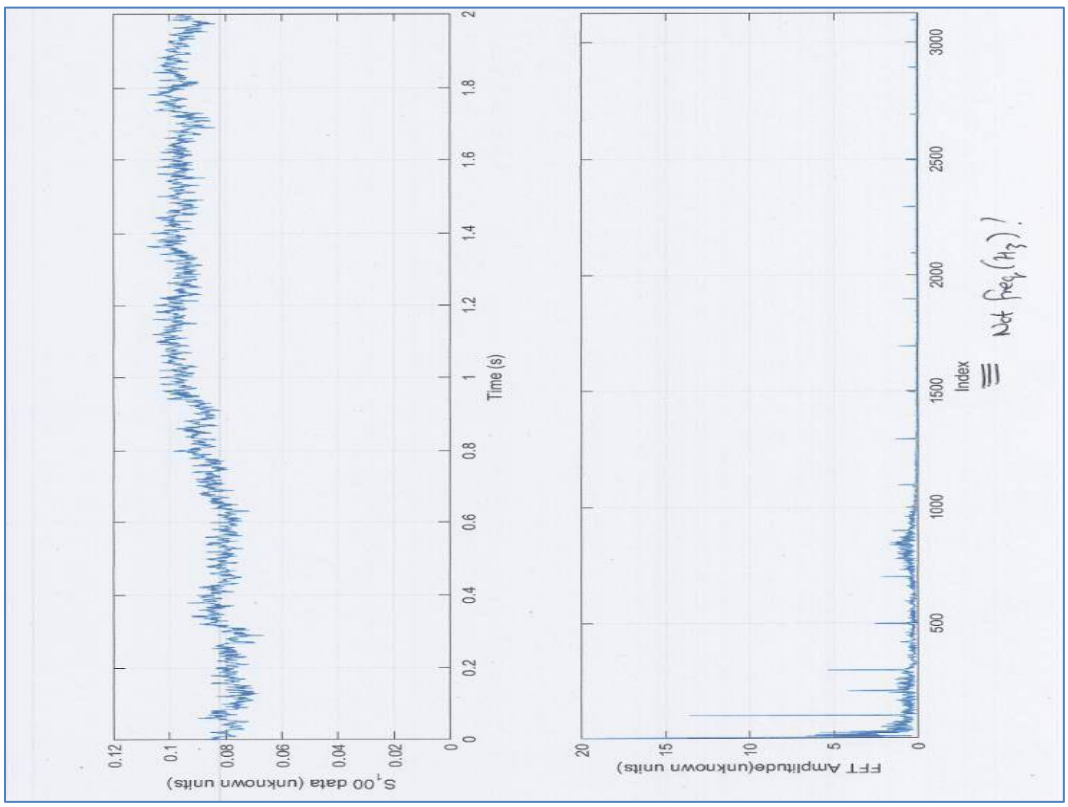
S100 data (unknown units)
Time (s)
FFT Amplitude(unknown units)
Index
Dat Freq (Hz)!

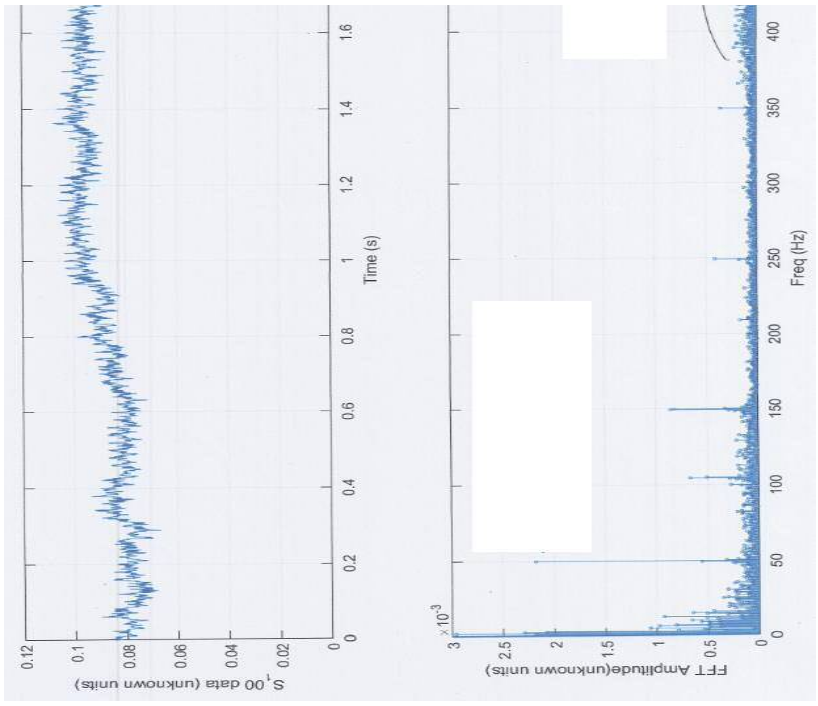
S100 data (unknown units)
Time (s)
FFT Amplitude(unknown units)
Freq (Hz)